PHASE II – FINAL REPORT
Exploration of Jovian Atmosphere Using Nuclear Ramjet Flyer

George Maise, Principal Investigator

March 1, 2003

Note: The work reported in this Final Report was performed for Universities Space Research Association (USRA) under NIAC Phase II Grant 07600-061, Prime Contract Number NAS5-98051. The period of performance was 24 months; form March 1, 2001 through March 1, 2003.

PLUS ULTRA TECHNOLOGIES, INC.
25 East Loop Road
Stony Brook, New York 11790-3350

CONTRIBUTORS

Many individuals contributed to the success of this project. The team was composed of Plus Ultra in-house staff, and consultants. The contributors, in alphabetical order, were:

Gilbert Carpenter, Consultant	Stability and Control
Randy Chue, GASL	CFD
Timothy Dowling, U. Louisville	Planetary Science & Instruments
Edward Kush, Consultant	Ramjet Propulsion
Robert Lecat, Consultant	Vehicle Conceptual Design
Hans Ludewig, BNL	Nuclear Physics
George Maise, Plus Ultra Technologies	Principal Investigator
John Paniagua, Plus Ultra Technologies	Mission Analysis
James Powell, Plus Ultra Technologies	Inventor of Concept, Neutronics
Sven Roosild, Consultant	Radiation Hardening
Pasquale Sforza, U. Florida	Flight Vehicle Aerodynamics
Jason Tyll, GASL	CFD, Ramjet Propulsion

Table of Contents

LIST OF FIGURES

.

Abstract

This report describes the status of the Nuclear Ramjet Flyer program at the conclusion of the NIAC Grant Phase II effort. The purpose of this project was to investigate the design, operation, and data gathering possibilities of a nuclear-powered ramjet flyer in the Jovian atmosphere. The MITEE nuclear rocket engine can be modified to operate as a ramjet in planetary atmospheres. (Note: MITEE is a compact, ultra-light-weight thermal nuclear rocket which uses hydrogen as the propellant.) To operate as a ramjet, MITEE requires a suitable inlet and diffuser to substitute for the propellant that is pumped from the supply tanks in a nuclear rocket engine. A flight vehicle, powered by such a ramjet would fly in the upper Jovian atmosphere, mapping in detail temperatures, pressures, compositions, lightning activity, and wind speeds, e.g., in the highly turbulent equatorial zone and the Great Red Spot. The nuclear ramjet could operate for months because: 1) the Jovian atmosphere has unlimited propellant, 2) the MITEE nuclear reactor is a (nearly) unlimited power source, and 3) with few moving parts, mechanical wear should be minimal. Our Phase II study has not revealed any issues which would make the concept unworkable. A number of changes (to the Phase I design) were necessary to make the concept more viable. We have abandoned the Galileo-type instrument package and replaced it with a state-of-the-art instruments which are much lighter and much more compact. Also, we are considering drosondes to complement the on-board instruments. The dropsondes can sample the Jovian atmosheres at altitudes lower than the flyer is able to fly. The MITEE nuclear engine, which was originally developed for rocket applications, was redesigned to provide improved performance for ramjet applications. Although the entire Ramjet Flyer system involves many disciplines, the focus of the current study has been on the design of the Flyer itself, i.e., its aerodynamic configuration and its nuclear powerplant.

1. INTRODUCTION

The Galileo probe which entered the Jovian atmosphere in 1995 was a great scientific achievement [Aichele, 1996]. It provided, for the first time, direct measurement of Jovian atmospheric properties. Because of the nature of the probe, atmospheric data was provided at one location on the planet and, at any particular altitude, at one instant of time. (It now appears that the probe entered a decidedly non-typical portion of the Jovian atmosphere. The entry location was one of the clearest and driest spots on the planet.) With the ramjet flyer, described in this report, we remove the restriction of space and time. We can sample the atmosphere at any location within the altitude restrictions of the flyer. We can observe time-dependent behavior since we can return to same location time and again to resample the atmosphere.

The Jovian atmosphere contains many puzzling features. The most famous, of course, is the Great Red Spot (GRS). It appears to be an enormous anticyclone, although its true nature is still unknown [Morrison, 1996]. In addition, there are many other less famous features that are lacking satisfactory explanations. For example, there are the three white oval spots (the size of Mars) near the GRS. There is the highly turbulent equatorial zone. It is expected that the Jovian flyer, with its enormous mapping capability (both spatially and temporally), could be instrumental in solving these and other riddles.

The project described in this report is aimed at the design, operation, and data gathering possibilities of a nuclear-powered ramjet flyer in the Jovian atmosphere. The MITEE nuclear rocket engine can be modified to operate as a ramjet in planetary atmospheres. MITEE is a compact, ultra-light-weight thermal nuclear rocket which uses hydrogen as the propellant. Its specific impulse is more than twice that of the best chemical rockets [Powell, 1998]. It is an outgrowth of the Particle Bed Reactor (PBR) which was initiated in the mid 1980's by the DOD/SNTP (Space Nuclear Thermal Propulsion) program [Ludewig, 1996]. While the program did not test a full-up engine, low power critical reactor tests were carried out and the various component hardware were developed and tested. Work on the PBR stopped in 1993 when its mission need disappeared at the end of the Cold War. While the PBR program was technically successful, the nuclear engine was still too large and heavy to be useful for present day space exploration missions. A new compact, ultra lightweight nuclear engine concept, termed MITEE (MInature ReacTor EnginE) was conceived to meet this need. Thus, MITEE is derived from the PBR, with modifications to substantially reduce the weight of the engine, simplify construction, and enhance performance.

To operate as a ramjet, MITEE requires a suitable inlet and diffuser to substitute for the propellant that is ducted from the supply tanks in a nuclear rocket engine. Such a ramjet would fly in the upper Jovian atmosphere, mapping in detail temperatures, pressures, compositions, lightning activity, and wind speeds. The nuclear ramjet could operate for months because: 1) the Jovian atmosphere has unlimited propellant, 2) the MITEE nuclear reactor is a (nearly) unlimited power source, and 3) with few moving parts, wear should be minimal. The ramjet is extremely simple and lightweight, with three components: 1) a diffuser to compress the incoming

atmosphere, 2) a heat source to heat the compressed gas, and 3) an exhaust nozzle to generate thrust. To perform the mapping mission, the flight vehicle must first be transported into the Jovian atmosphere. This is a technically demanding, but by no means impossible, task. We note that on December 7, 1995, the Galileo Probe, having a mass of 339 kg (approximately 50% payload and 50% thermal shield), successfully entered the Jovian atmosphere. In spite of an entry velocity of 47.4 km/s, stagnation temperatures of 15,500°C, and a peak deceleration of 230 g's, the probe performed successfully. The ramjet flyer will essentially duplicate the Galileo Probe mission until our entry vehicle has decelerated to about Mach 3.0 (v = 2.6 km/s). At that point, the ramjet flyer will detach from the entry vehicle, and the nuclear engine will commence operation to propel the flyer on its data gathering mission. Although this study has been directed at mapping the Jovian atmosphere, the technology is equally applicable for flying in and mapping the atmospheres of Saturn, Uranus and Neptune, as well as Sturn's moon Triton, the only moon in our solar system with an atmosphere.

From the standpoint of radiation safety, the nuclear ramjet is not hazardous. Until start up of the reactor, which will occur after entry into Jovian atmosphere, the nuclear fuel is not radioactive. During the launch phase (from Earth), safety systems would prevent reactor criticality for all conceivable accident situations.

Although the data gathered by the ramjet flyer will be similar to the data gathered by the Galileo entry probe, the advances in miniaturization of electronic components have led to much lighter and more compact instruments. The total mass of instruments on the Galileo probe, which were built with 1970's electronics, was 33.4 kg. Comparable instruments, which will provide all the data of interest to the planetary science community, will have a mass which is only a fraction of the Galileo instruments. In addition to on-board instruments, the flyer will will have an ability to carry drosondes which will be released from the flyer at specific locations. The flyer will then circle in a holding pattern receiving telemetry while the probe descends to an altitude corresponding to, say ~100 bars. At this point the flyer will quickly fly to a different latitude and repeat the process. In this way, the spatial variation of properties with latitude will be obtained.

The nuclear reactor design is a variant of the MITEE nuclear reactor. A modified design of the reactor for ramjet applications was necessitated as a result of thermal/hydraulic analyses of the MITEE nuclear reactor. It became evident that the geometry of the reactor, which was developed for nuclear **rocket** application, does not produce good performance as a **ramjet**. The basic problem is that while the rocket version of the MITEE operates at a uniformly high pressure (~70 atm), the ramjet, on the other hand, operates at a much lower pressure, which also varies appreciably depending on the flight conditions (altitude and Mach number). To produce adequate thrust, the flow passages in the ramjet core have to be much larger, leading to larger and heavier engines. These problems were largely overcome by modifying the core design in which the coolant enters at the center of each fuel element and flows radially outward through the annular core (opposite to the flow in the rocket version of MITEE). With this design, criticality is attainable for lighter weight engine than with the conventional MITEE design.

During its mapping mission in the Jovian atmosphere the Ramjet Flyer will have to respond autonomously to changing flight conditions. Any commands from Earth have a 55 minute built-in

delay. Although not addressed in any detail in this report, it may be noted that the U.S. military is developing robust technology for unmanned flight. This technology will have direct applications for guidance and control of the Ramjet Flyer. There are several ongoing unmanned air vehicle (UAV) development programs. Because UAV technology is maturing so rapidly, it is widely believed that the JSF will be the last manned fighter aircraft.

For completeness, we give here a brief historical sketch of earlier work on nuclear ramjets. During the period of 1957 - 1964 very extensive development work was carried out in the U.S. on a nuclear ramjet powered missile called the SLAM (Supersonic Low Altitude Missile) under the code name of Project Pluto [Herken, 1990]. This work was sponsored jointly by the U.S. Air Force and the Atomic Energy Commission. The mission of SLAM was strictly military, i.e., to deliver nuclear bombs on enemy targets. SLAM was designed to fly at near-treetop level (to avoid radar detection) at a Mach number of 3. It was powered by the Tory nuclear engine designed at the Livermore National Laboratory. In 1961 a full-sized static test of the Tory engine was conducted in the Nevada desert. The test was entirely successful, producing 513 Megawatts of power and 35,000 pounds (156,000 newtons) of thrust. No flight tests were ever conducted. In 1964 Project Pluto was canceled because the ICBMs became more attractive as strategic weapons.

The SLAM vehicle is, of course, very different from our Jovian Flyer in terms of mission requirements,, vehicle size and engine design. Project Pluto did demonstrate, however, that with a properly focused development program, nuclear ramjets are practical and will perform as intended.

2. MOTIVATION FOR STUDYING JUPITER WITH RAMJET FLYER

The Jovian atmosphere contains many puzzling features. The most famous, of course, is the Great Red Spot (GRS). It appears to be an enormous anticyclone, although its true nature is still unknown. In addition, there are many other less famous features that are lacking satisfactory explanations. For example, there are the three white oval spots (the size of Mars) near the GRS. There is the highly turbulent equatorial zone. It is expected that the Jovian flyer, with its enormous mapping capability (both spatially and temporally), could be instrumental in solving these and other riddles.

On a more fundamental level, understanding Jupiter is a central goal of NASA's strategic plan for exploring the Solar System. Four reasons for studying the planet that together underscore the need for an in situ observing platform like the ramjet are the following:

First, Jupiter is an extremely common planet type. It is likely that many solar systems have a dominant gas giant planet with an orbital radius in the neighborhood of 5 AU. Models of our Solar System's protoplanetary disk mark 5 AU as the "snow line," the distance from the protosun where the temperature drops to the point that ice is stable. Some planetary accretion models suggest that it may be no accident that Jupiter is located on the snow line. Jupiter has more mass than all the other planets in the Solar System combined, thus from a cosmochemical point of view accurate observations of its composition are crucial to the success of solar-system formation

models. Additionally, Jupiter serves as a prototype for Saturn, Uranus, Neptune, and for extrasolar gas-giants, approximately 80 of which have been identified to date.

Second, the meteorology that shapes the planet's outer appearance is simpler than on Earth, with a predictability horizon measured in years rather than weeks. However, the circulation patterns below the cloud tops are largely unexplored.

Third, Jupiter's magnetosphere is the largest in the solar system, with active aurora and strong interactions with its satellites and the solar wind. A high-order spherical harmonic mapping of the magnetosphere at close range is a sensitive way to probe the planet's interior structure.

Finally, because Jupiter is the closest gas giant to Earth, it is the easiest to observe using ground-based and Earth-orbiting telescopes, and because every probe sent to the outer solar system uses Jupiter for a gravity assist, it has had the largest number of close encounters with spacecraft. Thus, the scientific return from an in situ observing platform on Jupiter is significantly leveraged.

3. FLIGHT ENVIRONMENT

The ramjet flyer, designed to fly though the Jovian atmosphere, will encounter an atmosphere quite different from that on Earth. The Jovian atmosphere is composed primarily (99.7%) of hydrogen and helium. This gaseous outer layer extends approximately a quarter of the Jovian radius into the planet [Beebe, 1997]. Thus, the gaseous layer, in which convection currents dominate, is approximately 18,000 kilometers thick. (For comparison, the thickness of Earth's atmosphere is less than 100 km.) The upper atmosphere of Jupiter is covered by several cloud layers, as illustrated in Figure 3.1 [Morrison, 1996]. (Note: As there is no natural reference altitude on Jupiter, it is customary to take the reference altitude equal to the altitude where the atmospheric pressure is 1 bar.)

3.1 Thermodynamic Properties of Jovian Atmosphere

For the purposes of our performance calculations the atmospheric temperatures and pressures in the Jovian atmosphere were taken from Reference [Gierasch, 1996]. They are reproduced here as Figure 3.1.1. These data are a combination of Galileo and Voyager 1 probe measurements. Variations with altitude of the Jovian atmosphere were taken from actual Galileo probe measurements in the altitude range of -146 to +21 km Above 21 km, the atmospheric temperature is taken from Voyager 1 radio occulation data.

For the purposes of calculating the performance of the ramjet flyer, we have taken the Jovian atmosphere to be a binary mixture of 86.1 % hydrogen and 13.9 % helium. This hydrogen mole fraction was measured by the Galileo entry probe. We have accounted for the trace gases (CH_4, NH_4 and H_2O, which comprise a total of only 0.3 %) by increasing the helium mole fraction from 13.6 % to 13.9 %. The effect of this simplification on the ramjet performance is negligible. Based on this composition, with mean molecular weight of 2.278, we have calculated for mean values:

$$R = 3650 \text{ J/kg-K}$$

$$Cp = 12{,}100 \text{ J/kg-K}$$

$$\gamma = 1.42$$

3.2 Turbulence Characteristics

Virtually nothing is known about aircraft-scale turbulence on Jupiter. The scales of interest for safety concerns are well below the resolution of remote sensing. The Galileo Probe Doppler tracking time series shows some periodicities that have not yet been modeled, but these are most likely from the spin and pendulum motion of the probe under its parachute. The Probe's accelerometer data show some 1 m/s fluctuations, but because the sampling rate was low the vertical scale is about 200 mbar, which corresponds to distances much larger than the ramjet.

A conservative estimate of the largest turbulence amplitude on Jupiter is that it might be twice as strong as on Earth. We base this guess on a single fact, that the cumulus towers on Jupiter rise through 30 km instead of 8 - 10 km on Earth, in a roughly similar period of time, implying stronger vertical perturbations. These regions of active moist convection on Jupiter cover only a small fraction of the surface and their locations are well known, so avoiding them is not a problem. Jupiter's atmospheric heat flux is only 14 W/m^2, which is an order of magnitude less than Earth's, so it is conceivable that there are vast stretches on Jupiter where the turbulence is negligible, at least in the upper troposphere. But, the nature of deep disturbances that may initiate vertically propagating gravity (buoyancy) waves is unknown.

3.3 Radiation Environment

The Jovian radiation environment, which is very intense outside the atmosphere, drops to very moderate levels at the altitudes at which the flyer will be operating. The expert opinion is that the background radiation levels at the flyer operating altitudes in no worse than would be encountered by aircraft flying in Earth's atmosphere [Henry B. Garrett, JPL, private communication]. Since the radiation emitted by the unshielded MITEE nuclear reactor is quite intense, the background radiation in the Jovian atmosphere is negligible in comparison.

3.4 Lightning on Jupiter

The upper atmosphere of Jupiter contains very intense lightning storms. The energy in Jovian lightning strikes is about two orders of magnitude greater than on Earth. Such a strike could easily be catastrophic for the flyer. Fortunately, the lightning activity on Jupiter is confined to the lower regions of the water clouds, i.e., where the ambient pressure ranges from about 5 and 8 bar. Since the operating altitude of the ramjet flyer does not extend down to these altitudes, the flyer will not encounter the lightning. The dropsondes will, of course, descend through these lower altitudes, however, the time of exposure is very short and the probability of a lightning strike will be negligible.

4. DESIGN OF NUCLEAR RAMJET ENGINE - NEUTRONICS

The nuclear reactor is the first of the technical design issues to be addressed in this report. The compact light-weight reactor is the most novel component of the ramjet flyer system, and is also the one requiring the most development effort. Since the reactor has a minimum size in order to provide a critical mass to sustain fission, the reactor thus determines the minimum diameter of the fuselage and is the primary design driver for the size and the overall weight of the flyer. A small and light flyer is of course desirable to reduce the payload weight and the overall mission cost. Before describing the nuclear reactor selected for the ramjet flyer, we shall present some relevant background material and describe the various options that were considered in the reactor design process.

4.1 Overall Features of the MITEE Ramjet Nuclear Engine

Nuclear propulsion has the potential to dramatically enhance the capability for robotic and human exploration of of space, through its ability to deliver much greater ΔV to space craft than possible with chemical propulsion, and to operate for very long periods of time using in-situ extraterrestrial resources.

Over the past 50 years, a very extensive technology base on nuclear propulsion has been developed by programs in the United States and the Former Soviet Union (FSU). Components for nuclear rockets and ramjets have been developed and successfully tested, including nuclear fuels, moderators, control systems, pumps, etc. Operations of integrated nuclear engine systems have also been successfully demonstrated.

This technology base provides a strong foundation for nuclear propulsion engines for space exploration. In particular, for robotic exploration missions where compact, very lightweight, high thrust engines are required, the recent DOD/SNTP program on the Particle Bed Reactor (PBR) nuclear rocket is very relevant. The PBR engine design had a thrust output of 200,000 newtons and a mass of 500 kilograms, for a thrust-to-weight ratio of 40, comparable to that of high performance chemical engines, but with a much greater specific impulse, i.e., 1000 seconds compared to 430 seconds for hydrogen/oxygen.

The components for the PBR engine were developed and successfully tested. Thermal/hydraulic performance of the PBR fuel elements was verified in non-nuclear tests where high pressure H_2 propellant was blown through heated elements. Low power PBR critical assemblies were built and operated to verify PBR neutronics performance. The next step with the PBR program was to be ground testing of the engine, followed by in-space flight tests. However, these tests were not carried out, due to closing down of the PBR program when the Cold War ended in the early 1990's.

More recently, a derivative of the PBR nuclear engine, termed the MITEE engine, has been proposed for robotic space exploration missions. The MITEE engine is a smaller and much lighter version of the PBR that operates at lower power levels, so as to more closely match the

requirements for lightweight robotic spacecraft. It uses components and design approaches derived from the PBR and other earlier nuclear propulsion programs.

The compact ultra-light nuclear reactor engine termed MITEE (MIniature ReacTor EnginE) is very attractive for solar system exploration [Powell, 1998]. MITEE heats hydrogen propellant to 3000 K, achieving a specific impulse of 1000 seconds and a thrust-to-weight of 10. Use of nuclear rockets would enable major improvement in ΔV. Because pure H_2 propellant has low molecular weight, the I_{SP} for nuclear rockets is twice that for the best (hydrogen/oxygen) chemical rockets, with a practical limit on mission ΔV of ~22 km/sec. Using nuclear engines, flyby, orbiter, and lander missions require much less time and smaller, cheaper launch vehicles. They also enable new, unique missions, including the ability to hop to multiple sites on a planet or moon by using extraterrestrial propellant manufactured from in-situ resources (e.g., H_2 from ice). Using extraterrestrial propellant, MITEE can also return samples from distant planets (e.g., Pluto) and moons (e.g., Europa), asteroids, and comets.

The MITEE rocket engine is shown in 4.1.1. MITEE uses cermet fuel sheets instead of the packed beds of fuel particles employed in the PBR. The cermet fuel sheets consists of very small UO_2 particles imbedded in a refractory metal matrix (e.g., tungsten). The cermet W/UO_2 fuel was developed and tested in the 1960's for the 710 nuclear engine program. It has excellent resistance to hydrogen at temperatures of up to at least 3000 K, exhibiting virtually no fuel loss for operating periods of hours and multiple thermal cycles. The cermet fuel has also demonstrated the capability to survive very rapid rates of temperature change of ~10,000 K per second. The MITEE fuel element consists of an annular roll of multiple cermet fuel sheets (e.g., ~20 sheets), rolled together to form the annular element. The inner diameter of the annulus is typically about 1 centimeter, with an outer diameter of approximately 3 centimeters.

While most of the development work on nuclear thermal propulsion engines focused on nuclear rockets, there was also a substantial effort devoted to the development of nuclear ramjets [Herken, 1990]. The U.S. Pluto Project, in particular, aimed at developing an air-breathing nuclear ramjet that would fly at Mach 3 to deliver nuclear weapons. While never flight tested, the reactor portion of the engine was successfully ground tested.

The Pluto ramjet design was much too heavy to be practical for robotic space exploration missions. However, the MITEE design for nuclear rocket propulsion can be adapted for ramjet applications, to provide a very compact, lightweight engine that is practical for robotic flight in the atmosphere of Jupiter and other gas giants.

In a ramjet operating in the Jovian atmosphere, the propellant (86% H_2 - 14% He) flows radially inwards through the ~1 centimeter thick, annular fuel region emerging into the central flow channel at approximately 1500 K. The multiple cermet fuel sheets are perforated with many small holes providing a large surface area per unit volume of fuel element for heat transfer from the fuel sheet to the coolant.

Another key feature of the MITEE engine is its ability to achieve criticality in a very small and lightweight nuclear assembly. Three design features make this possible: 1) a very efficient and

low mass neutron moderator, namely, Lithium-7 hydride; 2) minimization of flux disadvantage effects in the heterogeneous core assembly; and 3) use of separated tungsten-184 isotope for the cermet fuel matrix, rather than natural tungsten. Lithium-7 hydride has a hydrogen atom density close to that of water, a lower mass density (0.7 g/cm^3, compared to 1.0 for water). Furthermore, ^{7}LiH has a much higher operating temperature capability (melting point of 950 K) than water. Other metal hydrides, such as ZrH_2, could be used in place of ^{7}LiH, but their weight would be much greater. There is a large stockpile (many hundreds of kilograms) of separated ^{7}Li in the US, produced as a byproduct of the US weapons program.

Flux disadvantage effects in MITEE are minimized by using a sufficient number of fuel elements so that neutronic behavior of the heterogeneous reactor approaches that of a homogeneous assembly, in which the fissile fuel would be incorporated in with the moderator. The 37 fuel element MITEE design achieves this goal.

Finally, natural tungsten has a high thermal neutron absorption cross section, 18 barns, compared to the order of magnitude smaller cross section for tungsten-184, namely 1.8 barns. The use of separated tungsten-184 results in a smaller lighter reactor that requires less fissile fuel. Tungsten-184 can be produced, and has been proposed for various nuclear applications.

However, some changes are necessary from the configuration described above for a ramjet version of the MITEE engine. The reactor geometry developed for nuclear **rocket** applications does not produce good performance as a **ramjet**. The basic problem is the size of flow passages in the system. In the rocket engine, the gas flowing through the core is pumped up to a uniformly high pressure (~70 atm) using a turbopump. The high-pressure (and high density) gas can readily flow through narrow flow passages in the core. The ramjet, on the other hand, operates at a much lower pressure, which also varies depending on the flight conditions (altitude and Mach number). To produce adequate thrust, the flow passages in the ramjet reactor have to be much larger, leading to a larger and heavier engine. A related problem is that, with the conventional MITEE design approach, it is difficult to increase the size of the hot flow channel (the central tube), which should be substantially larger than the cold flow channel. These problems have been overcome by modifying the core design approach to have the coolant enter at the center of the fuel element and flow radially outward through the annular fuel zone. Figure 4.1.2 compares the fuel element cross sections for the conventional and the new design approaches. We designate this new design MITEE-I for "inverted" or "inside-out." With this design approach the hot flow area is five times greater than the cold. Calculations with the MCNP neutronic code (Section 4.4) indicate that this approach enables criticality with a lighter-weight reactor than with the conventional MITEE approach.

The overall conclusion from the trade and design studies is that nuclear ramjets can operate in the atmospheres of Jupiter and other gas giants, using the reactor technology of nuclear fuels, moderators, thermal-hydraulics, etc. that has been developed and tested by previous nuclear propulsion programs. Developing such a nuclear ramjet does not require development of new materials and fuels, nor does it demand untested operating conditions. It is rather a matter of integrating already existing technologies into a system designed for atmospheric flyer missions.

4.2 Summary of Technology Base for Nuclear Ramjet Propulsion

Nuclear Thermal Propulsion (NTP) engines have undergone extensive development in the United States and in the Former Soviet Union (FSU). In the US, the NERVA system [Durham 1972, Koenig 1986] was developed and successfully ground tested. The NERVA reactor consisted of many hexagonal-shaped fuel elements each of which contained fissile material and axial flow coolant channels (Figure 4.2.1). Typically, the cores were about 1 m to 2 m in length, with length/diameter ratios of approximately unity. The reactors were graphite moderated, which was necessary since a large portion of the core operated at high temperature. Because graphite is a relatively poor moderator, the minimum diameter required for criticality was approximately 1 m. As a result, the reactor's power (and thrust) had to be high - otherwise the thrust/weight ratio would be impractically low (less than 1). The nominal power level for NERVA engines was 1000 MW, though reactors were tested with power levels of up to 5000 MW. Later designs included some hydrogenous material in an effort to reduce the critical size. This approach was not tested in a NERVA engine.

The FSU nuclear rocket was based on a somewhat different design approach [Goldin 1991]. The reactor fuel elements utilized bundles of many twisted cross-shaped rods (Figure 4.2.2). The bundles had an axial length of approximately 10 cm and were stacked lengthwise inside a ceramic tube with ceramic separators between bundles to form the final fuel element which had a total length in the range of 1 to 1.5 meters, depending on the reactor design power. The fuel elements were arranged in a hexagonal lattice, with each element surrounded by a moderator of ZrH_2 that operated at the reactor's inlet temperature fuel. Elements incorporating bundles of twisted fuel rods were successfully tested in the FSU, using flowing hydrogen coolant at temperatures above 3000 K for periods of approximately 1 hr. Full engine tests comparable to those carried out for NERVA were not performed.

Both of these nuclear rocket systems were inherently very heavy, which made them of limited utility for space application. Work on the US NERVA engine stopped in 1972, for lack of a defined mission. Work on the FSU engine continued until the early 90's, but it also lacked a clear mission. These engines typically weighed several tons, a consequence of their poor neutron moderating properties. To achieve criticality, the reactors had to be physically large and very heavy. A further limitation was their low thrust/weight ratio, which was at best only 5/1, compared to 50/1 for conventional chemical rocket engines. High thrust/weight ratios minimize burn times, enabling more efficient thrusting. Their low thrust/weight ratio was a consequence of low power density in the reactor. If the power density is low, the amount of power - and thrust - available from a unit volume of the reactor is low, resulting in a low thrust/weight ratio. Fuel element power densities in the NERVA and FSU reactors were in the range of 3 to 5 MW/L, with the average reactor power density substantially less.

This low power density resulted from two design features. First, the heat transfer area per unit volume of fuel element was very small (approximately 5 to 10 cm^2/cm^3), due to the relatively large dimensions of the coolant passages. This low heat transfer area limited the total heat flux per unit volume, resulting in low power densities. Second, the hydrogen coolant flowed axially along the NERVA and FSU fuel elements. Because of the long flow path, typically 1 m to 2 m, coolant flow

velocities had to be relatively low to achieve an acceptable pressure drop. This also limited fuel element power density. Finally, the NERVA and FSU engines had a long startup time (approximately 30 to 60 seconds), because of thermal stress limitations in the fuel elements. Chemical rocket engines typically start in a few seconds. Slow starts penalize performance, because propellant is not used efficiently, and gravity losses become important.

Recognizing these problems, the US DOD (Department of Defense) undertook a new development program, termed SNTP (Space Nuclear Thermal Propulsion) in the mid 1980's, with the objective of developing a compact, lightweight nuclear engine that had a thrust/weight ratio comparable to chemical rockets, and which could reach full power in a few seconds from a cold condition. The SNTP engine was based on the Particle Bed Reactor (PBR), a concept previously studied by Brookhaven National Laboratory (BNL) [Powell 1998 and Ludewig 1993]. Organizations involved in the SNTP program included Brookhaven National Laboratory, Sandia National Laboratory, Grumman Corporation, Babcock and Wilcox, Allied Signal, Hercules, and General Dynamics. The SNTP program continued until 1993, when the end of the cold war terminated the mission need for a compact, lightweight nuclear engine.

Program accomplishments [Ludewig 1996 and Powell 1997] included the development of small nuclear fuel particles capable of operating at 3000 K in high pressure hydrogen for more than an hour, experimental demonstration of 30 MW/L power densities in a PBR fuel element under transient non-nuclear blowdown conditions, nuclear criticality tests of the PBR reactor, initial nuclear testing of prototype PBR fuel elements, development and manufacture of suitable hot and cold frits, and detailed engineering designs of the PBR nuclear engine. At the close of the program the next step was to be the nuclear testing of PBR fuel elements in a compact reactor assembly, followed by the ground testing of a prototype PBR nuclear engine.

To overcome the limitations of the NERVA and FSU engines, three new design approaches were adopted for the PBR. First, a hydrogenous moderator was used. This is necessary for small size and weight (compact fast spectrum reactors are also possible, in principle, but the safety problems associated with hydrogen coolant and fast startup effectively preclude this option). Lithium hydride (using isotopically separated ^{7}Li, a material which is in plentiful supply) was chosen for the moderator. Lithium hydride has a low density (0.8 gm/cm^3) and high temperature capability (approximately 1000 K). Most of the PBR core volume was occupied by the Lithium hydride moderator, which was kept at low temperature by the incoming liquid hydrogen propellant. Neutronic tests of PBR critical assemblies verified that the small size PBR would operate as a critical reactor, and that the power distributions predicted by Monte Carlo analyses [Ludewig 1996], as well as, the other predicted reactor parameters (i.e., temperature coefficient, void coefficient, etc.) were correct.

Second, the heat transfer area in the PBR fuel element is greater by a factor of 10 than that in the NERVA and FSU elements. This enabled much greater power densities. The PBR fuel element consists of an annular packed bed of small diameter fuel particles positioned between two porous tubes termed "frits" (Figure 4.2.3). The fuel particles were directly cooled by hydrogen. The small diameter of the particles (typically 400 microns), resulted in a very high heat transfer area per unit volume of fuel element particle bed (approximately 100 cm^2/cm^3), enabling very high power

densities. Transient blowdown experiments on hot PBR fuel elements (non-nuclear heated) demonstrated approximately 30 MW/L capability. Refractory carbide coated nuclear fuel particles were tested at temperatures up to 3000 K in hydrogen, and demonstrated the capability to withstand corrosion attack for periods well in excess of one hour.

Third, a radial flow path through the annular bed of packed fuel particles was adopted, instead of the axial flow geometry used in the NERVA and FSU fuel elements (Figure 4.2.4). The much shorter path length (approximately 1 cm, compared to 100 cm for the NERVA and FSU fuel elements). enabled much greater coolant flow velocities, and correspondingly increased power densities. Local coolant flow rate was controlled by appropriate local adjustments in the effective porosity of the outer porous tube (cold frit), which accounted for the major portion of the total pressure drop through the fuel element. [The fuel bed and inner porous tube (hot frit) accounted for only a small portion of the total pressure drop.]

The locally varying porosity of the cold frit fully compensated for all of the axial and azimuthal variations in reactor power, enabling the hydrogen leaving the hot frit to be at the same temperature everywhere in the reactor. This maximized engine performance, since the mixed mean coolant outlet temperature then equaled the limit set by material properties. Thermal hydraulic experiments on prototype fuel elements demonstrated the ability to locally control coolant flow. In addition, they demonstrated the ability to operate with temperature gradients of approximately 3000 K/cm in the packed particle bed, and to withstand very rapid particle temperature changes during startup (approximately 10,000 K/sec). The capability to manufacture cold frits with the required porosity variation was also demonstrated, along with the capability to manufacture hot frits that could withstand 3000 K hydrogen.

After exiting the hot frit, the 3000 K hydrogen propellant flowed out through the cylindrical channel inside the hot frit. The diameter of the channel increased along its length in order to maintain a constant flow Mach number (design value of approximately 0.25). The PBR reactor assembly consisted of a hexagonal array of 19 or 37 fuel elements, depending on the power level and neutronic design. The hot coolant exiting from the elements then flowed into a common outlet plenum, which connected with the exhaust nozzle. The fuel element assembly and reflector elements were enclosed in a pressure vessel, which was integrally connected to the exhaust nozzle.

At the close of the SNTP program, all of the various neutronic, materials, and thermal hydraulic issues identified at program start were essentially resolved. The next step planned was to extensively test the PBR nuclear fuel elements under prototype conditions. If the SNTP (Figure 4.2.5) program had been completed, the PBR nuclear engine was anticipated to have the following capabilities: 1) ~ 800 kg total engine weight (including turbo-pump and controls), 2) ~ 1000 s specific impulse, 3) ~ 20,000 kg force of thrust (power = 1000 MW), 4) ~ thrust/weight ratio = 40/1, 5) 2 seconds startup time (cold to full power).

Although the PBR nuclear engine offers a major advance over the NERVA/FSU engines in terms of much lower weight, higher thrust/weight ratio, and fast startup, it still appears too heavy for

the new generation of lightweight, high performance spacecraft now envisioned for solar system exploration.

The PBR approach has been modified to enable a lower engine weight (e.g., approximately 200 kg), along with a more conservative (lower) operating power density (10 MW/L). This new concept, termed the MITEE (MIniature ReacTor EnginE) nuclear engine, would enable much higher performance for new exploration missions.

Figure 4.1.1 illustrates the basic MITEE concept. In contrast to the PBR, which had a single large pressure vessel, the MITEE core is of a set of hexagonal pressure tubes, each containing an outer shell of moderator and an inner cylindrical fuel element. Hydrogen coolant flows radially inward through each cylindrical fuel element, where the cold (~100 K) inlet hydrogen is heated to approximately 3000 K. Unlike the PBR, where the fissile fuel was coated small individual fuel particles (~ 400 microns OD), in MITEE the fuel fibers or particles are imbedded in a metal matrix sheet. The cermet sheets form a multi-layered annular fuel element, with each sheet in the roll perforated with optimally sized cooling holes. As in the PBR, there is a central hot gas channel inside the hot frit, where the hot hydrogen flows to exit through a nozzle. In contrast to the PBR, the MITEE hot gas channels do not exit into a common hot gas plenum and a single exhaust nozzle. Instead, each pressure tube has its own individual nozzle. The combined thrust from the nozzle assembly provides the total thrust. This results in a simpler and lighter engine.

Like the PBR, the MITEE core has 37 elements, each being a pressure tube, arranged in a hexagonal pattern. The core is surrounded by one or two rows (depending on design) of reflector elements, which have the same pitch as the fuel elements, and contain the same moderating material as the core. The moderator in the MITEE engine is Lithium-7 hydride held inside the beryllium tubes. Hydrogen cools the moderator in the reflector before flowing into the core.

The fuel element has three zones: 1) An outer zone of a beryllium metal matrix composite, containing graphite fibers that are infiltrated with uranium carbide or oxide, 2) A middle zone of molybdenum metal matrix composite, containing uranium oxide (UO_2) particles, and 3) An inner zone of tungsten metal matrix (the tungsten will be enriched in ^{184}W to reduce parasitic neutron losses) composite containing uranium oxide (UO_2) particles.

The heat transfer area in the perforated metal matrix is controlled by the hole diameter and number of holes. Studies indicate that a perforation fraction of ~ 25% results in acceptable heat transfer performance. The gas flow holes through the sheets are located in a grid pattern of slightly depressed channels formed in the sheets. When the sheets are layered together, the raised portions prevent closure of the holes in the sheets. Gas exiting through the holes in one sheet then flows to, and enters, the holes in the next sheet. This flow arrangement mixes the gas flow between sheets, and reduces the chance of thermal instabilities. The first sheet in the multi-layer stack has smaller holes in order to distribute and match the hydrogen flow to local variations in the radial, axial, and azimuthal nuclear power production. In effect, it functions like the cold frit in the PBR.

Most of the MITEE components - Be pressure tubes, ^{7}LiH moderator, cold frits and outer fuel sheets - are cooled by inflowing H_2 to well below their temperature limits. The only high temperature components are the inner W/UO_2 fuel sheets and TaC coated carbon-carbon nozzles. The 710 nuclear propulsion program [ANL 1966] operated W/UO_2 fuel for hundreds of hours in high temperature H_2 far longer than MITEE's ~1 hour burn period. The PBR program (6) demonstrated that TaC coated carbon-carbon and graphite hot frits and structures could operate for several hours in 3000 K H_2. Thus, suitable high temperature materials appear available for MITEE to maximize specific impulse, the H_2 radial flow rate into the elements is locally controlled so that the outlet H_2 exited from the hot frits everywhere at the same temperature, e.g., 3000 K. This control is achieved by axially and azimuthally varying the local flow resistance (i.e., porosity) of the outer fuel sheet so that the local flow rate matches local heating rate. Tests on fabricated aluminum sheets for the PBR demonstrated that the required local variations in porosity and flow rate could be achieved.

In addition to the US and FSU programs on nuclear rockets described above, there was substantial work by the US in the 1960's on nuclear ramjets. Project Pluto was aimed at developing an air-breathing ramjet that would fly at Mach 3 at treetop level, to deliver strategic nuclear weapons. The reactor for the ramjet, termed Tory, was successfully ground tested at a power level of 513 megawatts. Tory used beryllium oxide (BeO) moderator and UO_2 nuclear fuel, a choice dictated by the oxidizing nature of Earth's atmosphere. Since the payload was large and there was no need to launch into space (the ramjet operated close to ground level in the atmosphere), there was no urgent necessity to try to minimize reactor size and weight. While not directly relevant to the MITEE ramjet, results from the Pluto Program did indicate that ramjets could be powered by nuclear reactors, and that flight times and trip distances would not be limited by having to carry along propellant - that the ramjet could use available atmosphere for virtually unlimited flight.

4.3 Evaluation of Design Options for the MITEE Nuclear Ramjet

An evaluation study of design options for the nuclear reactor in the Jupiter flyer has been carried out. The goal of the study was to select the reactor technology options that best meet the various requirements for the ramjet. Emphasis was on existing and near term reactor technology, rather than long term development of radical new technologies. This greatly reduces the development time and cost required for Jupiter Flyer mission, and also minimizes technical risk.

The reactor requirements are summarized in Figure 4.3.1 The requirements are divided into three broads categories: 1) robust nuclear fuels; 2) acceptable reactor size, mass, and power level; and 3) ability to operate at low pressure with low pressure drops.

If the requirements shown in Figure 4.3.1 can be met using existing or near term technology, it is very desirable to base the reactor design on this technology rather than seek to develop new reactor technology. The cost and time needed to implement the Jupiter Flyer mission will be much less if it is based on existing technology.

Figure 4.3.2 summarizes the technologies for the above 3 areas that either already exist or can be developed in the near term with a modest amount of R&D. These reactor technologies have been developed by earlier programs on nuclear thermal propulsion in the US and USSR.

In the area of nuclear fuels, Figure 4.3.3 summarizes the reasons why the favored options , i.e., cermet fuel, were chosen. In general, there was no leeway in the choices – it is the only one that is practical.

The NERVA type fuel (Figure 4.2.1), which underwent major development in the US and USSR during the 1960's and 70's, simply is not compatible with long term operation in hot H_2. The graphite is rapidly transformed to gaseous methane. A ramjet reactor operating in Jupiter's atmosphere would only last a few hours at most. In the Particle Bed Reactor (PBR) program, ZrC and TaC coated UC particles were developed that could operate in 3000 K H_2 for several hours. Somewhat longer times could probably be achieved at the lower temperature (1500 K) of the Jupiter Flyer, but it is doubtful that lifetimes in excess of a few days would be possible.

The best and only choice for the nuclear fuel is the cermet fuel developed for the 710 nuclear engine in the 1960's. Figure 4.3.4 summarizes the principal features of the 710 nuclear engine fuel. In the cermet fuel, tiny UO_2 ceramic particles are imbedded in an enclosing metal matrix (tungsten for temperature above ~2000 K, molybdenum for lower temperatures). The matrix protects the particles against corrosion and attack by the hot coolant and minimizes the release of fission products. The metal matrix is ductile, strong, and can be shaped into the form desired for the reactor fuel elements. Figures 4.3.5 shows a photo of the 710 cermet microstructure. Figure 4.3.6 shows some of the data obtained on its ability to operate in hot H_2 propellant.

The 710 reactor program demonstrated capability to load up to 60 vol. % UO_2 in the refractory metal matrix. Both thin wafers and longer multi hole rod elements were tested in static and flowing high temperature hydrogen with a number of thermal cycles. Figure 4.3.6 shows fuel loss rates for thin wafers tested at 2500° C (2773 K) in hydrogen as a function of time at temperature and number of thermal cycles. Approximately 1% of the fuel was lost after 50 hours and 200 thermal cycles. According to the 710 program final report [Argonne National Laboratory 1966], "Additional tests of the W-UO_2 materials that were prepared by the conventional powder installing process were run at temperatures up to 2700° C (2973 K) with acceptable fuel loss rates for test periods up to 3-4 hours. In addition, other results described later indicate that UO_2 may be contained at temperatures as high as 2900-3000° C (3173 to 3273 K)."

Results on 7 hole fuel rods exposed to flowing and static 700 psia hydrogen at 2450° C (2723 K) are shown in Figure 4.3.7. Exposure times were up to 7.55 hours, and number of thermal cycles up to 30. Fuel loss rates were somewhat greater than those observed in the wafer tests, but still low.

Seven hole fuel rods were also exposed to rapid thermal transients in the pulsed TREAT reactor. Figure 4.3.8 summarizes the results of these tests. Temperature rise rates of more than 10,000 K/sec up to maximum temperatures of ~3000 K were experienced "without visible distortion or deterioration of the structure," with one specimen experiencing a total of 6 transient cycles.

Based on the 710 reactor experience, the 710 cermet fuel appears very attractive for the MITEE ramjet. It can be fabricated as thin sheets, with the perforation holes drilled by a laser. Cladding of the cermet composite with vapor deposited tungsten appears desirable to present contact of UO_2 with the hot hydrogen, which could affect the U/O ratio in the particles. In the 710 program 7 mils of tungsten coating was used; for the MITEE ramjet, a thinner coating - of ~3 to 4 mils would appear optimum.

At 2773 K (2500° C), the cermet fuel loses only 1% of its weight after 50 hours in hot H_2 and 200 thermal cycles. Since the goal of the 710 engine program was an operating temperature of $\geq$2750 K, data was not taken at lower temperatures. However, at 1500 K, it appears likely that the cermet fuel could last for many thousands of hours, since tungsten and molybdenum, the favored candidate materials for the metal matrix, do not react with H_2.

With regard to burnup capability, operating at 10 MW would burn up ~4 kg of ^{235}U per year or about 20% of the fissile inventory in the ramjet's reactor. Long-term burnup tests were not carried out in the 710 engine program, since the application involved an hour at most.

However, there is a vast body of experience (1000's of MW years) on high burn-up behavior of cermet fuels in water-cooled reactors. Cermet fuel elements have operated satisfactory with even higher burnups, and for periods of much longer than 1 year. Based on this experience, it appears very likely that the burnup goals for the Jupiter Flyer can be achieved. Use of a burnable poison, e.g., europium or gadolinium, in the fuel probably would be necessary to minimize the swing in reactivity as the ^{235}U is consumed. Use of such burnable poisons is standard in high burnup cermet fuels.

Turning now to the second category of options for the MITEE ramjet, that of small reactor size and mass (Figure 4.3.1), MITEE's size and mass performance will be determined by the choice of the fuels used, plus the choice of its moderator.

Nuclear reactors have a minimum size determined by neutronic criticality. In turn, the minimum critical size, together with the mass density of the components making up the reactor, determine its minimum weight. MITEE reactors must use a hydrogenous moderator to minimize critical size and mass. Reactors on Earth usually employ water as the moderator (though solid hydride moderators are also used). For the ramjet, however, water moderator does not appear to be a practical option.

Of the solid hydrogenous moderator options, the most promising are lithium-7 hydride (^7LiH), beryllium hydride (BeH_2), and zirconium hydride (ZrH_2). ^7LiH has been widely proposed in space reactor designs because of its low density (0.8 gm/cm^3) and high melting point. BeH_2 has also been proposed because it has a higher hydrogen density than ^7LiH, which could reduce reactor size and mass. However, it is difficult to fabricate, and has a low temperature for decomposition (~400 K). ZrH_2 has been used in a number of reactors on Earth. It has a high decomposition temperature (>1000 K) and a higher hydrogen density than ^7LiH.

^{7}LiH moderator must use the separated mass 7 isotope from natural lithium, because the mass 6 isotope has a thermal neutron cross section. However, tons of ^{7}LiH are presently stockpiled at DOE production sites.

There are three broad design approaches to minimizing the size and mass of the MITEE ramjet reactor:

1. Maximize reactor homogeneity.
2. Use a moderator with maximum hydrogen atom density.
3. Use of a high performance nuclear fuel.

The first approach, while available in principle, is not possible in practice. The size and weight of a MITEE reactor could be substantially reduced by eliminating voids in the moderator and mixing the nuclear fuel in it to form a homogenous MITEE reactor, rather than the present heterogeneous reactor, in which the high temperature nuclear fuel is separated from the moderator and there are flow channels for the high temperature hydrogen propellant. However, the maximum allowable temperature of the hydride moderator is only about 1000 K or less, depending on the choice of moderator, so that it must be physically separated from the high temperature nuclear fuel and hydrogen propellant. This separation necessitates separate regions for the fuel, moderator, and hydrogen propellant. Accordingly, significant reductions in the size and weight of the MITEE ramjet do not appear practical using the first approach.

The second approach offers possibilities. If an alternate moderator has a higher atom density of hydrogen than Lithium-7 hydride, and/or if it has another atom that is a better moderator than Lithium-7, MITEE's size and weight can be reduced, relative to that with ^{7}LiH moderator.

Options for such an alternate moderator are limited. The most promising alternate to ^{7}LiH appears to be BeH_2, which has both a greater atomic density of hydrogen, and beryllium, which is a better moderator than Lithium-7. ZrH_2 has a greater atomic density of hydrogen than ^{7}LiH, but its high density probably it out as an acceptable choice.

The third approach appears potentially promising. Since the predominant neutron loss mechanism is by leakage from the small reactor core, use of nuclear fuels that release a greater number of neutrons per neutron absorbed in the fissile atom than is the case for U-235, enables a smaller reactor size.

U-233 is a superior nuclear fuel to U-235 because of its greater η value (average number of neutrons released per absorption in the U-233 nucleus). The value of η for U-233 is 2.32 compared to 2.08 for U-235 while the neutron absorption cross sections are essentially equal.
Americium-242m (m refers to the metastable nuclear state of the Am-242 isotope) is superior to both U-233 and U-235 as a nuclear fuel, having both a considerably greater value of η, and a much greater neutron absorption cross section.

Four sets of detailed neutronic analyses of downsized MITEE NTP reactors have been carried out, using the 3-D explicit geometric representation MCNP neutronic code [Breimeister 1997].

As with earlier work, the results from these analyses accurately predict neutronic behaviors of actual reactors, including the multiplication factor (k_{eff}), 3-D power distribution, temperature coefficient, etc. The results, while directed at NTP applications, also apply to the MITEE ramjet. The four sets of MITEE analyses examine:

1. U-235 fuel with ^{7}LiH moderator
2. U-235 fuel with BeH_2 moderator
3. U-233 fuel with BeH_2 moderator
4. Am-242m fuel with BeH_2 moderator

For each analysis set, the effect of the following parameters on the multiplication factor, k_{eff}, was investigated:

1. Number of pressure tubes in the core
2. Number of fuel elements in the core (equal to or less than the number of pressure tubes)
3. Pitch to diameter ratio of the fuel elements in the core

Results from the parametric investigation are given shown in Figure 4.3.8. As the fuel element pitch to diameter decreases, k_{eff} and reactor mass both decrease, because the moderator volume decreases, causing neutron leakage to increase.

A practical operating point is at $k_{eff} = 1.05$. This value is sufficiently above $k_{eff} = 1.0$, (the actual critical condition) to allow for various effects like temperature change, etc. that affect reactor critically, but close enough to $k_{eff} = 1.0$ that a small number of control rods can quickly and accurately raise, lower, or maintain the desired thermal power released in the reactor.

The value of k_{eff} increases slightly if the number of fuel elements is smaller than the pressure tubes, due to a more optimum value for the moderator to fuel ratio. However, reducing the number of fuel elements also reduces the power output of the reactor, which may not be desirable.

Specification of the optimum number of fuel elements and pressure tubes for minimum engine mass will require a more detailed study. However, it is clear that U-233 fuel enables a considerably smaller reactor mass than U-235 fuel, while Am-242m fuel yields even smaller, lighter reactors.

As summarized in Figure 4.3.9, the minimum reactor mass for the U-235 fueled engine is 70 kilograms, 40 kilograms for the U-233 engine, 25 kilograms for the Am-252m engine. Total engine mass is taken to be twice that of the reactor mass. This actual engine mass should be significantly less, based on scaling factors derived from detailed analyses of PBR engines.

These engine designs represent the lowest possible weights for nuclear thermal propulsion, since they utilize the highest performance moderators and the best nuclear fuels. Further reductions in engine weight do not appear likely.

The choice of ^{7}LiH as the moderator for the MITEE ramjet appears clear, as summarized in Figures 4.3.9 and 4.3.10. ZrH_2 is too heavy to meet the mass requirement for the ramjet. BeH_2, while it would significantly reduce the mass of the ramjet, has a decomposition temperature that is too low for the nuclear ramjet application.

The choice of U-235 as the nuclear fuel for the ramjet is based more on availability issues rather than performance. From the standpoint of ramjet weight, U-235 results in the heaviest design. U-233 fuel reduces the reactor mass by approximately a factor 2, as compared to U-235 fuel. However, U-233 has a much shorter half life than U-233, i.e., 30,000 years compared to 500 million years. While U-235 does not pose a radiological hazard at launch, due to its very small inventory and long half life, U-233 fuel would rise issues of biological hazard due to its much shorter half life. Natural uranium is present in granites and some soils to ~1 ppm. Dilution by a relatively small volume of soil or seawater would reduce the alpha activity from U-235 to that from natural uranium already present. With U-233 fuel, however, the dilution volume would have to be over 10,000 times greater.

Americium presents even more of a radiological safety issue, because of its half life is much shorter than that of U-233 fuel. Accordingly, it seems desirable to minimize radiological launch safety issues by choosing U-235 fuel, even though it would result in a heavier ramjet.

Finally, turning to the third category of options for the MITEE ramjet, ability to operate at low pressure with low pressure drops (Figure 4.3.1), the challenge is to achieve high power capability and high power densities in the MITEE fuel elements, while operating at much lower propellant pressures than called for in the nuclear rockets, e.g., 1 atm instead of 50 to 100 atm.

Thermal hydraulic tests of PBR elements have demonstrated the ability to operate at very high power densities in the fuel region, up to 30 megawatts per liter. Pressure drops across the particle fuel bed are very low, a fraction of an atmosphere, even at these very high power densities.

The PBR flow geometry has been adopted for use in the MITEE nuclear rocket (Figure 4.1.1) which is similar in construction to the Jupiter nuclear ramjet. It uses perforated sheets of cermet W/UO_2 fuel in place of the packed bed of particles. The perforated sheets have a large surface area for heat transfer (Figure 4.3.12), on the order of approximately 130 square centimeters per cubic centimeter of fuel region. This is comparable to the surface area of the PBR fuel element, so that power densities well in excess of 10 MW/liter are achievable.

Accordingly, the radial coolant flow option is the only practical choice for the Jupiter ramjet, which probably will operate with power densities of a few megawatts per liter in the fuel region.

Figure 4.3.13 compares the main operating features of the MITEE ramjet with those of the MITEE rocket. The principal difference, and a challenging one, is that the MITEE ramjet must operate at a much lower coolant pressure than the MITEE rocket. The rocket version typically will operate at a pressure of ~70 to 100 atmospheres, while the ramjet must operate at a pressure of at most a few atmospheres (the operating pressure in the reactor will be a factor of 3 to 10

greater than the outside ambient atmospheric pressure, depending on the Mach number of the Jupiter flyer).

This very low operating pressure requirement is very important in determining the design approach. There are 2 basic ways to channel radial coolant flow in MITEE type fuel elements:

1. Radial inwards flow
2. Radial outwards flow

Figure 4.3.14 shows the 2 approaches. In Option 1, the spaces between the fuel elements is used as an inlet plenum for the cool H_2 propellant. The H_2 first flows radially inwards through the shell of ^{7}LiH moderator (which is supported and seated inside the element by a honeycomb structure of Be metal, and then through the fuel region where it is heated to high temperature). The hot H_2 then radially flows into the inner circular duct, along which it flows axially to the outlet nozzle.

In Option 2, the cool H_2 flows from the inner circular duct radially outwards, first through the inner ^{7}LiH/Be moderator shell and then through the outer perforated fuel sheet region. The hot H_2 then flows axially through the spaces between the fuel elements to the outlet nozzle.

Option 2 appears much more attractive than Option 1, because the outlet flow area between the elements is several times larger than the outlet flow area for Option 1, when the hot H_2 exits through the small ducts inside the fuel elements.

Option 3 (Figure 4.3.14) is a variation of Option 2, in which the outlet hot H_2 from the outer fuel regions in the fuel elements flow cross-wise through the duct that is outside of the reactor core. This outlet duct can have a larger flow area than the total area between the elements (Option 2), and still not have too great an effect on reactor criticality. Option 3, in turn has 2 versions: in Option 3A the outlet duct is an annular channel between the outside of the reactor's core and the inside of its neutron reflector; while in Option 3B, the outlet duct is outside of the reflector. (However, even though the outlet duct in Option 3B is outside the reflector, it does affect reactor criticality, because the reflector must be segmented to allow flow passages through it. These passages act to increase neutron leakage and reduce K_{eff}, the criticality constant.)

Figure 4.3.15 shows a cross section of the MITEE reactor core and reflector for Option 1, while Figure 4.3.16 shows a more detailed cross section of the Option 1 fuel element.

Figure 4.3.17 shows a cross section of the MITEE reactor core and reflector for Option 2, while Figure 4.3.18 shows a more detailed cross section view of Option 2.

Figure 4.3.19 illustrates the large difference in reactor power capability between Option 1 and Option 2 for the particular case of a Jupiter ramjet having a 37 element core and 1500 K H_2 outlet temperature. The central duct in each fuel element has a radius of 0.960 centimeters. The ratio of the flow area between the fuel elements to the flow area of the 37 central ducts is denoted by the term β. Here $\beta = 4.0$; that is, the flow area between the elements is 4 times larger than the flow area in the central ducts.

The hot H_2 flowing out through the duct s has a maximum Mach number of 0.25 at the outlet end of the core. (The Mach number in the outlet ducts increases linearly from zero at the inlet end of the core to its maximum value at the outlet end. At the core mid-plane, the Mach number would be 0.25/2, or 0.125).

At an operating pressure of one atmosphere in the reactor (the pressure level after ram compression), Option 2 allows a reactor power of 8.9 megawatts, while Option 1 only allows 1/4 of this value, or 2.2 megawatts. Using Option 3A and an outlet gas of 5.5 centimeters in width, the output reactor power increases to 21 megawatts. At an operating pressure of 3 atmospheres, the above power levels are increased by a corresponding factor of 3; at an operating pressure of 10 atmospheres, the power levels are 10 times larger than those for a pressure of 1 atmosphere.

A second issue is the pressure drop through the perforated fuel sheets. This should be a small fraction, e.g., less than 10% of the operating pressure, in order to have efficient aerodynamic performance. In general, as illustrated in Figure 4.3.20, this appears to be much less limiting on reactor power level than the Mach number constraint shown in Figure 4.3.19.

The pressure drop through a perforated fuel sheet is given by the Bernoulli relationship; that is, the pressure drop through the sheet is

$$\Delta P_i = (1/2)\, \rho_{H2}(T)\, V_{H2}^2(T)$$

where

$$\rho_{H2}(T) = P/RT$$

$$\rho_{H2}(T)\, V_{H2}^2(T)\, (C_p)_{H2}(T - T_{in})\, A_{flow} = P_0$$

$$Aflow = 37\, (2\pi r_3)\, L_R\, (f_H)$$

where

ΔPc	=	pressure drop, N/m^2
ρ_{H2}	=	density of H_2 at Pi and T, kg/m^2
V_{H2}	=	flow velocity of H_2 through the perforated holes at P_j and T, m/sec
$(Cp)_{H2}$	=	heat capacity of H_2, J/kg K
Tin	=	inlet temperature of cool H_2, K
T	=	temperature of heated H_2, °K
$\mathbf{A_{flow}}$	=	total flow area of holes in perforated sheet, m^2
Po	=	reactor power, watts
r_3	=	outer radius of fuel element, m
L_R	=	length of fuel element, m
f_H	=	fraction of sheet occupied by perforated holes

Taking the temperature T as 1500 K (the maximum temperature of the coolant, and the temperature of the last fuel sheet), with representative values of r_3 = 3.6 x 10^{-2} m, f_H = 0.25, L_R = 0.55 m, Tin = 300 K, and $(C_P)_{H2}$ = 7/2 R, the curves in Figure 4.3.20 are derived. The H_2 velocity through the holes increases linearly with power level and decreases as (gas operating pressure)$^{-1}$. The Option 2 cooling geometry is assumed.

The H_2 velocity through the holes is relatively low even at 1 atm, being 25 meters per second at 10 megawatts. The corresponding Bernoulli pressure drop through the last fuel sheet is only 6.7 x 10^{-5} atmosphere. At a power level of 30 megawatts, the pressure drop is still only 2 x 10^{-4} atmospheres. The 30 megawatt power level is over 3 times greater than the limit set by the Mach number. Accordingly, it appears that Mach number considerations will set the output power capability, rather than pressure drop. The Bernoulli pressure drop will increase with the number of fuel sheets. The pressure drop through the jth sheet will be

$$Pj = \{T_j/T_{out}) \Delta P_{out}$$

ΔPj is less than the pressure drop through the last fuel sheet, because the H_2 velocity for Tj < T_{out} is less than V_{H2} (out).

For a fuel region consisting of N sheets, in which temperature increases from Tin to Tout, the total Bernoulli drop is given by summation of individual pressure drops over N layers of fuel:

$$\Delta P_{tot} = \sum \Delta P_j = N (T_{av}/T_{out}) \Delta P_{tut} = (N/2) \Delta P_{out}$$

For a representative fuel element assembly of 8 fuel sheets, the corresponding total pressure drop is then about 4 times greater than the pressure drop through the last fuel sheet where T ~ 1500 K. This increases the total pressure drop through the fuel region in the fuel element from 6 x 10^{-4} atm to 2.4 x 10^{-3} atm at a power of 30 MW and pressure of 1 atm - still a negligible amount. Again, the 30 MW output is 3 times larger than the limit established by Mach number constraints.

Figure 4.3.21 shows the evaluations matrix for the 3 cooling geometry options. Clearly, Option 2 is much more attractive than Option 1. Option 3A also appears to be even more attractive, but neutronic analyses are required to determine the effect of the gap between the core and the reflector on reactor criticality.

Figure 4.3.22 summarizes the selections made for the ramjet reactor components in the Phase 2 study. The column headed Reason for Initial Selection gives the selections made for the design studies described in the first part of the Phase II study. The column headed Final Selection for Phase II Study gives the selections for the second part of the Phase 2 study. In general, the final selections were the same as the initial selections. When alternate options were analyzed, it was found that they usually did not result in higher performance - e.g., smaller size, lower weight, ability to operate at lower pressure for a given power level - than that provided by the initial selections. Even when an alternate option could result in higher performance, for example, ^{233}U is a superior fissile fuel to ^{235}U, and could result in a smaller, lighter reactor, it was concluded that

the issues raised by the alternate option - e.g., the launch of radioactive U-233 fuel rather than inert U-235 fuel - did not warrant using the alternate option. Given the selection of the reactor components, then a series of trade studies was carried out to determine an optimized baseline engine design that offers the greatest overall performance. Since the performance goals to a considerable extent are conflicting - e.g., a large, heavier reactor could operate at higher altitude - the final design inevitably is a compromise.

4.4 Neutronic Analysis of the MITEE Ramjet Reactor

4.4.1 Analytical Methods

The analytical methods that have been developed to predict the detailed neutronic behavior of nuclear reactors are very good. The most accurate method is the Monte Carlo MCNP computer code (Figure 4.4.1.1). MCNP uses pointwise nuclear cross sections and a full 3 dimensional representation of the actual reactor geometry. By following the fate of millions of neutron histories run in the reactor assembly, very detailed data on reactor criticality, spatial power distribution, temperature coefficients, void coefficients, etc. can be obtained.

MCNP treats all neutrons, photons, and electrons from 20 MeV down to thermal energies. In particular applications described in this report the neutron transport only is used, since the determination of a multiplication factor is of primary importance. MCNP employs a combinatorial surface/cell specification of the problem geometry, which permits modeling of the reactor configuration with minimal approximations. In addition MCNP employs nuclear data from the ENDF/B files in essentially un-approximated point-wise form, which avoids the complications associated with collapsing the data to a group structure and an a priori knowledge of the space-energy dependent spectra in the system. Finally, MCNP uses the $\mathbf{S(\alpha,\beta)}$ formalism for scattering off the bound molecules of moderators. The major limitation of Monte Carlo methods is the statistical nature of the results, this is inherent to the method, and creates difficulties when localized information is desired. In principle, however, the accuracy of the predictions is limited only by the accuracy of the nuclear data, the detail to which the actual geometry is modeled (which as noted above does not have to conform to the regular mashes required by most deterministic methods), and the number of particle histories considered. This last point is not trivial, and typical design calculations might place considerable demands on computer resources in terms of running time and storage. The MCNP code and its associated nuclear data has been extensively validated against experimentally determined measurements of critical assemblies. A series of experiments carried out on a particle bed reactor under the SNTP program were analyzed using MCNP with excellent agreement between measured and calculated parameters. The particle bed reactor is similar in composition and geometric configuration to the ramjet reactors being proposed here.

The MCNP code was used to predict the neutronics of the PBR (Particle Bed Reactor) during the DOD/SNTP program. Figure 4.4.1.2 compares the predicted value of various neutronic performance parameters with the actual experimental values for the small critical reactors. The

PBR is a highly heterogeneous, high neutron leakage reactor, and it is very impressive that the calculational and experimental results agreed so closely. (The numbers in parentheses for the calculated values correspond to the standard deviation for the calculation.)

It should be noted that these are the calculated values obtained before the experimental runs, so that there was no "adjusting" of data to try to match the experiments. The agreement is excellent, typically within one standard deviation. This benchmarking provides confidence that the predicted neutronics for the Jupiter Flyer reactor are correct.

4.4.2 Design Parameters Studied for the Jupiter Ramjet Reactor

A wide range of design parameter has been previously studied for the MITEE nuclear thermal propulsion rocket, as illustrated in Figure 4.4.2.1. This large data base provides excellent guidance in determining what the effect of various design parameters on the Jupiter Flyer reactor will be. For example, Figure 4.4.2.2 illustrates how reactor criticality varies with fuel element pitch/diameter ratio. The criticality constant, K_{eff}, increases with increasing pitch to diameter ratio, because the moderator to fuel ratio is increasing, making the reactor better moderated.

The reactor is critical (K_{eff} = 1.0) at a pitch/diameter (P/D) ratio of 1.0. Keff continues to increase as P/D increases, reaching a maximum of 1.11 at P/D =- 2.5. K_{eff} then begins to decrease as P/D increases further, because of the increasing absorption of neutrons by the hydrogen moderator. The optimum value of K_{eff} is ~1.05, which allows for an adequate margin for control rods and temperature effects. This value of K_{eff} is reached at P/D = 2.0. Similar analyses have been carried out for the Jupiter Flyer ramjet.

The effect of different moderators and fissile fuels on the K_{eff} and mass of the MITEE reactor are illustrated in Figure 4.4.2.3. Materials with greater moderating power, such as BeH_2, while a potential option for the MITEE rocket, is not a practical choice for the Jupiter Flyer, because of the Flyers greater moderator temperature and long operating life. More efficient fissile fuels like ^{233}U and ^{242}Am substantially reduce the mass of the MITEE reactor. However, as discussed in section 4.3, these have been ruled out for the Jupiter ramjet.

Figure 4.4.2.4 shows the design parameters studied for the Jupiter Flyer reactor. Figure 4.4.2.5 shows the geometrical relationships and nomenclature used in the MCNP analyses of the Jupiter Flyer for the radial outlet coolant flow option, the configuration adopted for baseline design of the ramjet.

The results of the calculations carried out on a series of reactor cores, using the method described above, are discussed in the following section. The objective is to determine the sensitivity of the reactor mass to the ratios α (moderator volume/fuel volume) and β (outlet duct area/inlet duct area), the fuel volume (V_f) and the radius of the inlet duct (r_1). In determining this functional dependence it is necessary to consider the sensitivity of the multiplication factor (k_{eff}) to the above variables. This is necessary since the reactor must be critical, and thus only reactors which have a

value of k_{eff} ~ 1.05 will be considered. The ~ 5 % margin in multiplication factor is considered a minimum contingency at the current stage of maturity of the overall vehicle design.

4.4.3 Results of Parametric Analyses of Ramjet Reactor

In order to vary the fuel/moderator ratio, and the inlet/outlet duct area ratio in a consistent manner over a range of values, the following assumptions were made:

1) Fuel volume = Total power/Average power density,
2) Height of core = seven x fuel element pitch – only for thirty seven element cores, and
3) Inlet duct diameter determined by flow rate and pressure drop requirements.

Thus by expressing the fuel volume in terms of the element radii, and element pitch relationships can be derived for the inner fuel layer radius, outer fuel layer radius, and element pitch as a function of the inlet duct radius and the two ratios described above. These parameters are defined below:

V_f = Fuel volume (Total power/Average power density)
α = Moderator volume/Fuel volume
β = Outlet duct area/Inlet duct area
r_1 = Inlet duct radius
r_2 = Inner radius of fuel
r_3 = Outer radius of fuel

The above relationships can be solved numerically for given values of V_f, α, β, and r_1, resulting in a geometrically consistent reactor configuration. These reactor configurations can then be analyzed using the MCNP code, described above, to determine the value of the multiplication factor.

The results of the calculations carried out on a series of reactor cores, using the method described above, are discussed in this section. The objective of these results is to find the sensitivity of the reactor mass to the ratios α (moderator volume/fuel volume) and β (outlet duct area/inlet duct area), the fuel volume (V_f) and the radius of the inlet duct (r_1). Before this functional dependence can be determined it is necessary to determine the sensitivity of the multiplication factor (k_{eff}) to the above variables. This step is necessary since the reactor must be critical, and thus only reactors which have a value of k_{eff} ~ 1.05 will be considered. The ~ 5 % margin in multiplication factor is considered a minimum contingency at the current stage of maturity of the overall vehicle design. Table 4.4.3.1 shows values of k_{eff} as a function of the variables of interest, and these results will be used to determine the systems for which the mass will be estimated. In the following tables all the dimensions are in cm., all masses in kg, and all volumes in liters.

Table 4.4.3.1 Criticality constant as function of α, β, V_f, and. r_1

Case	V_f	α	β	r_1	k_{eff}
1	25	4.5	4.968	0.9605	1.1689
2	25	3.5	4.968	0.9605	1.1223
3	25	3.0	4.968	0.9605	1.0809
4	25	2.65	4.968	0.9605	1.05
5	25	2.5	4.968	0.9605	1.0363
6	15	3.0	4.968	0.9605	0.9375
7	15	4.0	4.968	0.9605	1.0141
8	15	5.0	4.968	0.9605	1.0714
9	5	9.0	4.968	0.9605	0.8836
10	10	6.0	4.968	0.9605	1.0015
11	10	7.0	4.968	0.9605	1.0366
12	10	8.0	4.968	0.9605	1.0694
13	10	6.0	4.0	0.9605	1.0266
14	10	7.0	4.0	0.9605	1.0638
15	10	8.0	4.0	0.9605	1.0889
16#	10	6.0	3.0	0.9605	1.0575
17	10	5.0	4.968	0.68	1.0351
18#	10	5.5	4.968	0.68	1.0575
19	10	6.0	4.968	0.68	1.0767
20	10	7.0	4.968	0.68	1.1048
21#	10	5.0	4.0	0.68	1.0511
22	10	6.0	4.0	0.68	1.0888
23	10	7.0	4.0	0.68	1.1237
24	5	9.0	3.0	0.68	1.0170
25	5	10.0	3.0	0.68	1.0332
26#	5	11.0	3.0	0.68	1.0509
27	5	12.0	3.0	0.68	1.0629

Three reactor concepts (one corresponding to each β value) for each of the two values of r_1, and with a criticality constant of at least ~ 1.05 were chosen from the above table for a total of six

cases. Four of these cases are indicated in the table above (16#, 18#, 21# and 26#). The two remaining cases were determined by interpolating between cases with values of k_{eff} above and below the desired value of 1.05. Cases with the minimum fuel loading required to achieve the desired value for k_{eff} were used, since those cases with higher values of fuel loading resulted in heavier reactors. The estimated masses (kg) for these six reactors with relevant fuel element and core dimensions are shown on Table 4.4.3.2 below.

Table 4.4.3.2 – Selection of possible reactor designs (k_{eff} ~ 1.05)

(r_1 = 0.68 cm)

V_f	α	β	r_2	r_3	H=D	Mass+
5	11.0	3.0	3.2276	3.3649	47.53	130.2
10	5.0	4.0	3.0657	3.3445	48.14	157.4
10	5.5	4.968	3.1551	3.4177	49.85	165.0
			(r_1 = 0.9605 cm)			
10	6.0	3.0	3.2917	3.5337	52.07	173.0
10	6.6*	4.0	3.3710	3.5980	54.38	183.0
10	7.4*	4.968	3.4820	3.6927	56.91	200.0

*Interpolated from values in the above table
+ Mass includes fuel, moderator, and reflector.

These results show that for a constant fuel volume (V_f) increasing β implies a slow increase in the value of α. In the cases of r_1 = 0.68 cm and β = 3.0 the fuel volume of 10 liters implied a geometrically incompatible core (fuel element pitch/diameter < 1.0). Thus, a critical configuration had to be found with a lower fuel volume. It is clear that this implies a lower overall system mass. This is attractive from the standpoint of system mass; however, a lower fuel volume implies a lower reactor power if power density is is held constant, or a higher power density if the reactor power is held constant. These choices may not be achievable. Moreover, it should be pointed out that achieving an acceptable multiplication factor might not be possible for all values of β, since neutron leakage increases with increasing β.

The above reactors are all critical, and thus possible candidates for deployment in a ramjet driven vehicle. However, when integrated into the vehicle two shortcomings are apparent:

1) The pressure drop across the core is unacceptably high, implying that the inlet and outlet ducts need to be increased in cross sectional area, and
2) The overall diameter, which includes the core diameter (seven times the element pitch) plus twice the reflector thickness is too large.

These two issues were addressed by arranging for tapered inlet and outlet duct shapes, removing the reflectors, and adjusting the fissile loading in the fuel layer to compensate for the decrease in multiplication factor. The inlet duct entrance radius was increased to 1.4 cm (nominal values are 0.9605 cm or 0.68 cm), and the closed end radius was reduced to 0.4 cm. This results in a larger duct diameter in the section with the highest mass flow and a small radius were essentially no flow is expected, thus reducing the overall inlet duct pressure drop. In addition, the reduction in moderator mass at the inlet end is partially compensated for by the increase in moderator mass at the closed end where the duct diameter is small. A configuration with a multiplication factor of ~ 1.05 with the above inlet duct shape was defined by the following parameters:

$\alpha = 10.0$
$\beta = 3.5$
Pitch = 8.5213 cm
H = 59.6488 cm
$k_{eff} = 1.0542$

The above core had a reflector thickness of 10 cm, thus implying a reactor with an overall diameter of 79.6488 cm. In order to reduce the overall reactor diameter, and simultaneously maintain the value of k_{eff} in the acceptable range, the UO_2 loading in the W/UO_2 cermet fuel was increased from 30 % to 50 % (Note: 60 % volumetric loading has been successfully demonstrated in tests in the US and FSU). Increasing the fissile loading allows a reduction in the reflector thickness from 10 cm to 0.2 cm, while the value of k_{eff} increases from 1.0542 to 1.107. The overall reactor diameter has thus been reduced to 60.05 cm.

Finally, in order to reduce the pressure drop in the outlet duct, the outer surface of the fuel layer is tapered, thus progressively increasing the outlet duct flow area in the axial direction. The increase in the duct area increases the neutron leakage, and reduces the amount of moderator in the core. Both effects reduce the value of ke. However, since the starting point for k_{eff} is 1.107, which is well above the acceptable limit, it is felt that an acceptable point can be reached. A series of calculations was carried out with increasing taper angle of the outer fuel surface. The following sizes correspond to an acceptable configuration:

Inlet end
Inlet duct diameter = 2.8 cm
Element pitch = 8.5213 cm
Fuel outer diameter = 8.1945 cm

Outlet end
Inlet duct diameter = 0.4 cm
Element pitch = 8.5213 cm
Fuel outer diameter = 7.8366 cm

Multiplication factor = 1.0667
Reactor diameter = height = 60.05 cm

It is seen that the outlet duct, which occupies the space between the outer fuel element surface and the pitch, increases from the inlet to the outlet ends. The increase in area is approximately 40 %, which implied a reduction in the value of k_{eff} from 1.107 to 1.0667. Total reactor mass (fuel, reflector, moderator, structure, and controls) is ~160 kg.

4.5 Baseline Design of the MITEE Nuclear Ramjet Engine

The trade and option studies described above led to a baseline design for the MITEE nuclear ramjet engine. The overall features of the design are summarized in Figure 4.5.1, and the baseline design parameters are summarized in Figure 4.5.2. The design reflects an optimized engine capable of delivering high output power, e.g., on the order of 100 MW(th) at a fuel region power density of 10 MW/liter (at 1/3 of the 30 MW/liter demonstrated in tests of PBR elements in the DOD/SNTP program), while operating with alow pressure propellant, e.g., on the order of 1 atmosphere, with a total reactor mass of only 160 kilograms. This represents a major achievement in the design of nuclear ramjet propulsion engines for space exploration missions in terms of thrust/weight ratio, and the ability to operate in planetary atmospheres at high Mach number and low ambient pressure.

The key features that enable this high performance are:

- A robust, rugged nuclear fuel (W/UO2 cermet) that can operate for a long time in hot hydrogen propellant
- A fuel form (perforated cermet sheets) that achieves very high surface area per unit volume for heat transfer (~100 cm2/cm3), enabling very high power densities
- A coolant flow configuration (radial flow through a thin annular fuel region) that enables low pressure drops, even when operating at low at low ambient inlet pressure to the ramjet, and high reactor power
- A low density, high neutronic efficiency hydrogenous moderator (^{7}LiH) that enables a lightweight, very compact reactor

It is doubtful that this optimized design could be significantly improved unless one or more of the following options was chosen:

1) Use a higher efficiency fuel, e.g., U-233 or Am-242m.
2) Use a moderator, e.g., BeH_2, with higher moderating power.
3) Use a closed high-pressure coolant closed cycle reactor with a heat exchanger to transfer heat to the low-pressure open cycle propellant.

Using U-233 or Am-242m would raise issues since these fuels have a much greater (orders of magnitude) level of radioactivity than U-235 fuel. The second option raises issues about the long-term stability of BeH_2 with regard to both thermal and radiant energy. Very little is known about BeH_2 stability, and its temperature capability is much lower than ^{7}LiH. Extensive development testing of BeH_2 would be needed to determine whether it could be used in space reactors.

The third option, a high-pressure closed cycle reactor with an intermediate heat exchanger to transfer heat to the low-pressure open cycle coolant, raises issues of additional weight of the heat exchanger, and the mechanical reliability of the coolant circulator.

Based on the strong existing technology base for the design options selected, the above baseline design appears to be the best choice foe a high performance nuclear ramjet for exploration of planetary atmospheres.

5. DESIGN OF NUCLEAR RAMJET ENGINE - THERMAL/HYDRAULICS

5.1 Engine Configuration and Thermodynamic Cycle

The Jovian Flyer is propelled by a ramjet engine that uses the MITEE-I nuclear reactor as the heat source (in place of the combustor of a conventional ramjet). The engine is shown schematically in Figure 5.1.1 for a configuration wherein there is direct heat transfer from the reactor to the engine gas flow, and the reactor is an integral part of the engine. A Temperature-Entropy diagram of the (open) cycle is given in Figure 5.1.2.

The Jovian atmospheric gases, primarily hydrogen and helium are ingested by the inlet at the flight supersonic velocity and decelerated relative to the engine (and vehicle) to a subsonic velocity (points 1-3). Since the speed of sound in the hydrogen/helium mixture (0.86/0.14 by volume or mole fraction) is much greater than that of air at similar temperatures, the velocities are significantly greater than those encountered in Earth atmosphere flight at corresponding Mach numbers; but the process mechanisms are unchanged. The flow velocity is further decreased and static pressure increased, nearly isentropically, in the diffuser (3-4,5), with M_5 on the order of 0.25 to 0.4. For the present, points 4 and 5 are considered thermodynamically the same; but there will be some adjustment of properties in the transition of flow as guided into the reactor flow passages.

The Mach number entering the reactor must be low enough to allow the necessary heat addition and unavoidable friction pressure drop without choking, since both of these effects raise the Mach number toward 1 and decrease the total pressure. The nuclear reactions in the reactor continuously supply the source for direct heat transfer to the engine gas flow by sensible convection heat transfer (5-9). The maximum cycle temperature, $T_9{}^0$, determines the thrust and is limited by the allowable material temperature of 1500 K. The reactor exit flow is expanded in a converging-diverging nozzle to a supersonic velocity that is sufficiently greater than the flight velocity to provide the required thrust (9-11). Friction losses in the nozzle reduce the exit velocity slightly compared to an ideal isentropic expansion (point 11_s).

5.2 Ramjet Engine Components

5.2 1 Inlet

The type of inlet employed depends on the selected flight Mach number. The initial studies addressed steady flight at M_1 = 1.5, at which condition a normal shock type inlet would be employed since the total pressure loss across the shock is acceptable ($p_3^0/p1^0$ = 0.93). An alternative is to fly at a higher speed to gain mission advantages, and for flight above approximately M_1=2 the pressure loss of a normal shock would be prohibitive (e.g. at M_1 = 3, $p_3^0/p1^0$ = 0.32), requiring use of a more sophisticated design. The leading choice is an axi-symmetric spike type of inlet, which is depicted in the Figure 5.1.1 schematic and in more detail in Figure 5.2.1.1. Since the majority of flight will be at a nearly constant Mach number and the vehicle will not need to be accelerated from a lower Mach number (being delivered by the high speed interplanetary entry), a fixed geometry inlet can be used. This approach avoids the weight and mechanical and control complexity of employing axial translation of the centerbody and multiple bleeds and by-passes such as utilized in the SR-71 Blackbird which flew very successfully at Mach 3 with axisymmetric plug-type inlets (Figure 5.2.1.2.

The inlet total pressure recoveries used in the cycle analyses are listed by flight Mach number in Table 5.2.1.1. They were determined from estimates of shock strengths, isentropic turning and boundary layer loss coupled with references for previous theoretical and experimental results at the given Mach numbers [Seddon 1999, Mahoney 1990].

Table 5.2.1.1 Inlet Pressure Recoveries Used in Cycle Analysis					
M_1 or M_∞	1.5	2	2.5	3	3.5
η_{ram}	0.93*	0.87	0.85	0.79	0.71

* Normal shock

5.2.2 Nuclear Reactor (Thermal Source)

The reactor size controls the maximum diameter of the engine, hence that of the vehicle body. The diameter of the cylindrical reactor, not including the radiation containment at the outer periphery, is 58.13 cm, and the length is equal to the diameter. In the present design, shown in Figure 4, there are 37 modular elements each with axial passages that feed multiple rows of small diameter radial passages that pass through the moderator and fuel annuli and exit into annular axial passages (in contact with the fuel) leading downstream to the reactor exit. For the initial design the diameter of the inlet passages was a constant 1.921 cm, giving a total inlet flow area of .01069 m^2. This was increased to a diameter of 2.8 cm at inlet, tapering to 0.8 cm at the downstream end, giving a total inlet flow area of 0.02277 m^2. The total flow area of the radial passages was chosen as approximately twice the inlet area. The annular flow area was initially a constant 0.03763 m^2, and this was modified to taper up to.05431 m^2 at reactor exit.

The design material temperature in the MITEE-I reactor is 1500 K, in order to minimize fuel erosion and provide for the long operating life (months). The gas outlet temperature will be somewhat lower, depending on the convective heat transfer coefficient between the fuel surface and the gas. Very high surface-to-volume ratio in the core (because of large number of small flow

passages) provides a large heat transfer surface to accomplish the needed temperature rise while minimizing the (total) pressure drop through the reactor.

5.2.3 Nozzle

The exit nozzle is axisymmetric and converging-diverging in area, such that the reactor exit flow accelerates to Mach 1 at the throat and then expands fully to the local atmospheric pressure at the design point. This "full expansion" provides maximum thrust and can be used without an additional external drag penalty ($A_{11} > A_1$) because the reactor diameter dominates. The flows from the 37 separate annuli exiting the reactor must mix at the nozzle entrance section, and suitably faired afterbodies will be used to facilitate smooth mixing with low total pressure loss.

5.3 Cycle Analysis and Thrust Calculations

5.3.1 Overview

Thermodynamic cycle calculations were carried out to determine the state points and velocities in the ramjet engine and evaluate the thrust produced over a range of flight Mach numbers and Jovian altitudes. Three separate stages of calculations were utilized: (1) initial screening and effect of parameters, (2) refined variables and combined thrust and drag analysis to define flight envelope, (3) finalized calculations with established geometry and flight envelope.

In all calculations the composition taken for the Jovian atmosphere was 86 % hydrogen/14% helium by mole fraction, and the corresponding mixture properties were obtained from the NIST thermophysics code REFPROP [Lemmon 2002], which models real gas effects, and from standard property tables for the individual gases using mole or mass averaging. By comparing the two methods it was verified that the mixture can be appropriately treated as a thermally perfect gas within the range of temperatures and pressures of mission relevance. The mixture must be treated as calorically imperfect, however, with $c_p = f(T)$ and the ratio of specific heats = $\gamma = f(T)$. The latter can be correctly used for the isentropic exponent, given in real gas dynamics as $k = [(\partial p/\partial \rho)_s]^{1/2}$, which facilitates computations. The values of c_p and γ vary with mixture temperature because those of hydrogen vary (those of helium do not). The values of γ were calculated as $c_p/(c_p - R_u)$.

A critical factor in the design of the nuclear ramjet is the relative magnitude of the flow areas in the engine. If there is direct heat transfer from the reactor to the ramjet engine flow, then the engine envelope dimensions (diameters) are dictated by the reactor size. The reactor diameter is on the order of 60 centimeters, but the cross-sectional area available as flow passage is much smaller. That is, the reactor diameter of 58.13 cm gives a gross cross-section area of 0.2653 m^2; but the actual flow passage area at the entrance to the core is only 0.02276 m^2 or 8.6% of the total area. In order to maintain the reactor entrance Mach number at a low enough level for necessary heat addition with pressure drop, the engine inlet area, A_1, must be sized correspondingly small. This, however, limits captured mass flow and thrust, and careful trade-offs are necessary.

5.3.2 Cycle Calculations- Stage 1

The initial calculations were used to assess performance level over a range of flight Mach numbers and altitudes, establish area requirements and relationships, and evaluate the effects of parameters, particularly reactor exit temperature and friction pressure loss. They were carried out using an in-house developed Fortran computer program over the variable ranges and approach listed in Table 5.3.2.1. All calculations utilized a single reference ambient pressure p_1 = 0.068 atm (=1 psia). Altitude variations for a given flight Mach number were evaluated by scaling thrust and cycle pressures with Jovian pressure altitude (as given in Figure 3.1.1), since caloric properties are not influenced significantly by pressure in the applicable range.

For each flight Mach number (M_1), a reactor inlet Mach number (M_5) was selected as being high enough to allow as large an inlet capture area (A_1) as possible while remaining low enough to permit sufficient heat addition, resulting in a range of M_5 = 0.23 to 0.29. Then a series of cycle calculations was performed with varying reactor exit total temperature (T_9^0). A baseline calculation was first made for each temperature corresponding to heat addition at constant area with no pressure loss (i.e. a Rayleigh Line process.) Then calculations were made for assumed additional total pressure losses of 10 and 20% above the heat addition p^0 loss. Typically, friction pressure losses much greater than 20 % could not be sustained without choking for the M_5 values used. This held particularly at high T_9^0 and lower M_1 because the total temperature T_9^0/T_5^0 becomes too large. Preliminary estimates indicated that pressure losses can be held to the 20 % range if there is sufficient passage area.

Table 5.3.2.1 . CYCLE ANALYSIS PARAMETERS AND ASSUMPTIONS

- Engine geometry is specific to each flight Mach number ("rubber" engine")
- Fluid is H_2(0.86)/He(0.14) by volume, $\gamma = f(T)$
- M_0 = 1.5, 2, 2.5, 3, 3.5
- T_0= 167 K
- p_0=.068 atm (1 psia), results scaled to other pressure altitudes
- Inlet pressure recovery from Table 5.2.1.1
- Diffuser exit is essentially a plenum, M_4 = 0.02; take 2% total pressure loss (3-4)
- Reactor inlet M_5 = 0.23 to 0.29
- Reactor exit total temperature varied from 889 to 1500 K
  (1) A = const, $\Delta p^0_{friction} = 0$ (Rayleigh line)
  (2) Include nominal $\Delta p^0_{friction}$ values as %
- Nozzle isentropic expansion with C_v = 0.985 applied; $p_{11} = p_1$ (check $A_{11} = A_1$)
- Standard thrust = $F_{st} = w/g(V_{11} - V_1) + (p_{11} - p_1)A_{11}$
- Internal Thrust = $F_T = w/g(V_{11} - V_1) + [p_{11}A_{11} - p_1A_1]$
- Normalize thrust with A_1, i.e. F_T/A_1 ; $C_F = F_T/ A_1q_1$

The geometry was allowed to vary for each flight Mach number, often termed a "rubber engine". The areas at each engine station were normalized by the free stream capture area, A_1, since the size at this stage was not defined, and this approach allowed parametric study of the mass flows and required heat addition attendant to capture area. The F_T/A_1 values were non-dimensionalized by the free stream dynamic pressure q_1 to yield a thrust coefficient, $C_T = F_T/A_1q_1$.

The calculated values of C_T for M_1=3 are plotted versus cycle temperature at reactor exit, T_9^0, in Figure 5.3.2.1 for the reference case of friction $\Delta p^0_{5\text{-}9} = 0$ and for $\Delta p^0 = 10\%$ and 20% of reactor entrance value. The rate of increase in thrust with temperature is exhibited, and the loss with friction pressure drop is seen to be relatively small. The latter is influenced by the fact that full expansion is considered in the nozzle, so that even with these total pressure losses there remains sufficient pressure ratio to produce a high exit velocity.

Table 5.3.2.2 lists the engine area ratios vs. flight Mach number obtained from the Stage 1 cycle analyses together with the resulting inlet areas and mass flows corresponding to the original reactor inlet area of .01069 m^2 . At M_1=3 the ratio of the area after compression and diffusion (reactor inlet area) to the inlet capture area is $A_5/A_1 = 0.645$, dictating an inlet area of $A_1 = 0.01069/0.718 = 0.0149$ m^2, or $d_0 = 13.76$ cm. This, of course, is very small compared to that of the vehicle and would dictate a "fat" vehicle shape with a large area of profile drag on the cowl exterior. Even more importantly, the small inlet limits mass flow and thrust in direct proportion to area as discussed above. Flight at lower M_1 exacerbates the situation, since there is less area reduction in the inlet (A_3/A_1), and the reactor inlet area actually becomes larger than A_1.

Table 5.3.2.2 Area Ratios and Inlet Areas for Varying Flight Mach Number

M_1	M_5 Reactor Entrance	A_3/A_1 Inlet Comp Ratio	A_5/A_1 Reactor/Inlet at M_5	A_1 for A_5 = 0.01069 m^2	d_1 cm
3.5	0.29	0.282	0.528	0.0203	16.08
3	0.27	0.345	0.718.	0.0149	13.76
2.5	0.24	0.511	1.188	0.0090	10.71
2	0.23	0.726	1.814	0.0059	8.67
1.5	0.21	1.0	2.821	0.0038	6.96

The inlet could be made physically larger, but the design then would need to be tailored to allow flow spillage. This would cause spillage (or additive) drag as a trade-off with profile drag, and mass flow would not appreciably increase. The value of A_5/A_1 could be varied slightly for any M_1 but not enough to qualitatively alter the situation, since it is intrinsic to the aerothermodynamics of reducing the free stream velocity to a level suitable for the heat addition. Note that the area compatibility improves at increased flight Mach numbers. For example at $M_1 = 3.5$, A_5/A_1 is on the order of 0.53 (for $M_3 = 0.29$), yielding $A_1 = 0.0203$ m^2 or d_1=16.08 cm; but this is still too small, and there are some drawbacks to using too high a flight Mach number.

The options to address this situation included:

(1) Increase the reactor flow passage area significantly

(2) Use indirect heat transfer from the reactor to the ramjet flow with an intermediate fluid loop and heat exchanger in the engine.
(3) Fly at a higher Mach number with better area matching between engine and reactor.
(4) Use the annular area around the reactor periphery as flow area where there would be reduced heat transfer but increased mass flow (i.e. in effect a "by-pass").

5.3.3 Cycle Calculations - Stage 2

5.3.3.1 Thrust Calculation Procedure and Results

Based on the information gained in Stage 1 and a review of the details of the heat transfer in the reactor, Option (1) above was selected, and the decision was made to modify the reactor inlet geometry to an increased area. This was done by increasing the reactor inlet diameter to 2.8 cm initially with a linear decrease to d = 0.8 cm at the downstream end of the axial passages. The linear decrease approximately matches the decrease in mass flow as flow enters the equally spaced array of radial outflow holes. Furthermore, the calculations were modified to consider a higher M_5. Both of these steps allow larger capture areas and thereby higher mass flows, leading to increased thrust and capability to remove heat from the reactor fuel.

The calculations in Stage 2 were done both manually and by use of a Fortran computer code specially written for the task. Flexible engine geometry was again used for varied Mach number and for nozzle exit area with varying temperature. Ambient temperature (300 K) and pressure (1 psia scaled) were initially taken as constant and then varied with altitude per the Jovian Standard Atmosphere of Figure 3.1.1. The diffuser exit area, A_4, was taken as the entire face area of the reactor entrance, 2653 cm^2, yielding a very large value for A_4/A_3, which produces an M_4 only on the order of 02, thus essentially a plenum in front of the reactor passages. In the cycle calculation, then, full velocity head at Station 4 was considered lost, but this is a very small amount because of the low velocity. Total pressure loss of 3% was assumed in the diffuser (Station 3 to 4), and an additional 3% loss for mixing was taken at the reactor outlet (Station 9 to 10). No entrance losses to the reactor passages were included since there will be carefully radiused entrances. Thrust was calculated as Internal Thrust (see Table 5.3.2.1) and was expressed in dimensional force units (rather than C_T) to account for actual capture area and for direct comparison with drag values. .

Figure 5.3.3.1.1 shows a plot of thrust variation with temperature for four flight Mach numbers at a constant altitude of 50 km for M_5 in the 0.23 to 0.29 range and A_5 = 0.245 ft^2. The steeper thrust increase with temperature at higher Mach numbers demonstrates the capability to take advantage of available heat and to provide modulation via reactor output. The marked decrease of thrust at low M_1 is due mainly to the necessarily smaller capture areas (see Table 5.3.2.2) and also to the intrinsic cycle thermodynamics.

5.3.3.2 Thrust vs. Drag Comparisons; Flight Envelope

At this stage the available thrust was compared to calculated drag levels for the complete Jovian Flyer. It was found that additional thrust was required to provide a sufficient working flight

envelope. To this end the level of reactor inlet Mach number, M_5, was increased to the range of 0.4 to 0.45, which allowed a larger inlet diameter and greater mass flow through the engine. Analysis of the flow and heat transfer details in the reactor passages indicated that this approach was realistic because the majority of heat would be added in the fuel matrix sheet wherein the Mach numbers would be quite low (below 0.2). These analyses also indicated that the total pressure loss in the reactor would be in the range of 20%, and this value was used for subsequent cycle calculations.

Figure 5.3.3.2.1 is a plot of thrust vs. altitude for flight Mach numbers from 1.5 to 3, showing two temperature curves for each Mach number. The temperatures are 2300 R and 1600 R (except 2000 R is the upper curve for M_1=1.5 because the low total temperature causes excessively high temperature ratios for further heat addition). This graph conveys similar information to Figure 5.3.3.2.1 with the addition of showing altitude effects and a first estimate of flight envelope potential via the lines of drag for several levels of L/D. The indication is that M_1 must be at least 2.5 in order to obtain a sufficiently wide range of altitudes.

The internal thrust and the calculated vehicle drag for three vehicle configurations are plotted vs. altitude for M_1=3 in Figure 5.3.3.2.2. The drag is decreased by lengthening the nose to produce a shallower angle after the inlet as diameter is increased to the maximum at the reactor, hence the decreasing level of drag in the "Shortnose", "Midnose", and "Longnose" curves. There are two curves for each configuration, corresponding to inlet diameters of 20 and 25 cm. The engine inlet diameters fall within this range for M_5 values of 0.4 to 0.45. The parabolic nature of the drag curves occurs because profile drag dominates at the low altitudes and induced drag (due to lift) is the major contribution at high altitudes (low pressures and densities).

Based on vehicle mission, weight, equipment and structural considerations it was concluded that the Longnose profile and its lower drag advantages may be used for the final vehicle design. Figure 5.3.3.2.2, then, shows that there is theoretically sufficient thrust to fly up to an altitude of z = 50 km and as low as z=0 or below based on availability of thrust over drag. A more practical lower limit, however, would be in the vicinity of z = 20 km due to two issues: (1) lift coefficient, C_L, becomes quite small, on the order of 0.05 at 15 km, creating potential stability problems, particularly in the gusty Jovian atmosphere, and (2) internal pressures increase to levels that produce demanding structural requirements inconsistent with maintaining sufficiently light weight It is possible to modify the wing design to allow a lower altitude, but overall stability and control issues must also be considered.

Decreasing flight Mach number is beneficial to allowing flight at lower altitudes because C_L increases, internal pressure decreases, and power decreases for a given temperature. The reduction of M_1 is limited, however, because thrust becomes insufficient to overcome drag below approximately M_1=2.5. Another limiting factor is that with fixed geometry (designed for M_1=3), mass flow and reactor inlet Mach number become too high for the lowered flight Mach number and choking at the reactor exit (or before) can occur. Figure 5.3.3.2.3 shows a plot similar to Figure 5.3.3.2.2 for M_1=2.5. The drag curves are the same as those in Figure 5.3.3.2.2 (shown for d_1=25 cm only) and indicate thrust exceeding Long-nose drag for altitudes below 40 km.

The cycle temperature for the thrust curves in Figures 5.3.3.2.2 and 5.3.3.2.3 is 1278 K, which is conservative since temperatures close to 1500 K are possible. A plot of vehicle C_L vs. altitude with M_1 as parameter is given in Figure 5.3.3.2.4.

5.3.4 Stage 3 -Selection of Flight Mach Number and Flight Envelope

The third stage of cycle calculations entailed applying the previous results to defining a design flight Mach number and flight envelope and then finalizing the thrust capability over the flight range using a single fixed geometry. The flight design Mach number was selected as $M_1 = 3$ based as follows:

- the thrust is sufficient relative to drag to provide a wide basic flight envelope of 20 to 50 km with stable control
- the fixed geometry engine areas for M_1=3 can allow flight down to lower altitudes by decreasing M_1 to 2.5, with sufficient thrust to climb back (using design M_1 higher than 3 would make this impossible or very marginal)
- higher altitude (above 50 km) might be achieved using $M_1 = 3.5$ with the $M_1 = 3$ geometry.

As an alternative to increasing M_1 (above 3) for altitudes above 50 km, higher altitudes may be attained for short periods through use of transient "zoom" to gain altitude at the expense of kinetic energy. That is, the vehicle can be controlled to climb gradually until the vertical velocity reaches zero and then re-accelerate under the force of gravity to restore its original orbit.

The use of lowered M_1 (to the order of 2.5) for z = 0 to 20 km provides higher C_L and stability and decreased internal pressure, as well as decreasing the required power consumed at the increased ambient pressure and captured mass flow with fixed geometry. A plot of the required reactor power (equal to mass flow times enthalpy rise) in MW is shown versus altitude for M_1 = 2.5 and 3 and varying reactor exit temperature in Figure 5.3.4.1. These high levels of power are attainable from the reactor, but the life of the fuel and mission are reduced with increasing power requirement, and a tradeoff is dictated. The power is decreased with decreasing reactor outlet temperature, the allowable decrease being limited by the need to keep the thrust level above that of the drag at a given M_1

A final set of cycle calculations was performed with fixed inlet geometry, set to an average of those corresponding to the variation of temperature in the flight envelope and with fixed nozzle area ratio, averaged over the variations due to varied reactor exit temperature. These are tabulated in Table 5.3.4.1. The results for thrust are plotted in Figure 5.3.4.2.

Table 5.3.4.1 Values of Fixed Geometry Design for Final Cycle Calculations	
Inlet Area, A_1- m^2	0.04
Inlet Contraction Ration, A_3/A_1	0.385
Reactor Inlet Area, A_5	0.02276
Reactor Inlet Area/Inlet Area, A_5/A_1	0.569
Reactor Exit Area, A_9	0.05431

Nozzle Exit Area, A_{11}	0.10
Nozzle Exit Area/Inlet Area, A_{11}/A_1	2.5

5.4 Inlet Design

With the design flight Mach number established at M_1=3, detailed aerothermodynamic design of the inlet was undertaken using manual calculations of shocks and compression waves for a fixed geometry, axisymmetric centerbody/spike and cowl combination. This has entailed use of tables and charts for γ =1.4 and approximate characteristic methods. Initial results provided comparisons for various cone angles and amount of isentropic turning on the centerbody, the cowl positioning and wedge angle, and centerbody contour and blend to minimum (annular) area. A baseline configuration of a 15 degree cone angle followed by 10 degrees of isentropic turning has been established, with the bow conical shock positioned at the cowl lip and reflected by a 5 degree wedge, as shown in Figure 5.1.2. This is consistent with a total pressure recovery on the order of 0.8, a static pressure ratio across the inlet of approximately 20, and an area ratio across the inlet of $A_{min}/A_1 = 0.35$.

This design includes placing a normal shock taken at about M_2 = 1.5 at the minimum area (actually just downstream, in the expanding diffuser section). The ability to establish this properly depends on the downstream configuration, including the diffuser passage and the reactor flow passage areas and pressure drop; and final design must look at the overall engine. It is anticipated that a bleed passage will be used for final normal shock positioning and stabilization in the turbulent Jovian atmosphere.

5.5. Heat Transfer Analysis in Reactor

The fluid flow and heat transfer in the reactor occurs similarly in each of the 37 fuel-moderator modular elements so that only one representative element needs to be analyzed. There are four zones of heat transfer in each element, as shown in Figure 5.4.1 : (1) the axial inlet passage, (2) the radial holes through the moderator, (3) the layered fuel matrix, and (4) the axial exit annulus. The majority of the heat transfer by far will occur within the nuclear fuel. The flow passage, heat transfer details, and pressure loss phenomena are complex, and some simplifying assumptions are used to permit a practical analysis. For example, the flow through the multiplicity of radial holes is subject to somewhat varying inlet conditions and mass flows (unless specific design steps are employed for balancing), but herein it is assumed that all radial holes are of equal diameter, experience equal mass flow, and may be represented by an average inlet condition at the axial mid-point of the inlet passage.

The calculations have been carried out for a flight Mach number of M_1 = 3 across a Jovian altitude range of 0 to 50 km (0, 20, 40,50 km). This range entails a wide variation of engine captured mass flows because of the atmospheric density (pressure) decrease with increasing altitude, varying from 15.76 to 1.55 kg/sec. Reactor inlet pressure (total and static) varies in the same proportion, while reactor inlet temperature and Mach number vary slightly due to ambient

temperature variations with altitude. The calculation procedure for each of the four reactor heat transfer zones is detailed below, and example numbers for z=20 km are given For this case p_5^0 = 10.63 atm, T_5^0=397 K and the captured engine mass flow is 9.56 kg/sec.

5.5.1 Zone 1- Axial Inlet

The reactor inlet flow passages are axial to each element and circular in cross-section with inlet diameter d_5 = 2.8 cm (A_5 = 6.154 cm^2 pr element or 227.7 cm^2 total) tapering down to d = 0.8 cm (A = 0.5024 cm^2) at the end of the 59.65 cm length. The axial passage supplies the radial holes through the moderator but is not a "plenum" per se because the velocity is substantial, with M_5 on the order of 0.4.

There is some heat transfer to the flow via radial conduction through the hollow cylinder of moderator. This quantity, $q_{5\text{-}6}$, and the attendant radial temperature $T_{mod}(r)$ can be calculated from the steady-state solution for radial heat transfer through a hollow cylinder with the outer radius maintained at a constant temperature (say T_{fuel} = 1500 K) and a known (assumed constant) film coefficient at the inner radius:

$$q_{5\text{-}6} = 2\pi L[T_o - T_i]/(1/h_i r_i + \{\ln r_o/r_i\}/k)$$

where r_o= moderator cylinder OD=7.835 cm
ri= avg inlet passage radius=0.9 cm
T_o is the fuel temperature, typically 1500 K
T_i is the gas total temperature in the axial inlet, taken as T_5^0
k = thermal conductivity of the moderator, which is not known at this time but is approximated at 0.346 W/cm C based on the nature of the material and the value for Be in the mixture with Li_7H and carbon fibers
h_I = film coefficient at inner radius (wall of inlet passage)

The film coefficient, h_i, is a function of Reynolds number:

$$Re_{5avg} = (w/A_{5mid})d_{5mid}/\mu_5$$

where w is the mass flow rate per element, d_5 and A_5 are at the mid-point of the axial inlet passage, and μ_5 is evaluated at T_5. The values of Re_{5avg} are tabulated in Table 1 and indicate turbulent flow across the range of altitudes (e.g. 0.8 x 10^6 at z = 20 km). For turbulent flow in a circular tube, h may be determined from Nusselt number:

$$Nu_d = hd/k = 0.023(Re)^{.8}(Pr)^{.4}$$

where Prandtl number ($Pr = \mu c_p/k$) may be taken as 0.8 for the fluid mixture in the pertinent temperature range, and k_5 is evaluated at T_5 (k = 0.125 btu/hr f t F) The result for the example case is h_i = 1.34 W/cm^2 K.

Plugging all of the appropriate quantities into the equation for $q_{5\text{-}6}$ yields a value of q/L = 37.88 btu/sec per foot of axial length or 1.27 btu/sec per cm. For the average condition we use the axial passage mid-point, L = 59.65 cm/2 = 29.85 cm, and q=37.88 (.9785)=37.1 btu/sec. The average flow for the first half of the passage is ¾ times the inlet flow (assuming equal flow into each of the radial passages), which is 9.56 kg/sec=21.03 lb/sec total divided by 37 elements to give .258 kg/sec (.57 lb/sec) per element.

$$\Delta T_{avg} = q/wc_p = 37.1/[.57(3/4)x\ 2.92\ \text{btu/lb F}] = 30\ \text{F} = 16.7\ \text{K}$$

This is very small compared to the total temperature rise, and the total pressure loss due to heat addition (Rayleigh line loss) is likewise small, being evaluated for T_6^0/T_5^0 = 745 /715 = 1.042 and M_5 = 0.44 as p_6^0/p_5^0 = 0.983. The pressure loss due to friction may be evaluated from the Moody type equation:

$$\Delta p_{5\text{-}6\ \text{friction}} = f\,(L/d)\,\rho V^2/2g$$

Using $(L/d)_{avg}$=29.8 cm/1.8 cm= 16.56, a friction factor from the Moody chart based on nominal Re and roughness of f = 0.0135, and V_5 and ρ_5 gives $\Delta p_{5\text{-}6\ \text{friction}}$ = 0.61 psi = 0.413 atm for the example case. To address the turning and inlet loss from the axial passage into the radial holes it is reasonable to make the assumption that the total pressure in the radial hole (p_6^0) is equal to the local static pressure in the axial passage($p_{5'}$). Assuming the Mach number at 5' remains approximately the same as M_5, then for the example case $M_{5'}$=44 and p/p0 = 0.8755, yielding p_6^0 = [10.63(0.983) - 0.41] (0.8755) = 8.79 atm.

5.5.2 Zone 2- Radial Passage Holes

The total flow area has been selected to be approximately two times the axial inlet area ($A_5=\pi(2.8)^2/4$ = 6.154 cm^2) in order to keep the Mach number $M_{6\text{-}7}$ down. The hole diameter must necessarily be small but is taken as an order of magnitude greater than the fuel mesh holes (.018, 026 cm dia) as $d_6=d_7$=.25 cm. The flow area of each hole is then .0491 cm^2, and if there are four radial holes per row with rows spaced 1 cm apart for the 59.65 cm axial length there are 236 radial holes per element with a total area of 11.59 cm^2 (or 11.59/6.154=1.88 times the axial inlet area).

The value of M_6 can be obtained from the rearranged mass flow equation

$$f(M) = M/[1+\{(\gamma-1)/2\}\,M^2]^{(\gamma+1)/2(\gamma-1)} = w(T_6^0\,R/\rho_6)^{1/2}/p_6^0 A_6 \qquad [6]$$

For p_6^0 = 8.79 atm, T_6^0=414 K, and A_6=.11.59 cm^2, M_6 for the example case is 0.252.

The heat transfer can be calculated by a marching procedure in the radially outward direction via the following steps:

1. Divide the total moderator radial distance (r_{out}-$r_{in)}$ = (r_7-r_6) into j = N stations, giving Δr=(r_7-r_6)/N for each step where (r_7 - r_6)$_{avg}$ = (4 - 0.9) = 3.1 cm at the axial mid-point is used for the calculations
2. Obtain the wall temperatures T(r_j) from eq. [1]
3. Calculate Re and h from Eqs. [2] and [3] using the properties at Station 6 (inlet to an average radial hole) and assume h= const (1356 btu/hr ft^2 F in example case).
4. Calculate $q_j = hA_j[T_{avg}(r_j) - T_{fj}]$ where $A_j = \pi d_{hole}\Delta r$, $T_{avg}(r_j) = [T(r_{j+1}) - T(r_j)]$, and T_{fj} = fluid total temperature entering jth element, beginning at $T_{f(j=1)} = T_6^0$= 745 R
5. Calculate fluid temperature rise $\Delta T_{fj} = q_j/wc_p$
6. $T_{fj} + 1 = T_{fj} + \Delta T_{fj}$
7. Repeat steps 3 to 6 until j = N is reached at r_{out} = 4.005 cm

For the example case with N = 5, the result is T_7^0 = 512 K, a rise of 98 K in the moderator. From a Rayleigh line analysis the accompanying total pressure loss is given by p_7^0/p_6^0 = 0.988 for the example case inlet M_6 of 0.252.

The friction pressure drop in the radial holes (6 to 7) can be evaluated from Eq.5 using Re_6 (34,080 for the example case) and an assumed roughness ($\varepsilon = 5 \times 10^{-6}$ ft) to give friction factor, f (0.024 for the example), plus the use of average values for V and ε. For the example case this yields $\Delta p_{f6\text{-}7}$ = 0.415 atm, and p_7^0 = 8.79(0.988) - 0.415 = 8.27 atm.

5.5.3 Zone 3- Fuel Matrix Sheets

The fuel annulus is .180 cm thick and is made up of seven wrapped layers as shown in Figure 13 and described in Section _ of this report. Each layer contains a multitude of small diameter (radial) passages which produce a very large flow area (considerably larger than that of the total of radial holes in the moderator); and the ensemble of layers provides a very large heat transfer area to allow effective heat transfer even in the short transit distance. The radial passages of the individual layers do not necessarily line up with those of the adjacent layers, but a continuous flow passage is provided by the orthogonal array of recessed channels contiguous to the holes. The open area for flow is calculated from Figure 13 as 23% of the fuel circumferential area, the average of which is (π x 8.015 x 59.65) = 1502 cm^2 yielding $A_{flow} = A_7 = A_8$ = 0.23(1502) = 345.4 cm^2 per fuel element Dividing this by the hole area of $A_{1\ hole} = \pi/4(.018)^2$ = 0.000253 cm^2 indicates n = 1.358 x 10^6 holes per element.

A typical passage through one layer of the fuel sheet includes passing through a short distance of channel, then through 0.018 cm length of the 0.012 cm diameter hole, and then another short distance of channel. A non-rigorous geometric analysis using overlays of adjacent layers to estimate the average distance of travel through channels to the nearest radial hole in the subsequent layer yielded an average heat transfer area of 0.002374 cm^2 per hole per layer, or .01662 cm^2 for seven layers, and an average hydraulic radius of d_h = 0.0152 cm. The total heat transfer area per element is then 1.358 x 10^6 (0.01662) = 22,569 cm^2.

The average velocity entering the fuel layer is determined from $w/(\rho_7 A_7)$, where ρ_7 can be well-approximated by ρ_7^0 as determined from p_7^0 and T_7^0. The value of V_7 is very low for all cases of interest, 16 m/sec (52 ft/sec) for the example case, with corresponding $M_7 \sim 0.01$. The low velocity combined with the small hydraulic radius cause $Re_7 = (\rho_7 V_7 D_h)/\mu_7$ to be very low (69 for the example case) and correspond to laminar flow for the entire flight envelope. The velocity increases markedly through the fuel layer as the temperature and speed of sound rise, but the quantity $\rho V = w/A$ remains constant and the Reynolds number decreases due to increasing viscosity. For the example case $Re_8 = 34$ and $Re_{avg} = 52$.

The standard Nu for developed laminar flow and constant wall temperature is 3.65 but this is increased in developing entrance regions and an estimated value of $Nu_{7-8} = 4$ is used, giving $h_{7-8} = Nu(k)/d_h = 4(.304$ btu /hr ft F)/(.015 cm x 1/30.48 ft/cm)=2471 btu /hr ft^2 F = 0.6864 btu /sec ft^2 F. The film coefficient is, thus, large due to the small passage dimensions (high k/d). Applying the NTU method to evaluate effectiveness in the case of one fluid (or wall) temperature held constant in a heat exchanger:

$$\text{Effectiveness} = \eta_{7-8} = (T_8 - T_7)/((T_{fuel} - T_7) = 1 - e^{-NTU} \qquad [7]$$

where $NTU = UA/wc_p = hA/wc_p = 0.6864(24.29)/.570(3.04) = 9.62$ for the example case. Sustituting this value into Eq. 7 yields $\eta = 0.999$ indicating that the fluid exit temperature reaches the fuel element temperature. At altitudes above 20 km the engine mass flow is decreased (from w=.57 lb/sec=.259 kg/sec) so that the NTU will increase and give the same result of effectiveness very close to one. At a lower altitude of z=0, the mass flow increases to .939 lb/sec and NTU=5.84 and $\eta = 0.997$, essentially the same result.

To evaluate the pressure loss through the fuel sheet, it is first noted that the total pressure decrease due to heat addition is negligible because the inlet Mach number is very low (increases from about .01 to .015). The friction pressure loss calculation uses Eq 5 followed along the typical path described above consisting of .022 cm of channel, .012 cm of round (d = 0.018) hole, and 0.0065 cm of d = 0.026 hole, yielding an estimated $L/d_h = 19$. The friction factor for laminar flow is $64/Re_{avg}$ (f = 0.853), and the average velocity is 100 ft/sec. Considered also are a 90 deg short-radius turn into the central hole, a nominal expansion from channel to hole, the initial 90 deg turn from the radial hole into the first channel, and the final 90 deg (long radius) turn into the outer exit annulus. For the example case these add to a pressure loss of Δp_{7-8} of 0.06 atm and $p_8^0 = 8.27 - 0.06 = 8.21$ atm.

5.5.4 Zone 4 - Axial Exit Annulus

The exit annulus inner surface is formed by the outer surface of the fuel sheet, which originally was cylindrical (d = 8.1945 cm) but was modified to taper from this diameter at the upstream end down to d=7.8366 cm at the exit. The outer surface of each annulus is considered as the imaginary hexagonal profile defining the division between elements (see Figure 4), which has a pitch across flats of 8.5126 cm and an enclosed area of 62.886 cm^2. There is no wall or divider located at this boundary, the flow area is continuous to the adjacent fuel element surfaces, but it

represents a locus of planes of symmetry for the flow. The tapering, though small in angle, provides substantial axial flow area increase in the annulus (10.173 to 14.68 cm^2) which accommodates the continual step increases in hot flow from the radial moderator/fuel passages without presenting choking limitations.

Given the results from Zone 3, no heat transfer occurs in the annulus because the fluid has already attained the fuel wall temperature; thus there is no total pressure decrease due to heat addition. The friction pressure loss is calculated by a step-wise procedure in the flow direction that considers the local area and how much flow has entered the annulus (assumed linear with axial distance) at a given station, then calculating the Mach number from the mass flow equation using the known total pressure and temperature. This allows calculation of the static properties, speed of sound, and velocity and evaluation of the viscosity and Re (turbulent ranging from 50 to 100 x 10^6). The friction factor can then be evaluated using references for concentric annuli at the local d_h (note that 2{4A/P} was actually used for d_h to account for the outer boundary being a plane of symmetry, not a wall). The incremental Δp was then calculated from Eq. 5 and subtracted to give the new p^0. For the example case the total Δp was calculated as .27 atm, giving $p_9^0 = 8.21 - 0.27 = 7.94$ atm and $p_9^0/p_5^0 = 7.94/10.63 = 0.75$. This value is sufficiently close to the originally estimated values (initially 0.8, then 0.77) in the cycle calculations, particularly given that the parametric results showed relatively small decrease in thrust with increasing reactor pressure loss as long as choking was avoided. The exit Mach number was calculated as $M_9 = 0.478$ for the example (z = 20 km).

6 AERODYNAMIC DESIGN OF RAMJET FLYER

6.1 Introduction an Preliminary Design

6.1.1 Supersonic Cruising Flight in Jupiter's Atmosphere

The Jupiter Flyer is a supersonic vehicle designed to cruise continuously in the atmosphere of Jupiter. The stipulation of supersonic flight arises from the characteristics of the proposed innovative energy source and the proposed long-term mission. We have a compact nuclear reactor that acts as a high-energy heat exchanger, an atmosphere comprised primarily of hydrogen, a high-performance propellant, and the need for a high level of reliability for the long-term mission of exploring Jupiter's atmosphere. The simplest propulsion system incorporating all those requirements is the ramjet. The ramjet's simplicity of operation depends on passive aerodynamic compression of the atmospheric gases through properly designed shock wave systems. Such compression is effective only at supersonic speeds. The optimum speed for such systems is in the Mach number range of 2 to 4. Below M = 2 the compression afforded is minimal, while above M = 4 the compression heating of the gases precludes effective additional heat addition. Thus our attention is focused on the Mach number range between 2 and 4.

The fundamental equilibrium conditions of cruising flight are that the sum of all forces and moments acting on the vehicle are zero. That is the lift equals the weight, L = mg, the thrust equals the drag, F = D, and the sum of the moments about the center of gravity (c.g.) are zero

(trimmed flight), $\Sigma M = 0$. The lift and the drag are characterized by their respective coefficients so that $L/qS = C_L qS$ and $D/qS = C_D$. Here the quantity S is the representative area of the wing which is taken as the projected planform area while q is the dynamic pressure based on the flight conditions (subscript 0), $\rho_0 V_0^2/ 2 = \gamma P_0 M_0^2/2$. In these equations ρ, P, and V represent density, pressure, and speed, respectively. Since we are considering supersonic flight it is convenient to work in terms of Mach number rather than speed. The Mach number is $M_0 = V/a$, where the sonic speed in the gas is $a = \gamma P_0/\rho_0 = (\gamma R T_0)^{1/2}$. The atmospheric gas properties $\gamma = C_p/C_v$ and $R = C_p - C_v$ represent the isentropic exponent and the gas constant based on the specific heats.
The units used here are SI and the standard material and environmental properties that will be used in this study are listed in Table 6.1.1.1.

Table 6.1.1.1 Standard property values used for Jupiter

Property	Value
Acceleration of gravity, $g_{Jupiter}$	22.96 m/s^2 or 2.34g_{Earth}
Ratio of specific heats, γ	1.428, otherwise $\gamma(T)$ as required
Gas constant, R	3.650 kJ/kgK
Specific heat at constant pressure, C_p	12.10 kJ/kgK

The usual mission specification for flight vehicles on Earth is range or endurance, quantities constrained by the consumption of fuel. The Jupiter Flyer is nuclear powered so that the fuel consumption rate is negligibly small and therefore range or endurance is virtually unlimited. Aerodynamic heating is not a major problem for the Jupiter Flyer, because the ambient temperature on Jupiter in the altitude range of interest is much lower than on Earth at comparable ambient pressures. For example, the nominal temperature at ambient pressure of 1 bar is 25°C on Earth and -109°C on Jupiter. The corresponding stagnation temperatures at Mach 3 are 562°C on Earth and 207°C on Jupiter. An aircraft structure with a maximum temperature of ~200°C does not require exotic materials. Another important consideration is reliability and autonomous operation; the Jupiter Flyer must operate continually, even if not optimally.

6.1.2 General Features of Vehicles Designed for Supersonic Cruise

One approach to classifying airplane designs in terms of their intended flight regime has been suggested by Kuchemann (1978). Aircraft designed for the supersonic speed range are characterized by slender configurations where the ratio of the semi-span of the wing, b/2, to the total airplane length, *l*, is less than the tangent of the Mach angle, i.e., $b/2l < (M_0^2 - 1)^{-1/2}$. This geometry is one where the wings are highly swept, ensuring that the flow normal to the swept-back leading edge of the wing is subsonic, leading to weaker shock waves and reducing supersonic drag while permitting the use of rounded leading edges that enhance the low-speed characteristics of the airplane. This implies that airplanes designed for supersonic flight tend to have a low aspect ratio, A, where $A = b^2/S$. It is instructive to examine the design features of aircraft that have flown missions similar to that proposed for the Jupiter Flyer and this is facilitated by the typical results shown in Table 6.1.2.1.

Table 6.1.2.1 Characteristic features of supersonic cruisers

Aircraft	b/2l	W/S (N/m^2)	A	M_0	Engine
Concorde SST	0.20	3974	1.83	2.1	Turbojet
Tu-144	0.22	3351	1.89	2.2	Turbojet
XB-70	0.22	2633	1.30	2.7	Turbojet
SR-71	0.24	3351	1.93	3.0	Turbojet
Burya (USSR)	0.24	6700	1.72	3.2	Ramjet

It is clear from the table that the basic characteristics are similar. The low value of b/2*l* is dictated by drag reduction considerations, but also by utilization of the additional volume the long length provides for the requisite fuel load. Fuel consumption rates for turbojets and ramjets in supersonic flight are several times that for subsonic flight. This fact provides the major obstacle to development of an economical commercial supersonic transport. Corning [1960] points out that because of "the slight advantage in L/D, and decided advantage in stability and control, as well as the structural and mechanical advantages possible with a straight (i.e., unswept) trailing edge, the delta wing has been chosen at this time for the supersonic transport." He notes that this is likely not an optimum design, and the evolution of SST designs ultimately led to an arrow wing, as described by Harris [1992]. However, this result is due to the requirement of reducing drag to raise L/D to reduce fuel consumption to ultimately achieve economic viability and involves substantial sophistication in design integration. The present mission has no fuel constraint so that the requirements of reliability prevail, and these are based on maintaining simplicity throughout the design. Ed Heinemann, famous designer of aircraft for Douglas had as his design philosophy "simplicate and add lightness." The other advantage of the delta wing is the long chord length in the flight direction, enabling a thin airfoil section to be used while still providing substantial physical depth to the wing for strength as well as space for control systems, instrumentation cables, etc. The typical value of maximum thickness to chord ratio, t/c, for supersonic cruise aircraft is about 3% to 4%, a range also to be considered here.

6.1.3 Layout of a Conservative Jupiter Flyer Design

Since the start of this program a variety of vehicle designs were considered. Initially, a flight Mach number of 1.5 was considered. Later, the Mach number was raised to 3 to provide better performance. Both swept wing and delta wing designs were considered. The instruments were initially located in wing-tip pods. These were found to result in a high drag coefficient and were eliminated. Eventually, the design which evolved comprised a vehicle with a delta wing, multiple shock inlet, and the radiation-sensitive instrumentation in the inlet center-body (Figure 6.1.3.1).

Considerations regarding center of mass location, structural stiffness, and efficient shock compression led to the delta wing version for the Jupiter Flyer. Storing the instrumentation in the inlet centerbody along with the needed shielding (Figure 6.1.3.2) moves the center of gravity forward, a prime requisite for aerodynamic stability of the vehicle. In order to provide directional stability, a clean wing, and some roll stiffness, a parasol wing was selected. The mast of the

parasol wing can also provide space to house various subsystems. For additional directional stability canted tail fins were chosen. By rotating the two fins in concert or differentially, control in pitch yaw, and roll can be achieved. Of course, sizing of these components depends upon attention to aerodynamic details and will be carried out in subsequent sections of this report.

Taking as a general packaging constraint for delivery of the Jupiter Flyer to Jupiter that it should fit into a container measuring 3m by 2m by 1m, it is clear that, with no folding or moving parts to the vehicle, filling the package suggests that a value of b/2*l* down to around 0.33 is achievable. This is larger than the rule of thumb slenderness criterion when the flight Mach number goes beyond 2.8, but that is primarily a classification mechanism, driven in part by fuel volume requirements, as indicated previously. Starting with a vehicle concept somewhat smaller than the full package, we assume a total fuselage length l = 2m and a simple delta wing planform of span b = 1.41m, which yields a slenderness ratio b/2*l* of 0.35. Choosing an aspect ratio A= 2, like those of the surveyed aircraft yields, an area of 1 m^2, signifying a root chord length equal to 1.41 m and a leading edge sweepback angle $\Lambda_{LE} = 45^o$, consistent with those in Table 6.1.2.1. A layout of the prototype vehicle is shown in Fig. 6.1.3.3.

6.1.4 Drag Considerations

The second equilibrium condition is that the thrust is equal to the drag and therefore

$$F = D = L/(L/D) = mg/(L/D)$$

For the present notional design where the mass is assumed to be 270 kg, the thrust, F (in N), is equal to 6200/(L/D). The aerodynamic drag is given by $D = C_D qS$ where the drag coefficient, C_D, is comprised of two terms, the zero-lift drag, $C_{D,0}$, and the induced drag coefficient, $C_{D,i}$, which arises due to lift. The drag coefficient is usually expressed in terms of the lift coefficient as follows (see Raymer, 1989):

$$C_D = C_{D,0} + C_{D,i} = C_{D,0} + kC_L^2$$

This is the equation of the drag polar; the quadratic dependence of the induced drag coefficient on the lift coefficient is found to be generally acceptable for reasonably conventional designs. The zero-lift drag coefficient in supersonic flight is made up of several components, as shown below:

$$C_{D,0} = C_{D,friction} + C_{D,wave} + C_{D,misc} + C_{D,L\&P}$$

The first term represents the drag due to skin friction and is proportional to the wetted surface area of the vehicle and is typically formulated in terms of the skin friction coefficient, C_f, as $C_{D,friction} = \Sigma(C_{f,i}S_{i,wetted})/S$, where the subscript i denotes the element of the wetted area under consideration. The skin friction coefficient in supersonic flow is a function of Mach number, Reynolds number, and surface temperature. However, the for moderate Mach numbers like those considered here the deviation from the low speed results is not great and is described in Schlichting (1987). For the purposes of illustration, the situation in the present study, with

Reynolds numbers on the order of 10^7 per meter of length, a reasonable average value of the skin friction coefficient for a flat plate is C_f =0.002. As a rule of thumb the ratio of wetted area to planform area varies between 2, for planar bodies, and 3, for axi-symmetric bodies. For the notional delta wing Jupiter Flyer design shown in Fig. 6.1.3.3 the zero-lift drag coefficient contribution from skin friction may be conservatively estimated to be $C_{D,friction} = 0.006$.

The second term represents wave drag, the pressure drag due mainly to the presence of shock waves generated by the airplane, and it usually accounts for the major portion of the zero-lift drag of supersonic flight. The wave drag depends strongly on the flight Mach number and the slenderness of the body and is often larger than the sum of all the other drag components. An estimate of the wave drag contribution for the vehicle can be performed following the approach of Corning [1960]. The contribution of the wing is determined from curves of $\beta C_{D,wave,wing}/(t/c)^2$ as a function of $\beta \cot \Lambda_{LE}$ for various values of βA. For the present notional design and flight conditions a range of 0.0014 to 0.0030 for the wing's contribution to the wave drag coefficient. The major contribution for the wave drag will come from the fuselage because the packaging constraints on vehicle length coupled with the substantial reactor diameter limit the slenderness achievable. Preliminary estimates suggest the contribution to the wave drag from the fuselage to be around 0.04, because of its relatively small fineness ratio, but this will be considered more accurately in analyses presented subsequently.

The third term represents miscellaneous drag contributions due to carriage of external stores, exposed landing gear, etc., while the fourth term accounts for leaks and protuberances, the former of which occur at fasteners and seams and the latter at small bumps and gaps like those due to antennas and instrumentation ports. The magnitudes of these contributions are usually uncovered in testing final designs and are incorporated into the preliminary design process as a fixed percentage, say 5 percent, of the total predicted drag.

Raymer (1989) shows a zero-lift drag coefficient range of $0.02<C_{D,0}<0.05$ for a variety of operational supersonic aircraft over the Mach number range $1.5<M_0<3.0$. As a first approximation then it seems reasonable to select some parametric $C_{D,0}$ values to work with for the delta wing Jupiter Flyer shown in Fig 6.1.3.3. The results of the approximate estimation of drag described above suggests that for these initial evaluations $C_{D,0}$ be taken as 0.05, an optimistic value consistent with Raymer's data mentioned above, and 0.10, a conservative value.

The drag due to lift depends on the factor k, which Raymer [1989] suggests be represented, in supersonic flight, as

$$k = A(M_0^2 - 1)\cos\Lambda_{LE}/[4A(M_0^2 - 1)^{1/2} - 2]$$

Then the lift to drag ratio

$$L/D = C_L/[C_{D,0} + kC_L^2] = [C_{D,0}/C_L + kC_L]^{-1}$$

The lift coefficient for maximum L/D is found by setting the derivative of the preceding equation to zero and finding the corresponding lift coefficient. This results in $C_{L,max(L/D)} = (C_{D,0}/k)^{1/2}$. If $C_{D,0}$ = 0.05 is selected, the lift coefficient for maximum L/D is around 0.25 and the lift to drag ratio is $(0.2 + 0.25k)^{-1}$, or around 4, depending on the Mach number. For the conservative value of $C_{D,0}$ = 0.1 the lift coefficient for maximum L/D is around 0.4 and $(L/D)_{max}$ is diminished to around 2. These simple illustrations demonstrate the importance of maintaining as low a value of zero-lift drag coefficient as possible.

Subsequent detailed drag calculations for all components of the Jupiter Flyer vehicle were carried out primarily using the preferred standard methods described in the USAF Stability and Control DATCOM [Hoak 1970].

6.1.5 Wing Sizing for the Jupiter Flyer

The wing area is limited not only by the package size constraints, but also, and to a greater extent by the altitude and flight Mach number ranges required. In cruise, the second equilibrium condition is that the lift of the vehicle is equal to the weight so that $L=W=C_L qS$, and the important parameter is the wing loading, $W/S = C_L q = \frac{1}{2} \gamma p M^2 C_L$. In the atmosphere of Jupiter, over a pressure range of 1 bar down to 10^{-2} bar, the temperature varies between 112K to 170K, with a minimum temperature of 112K at 10^{-1} bar, as shown in Table 6.1.5.1.

Table 6.1.5.1 Atmospheric Characteristics of Jupiter

Pressure (bar)	Altitude above 1 bar (km)	Temperature (K)
1	0	170
0.1	40	112
0.01	80	137

With the temperature almost constant, it is reasonable to suppose an exponential atmosphere such that $p/p_0 = \delta = \exp(-Z/H)$, where p_0 is the pressure at the altitude Z=0 and H is the scale height of the atmosphere. In this instance, the value H =17.37 km yields excellent agreement with the actual pressures.

Now the relationship between wing loading and altitude as a function of lift coefficient and Mach number may be written as $W/S = 72.12\delta C_L M^2$ in units of kPa. It has already been shown that for expected levels of the drag coefficient, flight at reasonable values of L/D requires lift coefficients around 0.2 to 0.4. Furthermore it has been suggested previously that flight Mach numbers of around 2.5 or 3 will provide the best thrust performance for ramjets. To demonstrate the implication of these parameter constraints, a plot of wing loading as a function of altitude for appropriate pairs of Mach number and lift coefficient is presented in Fig. 6.1.5.1. From that figure it is seen that the design region requires a relatively small wing, with correspondingly high wing loading, in order to function effectively over a band of altitude that ranges on either side of the design altitude of 40 km (0.1 bar). As an illustration, the wing areas for a 326 kg Jupiter Flyer are

also shown in the figure, and it is clear that a wing of only 0.5 m^2 area is probably best suited to the high speed mission considered here.

This result indicates an altitude range of $20<Z<60$ km should be achievable with the nuclear powered ramjet and a conventional airframe design permitting reasonable L/D values while operating in the Mach number range of $1.5<M_0<3.0$. On the other hand, flight at altitudes below Z=20 km will require more careful study since the flight Mach number will become quite low and the propulsion requirements will be more stringent.

Note that the square of the Mach number appears in the wing loading equation so doubling W/S will increase M_0 by only 41%. It is generally true that the weight of a vehicle increase during the design process, and the wing area can be readily reduced, so that there is reasonable design control over the flight envelope possible for the vehicle. Although the lower Mach numbers admit flight at lower altitudes, engine calculations will show that the ramjet generates insufficient thrust at the slower speeds. Indeed, the optimum performance occurs around a Mach number of 3, a result determined a half-century ago for nuclear powered ramjets designed for flight in Earth's atmosphere, see, e.g., Merkle [1959].

6.1.6 Delta wing characteristics

The sweepback angle $\Lambda = \tan^{-1}(2C_r/b)$, the aspect ratio $A = b^2/S$, and the planform area $S = bC_r/2$, where b and C_r are the span and root chord of the delta, respectively. Thus $A = 2b/C_r$ and $\Lambda = \tan^{-1}(4/A)$ or $A = 4/\tan\Lambda$; also, $S = b^2\tan\Lambda/4$.

The thickness to chord ratio, t/c, is taken to be 5% and the mean aerodynamic chord, $\underline{c}$, a parameter of the planform of importance in stability and control considerations, is defined as

$$\underline{c} = 2c_r\{1 + \lambda - [\lambda/(1 + \lambda)]\}/3$$

In the above equation c_r denotes the chord length at the root of the complete wing planform. The mean aerodynamic chord is located on the planform at the distance

$$Y_{MAC}/(b/2) = [(1 + 2\lambda)/(1 + \lambda)]/3$$

as measured along the y-axis of the wing, i.e., normal to the aircraft centerline. In these equations the quantity $\lambda = c_t/c_r$ is the taper ratio of the wing. For a delta wing with sharp tips the tip chord is $c_t=0$, therefore $\lambda = 0$.

The normal force due to pressure for deltas with unswept trailing edges is given by

$$C_N = C_L\cos\alpha + C_D\sin\alpha$$

For small angles of attack the gradient of this force may be approximated by

$$dC_N/d\alpha = C_{N,\alpha} \approx dC_L/d\alpha = C_{L,\alpha} = 4/\beta = 4/(M^2 - 1)^{1/2}$$

The parameter β is called the Prandtl-Glauert factor. The induced drag factor k described in the section on drag characteristics is given by $k = (C_{N,\alpha})^{-1}$, and is significantly higher than that used for high aspect ratio wings at lower speeds, i.e., $(\pi eA)^{-1}$, where the quantity e is the Oswald span efficiency factor. Thus the wing drag is given by

$$C_D = C_{D,0} + (C_{N,\alpha})^{-1} C_L^{\ 2}$$

Three delta wings spanning the wing areas appropriate to our design region, as described in Fig. 6.1.5.1, were considered in the preliminary design process; they are described in Table 6.1.6.1. As mentioned in the previous section, propulsion considerations determined that Mach 3 is the preferred flight speed and thus the smallest wing, i.e., Wing 3, with area $S = 0.5\ m^2$ was selected for the configuration.

Table 6.1.6.1 Three wings studies

Wing	S (m^2)	L (degrees)	A	b (m)	C_r (m^2)
1	1.73	60	2.31	2.0	1.73
2	1.2	50.2	3.33	2.0	1.2
3	0.5	50.2	3.33	1.29	0.78

6.1.7 Thrust Required

Using the results of the previous sections it is reasonable to consider a net thrust F = mg/(L/D) of 1550 N for the optimistic case of $C_{D,0} = 0.05$, while for $C_{D,0} = 0.1$ the requirement expands to about 3100 N, still well within the capacity of the nuclear ramjet.

6.1.8 Estimation of Fuselage Drag

The fuselage has a relatively low fineness ratio since the reactor diameter fixes the fuselage diameter at about 0.6m, while the length is confined, by packaging restrictions, to less than 3m. We consider the fuselage to be comprised of basically four components: an open circular cone frustum forebody, a circular cylinder centerbody, an open circular cone afterbody, and an annular base plate covering the area between the nozzle opening and the diameter of the after body at the end of the fuselage. These components and their geometrical idealization, along with their contribution to the drag of the fuselage is shown in Table 6.1.8.1. The intake diameter at the inlet tip and the nozzle diameter at the end of the fuselage are fixed by the propulsion considerations described elsewhere in this report. The length of the reactor is fixed, and though the nozzle length can be small it cannot be less than that reported in Table 6.1.8.1. Thus, the only real design variables are the angles of the forebody and afterbody cone frustums.

Table 6.1.8.1 Components comprising Flyer fuselage

Component	Geometry	Drag contribution	Size determinants	Nominal dimensions
Forebody	Open cone frustum	Primary: wave drag.	Inlet and fuselage diameters	20-25cm inlet, 60cm outlet, length variable
Centerbody	Circular cylinder	Tertiary: friction.	Reactor diameter and length	60cm diameter, 70cm long
Afterbody	Open cone frustum	Secondary: separation.	Nozzle exit and fuselage diameters	60cm inlet, 50cm outlet, 50cm long
Base	Annular disc	Secondary: separation.	Nozzle exit diameter and drag increment	30-38cm inner diameter, 50cm outer diameter

The afterbody slope is determined from considerations of separation dynamics. For a shallow enough slope, say, less than 8 degrees, the boundary layer will stay attached and the drag will be minimized. Furthermore, as pointed out by Kuchemann [1978], a propulsive jet will give a positive base pressure, i.e., a thrust, so that the drag of the afterbody and the base will be less than the afterbody drag alone. Taking a conservative approach, we keep the afterbody confined to a shallow slope to minimize its drag and we assume, because of the propulsive jet issuing from the nozzle, that the base drag is zero.

In particular we choose the afterbody slope to be 5.7 degrees so that the 60cm fuselage diameter is linearly reduced to 50cm over an afterbody length of 50cm. That leaves only the forebody cone angle as a parameter with which to deal. Six cone angles were studied, covering two intake diameters and three lengths keeping the exit diameter of the inlet equal to 60cm, the centerbody diameter and remaining within the overall length restriction of 3m. The inlets were thus characterized as short, mid-length, or long, and they are listed below in terms of their cone angle.

I	Inlet d=20cm	Inlet d=25cm
Short nose	16.6^{o}	14.6^{o}
Mid-length nose	12.5^{o}	11.0^{o}
Long nose	8.5^{o}	7.45^{o}

Results for the profile, or zero-lift drag coefficient, of the fuselages with the different cone angles as a function of Mach number are shown in Figure 6.1.8.1 for the altitude of 40 km. Similar result are obtained for 0 and 80 km altitudes. In order to keep the drag of the Jupiter Flyer as low as possible, the JF-6, with a forebody slope of 7.45 degrees and an intake diameter of 25 cm was selected. This vehicle has an overall length of 2.84 m, and with its wingspan of 1.29 m the JF-6 has a slenderness ratio, b/2*l*, of 0.23. This is in close correspondence with the survey aircraft described in Table 6.1.2.1.

6.1.9 Total Drag of the Jupiter Flyer

The total drag, i.e., profile plus induced drag, was calculated for all 6 complete versions of the Jupiter Flyer vehicle, i.e., 3 slenderness ratios and 2 intake diameters. The range of airframes selected covered configurations expected to be consistent with thrust capability of the engine. The drag was calculated for each configuration at altitudes of 0, 20, 40, 60, and 80 kilometers and Mach numbers of 2, 2.5, and 3. The "long nose" configuration, i.e., the JF-6 vehicle, which combined the most slender fuselage design and the largest intake diameter possible for effective engine performance, gave drag values that were within the thrust capability of the engine, a characteristic not achievable with the earlier "short nose" airframes studued earlier. The JF-6 configuration selected is shown in Fig. 6.1.3.2.

The drag results were compared with the engine thrust predictions to and demonstrated the possibility of cruising flight at a Mach number of 3 over a range of altitude from about 20 to 50 km, as well as at M=2.5 over a narrower band of altitudes. These results are described in Section 5.0: Design of Nuclear Ramjet Engine – Thermal/Hydraulics.

6.1.10 Lift Characteristics of the Jupiter Flyer

Lift characteristics of the wing at Mach 3 were calculated using the USAF Stability and Control DATCOM [1970] methodology. The flow over the wing is divided into several regions as a function of angle of attack: shock attachment, transition to detachment, and fully detached shock. This provided the lift coefficient as a function of angle of attack. The variation of the lift coefficient, drag coefficient, and lift to drag ratio with angle of attack was computed and is shown in Figure 6.1.10.1. Lift coefficients required for all cases were calculated to aid in determination of the envelope of altitude and Mach number for achievable states of steady level flight

The variation of the lift coefficient, drag coefficient, and lift to drag ratio with angle of attack was computed and is shown in Figure 6.1.10.1. Having this data it is also possible to generate the drag polar for the JF-6 long nose flyer at the design point of Z = 40 km and M = 3. The drag polar will change slightly at the other altitudes because of the corresponding slight changes in the drag coefficient; the lift coefficient is independent of altitude at the present level of precision. Using the same method the lift characteristics of the tail was also generated. This information is necessary in the analysis of the stability and control of the flyer. The drag polar is shown in Figure 6.1.10.2.

6.2 Perfprmance of Selected Design, the JF-6

6.2.1 Center of Mass

Moments about the x-, y-, and z-axes were taken in order to locate the center of gravity of the flyer. First it was necessary to estimate the mass of each of the components of the JF-6. Then the center of mass location of each component was estimated based on the component masses (see Table 6.2.1.1). From this data the center of mass location of the complete JF-6 was estimated.

Table 6.2.1.1 Masses, moment arms, wetted areas, and JF-6 center of mass location

Vehicle component	Mass (kg)	Moment arm X(cm) from spike tip	Moment arm Z(cm) from fuselage bottom	Wetted area (m^2)
Wing	14	195	80	1.00
Mast	6.9	206	69	0.48
Tail	6.3	265	9	0.45
Forebody	25[(1)]	106	30	1.80[(1)]
Centerbody	19	200	30	1.32
Afterbody	12	259	30	0.87
Reactor	180[(2)]	200	30	
Inlet body	8	55	30	
Instruments	40	35	30	
Shielding	15	85	30	
Com. system				
Controls/aero				
Controls/reac				
Nozzle				
GNC system				
Aux. Power				
Total	326.2	167	33	

6.2.2 Mass Estimation

The mass estimation is based on the techniques used for preliminary design reported by Torenbeek (1982). The fuselage is the major element in the JF-6 and it has the attributes of both a fuselage and an engine nacelle. Formulas for estimating the mass of these two components are given by Torenbeek. For the fuselage he suggests

$$m_f = 0.23[V_D(l_t/2d_f)]^{1/2}S_w^{1.2}$$

and for the nacelle he proposes

$$m_n = 0.405[V_D]^{1/2}S_w^{1.3}$$

where l_t is the moment arm of the tail described later in the determination of longitudinal stability, d_f is the diameter of the fuselage, V_D is the design dive speed, and S_w is the wetted area. Since these both have much the same form it seems appropriate to use an average of the two to form

the equation for the mass of the JF-6 fuselage. As a conservative estimate the exponent of the wetted area S_w will be kept at the higher value so that

$$m_{fus} = [0.12(l_t/2d_f)^{1/2} + 0.2]V_D^{1/2}S_w^{1.3}$$

In the present configuration the JF-6 has l_t = 1.0m and d_f = 0.6m so that $m_{fus} = 0.31V_D^{1/2}S_w^{1.3}$ and this equation was used to calculate the mass of the elements of the fuselage as listed in Table 6.2.1.1. The resulting mass of the fuselage of approximately 63 kg was used to generate a mass per unit external wetted area of roughly 14 kg/m^2. This specific mass was used to estimate the mass of the wing, tail, and inlet centerbody, including the instrument package. The mass of the reactor, instruments, and shielding was taken from the Phase I Final report. The last line of Table 6.2.1.1 shows the resulting mass of the Flyer to be about 326kg and the center of mass to be located approximately 167cm aft of the tip of the inlet spike and 33cm above the fuselage bottom, i.e., slightly above the centerline.

6.2.3 Design Dive Speed

An important parameter in the mass estimation method is the design dive speed, or Mach number. This is the maximum speed at which the structure is designed to withstand particular loads required by airworthiness regulations, e.g., a gust load due to a specified gust velocity. For our preliminary design purposes the design dive speed is taken to be the speed corresponding to the cruise Mach number of 3. In terms of equivalent airspeed on Earth this is given by

$$V_D = M_{cr}a_{cr}$$
$$V_{D,EAS} = (\rho_{alt,jup}/\rho_{sl.Earth})^{1/2}V_D$$

This yields the airspeed on Earth that has the same dynamic pressure as experienced by the vehicle under its cruise condition. For supersonic flight is more appropriate to deal with Mach number so we may use the dynamic pressure in the form

$$Q = (½)\rho V^2 = (½)\gamma p M^2$$

Then, with the pressure p in bars, we may set

$$M_{D,EAS} = [(\gamma_{Jup}/\gamma_{Earth})p]^{1/2}M = [(\gamma_{Jup}/\gamma_{Earth})\exp(-Z/17.37)]^{1/2}M_D$$

At the design altitude of 40 km the pressure p = 0.1 bar and with M_D = 3 the design dive Mach number is $M_{D,EAS} = [(0.1)(1.57/1.4)]^{1/2}(3) = 1.0$. That is, the ambient conditions are such that the vehicle is operating under loading conditions that would be experienced flying at Mach=1.0, or 750mph, at sea level on Earth. Obviously, as the flyer descends into Jupiter's atmosphere at M = 3 toward the level where the pressure is one atmosphere, the design dive Mach number will approach the flight Mach number of 3. The loading on the vehicle will then be almost an order of magnitude greater than it was at Z = 40 km. Obviously at some later design iteration the effect of this loading increase will have to be evaluated in some detail because it will influence the weight

of the flyer and/or the actual minimum altitude possible. On the other hand, more detailed optimization analyses would focus attention on trade-offs between Mach number and altitude in order to more completely define the flight envelope. Such trade-offs would involve reducing the Mach number as the altitude is reduced. This requires a variable geometry inlet, which is quite feasible, but is outside the scope of the present study.

6.3 Aerodynamic Stability and Control of JF-6 Flyer

6.3.1 Longitudinal Stability

The fuselage generally contributes to a reduction of stability because the long fuselage needed for drag reduction provides a substantial moment arm that exaggerates the effect of forces on the fuselage. The USAF Stability and Control DATCOM [Hoak 1970] techniques were used to estimate the moment coefficient contribution for all components of the JF-6. The method is particularly tedious for the fuselage, requiring consideration of the fuselage as a body composed of the conical fore-body, the cylindrical after-body and the conical boat-tail. As expected, the fuselage is destabilizing in pitch and requires significant nose-down moment. However the aft high-wing configuration resolves this problem. Indeed, no lift, and therefore no induced drag, is required from the tail (i.e., it is set at zero incidence) and therefore the drag penalties for trimming are minimized by the design.

The pitching moment coefficient was estimated for the JF-6 and is shown as a function of angle of attack in Fig. 6.3.1.1. The vehicle is trimmed at zero angle of attack of the fuselage centerline at the required lift coefficient of about 0.21, which corresponds to a wing incidence angle of about 8.4 degrees (see Figure 6.1.10.1) and with the incidence angle of the tail equal to zero.

6.3.2 Rolling Characteristics

Roll of an aircraft around its x-axis (the fuselage centerline) results in no first order changes in the aerodynamics if the x-axis is coincident with the aircraft's velocity vector. A second order effect arises if the roll axis and the velocity vector are separated by an angle of attack α_x because in that case the effective angle of attack α_x induces a sideslip angle β. In that case a roll stiffness parameter arises through the stability derivative $C_{l\beta}$, the change in rolling moment coefficient with respect to sideslip angle β. It may be shown that the change in rolling moment C_l with respect to the roll angle ϕ is approximately equal to $C_{l\beta}\alpha_x$. Since $C_{l\beta} < 0$, the tendency of the roll stiffness is to reduce the roll angle disturbance, thus helping keep the wings level. The high wing position of the JF-6 provides a dihedral effect adding to this roll stiffness even though the wing has zero dihedral angle.

6.3.3 Control Authority in Pitch, Yaw, and Roll

In order to reduce the number of moving parts on the JF-6 an attempt has been made to provide control in all three axes using the canted tail fins alone. The basis for this approach is that each tail fin generates a normal force that may be decomposed into both vertical (Z-direction of the JF-6) and side (X-direction of the JF-6) forces depending on the deflection imposed on the fin. Since

each fin may be moved up or down independently there are four possible configurations for equal magnitude deflections, as follows:

$\alpha_{left} > 0$, $\alpha_{right} > 0$: pitch down, no roll; l=0, m<0, n=0
$\alpha_{left} < 0$, $\alpha_{right} < 0$: pitch up; no roll; l=0, m>0, n=0
$\alpha_{left} < 0$, $\alpha_{right} > 0$: coordinated turn to port; l<0, m=0, n<0
$\alpha_{left} > 0$, $\alpha_{right} < 0$: coordinated turn to starboard; l>0, m=0, n>0

The general vector moment coefficient achievable by the canted fin system is given by

$$C_M = C_L\mathbf{i} + C_M\mathbf{j} + C_N\mathbf{k}$$

Here the quantities **i**,**j**,**k** denote unit vectors in the x,y,z coordinate system of the JF-6 with the origin at the center of mass. In this right-handed system the x-axis is positive in the direction of flight, y is positive in the starboard direction, and z is positive down, The quantities L ,M,N denote the moments about the x,y,z directions; as subscripts they also serve to denote the designated moments normalized by the quantity qS$\underline{c}$ where $\underline{c}$ is the mean aerodynamic chord of the wing. For the JF-6 the general moment coefficient is given by

$$C_M = [0.00474(\alpha_{t,port} - \alpha_{t,starboard})]\mathbf{i} + [-0.0055(\alpha_{t,port} + \alpha_{t,starboard})]\,\mathbf{j}$$

$$+ [0.00930(\alpha_{t,port} + \alpha_{t,starboard})]\,\mathbf{k}$$

In this configuration setting $\alpha_{t,port} = \alpha_{t,starboard}$ results in the pure pitch motion while setting $\alpha_{t,port} = -\alpha_{t,starboard}$ results in a coupled roll and yaw to provide coordinated turns.

6.3.4 Inertia Characteristics

In order to carry out any dynamic studies of the JF-6 it is important to develop the moments and products of inertia of the vehicle. Though this can be a laborious process, in the present study the components of the vehicle will be idealized to expedite calculations. The vehicle components and their geometrical idealizations and related quantities shown in Table 6.3.4.1 were used to calculate the necessary moment and products of inertia.

Table 6.3.4.1. Mass and geometric characteristics of the major components of the JF-6

Component	Shape	Mass (kg)	Center of mass (X,0,Z) Origin at spike tip and fuselage bottom
Inlet centerbody	Cylindrical shell	8	55,0,30
Instrument package	Cylindrical solid	40	35,0,30
Shielding	Cylindrical solid	15	85,0,30
Inlet forebody	Conical shell	25	106,0,30
Centerbody + reactor	Cylindrical solid	199	200,0,30

Afterbody	Conical shell	12	259,0,30
Mast	Rectangular plate	7	206,0,69
Wing	Triangular plate	14	195,0,80
Tail fins	Triangular plate	13	265,0,9

6.3.5 Moment of inertia characteristics

The moment of inertia characteristics of the JF-6 have been evaluated on the basis of the mass characteristics and center of gravity information provided in previous progress reports. The moment of inertia tensor is described by the following array:

$$\mathbf{I} = \begin{matrix} I_{xx} & I_{xy} & I_{xz} \\ I_{yx} & I_{yy} & I_{yz} \\ I_{zx} & I_{zy} & I_{zz} \end{matrix}$$

The symmetry of the JF-6 about the x-axis and the z-axis, like most aircraft, forces some of the products of inertia to be zero, reducing the above equation to the following form:

$$\mathbf{I} = \begin{matrix} I_{xx} & 0 & I_{xz} \\ 0 & I_{yy} & 0 \\ I_{zx} & 0 & I_{zz} \end{matrix}$$

Since $I_{xz} = I_{zx}$ there are only 4 components of the moment of inertia tensor which must be satisfied. The magnitude of I_{xz} is typically one or two orders of magnitude lower than that of the other components so the moment of inertia tensor is nearly diagonal. The approximate values for the JF-6, normalized by the product mlb, were determined to be as follows:

$I_{xx}/mlb = I_x/mlb = 0.7x10^{-2}$

$I_{yy}/mlb = I_y/mlb = 11x10^{-2}$

$I_{zz}/mlb = Iz/mlb = 11x10^{-2}$

$I_{xz}/mlb = 0.1x10^{-2}$

Here m is the vehicle mass, *l* is the overall length, and b is the wing span; the quantity m*l*b=1213 kg-m^2. The normalized values for the moment of inertia components are in agreement, within a factor of 2, with known corresponding values, normalized in the same fashion, with those of three other vehicles of widely varying mass, one of which is the Boeing 747. Relative to these other aircraft the JF-6 is somewhat easier to roll, while more difficult to pitch and yaw. The moment of

inertia components may change as the details of mass and center of gravity location are refined, but the deviations from the approximate values already given should be slight.

6.3.6 Moment of Inertia Summary

The moments of inertia calculated for the JF-6, along with those of several other aircraft, are shown in Table 6.3.6.1. The X-24C was a hypersonic (M>4) airplane design that was flown only at low speed, the Supermaneuver was a design study for highly maneuverable Mach 2 fighter that was never flown, and the Boeing 747 is the well-known high speed commercial jetliner. Though the masses span three orders of magnitude it is clear that the appropriate non-dimensional parameters are quite close. The length to span ratio, l/b, is around 2 for the supersonic aircraft while it is around unity for the transonic jetliner, both falling in ranges typical for the aircraft type considered. The wing loadings for the X-24C and the Supermanueuver fighter are low because of design constraints posed by landing requirements. The Boeing 747 needs the high wing loading to satisfy economical cruise at transonic speeds; landing requirements are met by the use of sophisticated high lift devices. The JF-6 has no landing requirement so the wing loading is optimized for the high speed needed for effective operation of the nuclear ram jet engine.

Table 6.3.6.1. Moments of Inertia of the JF-6 and other vehicles

Variable	JF-6	X-24C	Supermaneuver	Boeing 747
I_{xx}/mlb	$1.43\text{x}10^{-2}$	$0.766\text{x}10^{-2}$	$0.757\text{x}10^{-2}$	$2.04\text{x}10^{-2}$
I_{yy}/mlb	$11.6\text{x}10^{-2}$	$12.5\text{x}10^{-2}$	$5.59\text{x}10^{-2}$	$3.71\text{x}10^{-2}$
I_{zz}/mlb	$11.3\text{x}10^{-2}$	$13.2\text{x}10^{-2}$	$6.58\text{x}10^{-2}$	$5.56\text{x}10^{-2}$
I_{xz}/mlb	$0.127\text{x}10^{-2}$	$0.107\text{x}10^{-2}$	$0.0789\text{x}10^{-2}$	$0.109\text{x}10^{-2}$
m(kg)	$3.26\text{x}10^{2}$	$7.31\text{x}10^{3}$	$1.46\text{x}10^{4}$	$2.88\text{x}10^{5}$
b(m)	1.31	7.56	12.2	59.4
l(m)	2.84	14.7	23.2	70.4
l/b	2.18	1.95	1.90	1.19
x_{CM}/l	0.59	0.66	0.61	0.46
W/S(N/m^2)	$15.0\text{x}10^{3}$	$1.40\text{x}10^{3}$	$2.36\text{x}10^{3}$	$5.40\text{x}10^{3}$

6.3.7 Equations of motion of the JF-6 as a rigid body

It is assumed that the aircraft is symmetric and flying at zero angle of sideslip, $\beta = 0$. It is further assumed that any lateral motions are small enough to have negligible effect on the longitudinal aerodynamics, and, conversely, the longitudinal motions are small enough to have negligible effect on the lateral aerodynamics. In this sense the longitudinal motions are considered to be uncoupled from the lateral motions so that each may be investigated separately. In the same manner, it is assumed that the Mach number, Reynolds number, dynamic pressure, velocity, engine parameters, etc., change so little that the non-dimensional aerodynamic coefficients are unaffected. The equations of motion under these conditions are derived from those given in standard textbooks on the subject, e.g., Etkin [1996], and are not be repeated here.

The equations are of the form $x'_i = A_{ji}x_i + X_i$ where x'_i is the column matrix denoting the time derivative of i components of the motion, x_i, A_{ji} is the square matrix of aerodynamic influence coefficients involving the stability derivatives, and X_i is the column matrix of the forcing functions for the components of the motion. The longitudinal motions are described by 4 components: $x_1 = \Delta u$, the change in x-component of velocity from the reference velocity u_0; $x_2 = w$, the change in the vertical velocity from the reference value $w_0 = 0$; $x_3 = q$, the angular pitch rate about the y-axis; and $x_4 = \Delta\theta$, the change in the Euler angle describing pitch. The lateral motions are likewise described by 4 components: $x_1 = v$, the change in the y-component of velocity from the reference lateral velocity $v_0 = 0$; $x_2 = p$, the angular roll rate around the y-axis; $x_3 = r$, the angular yaw rate about the z-axis; and $x_4 = \phi$, the change in the Euler angle describing roll.

An appreciation for the aerodynamic influence coefficient matrix for the uncoupled equations is given below under the condition that the stability derivatives involving rates of change of angle of attack and of angle of sideslip are negligible compared to other quantities:

$A_{11} = \rho u_0 S[C_{w0}(\sin\theta_0 + \tan\theta_0) - C_{D0} - M_0(dC_D/dM)]/m$
$A_{21} = \rho u_0 S[C_{w0} - C_{D\alpha}]/2m$
$A_{31} = 0$
$A_{41} = -g\cos\theta$

$A_{21} = \rho u_0 S[-(W/S)\cos\theta/p_{dyn} - (M_0/2)\,dC_L/dM]/m$
$A_{22} = -\rho u_0 S[C_{L\alpha} + C_{D0}]/2m$
$A_{23} = [-\rho u_0 S\underline{c}(a_T V_H)/2m] + u_0$
$A_{24} = -mg\sin\theta_0/m$

$A_{31} = [\rho u_0 S\underline{c} M_0(dC_D/dM)/2]/I_y$
$A_{32} = -\rho u_0 S\underline{c} C_{m\alpha}/I_y$
$A_{33} = -\rho u_0 S\underline{c} a_T V_H l_t/2$
$A_{34} = 0$

$A_{41} = 0$
$A_{42} = 0$
$A_{43} = 1$
$A_{44} = 0$

The quantities shown are now reasonably well in hand for the JF-6 and may be described as follows:

- m, g, S, $\underline{c}$, I_y, a_T, l_T, V_H denote vehicle mass, gravitational acceleration, wing planform area, mean aerodynamic chord, moment of inertia about the y-axis, lift slope of the tail, distance between the aerodynamic center of the tail and the center of mass, and the volume coefficient of the tail, $l_T S_T/\underline{c}S$, respectively. These quantities are all known from the design information presented in previous reports.

- ρ, u_0, M_0, θ_0 denote reference flight conditions of density, flight speed, flight Mach number, and pitch angle. These quantities may be selected as required.

- $C_{L\alpha}$, $C_{m\alpha}$, $C_{D\alpha}$ denote the variation of lift, pitching moment, and drag coefficients as a function of angle of attack. These quantities have been calculated in previous reports.

- C_{w0}, C_{D0}, dC_L/dM, dC_D/dM denote the lift coefficient in the reference state, the zero lift drag coefficient, the variation of lift coefficient with Mach number, and the variation of drag coefficient with Mach number. These quantities were determined in previous reports.

There is a similar set for the lateral motions but there the motion is considered to be dominated by the effects of the tail and are not as fully developed as the present set for longitudinal motion.

6.3.8 Sensors and actuators

The selection of sensors and actuators is an important aspect of the control system design, particularly for a new type of vehicle for which no "standard" configuration of control hardware has been established. It is expected that the primary sensors will be inertial, i.e., accelerometers and gyros of the "strapdown" type that are fixed to the airframe thereby providing measurements of forces and angular velocities projected onto the body axes of the vehicle. Since such sensors will be needed on the vehicle for navigation they will also be available for the purposes of flight control. At least two sets of sensors are necessary to provide some redundancy, and one of the sets should be placed as close to the center of mass of the vehicle as permitted by the details of the design. The fact that the center of mass is located within the body of the reactor requires a location for the inertial sensors somewhere in the mast, perhaps directly above the axial location of the center of mass. A major advantage of using inertial instruments of navigation quality in the flight control system is that errors are all but negligible in comparison to typical flight control hardware. Although gyros and accelerometers are the sensors of choice, the possibility of using air data sensors may be considered, particularly for the role they can serve in monitoring critical parameters, like reactor exit temperature.

In the flight corridor expected for the Jupiter Flyer aerodynamic controls should be suitable and recourse to exotic approaches like thrust vectoring is unnecessary. It has been poined out earlier that all motions can be provided by the canted tail fins of the JF-6. Each fin can have a shaft attached with an axis of rotation coincident with the center of pressure so that torque required for rotation of the fin remains small. Then geared electric motors can be directly attached to those shafts to provide specific adjustments of the angle of each fin.

The forcing functions may be described as follows:

$X_1 = \Delta X_{control}/m$
$X_2 = \Delta Z_{control}/m$
$X_3 = \Delta M_{control}/I_y$
$X_4 = 0$

As noted earlier, the canted tail fins produce a general moment coefficient in the form

$\mathbf{C_M} = C_l\mathbf{i} + C_m\mathbf{j} + C_n\mathbf{k} = \mathbf{C_M}(\alpha_{port}, \alpha_{starboard})$

Thus the change in moment about the pitch axis alone due to control actuation is

$\Delta M_{control} = C_m p_{dyn} \underline{c} S$

The resulting forcing functions for directions along and normal to the flight path can be determined from the details of the forces generated by the fins. For example, drag will be produced when deflecting the tail fins to trim out the vertical forces. Throttling the engine also produces forces.

6.3.9 Control system design

It is expected that one of the critical control requirements is to track a slowly time-varying flight path angle with great accuracy over a range of Mach numbers and altitude. Other maneuvers that merit consideration include synergetic plane change, steady turn, and optimum ascent. The characteristics of the JF-6 have been calculated diligently and they may be used to develop a preliminary flight control system. An important maneuver to be considered is a change in flight path angle. The flight control system is to be designed so as to provide accurate control of this angle. With this requirement in mind, the dynamics may be formulated with the error between the actual and desired flight path angle as a state variable. The system dynamics may be expressed in state-space form with the error in flight path angle, the inertial pitch angle the pitch rate the control surface and the commanded flight path angle as state variables, as follows:

$$X = [e\gamma, \theta, q, \delta, \gamma_c]$$

The commanded surface deflection is the control input and if inertial instrumentation is assumed there are two outputs available: normal acceleration and inertial pitch angle. This approach will be used to assess some of the characteristic responses of the vehicle since the implementation of a full 6-degree of freedom (6-DOF) analysis is beyond the scope of the present study.

6.3.10 Aerodynamic Influence Coefficients for Longitudinal Modes

The aerodynamic influence coefficients for the uncoupled equations are summarized below. Under the condition that the stability derivatives involving rates of change of angle of attack and of angle of sideslip are negligible compared to other quantities:

$A_{11} = \rho u_0 S[C_{w0}(\sin\theta_0 + \tan\theta_0) - C_{D0} - M_0(dC_D/dM)]/m$
$A_{12} = \rho u_0 S[C_{w0} - C_{D\alpha}]/2m$
$A_{13} = 0$
$A_{14} = -g\cos\theta$

$A_{21} = \rho u_0 S[-(W/S)\cos\theta/p_{dyn} - (M_0/2)\, dC_L/dM]/m$
$A_{22} = -\rho u_0 S[C_{L\alpha} + C_{D0}]/2m$
$A_{23} = [-\rho u_0 S\underline{c}(a_T V_H)/2m] + u_0$
$A_{24} = -mg\sin\theta_0/m$

$A_{31} = [\rho u_0 S\underline{c} M_0 (dC_D/dM)/2]/I_y$
$A_{32} = -\rho u_0 S\underline{c} C_{m\alpha}/I_y$
$A_{33} = -\rho u_0 S\underline{c} a_T V_H l_t/2$
$A_{34} = 0$

$A_{41} = 0$
$A_{42} = 0$
$A_{43} = 1$
$A_{44} = 0$

6.3.11 Reference State Conditions

The reference conditions, denoted by the subscript 0, are those of steady level flight at a given altitude and Mach number. Here we choose the design altitude of 40km and a flight Mach number of 3. The corresponding input data relating to the atmospheric environment and to the configuration of the JF-6 are given in the Table 6.3.11.1.

Table 6.3.11.1 Environment and Configuration Parameters

Variable	Value
Altitude, Z	40 km
Mach number, M	3
Density, ρ_0	0.025 kg/m^3
Temperature, T_0	112 K
Isentropic exponent, γ	1.57
Speed of sound, a_0	798 m/s
Flight velocity, u_0	2393 m/s
Dynamic pressure, $p_{dynamic}$	71.24 kPa
Gravitational acceleration, g	22.96 m/s^2
Mass, m	326 kg
Moment of inertia about y-axis, I_y	139.24 kg-m^2
Weight, W	7485 N
Wing area, S	0.5 m^2
Wing loading, W/S	14,970 N/m^2
Mean aerodynamic chord (MAC), $\underline{c}$	0.517 m
Horizontal tail moment arm, l_t	0.98 m
Horizontal tail area, S_t	0.222 m^2

Horizontal tail volume coefficient, $S_t l_t / S\underline{c}$	0.842
Zero lift drag coefficient, C_{D0}	0.088
Induced drag coefficient factor, k	0.707
Wing sweepback angle, Λ	50.2 deg
CG position as fraction of MAC, h	-0.068

The lift coefficient at the reference state is $C_{w,0} = (W/S)/p_{dynamic} = 0.21$ and the drag coefficient at the reference state is $C_{D,0} = C_{D0} + kC_{w,0}^2 = 0.119$. We can now proceed to get the aerodynamic coefficients and stability derivatives required.

6.3.12 Variation of coefficients with angle of attack

Lift coefficient - The variation of lift coefficient with angle of attack is $C_{L\alpha}$ and this is estimated from the results for lift coefficient as a function of angle of attack for a Mach number of 3, which is given by $C_L = 0.175 + 0.075\alpha$. Note that the angle of attack is taken as that of the fuselage; the wing and tail surfaces being set at appropriate incidence angles to trim the vehicle at the reference condition. Thus $C_{L\alpha} = 0.584$ per degree = 3.35 per radian.

Drag coefficient - The variation of drag coefficient with angle of attack at the reference condition is $dC_D/d\alpha = C_{D\alpha} = 2kC_L(dC_L/d\alpha) = 2kC_LC_{L\alpha} = 0.3$ per radian.

Moment coefficient - The variation of moment coefficient with angle of attack $dC_m/d\alpha = C_{m\alpha}$ and this may be determined by taking the derivative with respect to angle of attack of the general equation we developed for the JF-6 moment coefficient. The resulting equation is

$$C_{m\alpha} = [- C_{L\alpha}\underline{x} + C_{D\alpha}\underline{z}]_{wing} - C_{D\alpha,mast}\underline{z}_{mast} - C_{L\alpha,t}(S_t/S)\underline{x}_t\cos\omega - C_{D\alpha,t}(S_t/S)\underline{z}_t + C_{m\alpha,fus}$$

In this equation $\underline{x}$ and $\underline{z}$ are the moment arms for the indicated component normalized by the wing aerodynamic chord, $\underline{c}$, while ω is the cant angle of the horizontal tail fins. We can also just estimate the derivative from a plot of C_m vs. α, which gives us $C_{m\alpha} = 0.728$ per radian.

6.2.13 Variation of coefficients with Mach number

Lift coefficient - The variation of lift coefficient with Mach number is taken from Etkin and Reid [1996] who provides an estimate applicable to subsonic and supersonic flow as follows: $dC_L/dM = C_wM\cos^2\Lambda/(1 - M^2\cos^2\Lambda)$. In the reference state $dC_L/dM = -0.0788$.

Drag coefficient - The variation of drag coefficient with Mach number arises directly from the definition $C_D = C_{D0} + kC_L^2$. Thus $dC_D/dM = dC_{D0}/dM + 2kC_LdC_L/d/M = -0.0324$ where the quantity $dC_{D0}/dM = -0.028$ is estimated directly from calculations of the zero-lift drag coefficients at M = 2.0, 2.5, and 3.0.

Moment coefficient **-** The variation of the pitching moment coefficient can be obtained in a manner similar to that presented previously for its variation with lift coefficient. Then

$dC_m/dM = [-(dC_L/dM)\ \underline{x} + dC_D/dM)\ \underline{z}]_{wing} - (dC_D/dM)_{,mast}\underline{z}_{mast} - (dC_L/dM)_t\ (S_t/S)\underline{x}_t\cos\omega - (dC_D/dM)_t(S_t/S)\underline{z}_t + (dC_m/dM)_{fus}$

Using the values developed previously we find $dC_m/dM = 0.0198$

6.3.14 Coefficients of the Longitudinal Stability Matrix

Now the aerodynamic influence coefficients may be calculated from all the information given in the preceding sections of this report.

$A_{11} = -0.00362\ sec^{-1}$
$A_{12} = -0.00413\ sec^{-1}$
$A_{13} = 0$
$A_{14} = -22.96 m/sec^2$

$A_{21} = -0.00843 sec^{-1}$
$A_{22} = -0.159\ sec^{-1}$
$A_{23} = 2393\ m/sec$
$A_{24} = 0$

$A_{31} = 0.00329\ (m\text{-}sec)^{-1}$
$A_{32} = -0.0403\ (m\text{-}sec)^{-1}$
$A_{33} = -0.0681(1+Q)\ sec^{-1}$
$A_{34} = 0$

$A_{41} = 0$
$A_{42} = 0$
$A_{43} = 1$
$A_{44} = 0$

The quantity $Q = C_{m,d\alpha/dt}/C_{m,q}$ represents the effect of pitch rate on the dynamics of the vehicle. The coefficient $C_{m,d\alpha/dt}$ is usually determined from unsteady aerodynamic analysis, which is beyond the scope of the present study.

The general equation was given previously in the form $x'_i = A_{ji}x_i + X_i$ where x'_i is the column matrix denoting the time derivative of i components of the motion, x_i, A_{ji} is the square matrix of aerodynamic influence coefficients involving the stability derivatives, and X_i is the column matrix of the forcing functions for the components of the motion. Solutions are of the form $x(t) = x_0\exp(\lambda t)$ where x_0 is an eigenvector and λ is an eigenvalue of the system. Thus $(A_{ji} - \lambda I)x_0 = 0$ where I is the identity matrix. The scalar form of this is a set of N homogeneous equations that possess non-zero solutions for x_0 only if the determinant of $(A_{ji} - \lambda I) = 0$. The result of this

equation is an Nth order polynomial in λ called the characteristic equation. In the present case this is the 4^{th} order equation $A\lambda^4 + B\lambda^3 + C\lambda^2 + D\lambda + E = 0$ with the values for the coefficients given as follows:

A = 1
B = 1.163 + 0.0681Q
C = 96.4 + 0.011Q
D = 0.62
E = 0.0207

The fact that all the coefficients are positive and that the quantity $D(BC - AD) - B^2E > 0$ assures us that there are no unstable modes for this system. The solution to the characteristic equation is

$x_{1,2} = -0.00237 \pm 0.01414i$
and

$x_{3,4} = -0.5790 \pm 9.801i$

This pair of results displays the usual long-term, or phugoid, mode and the short-term mode, respectively. Calculation of the nature of the motion yields the results shown in the Tables 6.3.14.1 and 6.3.14.2.

Table 6.3.14.1 Oscillation characteristics in the long-term, phugoid, mode

Variable	Exact phugoid solution	Approx. phugoid solution
Damping exponent, n	-0.00237	-0.00869
Frequency, , ω, sec^{-1}	0.01414	0.0143
Period, T, sec	444	438
Damping ratio, $\xi = -n/\omega$, sec	0.167	0.608
Time to half, $t_{1/2} = -0.693/n$	257	79.7
Cycles to half, $N_{1/2} = -0.11\omega/n$	0.659	0.181

Table 6.3.14.2 Oscillation characteristics in the short-term mode

Variable	Exact short-term solution	Approx. short-term solution
Damping exponent, n	-0.5790	-0.114
Frequency, ω, sec^{-1}	9.801	9.82
Period, T, sec	0.64	0.64
Damping ratio, $\xi = -n/\omega$, sec	0.059	0.012
Time to half, $t_{1/2} = -0.693/n$	1.19	6.08
Cycles to half, $N_{1/2} = -0.11\omega/n$	1.86	9.17

The approximate solutions were carried out according to Etkin and Reid [1996] as a check on the full calculations and the relationship between the two sets are typical. The short-term mode has a very high natural frequency that may require some additional damping to make the response of the JF-6 more benign. The reduced frequency in the short-term mode is $k = \omega\underline{c}/2u_0 = 1.06 \times 10^{-3}$ which is extremely small due to the very high speed of the JF-6. It must be noted that we have neglected the variation of pitching moment coefficient with rate of change of angle of attack, $C_{md\alpha/dt}$, because there is no simple estimation method available and model tests or computer simulations are beyond the scope of the present study. However, large negative values for this variable can strongly enhance the damping, though it will scarcely affect the frequency.

Studies of plunging wings have been applied toward the study of $C_{md\alpha/dt}$ leading to the following estimate:

$$C_{md\alpha/dt} = \pi (h - \tfrac{1}{2}) + 2\pi[G(k)/k](h - \tfrac{1}{4})$$

In this equation G(k) is the imaginary part of the Theodorsen function developed for the study of flutter problems. The difficulty in application is that the quantity G(k)/k is unbounded as $k \rightarrow 0$, although it seems to have been useful even down to values of k=0.001. Using the JF-6 properties we find $C_{md\alpha/dt} = -1.27 - 0.963G(k)/k$. However, $G<0$, and thus as $k \rightarrow 0$, the G/k will be a large positive number and will reduce the damping of the high frequency oscillations. For example, Theodorsen [1940] presents a tabulation of G(k)/k which stops at k = 0.01 at which G/k = -4.82, so that it's clear that $C_{md\alpha/dt} > 0$ and there will be no help from the wing as far as damping goes. On the other hand, the fuselage contributes as much lift and pitching moment as does the wing and therefore its dynamic response will affect the magnitude and sign of $C_{md\alpha/dt}$. The extent of this effect is beyond the scope of the present project.

6.3.15 Flight Management System

Control system design methodologies have evolved to the point where we can successfully control variable configuration aircraft such as the F-14, flying wing configurations like the B-2, and even statically unstable aircraft such as the X-29. The task of designing the control system for the flyer should not be as great as for the configurations mentioned because the flyer will operate over a narrower Mach number range. It's the wide Mach number variation that causes significant nonlinear changes in the flight dynamics of the aircraft that presents the challenge in designing the control system. Based on the success of the aircraft shown we don't anticipate any insurmountable problems in developing the Stability Augmentation System (SAS) for the three attitude channels of roll, pitch, and yaw for the Ramjet Flyer. A typical SAS design for the pitch channel of a high performance military aircraft including gust alleviation is shown in Fig. 6.3.15.1.

The next step in designing an advanced flight management system for the flyer is to investigate the capabilities of the state-of-the-art autopilot designs. Current technology autopilot designs provide 'command' and 'hold' modes of operation for vehicle: altitude, heading, attitude, and Mach number/airspeed (throttle). Present autopilot designs allow for only moderate perturbations in aircraft attitude thus the question is: Will these designs be sufficient to control the unmanned

flyer through the turbulent storms generated in the Jovian atmosphere and have it survive? In order to design the SAS a statistical model representing the atmospheric turbulence is required to guarantee a stable system. To determine if a statistical turbulence model of the Jovian atmosphere exists we investigated the atmospheric data measurements taken during the Voyager and Galileo missions and the simulation models that have been developed based on these databases.

Figure 6.3.15.2 summarizes the mean zonal wind speeds found in the Jovian atmosphere for the zones or bands found from 60 deg north latitude to 60 deg south latitude. The wind speeds are average from data recorded from both Voyager I and II missions. Note that almost every other band flows in a westward or retro direction and that several of the zones have a mean speed in excess of 100 m/sec. From time lapse imagery of several of the zones it appears that at the juncture between the zones there is the possibility of significant shear flows generating dangerous turbulence for the flyer in these regions.

The plot in Fig. 6.3.15.3 summarizes the wind speed data recorded by the Galileo probe which entered the the Jovian atmosphere in 1995. This data represents the only in situ data that shows the variation in local wind speed as a function of altitude. The descent lasted 58 minutes, during which the probe measured winds in excess of 175 m/sec (four-hundred miles per hour) - stronger than anything on Earth. The probe melted as it reached a pressure of approximately 22 bars and vaporized by the intense heat of the atmosphere. It should be noted that the greatest variation in speed occurs in the altitude range corresponding to a pressure change of from 1 to 4 bars, a region within the flight envelope of the Ramjet Flyer.

Atmospheric planetologists have invested a great deal of effort in analyzing and modeling the Great Red Spot on Jupiter. The Great Red Spot is a great anti-cyclonic (high pressure) storm akin to a hurricane on Earth, but it is enormous (three Earths would fit within its boundaries) and therefore not likely to provide relevant local turbulence data for the Ramjet Flyer. The plot in Fig. 6.3.15.4 summarizes the rotation velocity field determined by averaging photo data of the Great Red Spot recorded by Voyager I and II.

The data from both the Voyager and Galileo missions provides wind and turbulence data only at a large global scale, unfortunately not at the scale of the flyer itself. As shown in Figure 6.3.15.5, a statistical model of the turbulence must be representative of the disturbances the flyer will encounter in its immediate vicinity that is typically taken to be approximately one half kilometer. The local turbulent wind gusts are used to insure both the structural integrity and the controllability of the vehicle design.

The next step in designing an advanced flight management system for the flyer is to investigate the capabilities of the state-of-the-art autopilot designs. Current technology autopilot designs provide ‘command’ and ‘hold’ modes of operation for vehicle: altitude, heading, attitude, and Mach number/airspeed (throttle). Present autopilot designs allow for only moderate perturbations in aircraft attitude thus the question is will these designs be sufficient to control the unmanned flyer through the turbulent storms generated in the Jovian atmosphere and have it survive.

Since the round trip transit time to send data and receive a reply from the flyer's data computer is in excess of 90 minutes it will be impossible to fly the Ramjet Flyer in real time from a terrestrial ground station. Thus the requirement for an autopilot must be expanded to the concept of an 'Advanced Flight Management System' which will provide complete autonomous control of the Ramjet Flyer. The system will have to include capabilities based on AI technologies, neural nets, and genetic learning algorithms in order for the system to adapt to the unknown turbulent environment.

Figure 6.3.15.6 is a block diagram representation of a proposed autonomous flight management system for the Ramjet Flyer. It consists of tasks including: mission planning, navigation, and sensor integration. It will also be responsible for specific mission related events including atmospheric insertion (de-orbit), sona buoy deployment, and vehicle recovery from a turbulent upset.

6.3.16 Construction Aspects of the JF-6

Characteristics of the design are presented in Figure 6.1.3.2 illustrating a concept for the construction of the JF-6. The reactor is the major component of the JF-6 in that it represents more than half the mass of the vehicle and its maximum diameter. The wing is shown in the figure set to its proper incidence for ensuring the correct trimmed lift of the JF-6 at the design point of M=3 at an altitude of 40km.

6.3.17 Subsystems for the JF-6

The major subsystems on the JF-6 are the instrumentation package, the communication equipment, the flight control system, and the tail fin actuation system. The packaging of these systems is illustrated in schematic fashion in Figure 6.1.3.2. For power requirements on the order of 1kW, individual, co-located, RTG units or a centralized direct thermal to electric conversion using reactor heat can serve. The mass of such systems would be around 5 to10kg. Larger power requirements could be readily handled if packaging restrictions were relaxed. The nuclear reactor can provide sufficient extra power to operate a closed cycle turbine-generator unit, as was generally considered for nuclear thermal rocket vehicles requiring more than 10kW of electric power [Hesse and Mumford 1964] although this is relegated to follow-on studies.

7. MISSION ANALYSIS

7.1 Flight from Earth to Jupiter

Nuclear propulsion offers the opportunity to dramatically increase the capability for planetary science and exploration, compared with now available using chemical rockets. In nuclear thermal propulsion (NTP), a reactor heats hydrogen propellant to high temperatures, e.g., up to ~3000 K in some designs. The combination of low molecular weight and high temperature results in a specific that approaches 1000 seconds – over twice the ~450 seconds achieved by the best chemical propellant, hydrogen/oxygen. The high specific impulse and high thrust capability of NTP enables spacecraft ΔVs that are over twice that from chemical rockets. This enhanced ΔV

capability can allow much shorter trip times to the outer planets, elimination of the need for planetary gravity assists, and the use of smaller, lower cost launch vehicles. Accordingly, for the Jupiter Ramjet Flyer mission, nuclear thermal propulsion (NTP) appears to be the best and probably only choice for a robust exploration program.

An initial parametric analysis of the entire mission design was completed for the Jupiter Ramjet Flyer/Orbiter spacecraft. The mission design analysis was focused on framing the envelope for the many parameters and factors that influence the overall spacecraft and mission designs. The launch vehicle selection parameter is dictated not by its payload-lifting capability, but by the payload fairing volume of the booster. This is due to the nature of nuclear thermal propulsion (NTP) systems, which utilize low-density hydrogen propellant exclusively. NTP vehicles require five times the tank volume of chemical systems for the same propellant loading, resulting in decreased mass efficiency. The Jupiter Ramjet Flyer mission considered in this analysis is restricted to starting from LEO only after being placed in a stable orbit by a chemically powered launch vehicle. This simplifies and eases the safety issues and mitigates political concerns.

The Jupiter Flyer Mission falls into the category of orbital capture missions, which require additional propellant, as compared to fly-by missions. The MULIMP trajectory code was used to calculate IMLEOs for a 2009 Earth departure opportunity. No gravitational assists were employed in this analysis. The spacecraft payload is set to 800 kg for Jupiter Ramjet Flyer/Thermal Shield/Orbiter configuration. Mission durations analyzed have two and three-year time-of-flight (TOF) outbound direct trajectories.

Because orbital capture missions must perform multiple burns, they require long-term storage of propellant. Since nuclear and solar propellant heating both would act to boil-off this stored propellant, mitigation strategies include tank insulation, use of slush hydrogen, and active refrigeration. The system weight of the MITEE engine(LEO to Jupiter rocket) is estimated at 300 kg. IMLEO optimization studies resulted in a single-stage vehicle configuration with two propellant tanks. The first propellant tank, used for Earth departure, is a disposable lightweight tank of 10% tankage fraction that is jettisoned after the burn is completed. The single stage is powered by 900 sec Isp MITEE engine with restart capability. The second propellant tank also has a 10% tankage fraction, and is used for the Jovian system insertion burn and subsequent orbital capture at Jupiter. Adding restart capability to the MITEE engine, required in increased design margins requirements and decay heat removal capability. This, is effect, would result in lowering the Isp to 900 sec instead of MITEE's 1000 sec Isp design parameter value.

The decay heating rate after engine firing is sufficient for core meltdown if cooling flow is not provided. The required cooldown propellant is typically an appreciable fraction of the impulse propellant and does amount to extra propellant loading that adds to the MITEE engine system weight. For these reasons, for the two-propellant tank vehicle configuration is chosen where the first stage MITEE engine used for an Earth departure burn consumes the first propellant tank fuel and the empty tank is subsequently jettisoned. This ensures that the Jupiter capture propellant tank is full for the interplanetary coast and eliminates the issues of a partially full propellant tank.

Another factor that affects the ΔV and subsequently the Initial Mass in Low Earth Orbit (IMLEO) is the orbit height above Jupiter (in body radii) where the orbital capture burn is performed. Jupiter body radii of 5, 10, and 20 are used in the IMLEO calculations. IMLEO is estimated for an orbital capture at 10 body radii to be approximately 6,200 kg for the NTP system and 50,000 kg for the chemical propulsion system (currently no launcher large enough to lift 50 metric tons to LEO exists). Results are illustrated in Figure 6.1.

The NTP option results are volumetrically small enough to be housed inside the fairing of a Delta III launcher. The Delta III booster is the newest and most powerful version of the Delta family of medium capacity expendable launch vehicles. The Delta III can provide a payload lift capability of 18,400 pounds to low-Earth orbit and 8,400 pounds to geo-synchronous transfer orbit. Launch costs are in the $80 - $100 million range.

If the time-of-flight is increased to three years, then the IMLEO for the chemical option at a 20 body radii orbital capture decreases to 29,000 kg, which is at the limit of or beyond the capabilities of the heaviest launch vehicles in service today such as the Space Shuttle or the Titan-IVB.

For further study in IMLEO reduction, other mission designs to be analyzed include releasing the Jupiter Ramjet Flyer into the Jovian atmosphere for a ballistic-type re-entry (similar to Galileo) and having only the orbiter mass of approximately 250 kg involved in the orbital capture burn at Jupiter. In addition, instead of achieving circular orbits after the capture burn, IMLEO can be reduced by achieving highly elliptic orbits about Jupiter due to the lower ΔV requirements of the elliptic orbits. For example, a two-year TOF and an elliptical orbital capture, where the eccentricity is 0.60, IMLEO is further reduced to 4,100 kg for an NTP system and 19,000 kg for a chemical rocket.

The propulsion requirements for Jupiter orbital insertion can be further reduced so that the spacecraft size matches the payload volume limitations of the Delta II or Atlas IIAS. Therefore, a possibly more desirable approach to reduce IMLEO would be to launch direct to Jupiter, insert into the Jovian orbit, and then use the Jovian satellites to pump the spacecraft orbit down using gravitational assists to where the Europan orbit insertion and subsequent landing allows for optimum propulsion requirements. The proposed baseline schedule has the REE spacecraft launching in December 2009 on a direct trajectory to Jupiter. These trajectories are available every 13 months and result in a flight time of 2 years using MITEE. As the spacecraft approaches Jupiter, a flyby of one of Jupiter's moons, Ganymede, is used to lower the arrival velocity to lower the Jupiter Orbit Insertion (JOI) ΔV. JOI places the spacecraft into a highly elliptic orbit around Jupiter where the Jovian moons are subsequently used to place the spacecraft into circular orbit around Jupiter. The main design factor for the Jovian tour is to minimize the spacecraft Initial Mass in Low Earth Orbit (IMLEO) by minimizing the ΔV or propellant requirement by using as much natural or potential energy in the form of gravitational assists as possible.

7.2 Jovian Entry and Commencement of Powered Flight

It is proposed that the ramjet flyer will enter the Jovian atmosphere in a lenticular capsule similar to the one which transported the Galileo probe. To accommodate the 2 meter long and 2 meter wingspan vehicle, the diameter of the capsule will have to be about 2.5 meters. This makes it twice the diameter of the Galileo entry capsule. As in the case of the Galileo probe, the mass of the thermal shield is expected to be comparable to the mass of the payload. Thus, the total mass of our entry vehicle will be approximately 500 kg. While larger than the Galileo probe, it is not prohibitively massive. (With the relay satellite included the mass is 800 kg.)

A possible separation scenario is illustrated in Figure 7.2.1. The capsule enters the Jovian atmosphere in the conventional manner, i.e., with the thermally protected blunt end forward [see Figure 7.2.1 (a)]. It will remain in this orientation during the severe aerodynamic heating and deceleration phase. When the capsule has decelerated to a Mach number somewhat higher than its intended cruising speed, a small drogue parachute is ejected from the side of the capsule nearest the aft end of the flyer. This action will rotate the capsule 90 degrees so that the front end of the flyer points downward [see Figure 7.2.1(b)]. After a few oscillations, the capsule will assume a steady orientation as shown in the diagram. At this point the two halves of the capsule will separate, by means of small explosive charges [see Figure 7.2.1(c)], and the ramjet flyer will be exposed to the free stream conditions at its cruising Mach number. At this point, the control rods in the nuclear engine will be rotated, starting the fission and the heat production. Using the horizontal control surfaces the flyer will be maneuvered out of the dive into level flight to commence its mapping mission.

8. SCIENTIFIC EXPLORATION OF JUPITER

8.1 Past Missions

Primary spacecraft missions to Jupiter include the Pioneer and Voyager flybys and the Galileo orbiter. Because it has the most modern detectors, the highest quality remote-sensing data come from the Cassini Saturn-Titan Mission flyby in December 2000, but the Galileo Orbiter provides the longest spacecraft baseline.

There has been only one probe sent into Jupiter's atmosphere, the Galileo Probe; everything else known about the planet is inferred from remote sensing. Before the Galileo Probe, the vertical structure of Jupiter's atmosphere was determined reliably down to 1 bar by modeling the attenuation of spacecraft radio signals as they passed behind the planet. The Galileo Probe directly measured the atmospheric structure down to 20 bars at one horizontal position [Seiff 1997, seiff 1999], as shown in Figure 8.1. The Probe entry site turned out to be the southern rim of a 5-μm hot spot (a long-lived hole in the clouds that appears bright at infrared wavelengths centered at 5 μm).

Doppler tracking of the Galileo Probe [Atkinson, 1998] provided one of the most interesting results from the Galileo Mission, namely that the zonal (east-west) wind speed increases

significantly with depth down to about 4 bars and then becomes relatively constant. This vertical wind shear occurs in the region referred to as the radiative boundary layer. Fortuitously, Jupiter's radiative boundary layer coincides with the altitude range of the ramjet.

Modeling of hot spots [Showman 2000] suggests that the vertical wind shear seen by the Galileo Probe may only be associated with the southern rim of hot spots, and not the planet as a whole or even the 7^0N entry latitude. In particular, the model predicts that the opposite sign of shear (winds decreasing with depth) should occur on the northern rim of hot spots, and that away from the hot spots the vertical shear may be significantly weaker than inside them.

Another significant result to come from the Galileo Probe is that hot spots are not only cloud free, but also extremely dry (cloud free only implies a relative humidity less than 100%), with trace chemical species arranged in the expected order but deflected significantly downward into the planet. The current best hypothesis is that the hot spots are the troughs of large-amplitude waves [Showman, 2000].

The scientific importance of being able to sample the dynamics and chemistry of Jupiter's radiative boundary layer in situ across multiple latitudes with the ramjet cannot be overstated. Balloons have been successfully deployed into the Venusian atmosphere (the Russian-French VEGA mission), but they are a near impossibility in the hydrogen-helium atmosphere of Jupiter. However, the ramjet can be used to observe the vertical shear versus latitude for the entire planet, and correlate this with the horizontal shear, in particular the difference between cyclonic and anticyclonic regions. The ramjet can map the heterogeneity of the clouds, compare with the Galileo Probe results, fly multiple chords through long-lived structures like the Great Red Spot, hot spots, and cyclonic regions, and fly between eddies to establish background conditions.

An important practical advantage of the ramjet is that it can be steered clear of Jupiter's potentially hazardous regions at the start of the mission and then undertake higher-risk flight paths in later circumnavigations. Potentially risky paths include flying through tropospheric regions with active moist convection, and underneath stratospheric high-energy areas like the Io footprint (and other satellite footprints where the strong currents connected to the satellites enter the atmosphere) and the polar aurora. One of the most powerful observational techniques used by terrestrial meteorologists who study hurricanes is to drop small probes into the storms from airplanes. Figure 8.2 shows the belly pod of the NASA ER-2 with 16 dropsondes as it was configured for the 4^{th} Convection and Moisture Experiment (CAMEX-4) in Summer 2001. These dropsondes (sondes) were 0.39 kg in mass, 40 cm in length, and 7 cm in diameter. New sondes are under development that will be 0.2 kg in mass, 20 cm in length, and 4-5 cm in diameter. The sondes return temperature, pressure, and relative humidity. They also each carry a GPS receiver to determine winds speeds, but Jupiter sondes will not have this component, which will free up a substantial amount of mass and power (line-of-sight speed will be determined by Doppler tracking).

8.2 Science Goals

8.2.1 Atmospheric Chemistry

The photochemistry of Jupiter's stratosphere is better understood than the tropospheric chemistry, chiefly because the stratosphere is in view whereas much of the troposphere is hidden beneath the ammonia cloud tops, which are at about 670 mb. The following is a list of top open questions in Jovian tropospheric chemistry that can be addressed by the ramjet. First, the N/H and O/H ratios can be established, which bear on the origin and evolution of the atmosphere. Second, the NH_3 mixing ratio versus altitude can be mapped; currently the Galileo Probe, Galileo Orbiter, and Earth-based data all give different results. Third, the location and molecular form of sulfur can be established. Fourth, still unknown is the composition of the cloud chromophores (the chemicals that make the Great Red Spot red), but they may be established from in situ observations. Fifth, there are conflicting reports on the abundances of hydrocarbons in the upper troposphere. Sixth, both N_2H_4 and N_2 are predicted to be endpoints of NH_3 chemistry, but have not yet been observed. The primary instrument needed to answer all these questions is a gas chromatograph mass spectrometer (GCMS).

8.2.2 Atmospheric Dynamics

The optimal strategy for studying atmospheric dynamics with the ramjet is to fly across as many latitudes as possible. There is no other platform that can compete with this capability. Given the strong vertical shear discovered by the Galileo probe in the 0.5 - 4 bar range, the establishment of the vertical shear as a function of position, especially how it correlates with horizontal shear (cyclonic versus anticyclonic), is fundamental. Also important is to establish thermodynamical parameters and composition, most especially maps of the relative humidity of H_2O, but also NH_3, H_2S, PH_3, GeH_4, and HCl.

A major result from the Galileo Orbiter is strong evidence that the large convective bursts seen in localized areas on Jupiter, most notably to the northwest of the Great Red Spot, are the tops of enormous water-cloud thunderstorms that rise from about 5 bar up through the ammonia clouds to nearly the tropopause at 100 mbar. The Galileo data also show that Jupiter's lightning is coincident with these areas of active moist convection. A current idea put forward by the Galileo team (Ingersoll, Gierasch, et al) is that these thunderstorms are the means by which the planet's internal energy is transferred into the visible atmosphere, ultimately driving the alternating jets and maintaining the long-lived vortices.

Another important topic that can be addressed uniquely by the ramjet is the nature of eddy fluctuations and turbulence, which the ramjet can sample when parked (flown in a tight loop). Accelerometers and a clear-air turbulence (CAT) scanner can be used to make turbulence measurements. Also, the three-dimensional structure of the clouds can be determined from a stereo imaging system. (Note: Jim Powell pointed out that there is the possibility of using a neutron-beam from the ramjet's nuclear reactor to do significant remote sensing from the ramjet itself without increasing the payload).

8.2.3 Electromagnetism

Jupiter's magnetosphere is reasonably modeled by a tilted-dipole model that is similar to the one used to describe the terrestrial magnetic field (with the sense of north and south reversed from Earth's current configuration). This means that a magnetic compass will be a primary navigational instrument on the ramjet, just as it is on terrestrial jets. But it is the higher-order moments that are most interesting scientifically. By mapping these in the 4-15 Gauss range over several different great circles around the planet, the ramjet observations can illuminate the interior structure of Jupiter in a potentially significant way.

Much of the activity in Jupiter's atmosphere that is connected to its magnetosphere occurs in the upper stratosphere in the polar regions. The ramjet can be flown underneath the active polar auroral areas, and its precise navigational abilities can be used to target the relatively small, but extremely energetic, satellite footprints. The heightened magnetic activity in the stratosphere is expected to have an effect on the chemistry in the altitude range where the ramjet flies. The ramjet can also carry a lightning detector to map electromagnetic storms seated in the troposphere.

8.3 Ramjet Strawman Payload

Table 8.3.1 shows the major instruments needed to accomplish the scientific goals outlined above. Mass and power requirements tend to decrease with time, which will be beneficial to the ultimate ramjet design.

Table 8.3.1 Ramjet strawman payload

Instrument	Acronym	Location	Mass (kg)	Pwr (W)	Purpose
Gas chromatograph/ Mass spectrometer	CGMS	Inlet spike	14	20	Gas composition
Atmospheric structure instrument	ASI	Mast	4	5	T, p, ρ, μ; planet atmospheric dynamics
Magnetometer	MAG	Mast	4	16	Magnetic field; planet interior
Clear air turbulence scanner	CAT	Mast	11	80	Atmospheric dynamics
Stereo Imaging system	SIS	Wing tips	1	10	Visual images of clouds
Lightning/Energetic particles	LEP	Inlet spike	3	3	Electromagnetics Rad. environment

Dropsondes	SONDES	Ejected from side of mast	ε (Passive) 0.4 (Instrented)	9v bat	Atm. dynamics

A major goal is to be able to fit all the instruments inside the inlet centerbody and wing mast without the need for the wing pods considered in the Phase I report, because aerodynamic studies have revealed that such pods dominate the drag more than is desirable. Thus, we proceed under the assumption that the instruments all have a height of 4 cm or less. Consider that this is two laptops in thickness. We identify the goal of placing all the instruments inside the inlet centerbody and mast as an enabling technology that is realistic.

The laser (lidar) system needed for the clear-air turbulence scanner (CAT scanner), which will provide both valuable control-and-stability information and new science, may require the most power of all the instruments, and a large share of the mass. Thus, outfitting a CAT scanner for the ramjet may require some enabling technology. The mass and power specifications for the CAT scanner in Table 2 are very approximate.

The only two instruments that are especially sensitive to the radioactive environment of the ramjet's nuclear-fission engine are the GCMS and the energetic-particle detector of the LEP. These both may require enabling technology to harden against radiation. Care must also be taken to design the inlet to the GCMS to minimize the effects of the supersonic slipstream on chemistry and composition. The inlet may best be placed on the wing end.

8.4 Flight Trajectories

Circumnavigation 1 **-** The ramjet will most likely enter Jupiter's atmosphere near the equator, just as did the Galileo Probe. The first circumnavigation should start with a parked (tight-circle) position at the entry point to allow tests of the navigation and control systems, followed by an immediate northward heading. The ramjet should be steered in between hot spots on the first pass to avoid any large-amplitude fluctuations and to establish the background, and generally be steered clear of organized storms. Its altitude should be near the tropopause to limit turbulence, or the quietest altitude it encounters in this regard. A dropsonde should be deployed at the centers of an eastward and a westward midlatitude jet (1 and 2 of 6), and at a point where the wind speed is near zero (measured in System III, that is, relative to the magnetic-field rotation rate). In the north-polar region, the ramjet should be steered clear of active auroral regions and satellite footprints, again to establish the background and maximize safety.

A dropsonde (3/6) should be deployed near the north pole, and then the ramjet should start south again, this time targeting the center of an anticyclone and the center of a cyclone. As the ramjet approaches the equatorial regions it should be aimed for the center of a hotspot to maximize comparison with the Galileo Probe entry site, dropping a sonde (4/6) on the northern rim. Parking positions should be maintained at intervals to establish eddy fluctuations as the ramjet cuts through many latitudes.

As the ramjet passes to the southern hemisphere, it should be aimed for a long sortie in the vicinity of the Great Red Spot (GRS). Sondes 5 and 6/6 should be deployed in the center and edge of the GRS, completing the dropsonde experiments.

Circumnavigations 2-4 and Beyond - To maximize the magnetic-field mapping, the ramjet should be made to perform great circles that are optimized based on the best sampling model for determining higher-order moments. In addition, the high and low altitude operating envelope should be pushed to maximize the atmospheric chemistry scientific return. Details of later circumnavigations should be left open so that the data and lessons learned from the first pass can be fully incorporated into the flight plan.

We can anticipate that mission planning and execution for the ramjet trajectory will capture the attention of the world, based on the fascination the public and media gave during the Mars Pathfinder mission.

9. DEVELOPMENT PLAN AND COST

9.1 MITEE Ramjet Engine Development

Figure 9.1.1 shows an overall roadmap for the development of the MITEE nuclear ramjet engine. Three development phases are contemplated:

Phase 1: Testing of separate engine components
Phase 2: Testing of partially integrated engine systems
Phase 3: Testing of fully integrated engine under simulated flight conditions

There is no way to test the MITEE ramjet engine under actual flight conditions on Earth, so that the first operation of the the engine in an actual H_2/He atmospheres will have to be during the Jupiter mission. However, with careful and detailed testing of its individual components and systems, the engine engine should perform as expected during its mission.

During Phase 1, most of the development and testing would be concentrated in three areas:

A. Nuclear fuel temperature and burnup durability
B. Thermal/hydraulics and power output capability of the MITEE fuel elements
C. Neutronic design of the MITEE reactor

In area A, tungsten/UO_2 fuel would be tested at 1500 K for long periods (months) in flowing H_2/He to determine if the cermet corroded or degraded with respect to potential loss of UO2 content, mechanical strength, cracking, etc. These tests would be carried out using non-nuclear, electrically heated cermet fuel sheets. The results would be as valid as actual nuclear tests, and could be carried out much quicker and at much lower cost. The fuel sheets would be thermally

cycled in addition to long duration tests at constant temperature, to determine if thermal cycling degraded performance.

In addition to H_2 testing, samples of W/UO_2 cermet fuel sheets would be tested in a nuclear reactor at temperature for neutron fluxes, exposure times, and fissile fuel burnups that are representative of operating conditions for the actual Jupiter ramjet. The combination of the non-nuclear H_2 exposure and in-reactor burnup tests will demonstrate the time-temperature-neutron exposure capability of the W/UO_2 cermet fuel for the Jupiter flyer.

In area B, thermal/hydraulic testing would be carried out on full size MITEE ramjet elements using electrically heated metal sheets in place of nuclear heating. The thermal/hydraulics of the fuel elements could be fully tested under the operating conditions anticipated on Jupiter, including H2/He inlet temperature and pressure, outlet H2/He temperature, and projected power densities in the fuel region. The pressure drop across the element could be determined together with the temperature distribution inside the fuel element.

In area C, detailed neutronic designs of the ramjet reactor would continue, with the addition of burnup calculations to determine the effects of fission product buildup and fissile fuel depletion on the criticality constant and the local power density in the reactor. These analyses will help to determine what the limit on operational time is from the reactor neutronics perspective.

Additional reactor-related tests in phase 1 would include design studies of the reactor control system, analyses of transient power and temperature effects during reactor startup including xenon buildup, methods of matching local coolant flow to the local power distribution, reactivity Temperature coefficient, etc. Detailed study of these and other issues is necessary in order to arrive at a final engineering design.

Phase 1 is estimated to take 3 years, and would cost approximately $100 million. At the end of Phase 1, the various tests and analyses would provide sufficient information to proceed with the construction of a test reactor in Phase 2.

Phase 2 would take 3 years at a projected cost of approximately 300 million dollars. The principal tasks in Phase 2 would be:

1. Nuclear testing of a full size single prototype element of the ramjet engine at projected operating conditions in an existing reactor. The nominal power output of the element would be approximately 300 kW(th), and would require a h2/He flow loop capable of handling the required coolant flow rate at the anticipated inlet and outlet temperatures and pressures. A steady flow test loop circuit would be preferable, e.g., a loop at the Advanced Test Reactor (ATR) at INEL, or in a Russian test reactor. If such a loop were not possible, however, transient testing in a pulsed reactor, such as TREAT in the US, or IGOR in Kazakhstan would be acceptable. The tests would provide benchmark validation of the thermal/hydraulic and neutronic codes used to predict the performance of the elements in the ramjet engine. It would not be necessary to operate the element for long periods, since the burnup performance and the cermet fuel and the

steady-state thermal/hydraulic performance of the element would have been demonstrated in the Phase 1.

2. Neutronic tests of low-power actual assemblies that duplicated the configuration and nuclear design of the ramjet engine. These would not require a H2 flow loop, but simply would validate the detailed 3-D Monte Carlo neutronic analyses with regard to criticality constant, 3-D power distribution, moderator and temperature coefficients, control rod worth, etc. The effects of burnup and fission product buildup could also be verified by critical assembly tests using cermet fuel that simulated the U-235 depletion and fission product buildup as a function of operational time. The results from the critical assembly tests would be benchmarks that would validate the neutronic analyses carried out in Phase 1.

3. Construction of a closed cycle H2/He flow loop that would duplicate the coolant flow conditions encountered by the ramjet engine on Jupiter. This flow loop would be capable of handling the full anticipated operating power of the engine, e.g., on the order of 10 MW(th), and would have cleaning filters and absorbers to trap any radioactive releases, whether particular or gaseous in nature. Clearly, such a loop would have to be built in an existing nuclear facility at a national laboratory in the US, or some facility in Russia.

4, In conjunction with the H2/He flow loop facility built in Task 3 above, a full-up ramjet reactor engine would be constructed and integrated into the H2/He flow loop. The ramjet reactor and flow loop would be fully shielded and contained so that no radioactivity could be released to the environment. Initial low power critical reactor tests and cold flow tests would be carried out to verify operational capabilities, but full power, hot flow testing would not be carried out until Phase 3.

Phase 3 would involve full power, hot flow testing of the H2/He flow loop and the full-up ramjet reactor. The Phase 3 testing period would be 2 years, with a cost of approximately 200 million dollars. Assuming initial results were favorable, a decision to proceed with the Jupiter Flyer mission could start after 1 year of testing in Phase 3. The remainder of Phase 3 testing period would be used to verify the full range of operating conditions, e.g., equivalent Mach number and ambient pressure level anticipated for operation on Jupiter. Among the data taken would be pressure drop across the reactor core, local fuel and coolant temperature distributions in the reactor as a function of inlet temperature and pressure, and outlet temperature, moderator temperature distributions, etc.

The total development time for the three-phase reactor program is 8 years, with a total cost of 600 million dollars. To this must be added the development cost of for the airframe, control devices, scientific payload, system integration, and mission planning. The development costs would be allocated to multiple missions, however, since the same Ramjet Flyer could be used for exploring the atmospheres of the other giant planets, i.e., Saturn, Uranus, and Neptune. Spread out over the gas giants, the reactor development cost per mission would be $150 million.

10. CONCLUSIONS

1. The proposed Nuclear Ramjet flyer system permits detailed mapping of the Jovian atmosphere spatially as well as temporally. The flyer will operate for months to collect enormous amounts of data. To date, no issues have emerged which would make the concept unworkable.

2. The nuclear reactor design best suited for ramjet application is a modified version of the compact ultra-light MITEE nuclear rocket engine, initially proposed for robotic exploration of the solar system.

3. The nuclear engine best suited for the powering the ramjet flyer has the following characteristics: a) the fuel form is cermet sheets impregnated with UO_2 particles, a) the moderator is 7LiH, c) the propellant flows through the core (open cycle), and d) the flow direction through the annular fuel sheets is from inside out (opposite of the rocket version of MITEE). The total mass of the engine is 160 kg.

4. The ramjet flyer will operate at Mach 3, the optimum speed for a nuclear ramjet.

5. Based on aerodynamic and stability considerations, the flyer configuration which evolved has a delta wing lifting surface, canted control surfaces (to provide control in pitch, roll and yaw modes), and a spike ramjet inlet. The inlet spike contains the radiation-sensitive instruments. It is the optimum location for effective radiation shielding (from the engine).

6. The development cost of the nuclear ramjet engine is estimated at $600 million. (This is not the total mission cost.) The engine development time is 8 years.

7. The Jupiter Flyer, once developed, can also be used to explore the atmospheres of Saturn, Uranus, Neptune and Titan, thus spreading the development cost over several missions.

REFERENCES

Aichele, J.H., Ed. (1996): *Galileo, The Tour Guide and a Summary of the Mission to Date,* Jet Propulsion Laboratory, JPL D-13554, June 1996.

Argonne National Laboratory (1966): "Nuclear Rocket Program Technical Report." ANL-7236.

Atkinson, DH, Pollack JB, Seiff A. (1998): "The Galileo Probe Doppler wind experiment: Measurement of the deep zonal winds on Jupiter," *JGR*, 103, 22911-22928.

Beebe, R. (1997): *Jupiter, The Giant Planet*, Second Edition, Smithsonian Institution Press, Washington.

Breimeister, J.F., Ed. (1997), "MCNP4B2 ; Monte Carlo N-Particle Transport Code System," Los Alamos National Laboratory, Los Alamos, NM., Report LA-12625-m.

Corning, G. (1960): Supersonic and Subsonic, CTOL and VTOL, Airplane Design, G.Corning,College Park, MD.

Durham, F.P. (1972): "Nuclear Engine Definition Study Preliminary Report, Vol.1, Engine Description," Los Alamos Scientific Informal Report, LA-5044-MS.

Etkin, B. and Reid, L.D. (1996): Dynamics of Flight – Stability and Control, 3rd Edition, Wiley, NY.

Fischer, H.M., et al (1996): "High-Energy Charged Particles in the Innermost Jovian Magnetosphere," *Science*, v. 272, no. 5263, 10 May 1996.

Gierasch, P.J. (1996): Dynamics of the Atmosphere of Jupiter, *Endeavour*, vol. 20, no. 4, p. 144.

Goldin, A.Y., et al (1991): "Development of Nuclear Reactor Engines in the USSR," presented by J.R. Wetch at AIAA/NASA/OAI Conference on SEI Technologies, Cleveland , Ohio, AIAA Paper 191-3648.

Harris, R.V. (1992): "On the Threshold – The Outlook for Supersonic and Hypersonic Aircraft", Journal of Aircraft, Vol. 29, No. 1, Jan.-Feb., pp. 10-19.

Herken, G. (1990): "The Flying Crowbar," *Air & Space Magazine*, vol. 5, no. 1, April/May.

Hesse, W.J. and Mumford, N.V.S. (1964): *Jet Propulsion for Aerospace Applications*, Pitman, NY, NY.

Hoak,D.E., et al (1970): "USAF Stability and Control DATCOM, Flight Control Division, Air Force Flight Dynamics Laboratory, Wright-Patterson AFB, Dayton, OH.

Koenig, D.R. (1986): "Experience Gained from the Space Nuclear Rocket Program (Rover)," LA-10062-H.

Kuchemann, D. (1978): *The Aerodynamic design of Aircraft*, Pergamon Press, Oxford, U.K.

Lemmon, E. W., M.O. McLinden, and M.L. Huber: (2002): REFPROP (Reference Fluid Thermodynamic and Transport Properties) Computer Code, NIST Physical and Chemical Properties Division, Boulder, CO.

Liepmann, H.W. and Roshko, A. (1957): *Elements of Gasdynamics*, John Wiley & Sons, New York.

Ludewig, H., et al (1993): "Design of Particle Bed Reactor for the Space Nuclear Thermal Propulsion Program," Brookhaven National Laborator, BNL 52408.

Ludewig, H., et al (1996): "Design of Particle Bed Reactor for the Space Nuclear Thermal Propulsion Program," *Progress in Nuclear Energy*, Vol. 30, No. 1, pp 1-66.

Mahoney, J.J. (1990): *Inlets for Supersonic Missiles*, AIAA Education Series

Maise, G., et al (2000): "Phase I – Final Report, Exploration of Jovian Atmosphere Using Nuclear Ramjet Flyer," Plus Ultra Technologies Report, PUR-16, November 30, 2000.

Merkle, T.C. (1959): "Nuclear Reactors for Ramjet Propulsion," *Air University Quarterly Review*, Vol. IX, Nos. 3 and 4, Headquarters, Maxwell Air Force Base, Alabama.

Morrison, D. and Owen, T. (1996): *The Planetary System*, Second Edition, Addison-Wesley,Reading, Massachusetts.

Nielsen, J. (1960): *Missile Aerodynamics*, McGraw-Hill, NY.

Powell, J.R. (1988): "Particle Bed Reactor Orbit Transfer Vehicle," Brookhaven National Laboratory, BNL 40497.

Powell, J.R., et al (1998): "MITEE: An Ultra Lightweight Nuclear Enhgine for New and Unique Planetary Science and Exploration Missions," 49th International Astronautical Congress, Paper No. IAF-98-R.1.01, Melbourne, Australia, September 28 – October 2, 1998.

Powell, J.R., et al (1999): "A High Performance Nuclear Thermal Propulsion System for Near Term Exploration Missions to 100 A.U. and Beyond," *Acta Astronautica*, vol. 44, no. 2-4, January-February.

Raymer, D. (1989): Aircraft design, A Conceptual Approach, AIAA, Reston, VA.

Schlicting, H. (1987): Boundary Layer Theory, McGraw-Hill, NY.

Schlicting, H. and Truckenbrodt, E. (1979): Aerodynamics of the Airplane, McGraw-Hill, NY.

Seddon, J. and E.L. Goldsmith (1999): *Intake Aerodynamics, Second Edition*, AIAA Education Series.

Seiff A, Kirk DB, Knight TCD, Young LA, Milos FS, Venkatapathy E, Mihalov JD, Blanchard RC, Young RE, Schubert G. (1997): "Thermal structure of Jupiter's upper atmosphere derived from the Galileo Probe," *Science*, 276, pp. 102-104.

Seiff A, Kirk DB, Mihalov J, Knight TCD (1999): "Further evaluations of waves and turbulence encountered by the Galileo Probe during descent in Jupiter's atmosphere," *Geophys. Res. Let.*, 26, p. 1199.

Shames, I.H. (1962): *Mechanics of Fluids*, McGraw-Hill, New York.

Showman, A, and T. Dowling (2000): "Nonlinear simulations of Jupiter's 5-μm hot Spots,"*Science*, 289, pp.1737—1740.

Torenbeek, E. (1982): Synthesis of Subsonic Airplane Design, Delft University Press, Delft, The Netherlands.

Yeates, C.M., et al (1985): "Galileo: Exploration of Jupiter's System," NASA SP-479.

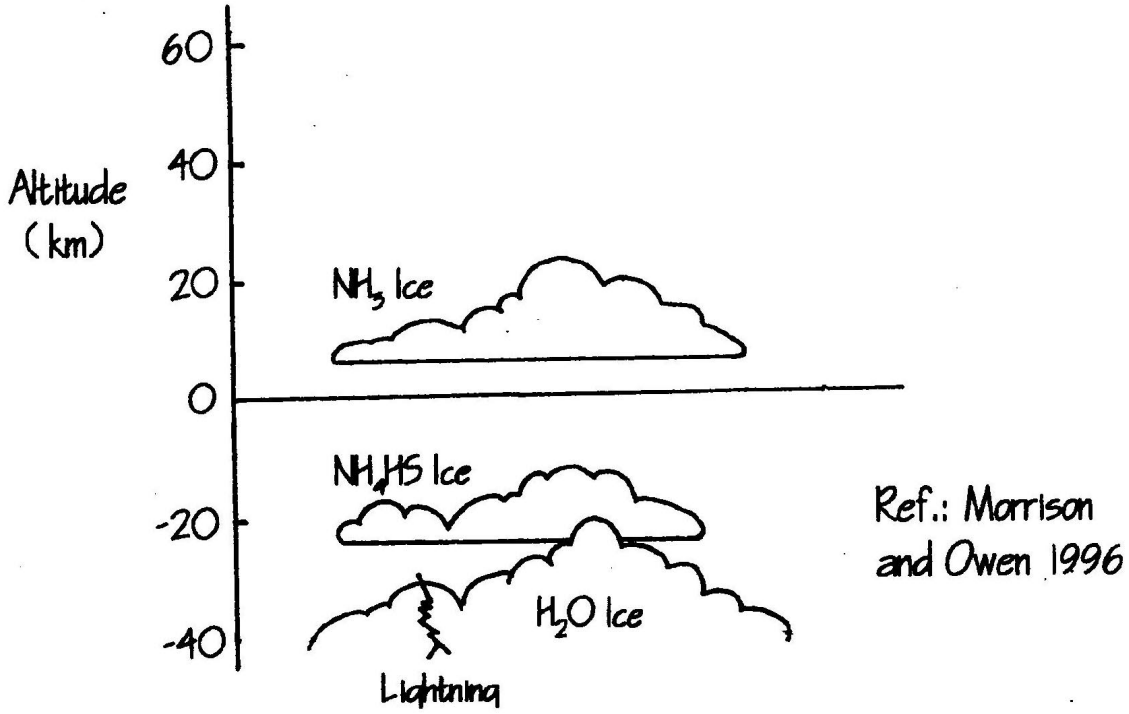
Altitude
(km)
60
40
20
0
-20
-40
NH_3 Ice
NH_4HS Ice
H_2O Ice
Lightning
Ref.: Morrison
and Owen 1996

Figure 3.1 Cloud layers in the upper atmosphere of Jupiter

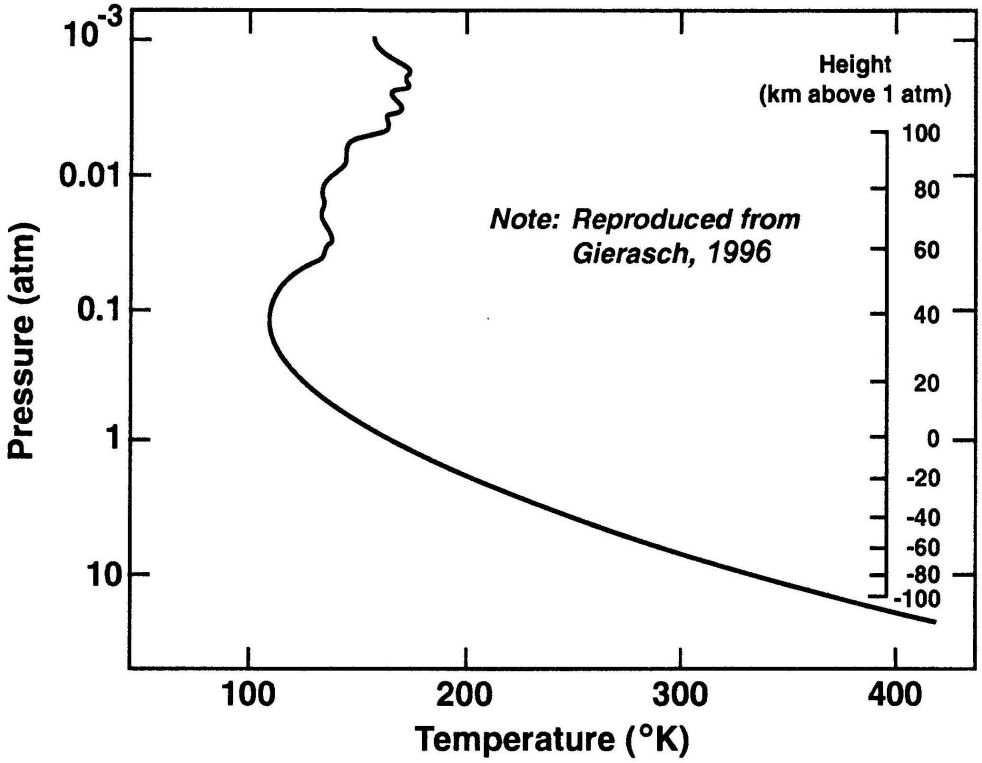

Figure 3.1.1 Temperature variation with ambient pressure in the Jovian Atmosphere

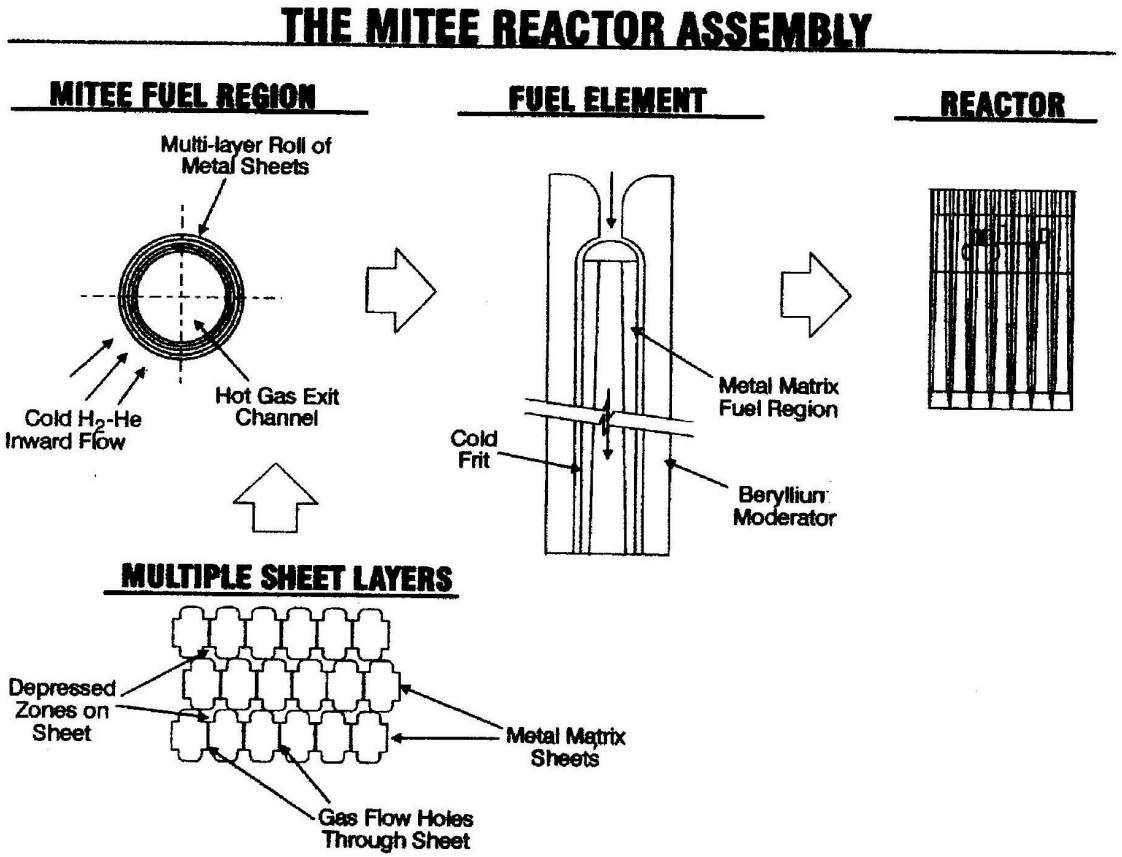

Figure 4.1.1 General Description of MITEE engine

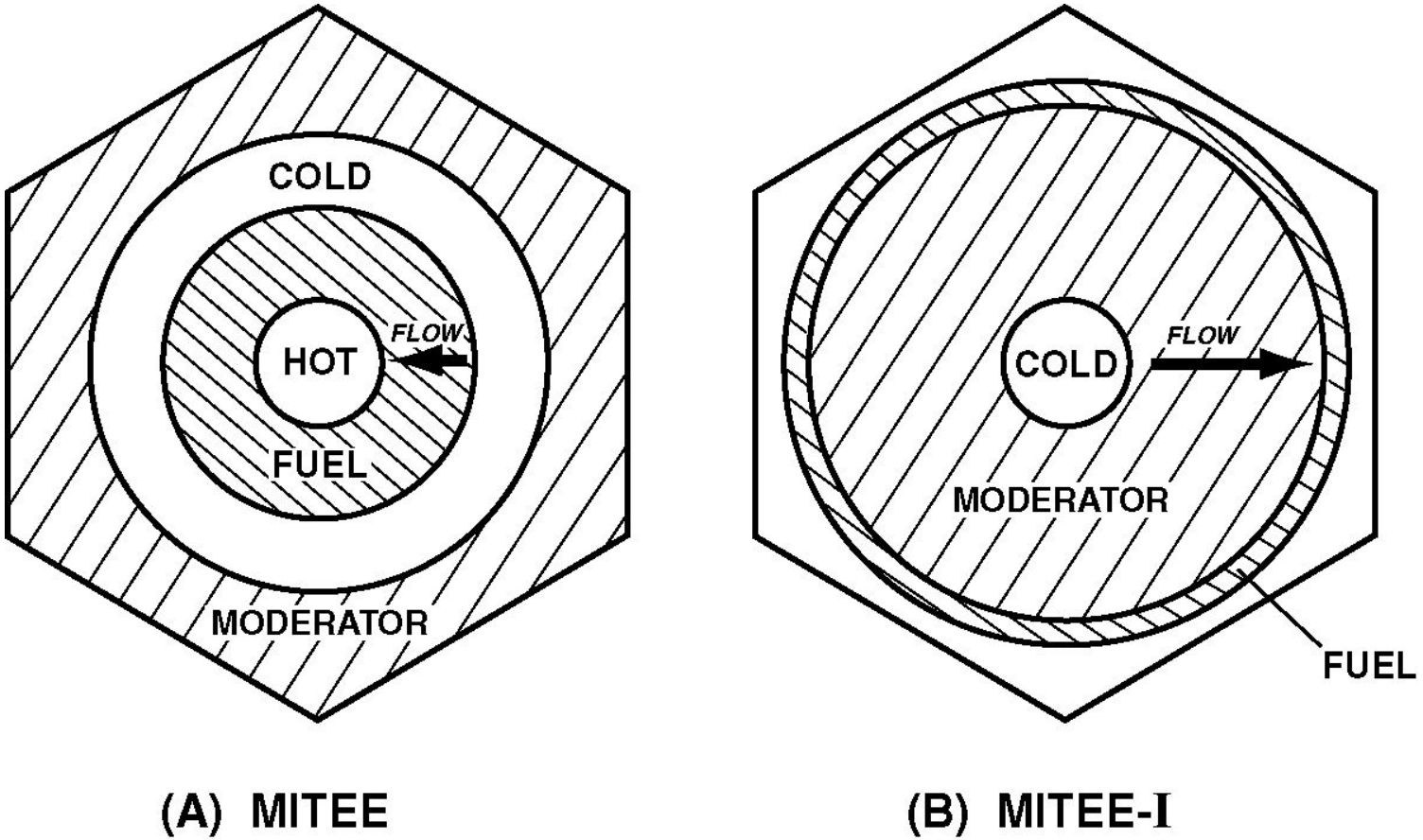

Figure 4.1.2 Comparison of fuel elements: (A) Conventional MITEE, (B) Inverted MITEE

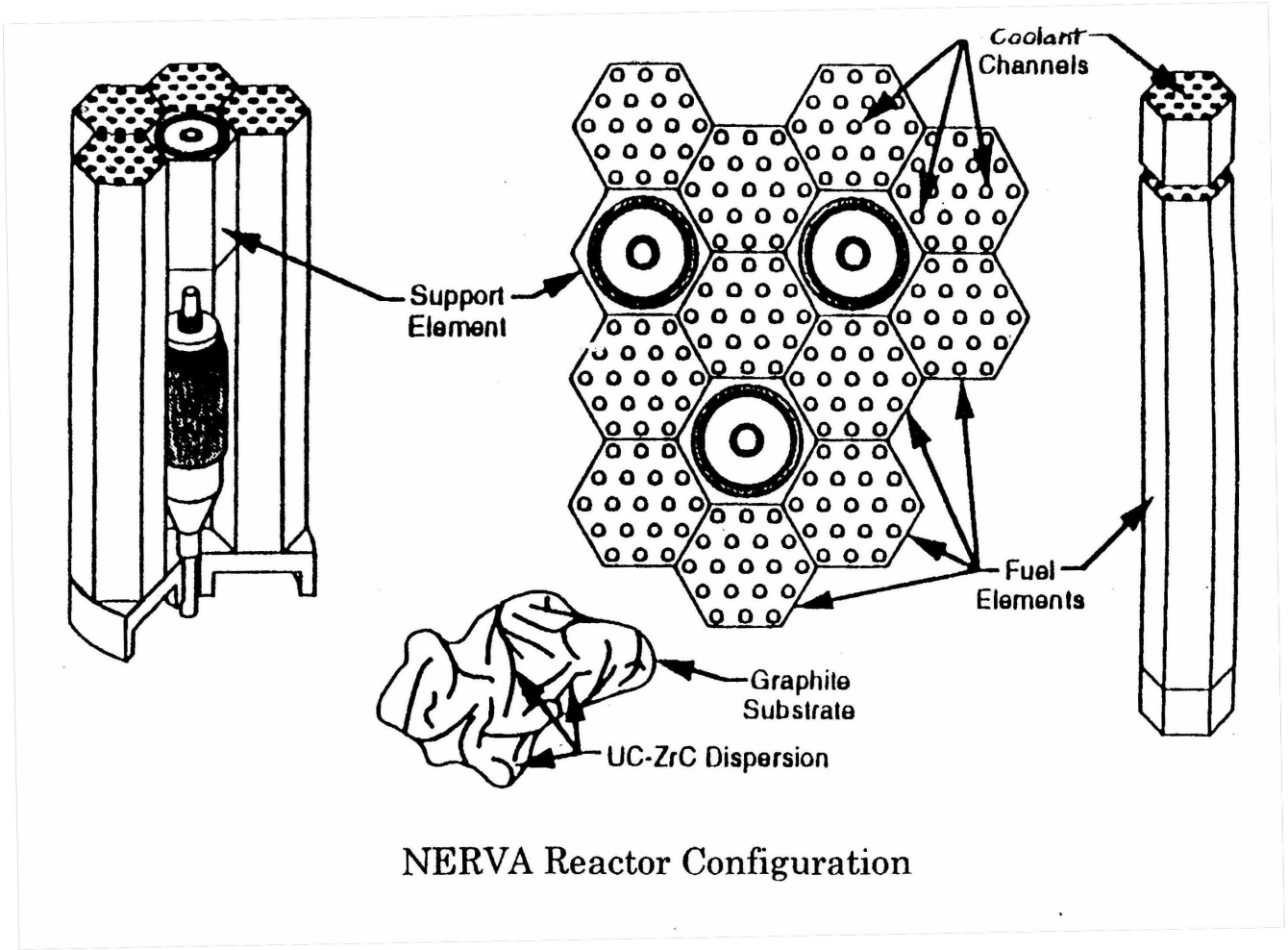

Figure 4.2.1 NERVA reactor configuration

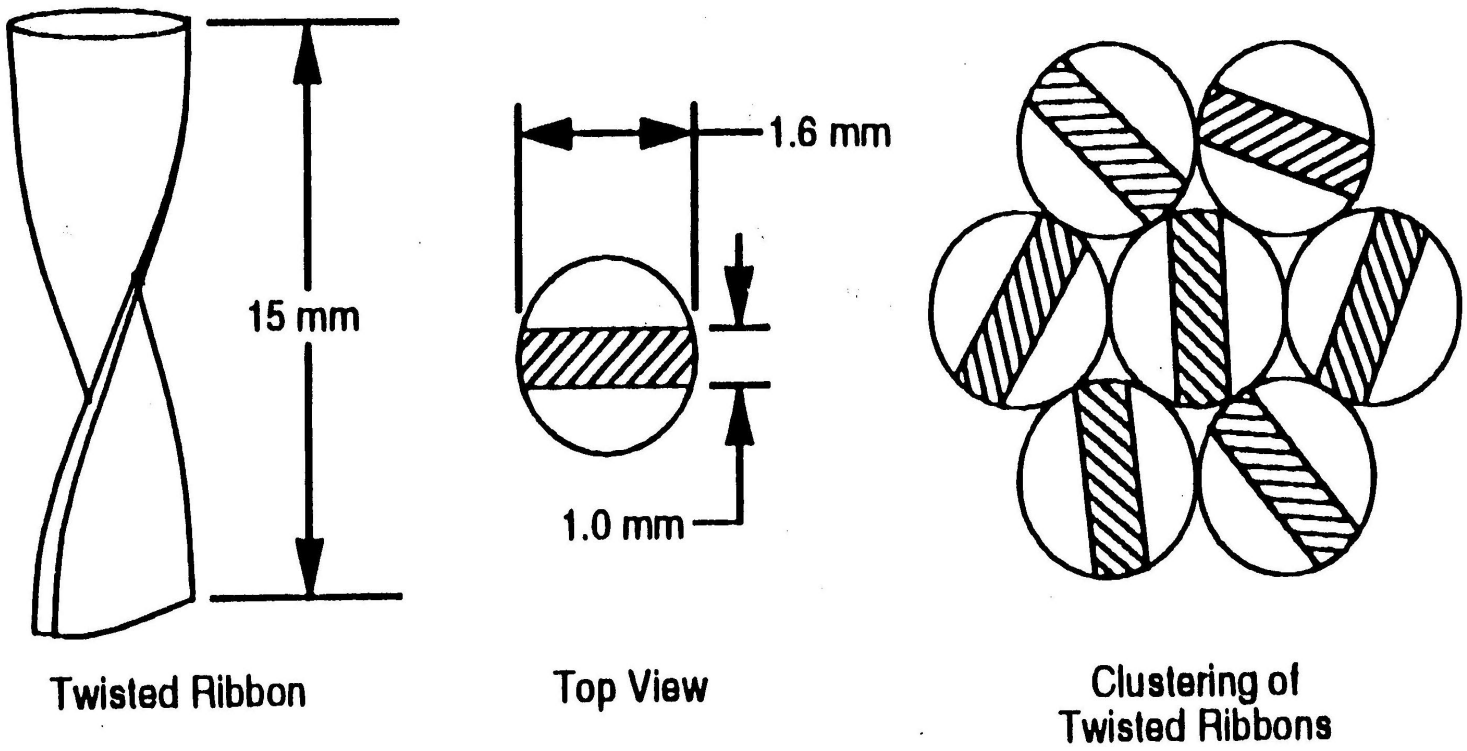

Figure 4.2.2 FSU reactor concept configuration

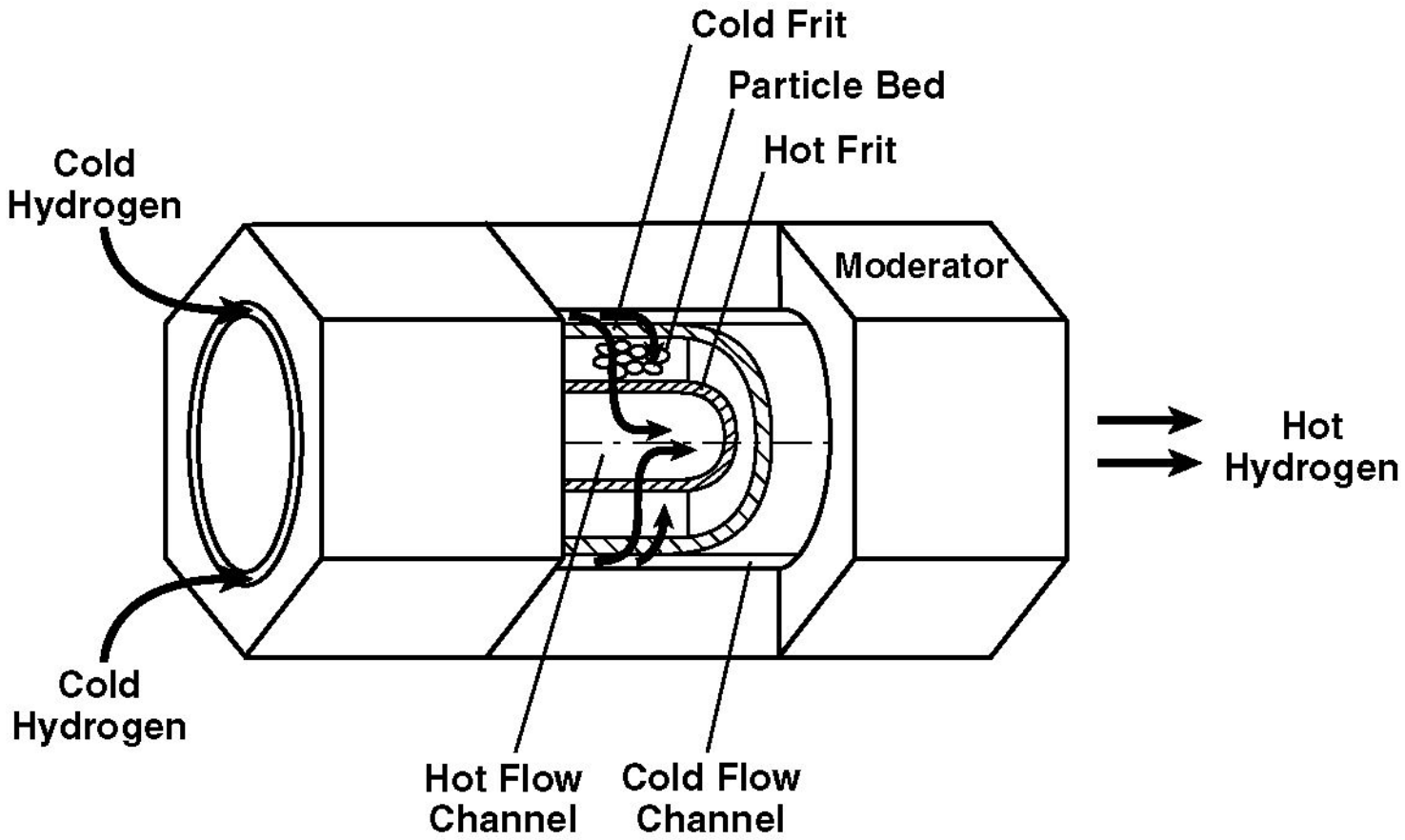

Figure 4.2.3 Particle bed reactor (PBR) fuel element

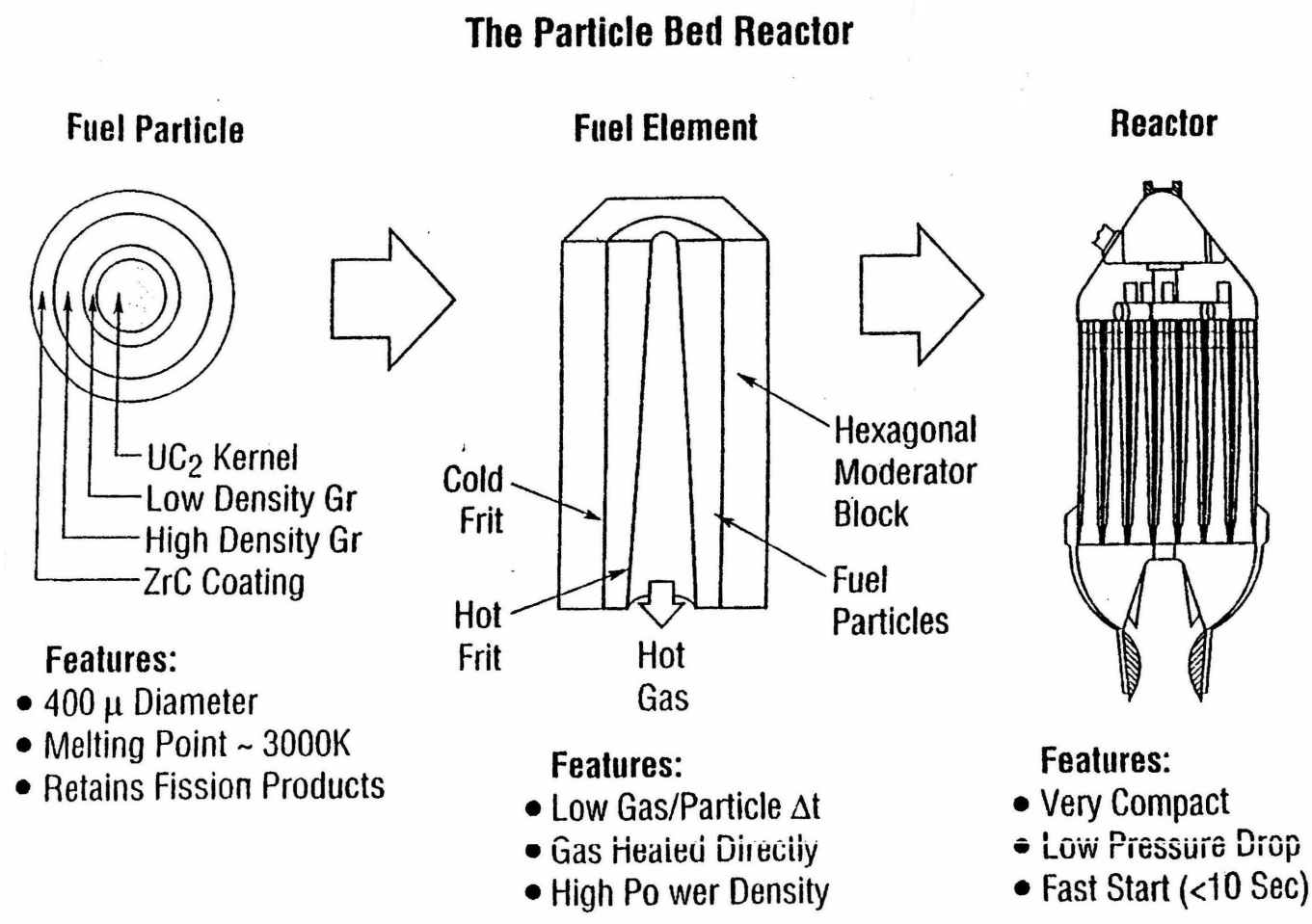

Figure 4.2.4 Particle bed reactor

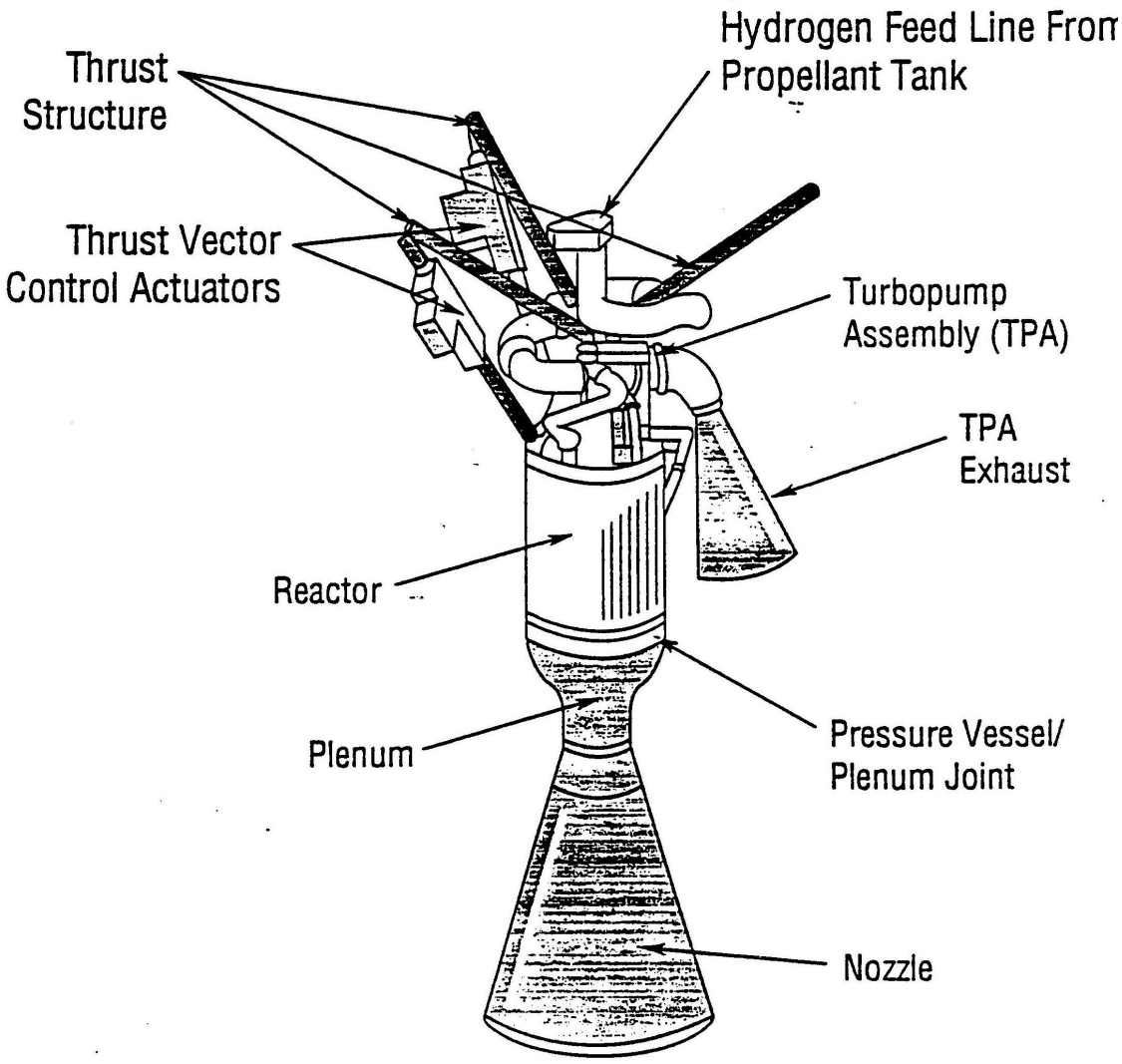

Figure 4.2.5 PBR engine description

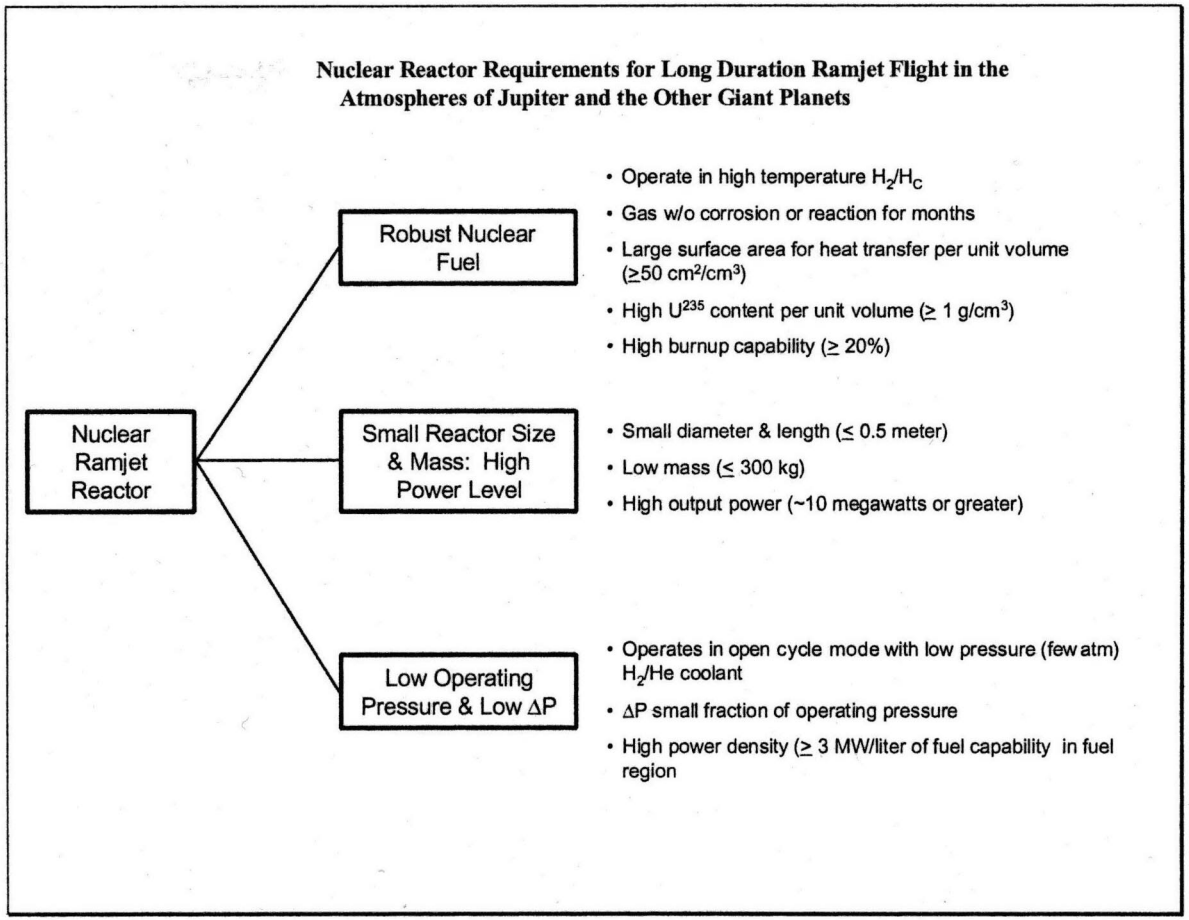

Figure 4.3.1 Nuclear reactor requirements for long duration ramjet flight in the atmospheres of Jupiter and other Giant planets

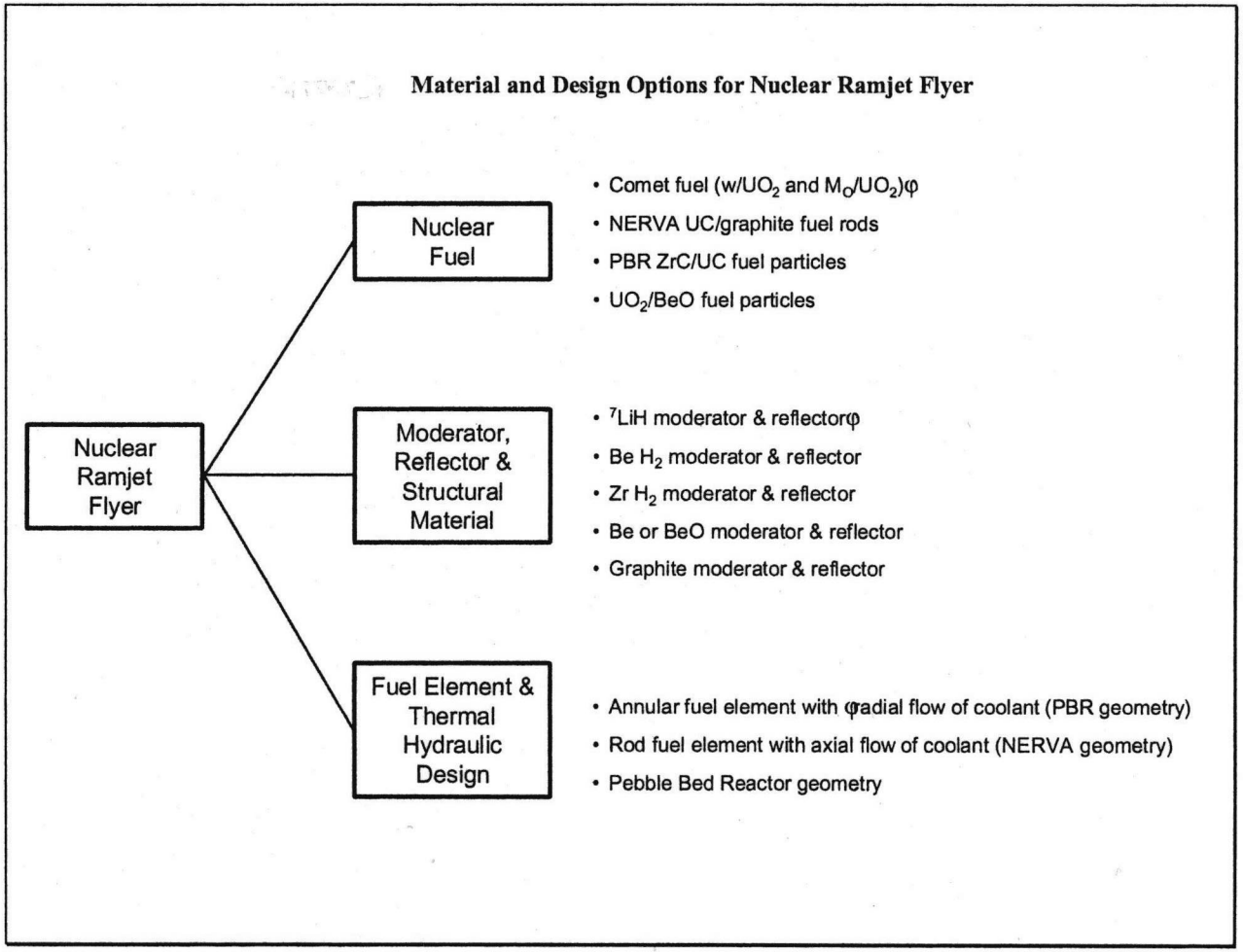

Figure 4.3.2 Material and design options for nuclear ramjet flyer

Evaluation Area	Cermets★ (W/UO_2 and M_O/UO_2)	NERVA (UC/Graphite)	PBR Particles	
			UC/ZrC	/BeO UO2
Can operate for months in 1500K /He2 H2	Yes - Minimal fuel loss for hundreds of hours in 2750K H_2	No - 1500K H_2 rapidly attacks graphite and UC	No - H_2 - H_2 rapidly attacks UC/ZrC particles	Very likely - UO_2/BeO should be stable in 1500K H_2
Large surface area for heat transfer $\geq$ 50 cm^2/cm^3	Yes - Cermet can be fabricated as perforated plates with large heat transfer area	No - Holes in NERVA fuel rods have limited heat transfer area	Yes - PBR particle fuel elements had ~100 cm^2 per cm^3 of bed	Yes - Same area as PBR UC/ZrC particles
High U^{235} content ($\geq$ 1g/cm^3)	Yes - Cermets with U^{235} contents up to ~5 g/cm^3 have been fabricated	No - NERVA criticality requires low U^{235} concentrates in graphite	Yes - U^{235} contents of PBR particles was up to 3g/cm^3	Yes - High UO_2 content in BeO is possible
High burnup capability ($\geq$20%)	Yes - High burnup capability cermet fuels have operated in DoD Reactors for 1000's of megawatt years	Probably - Though fission products would escape	Yes - HTGR type fuel particles have high burnup capability and do not release fission products	Uncertain - Ceramic particles might break up

Figure 4.3.3 Evaluation Matrix for Nuclear Fuel Options

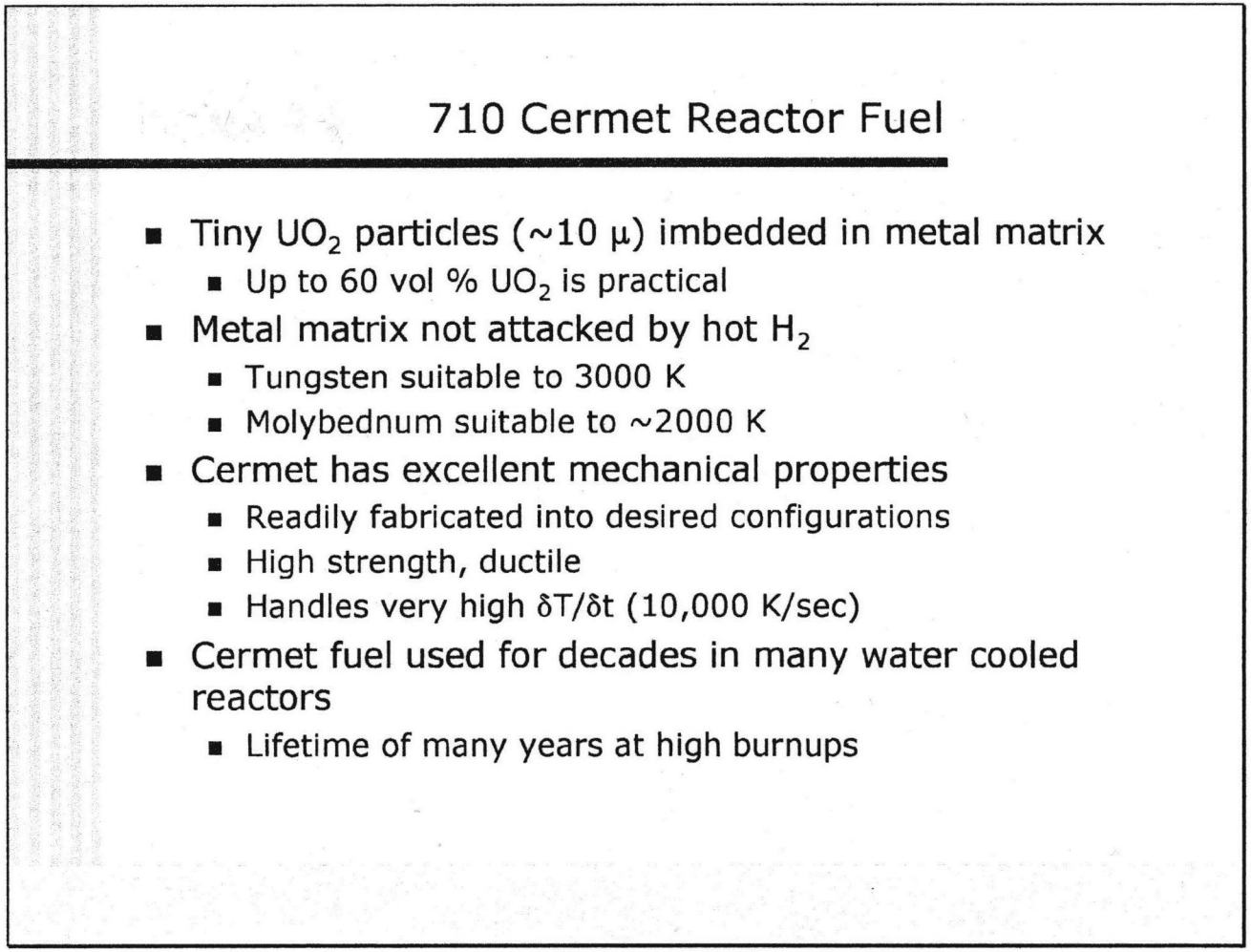

Figure 4.3.4 710 Cermet reactor fuel

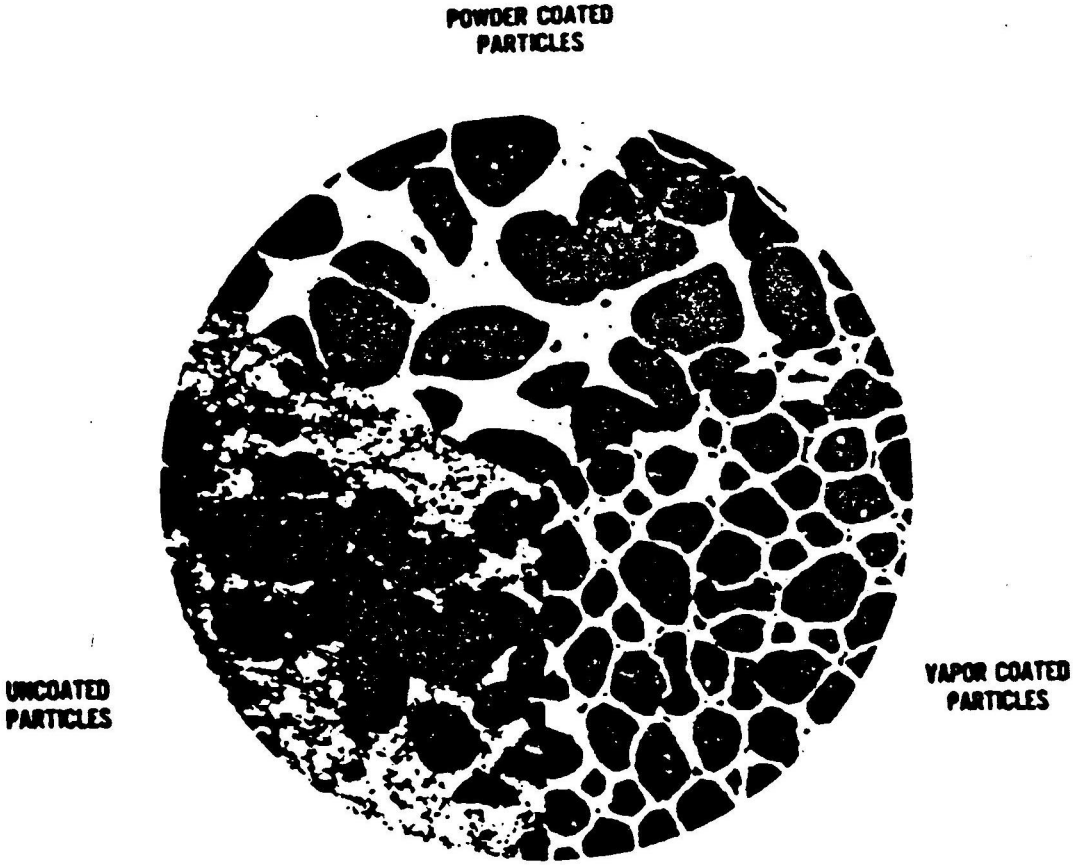

Figure 4.3.5 Effect of constituent preparation on microstructure of 710 fuel

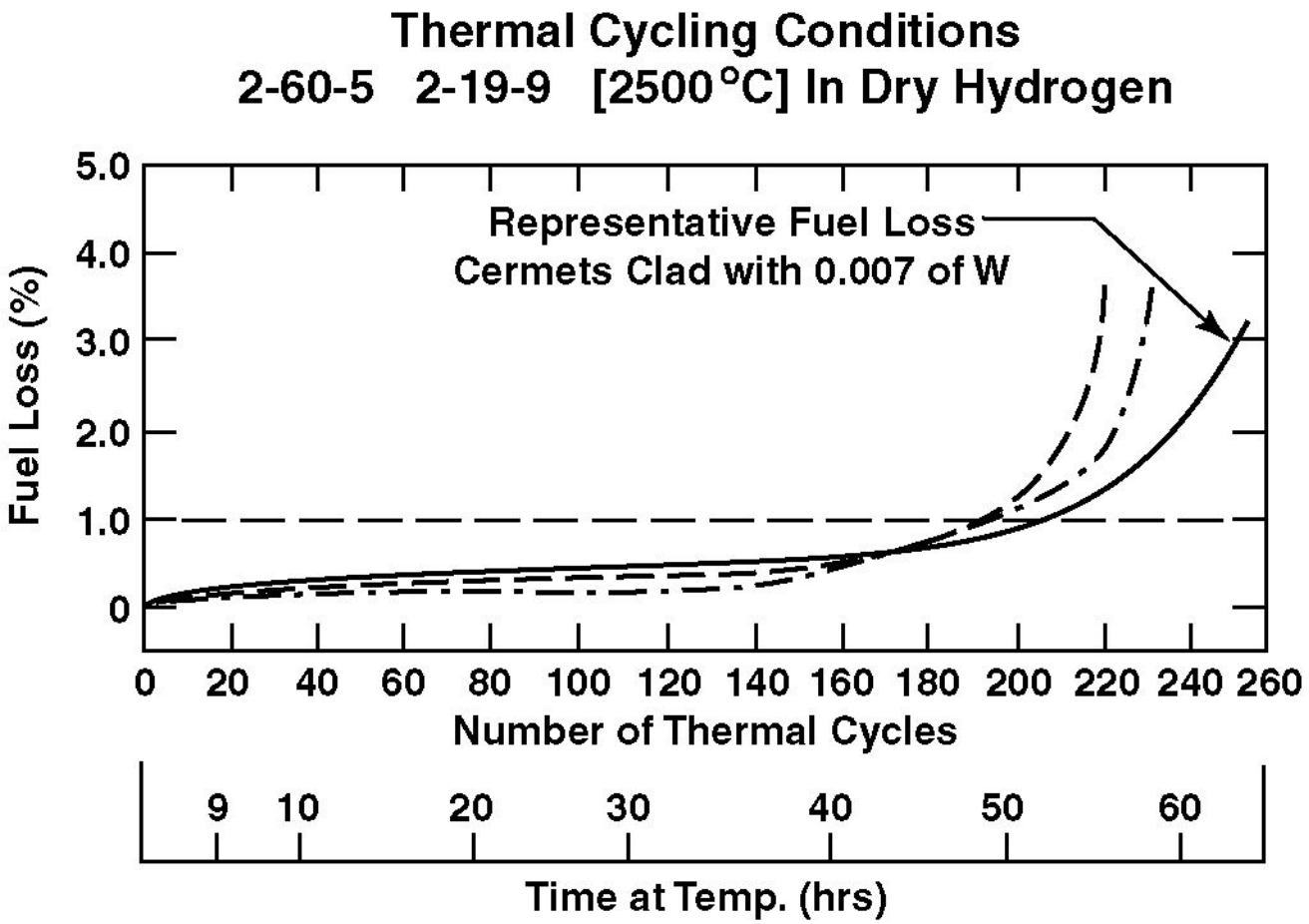

Figure 4.3.6 Fuel loss of 710 fuel

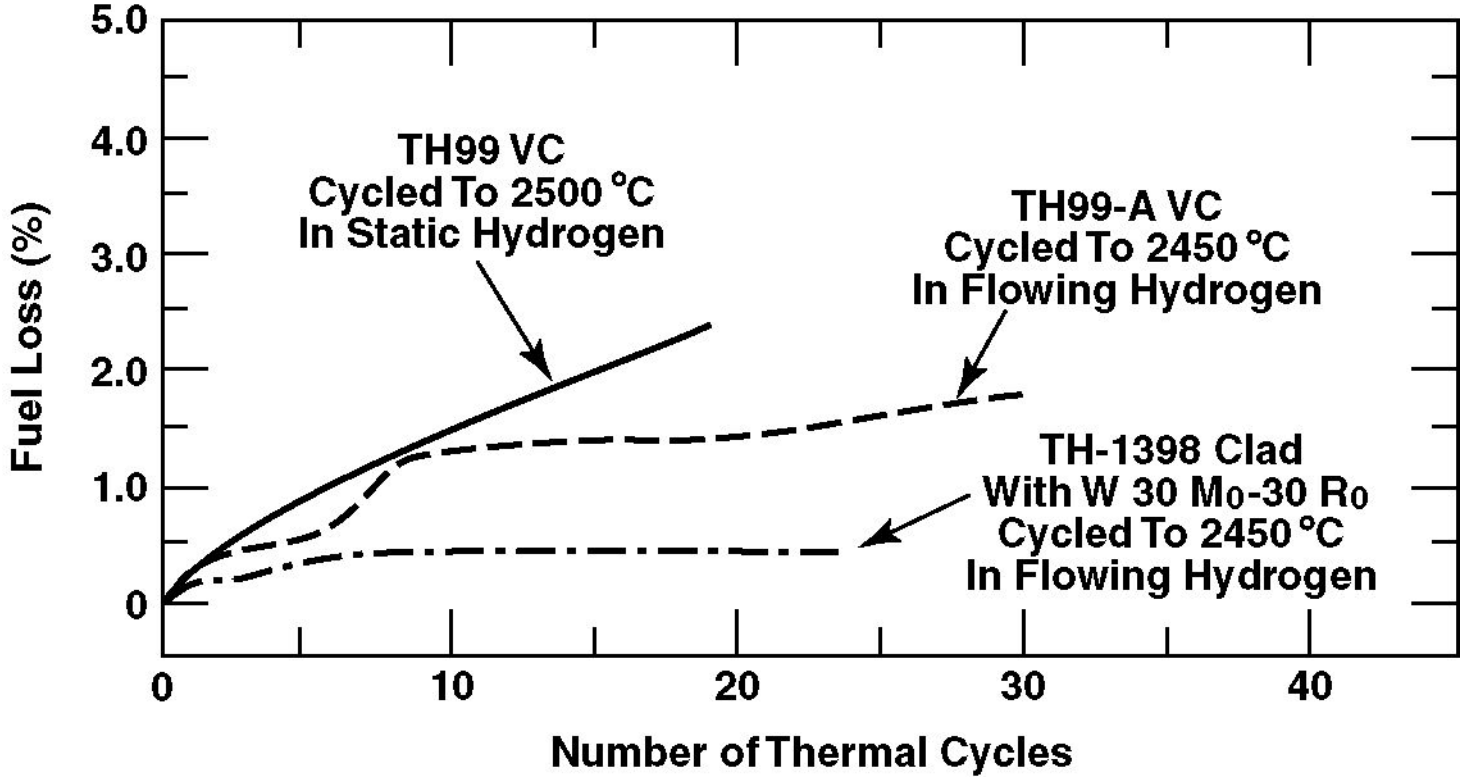

Figure 4.3.7 Cermet fuel loss comparison for static vs dynamic tests

Sample No.	Transient Duration (sec)	Reactor Integrated Power (MW-sec)	Maximum Recorded Surface Heating Rate (°C/sec)	Maximum Recorded Surface Temperature (°C)
1	0.43	164	1,700	800
1	0.3	284	3,900	1,460
2	0.3	377	5,600	1,790
3	0.2	487	8,000	2,200
4	2.1[a]	332	800	1,460
5	0.2	540	12,000	2,600
6	3.0[a]	495	1,400	2,050
7[b]	0.2	523	14,500	2,750
8[c]	0.2	532	16,000	2,750

[a]"Flat top" transient.
[b]Sample given two additional transients of same severity.
[c]Sample given five additional transients of same severity.

Figure 4.3.8 Summary of TREAT tests

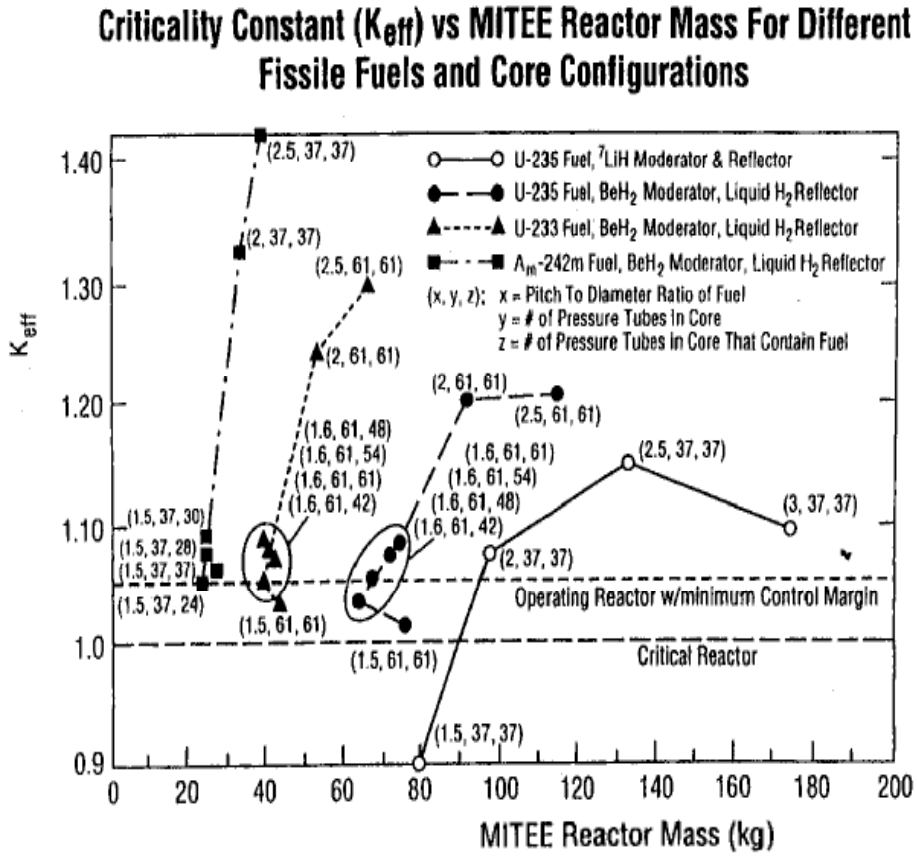

Figure 4.3.9 Criticality constant vs MITEE reactor mass for different fissile fuels and core configurations

Figure 4.3.10 Evaluation Matrix for Moderator Reflector and Structural Material Options

Evaluation Area	^{7}LiH	BeH_2	ZrH2	Be or BeO	Graphite
Reactor size - Diameter/Length (≤0.5 meter)	Hydrogenous moderator required to meet size requirement All 3 hydride materials yield acceptable size reactors			Probably will not meet size requirements	Cannot meet size requirements (>1 meter)
Reactor mass (Total ≤300 kg)	Can meet mass requirement $\left[\rho = \frac{0.8\,gm}{cm^3}\right]$	Can meet mass requirement $\left[\rho = \frac{0.8\,gm}{cm^3}\right]$	Cannot meet mass requirement	Cannot meet mass requirement	Cannot meet mass requirement
Operating temperature	Very high melting point (950K)	Decomposes at modest temp. (~400K)	Can operate to ~1000 K	Fiber reinforced Be can operate to ~1000 K	Attached by Hot H2
Moderator and reflector	Only practical moderator/-reflector option★	Not practical	Not practical	Not practical	Not practical
Internal structure	Not practical	Not practical	Not practical	Be only ★ practical structure	Not practical

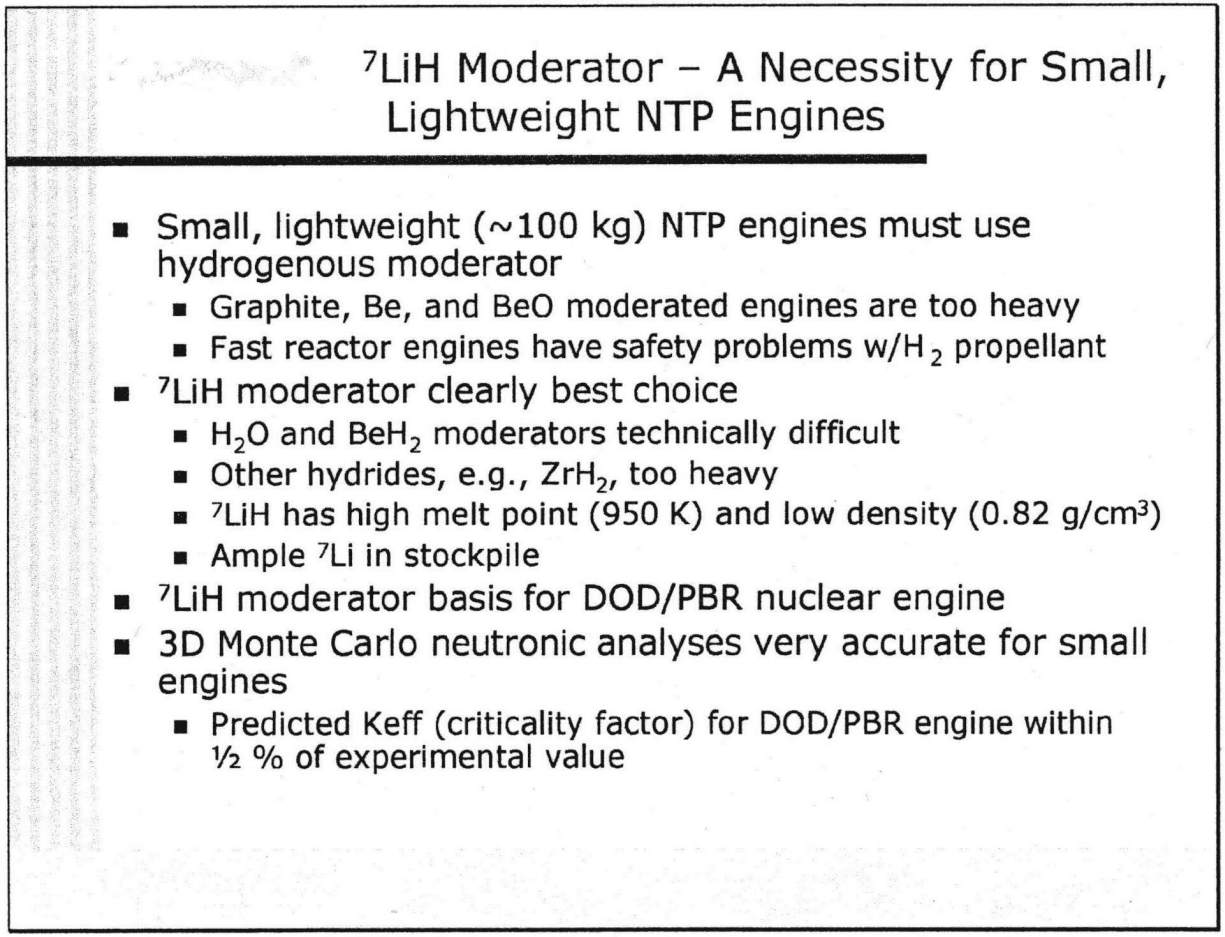

Figure 4.3.11 ^{7}LiH moderator – A necessity for small, lightweight NTP engine

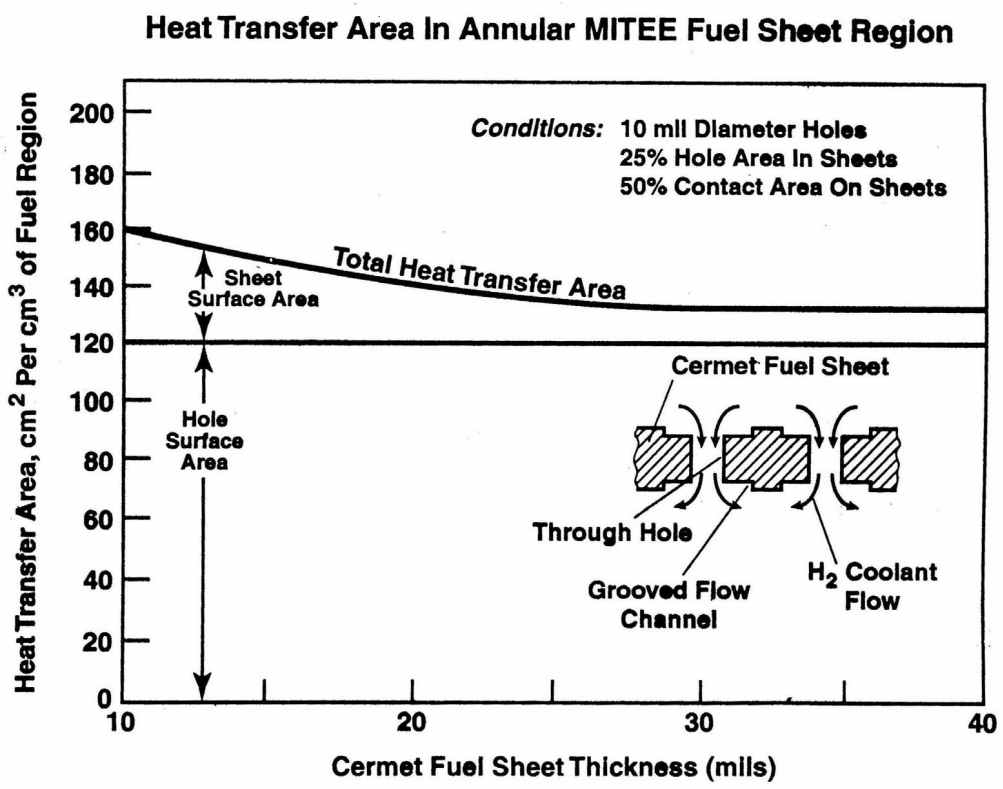

Figure 4.3.12 Heat transfer area in annular MITEE fuel sheet region

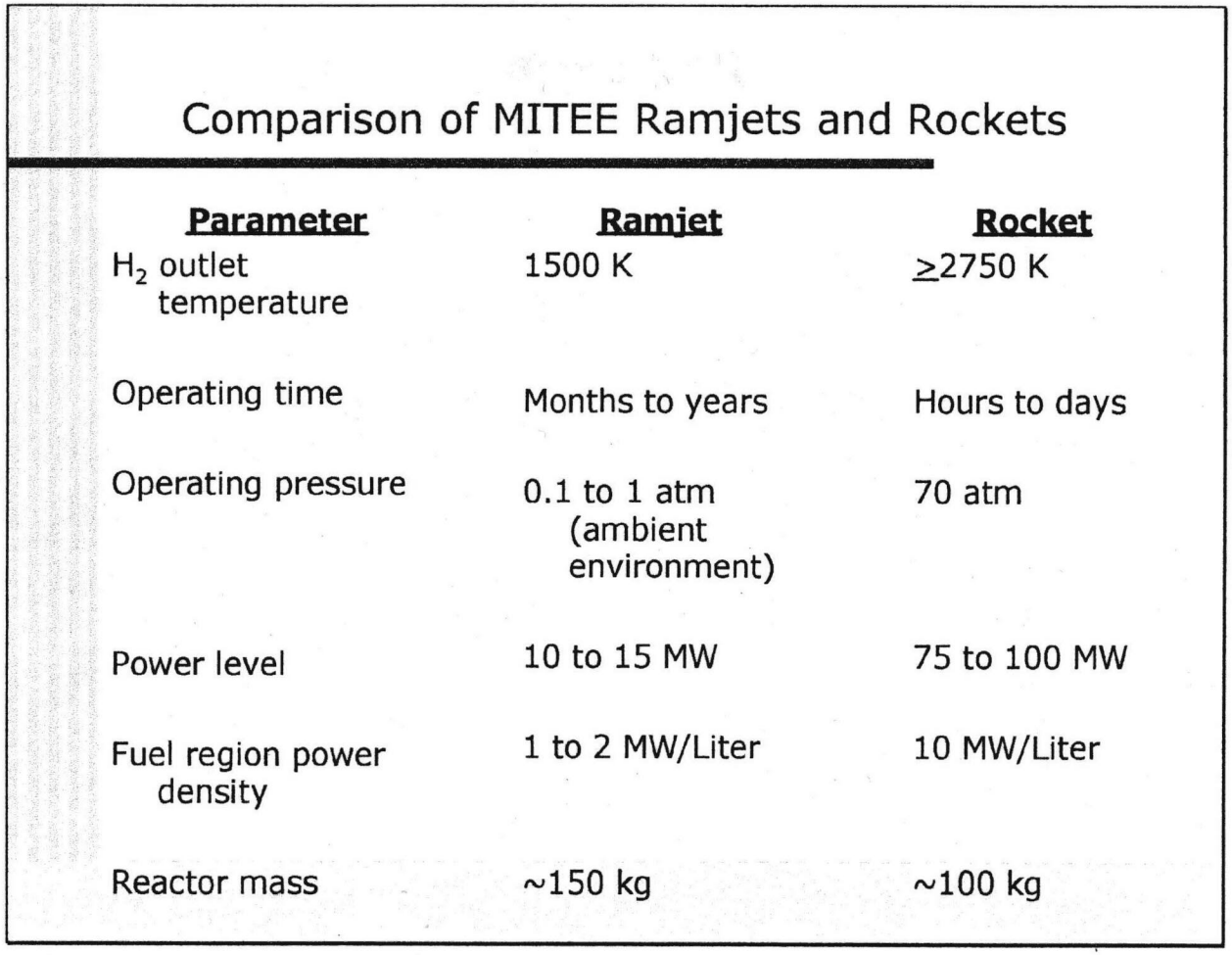

Figure 4.3.13 Comparison of MITEE ramjets and rockets

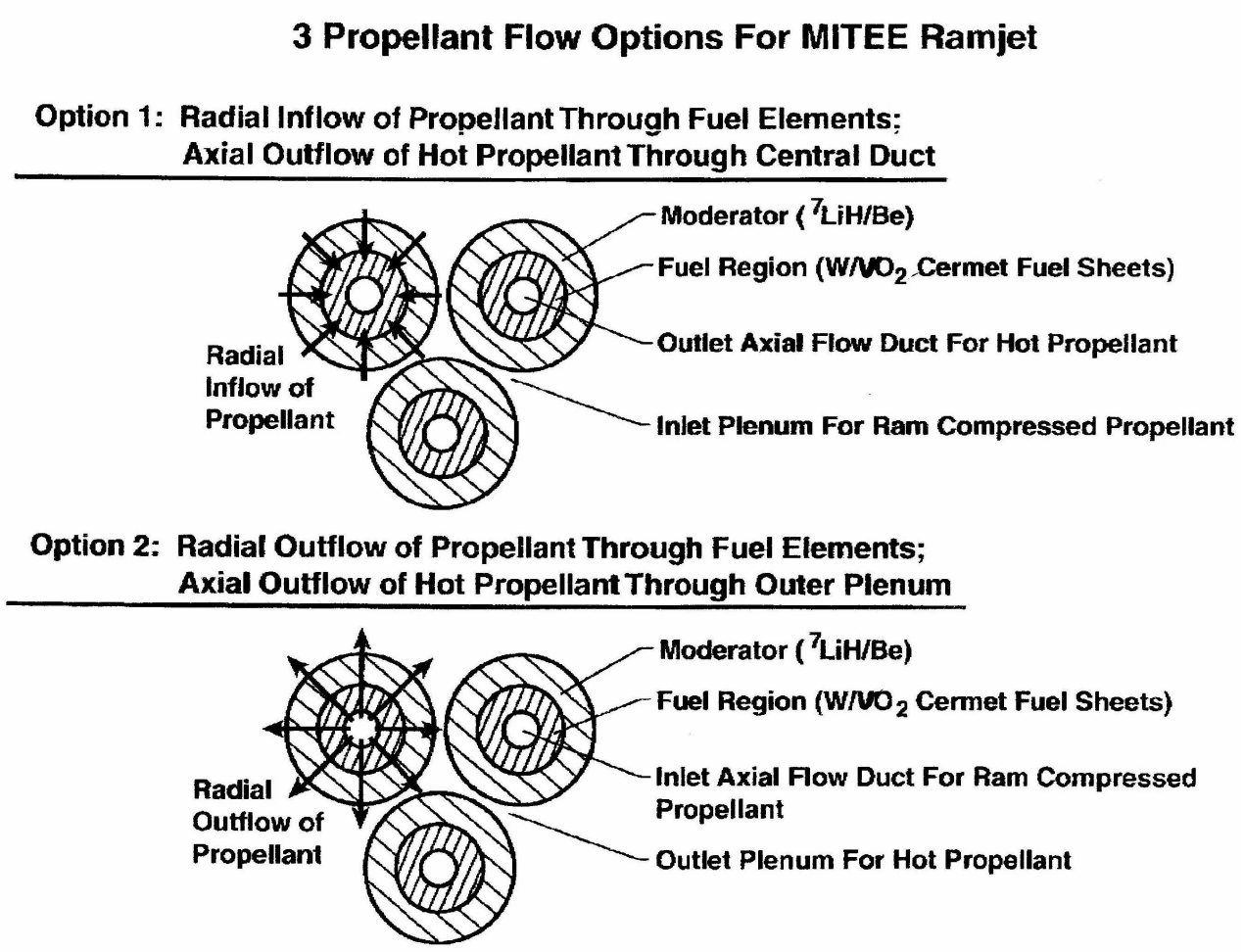

Figure 4.3.14 Three propellant flow options for MITTEE ramjet

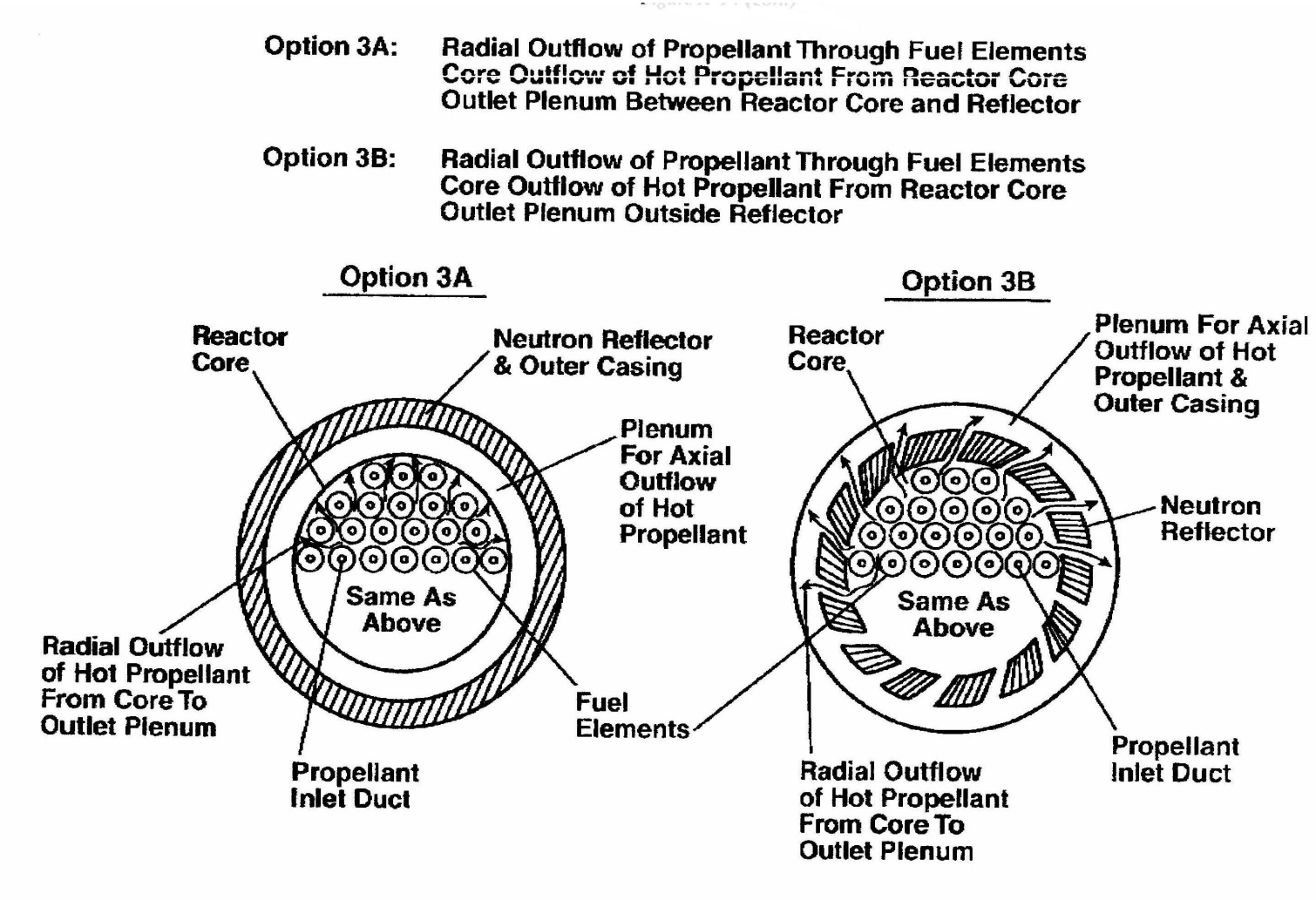

Figure 4.3.14 (Cont.)

Figure 4.3.15 Cross section through MITEE-B reactor

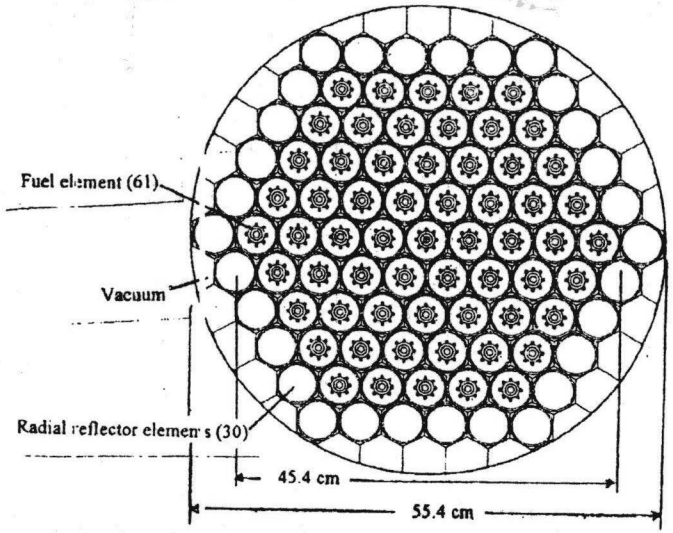

Figure 4.3.16 Cross section of MITEE-B pressure tube/fuel element for MITEE nuclear rocket

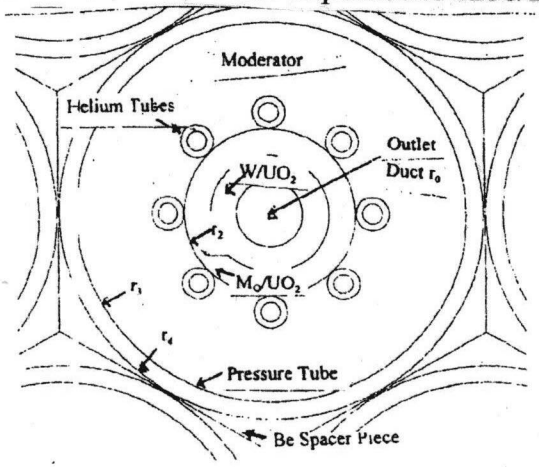

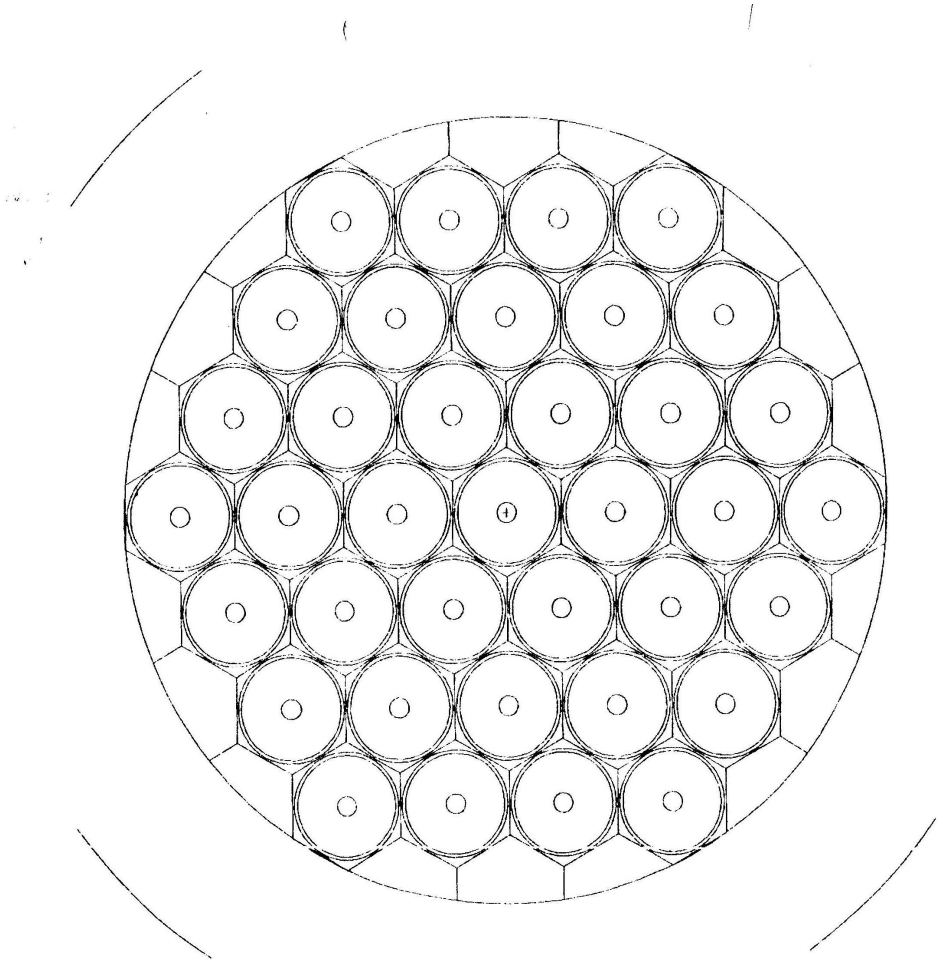

Figure 4.3.17 Cross section through MITEE reactor for ramjet application

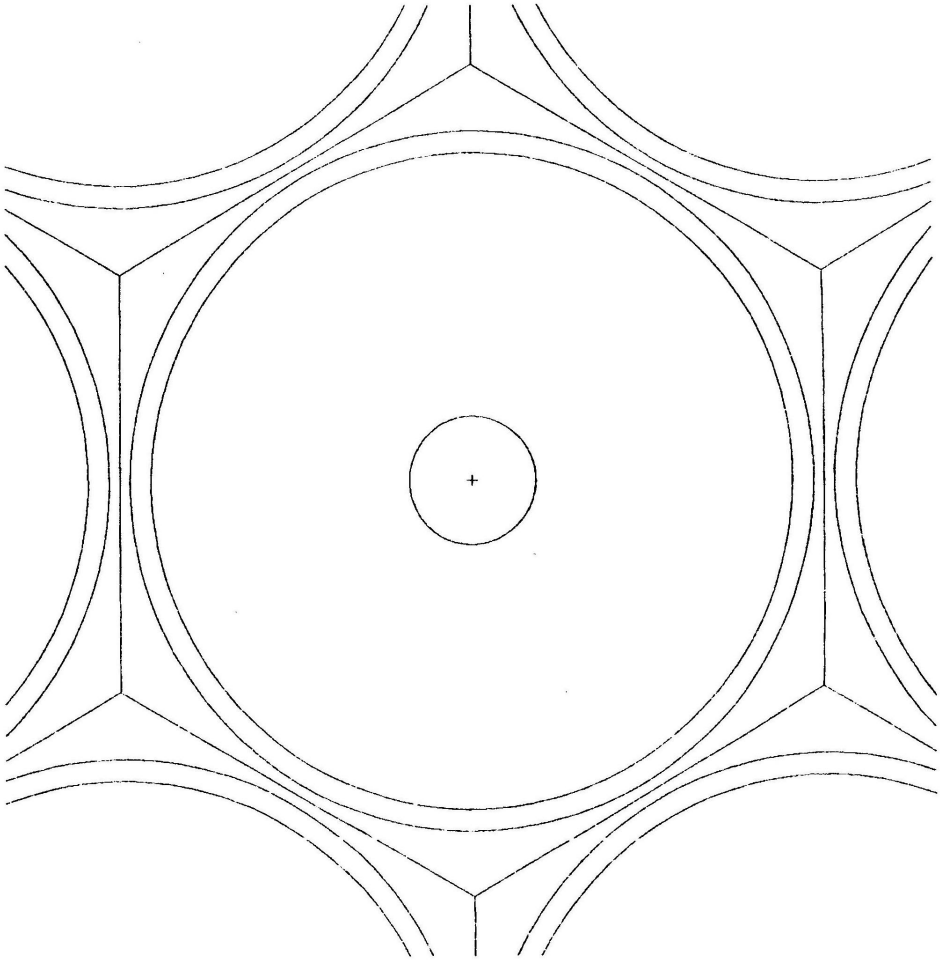

Figure 4.3.18 Cross section of MITEE pressure tube/fuel element for MITEE nuclear ramjet

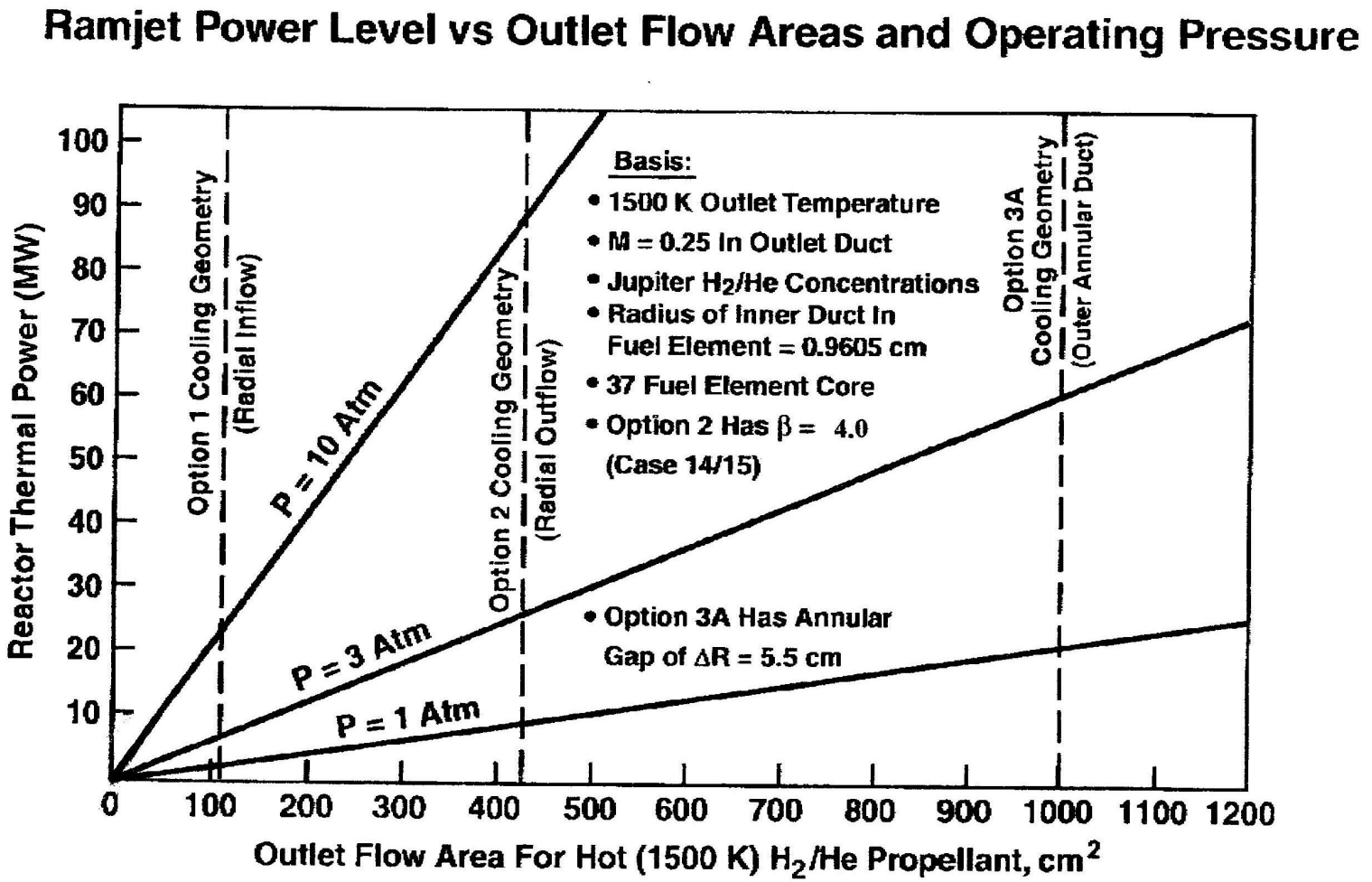

Figure 4.3.19 Ramjet power level vs outlet flow areas and operating pressures

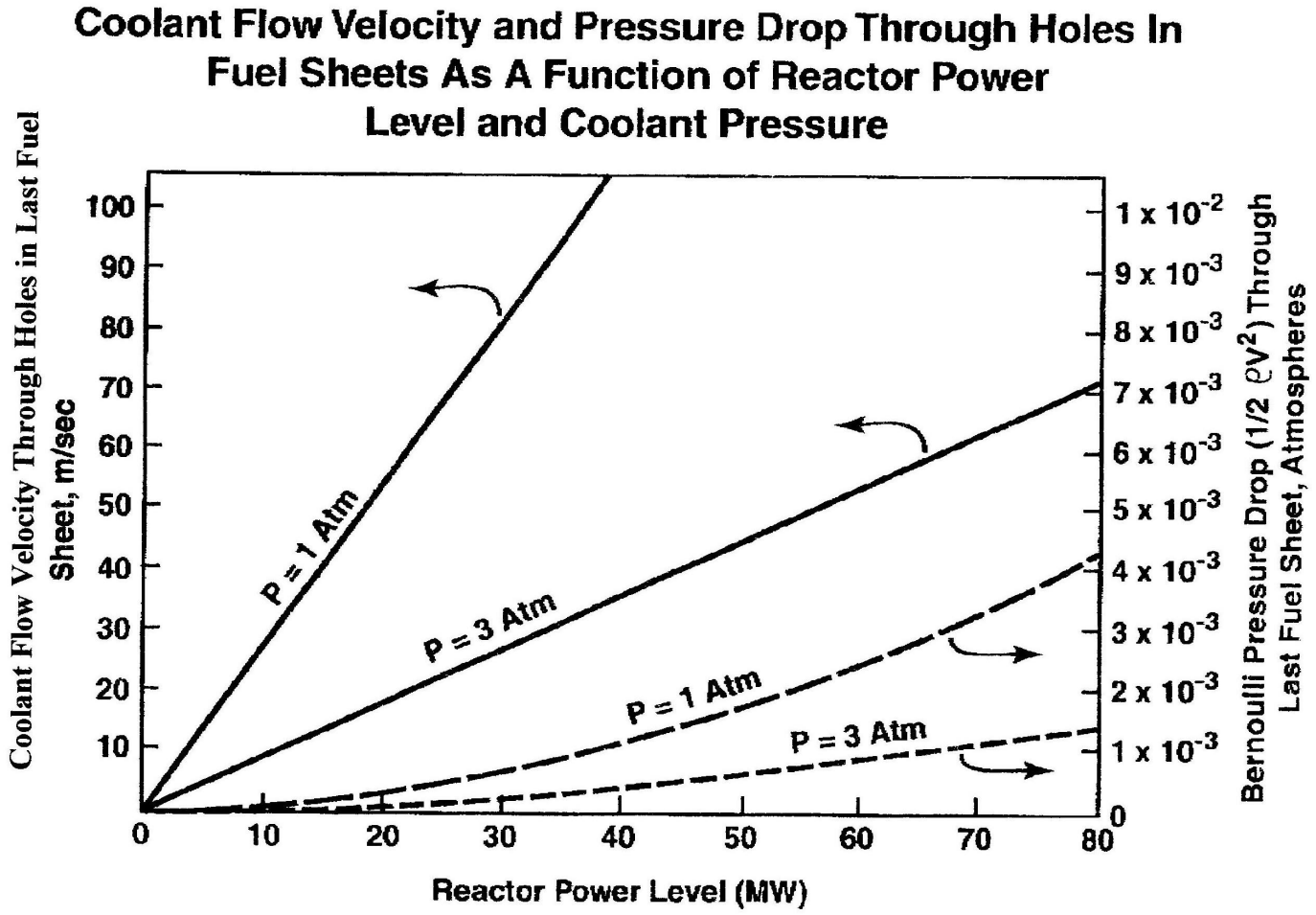

Figure 4.3.20 Coolant flow velocity and pressure drop through holes in fuel sheets as a function of reactor level and coolant pressure

Figure A 4.3.21 Evaluation Matrix for Reactor Cooling Geometry Options for MITEE Ramjet

Evaluation Parameters	**Option I (Radial Inflow)**	**Option 2 (Radial Outflow)**	**Option 3A Outlet Plenum Between Core & Reflector**	**Option 3B Outlet Plenum Outside Reflector**
Power limit due to Mach # in outlet ducts	Limits power to ~2 MW for P ≈ 1 Atm	Limits power to ~9 MW for P = 1 Atm	Limits power to ~25 MW for P = 1 Atm	Limits power to ~25 MW for P = 1 Atm
Bernoulli Pressure Drop in Fuel Sheets	Not limiting - allows much higher powers than Mach # limit	Not limiting - allows much higher powers than Mach # limit	Not limiting - allows much higher powers than Mach # limit	Not limiting - allows much higher powers than Mach # limit
Effect on Reactor Construction	Not as attractive as Options 2 & 3A - thick fuel region & outlet plumbing is complex	Very attractive - simple gap between fuel elements and fuel region is thin	Very attractive - simple gap between core and reflector and fuel region is thin	Not attractive - complex reflector structure is necessary
Effect on Reactor Neutronics	Good - yields lowest reactor mass. However, power level is limited	OK - yields acceptable reactor mass	OK - yields acceptable reactor mass	OK - yields acceptable reactor mass

Figure 4.3.22 Initial Selections for Reactor Components in Phase 2 Ramjet Study

Component	Reason for Initial Selection	Alternate Selections for Future Study
Cermet nuclear fuel	Only fuel that can operate for months in hot H_2	No change
^{7}LiH moderator and reflector	Required for low mass compact reactor	No change
Be structure	Lightweight, H_2 resistant, and neutronically attractive	No change
^{235}U fissile fuel	Standard fissile isotope	^{233} U - possible smaller, lighter reactor
Radial coolant flow in fuel element	Radial outflow (Option 2) yields higher power capability	No change
Outlet path for Hot H_2	Axial flow in spares between fuel elements (Option 2)	Axial flow in channel between core and reflector (Option 3A) - greater power capability
37 fuel elements	Used in previous studies on MITEE rocket	61 fuel elements - possible smaller, lighter reactor

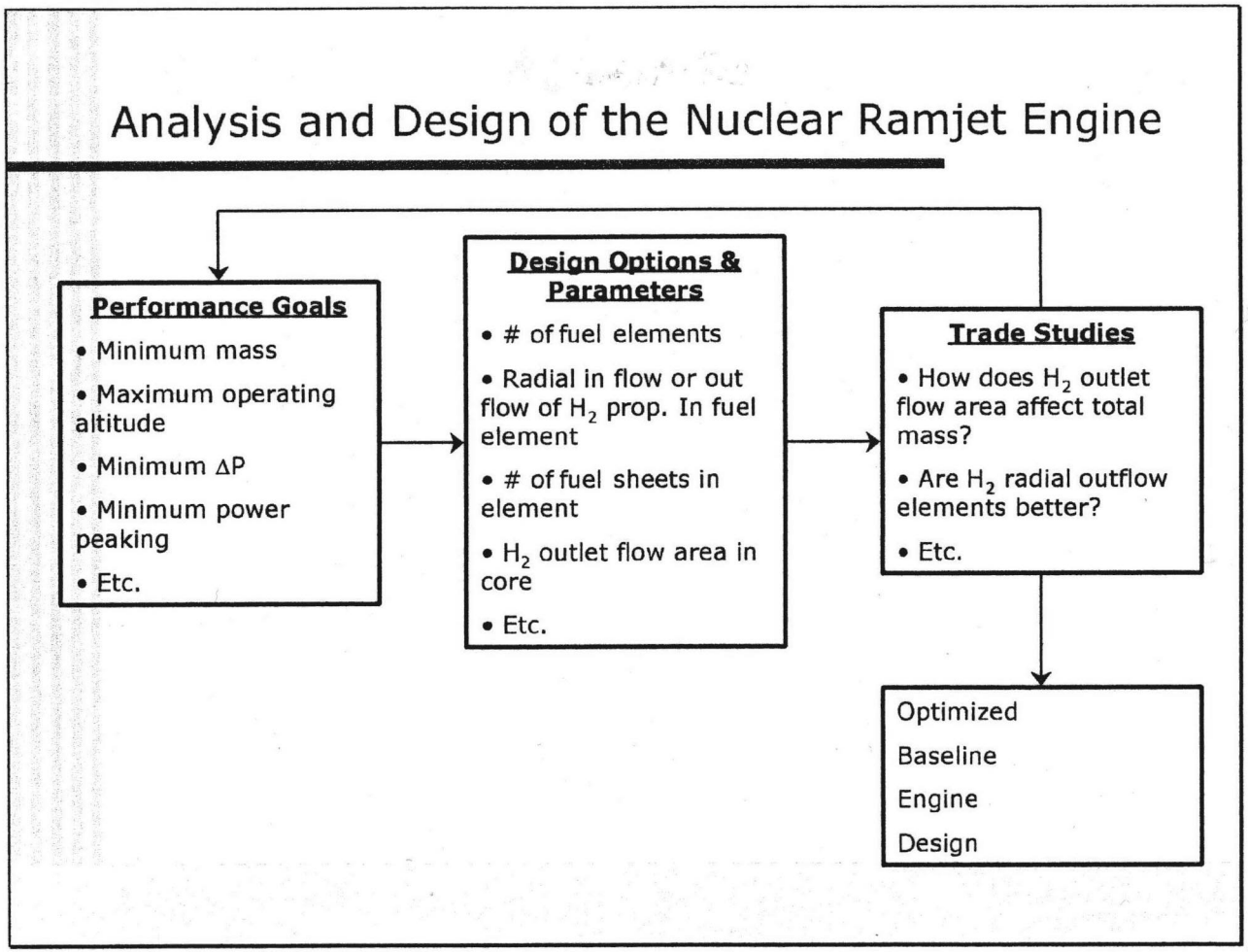

Figure 4.3.23 Analysis and design of the nuclear ramjet engine

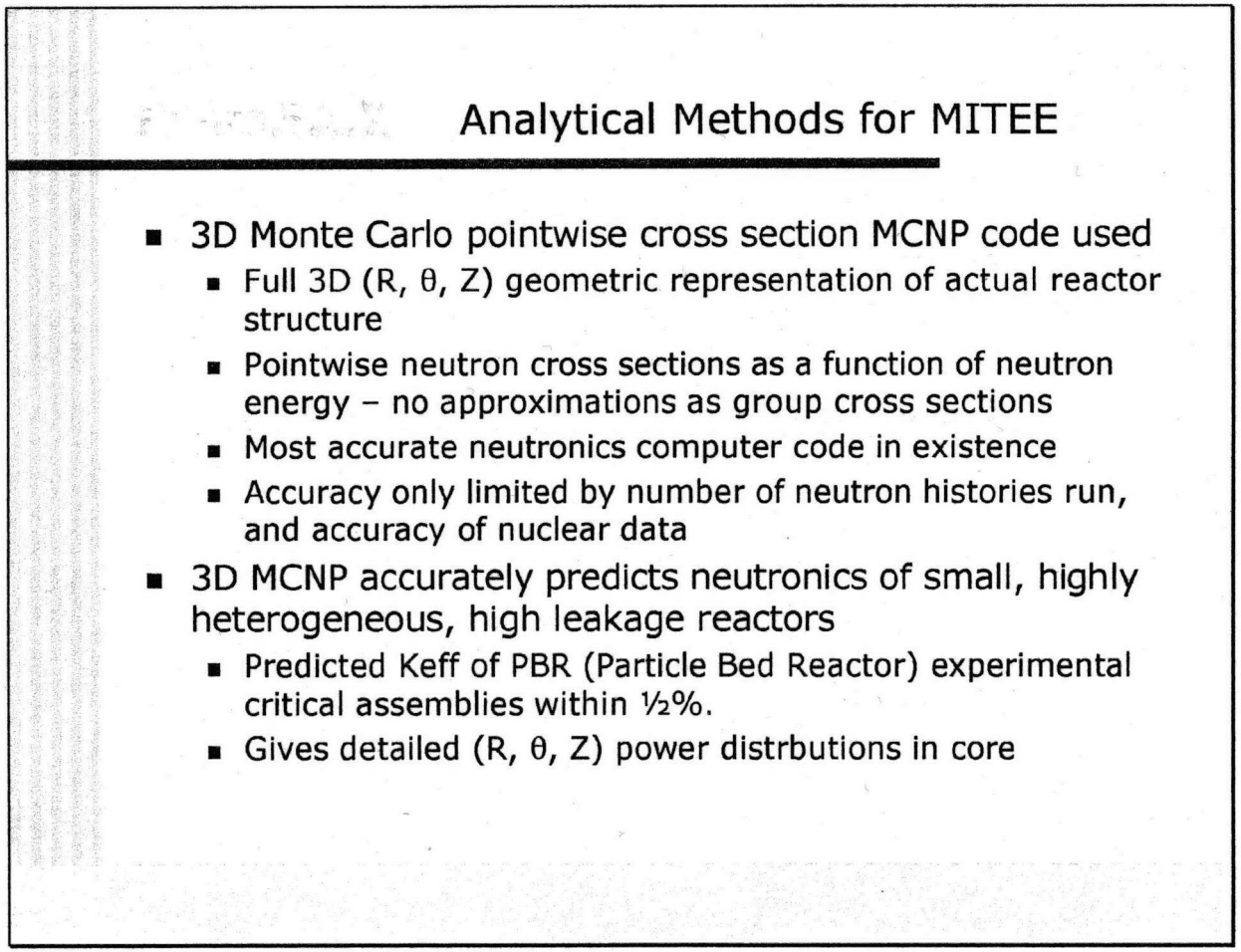

Figure 4.4.1.1 Analytical neutronic methods for MITEE

SPACE NUCLEAR THERMAL PROPULSION PROGRAM
MCNP BENCHMARK ANALYSES OF CRITICAL EXPERIMENTS

Particle Bed Reactor Critical Experiments Conducted at the Sandia National Laboratory Reactor Facility Using a Nineteen Element Light Water Moderated and Reflected Thermal Reactor System

MCNP Benchmark Data

	Experiment	Calculation
■ **Initial Criticality/ Excess Reactivity**		
▸ ΔK_{EFF}	0.016	0.015 (.001)
▸ Critical Boric Acid Concentration, ppm	65.8	61
▸ Boric Acid Worth, $/ppm	0.03	0.03
■ Prompt Generation Time, μsec	33.3	34.7 (0.1)
■ Worth of Polyethylene Plug, $	0.72	0.74 (0.18)
■ Moderator Temperature Coefficient of Reactivity, ¢/ K (283 to 353 K)	+3.5	+3.6 (0.3)
■ Worth of Cryogenic Polyethylene, $ (97 to 296 K)	1.65	1.62 (0.17)

Figure 4.4.1.2 Space nuclear thermal propulsion program MCNP benchmark analysis for critical experiments

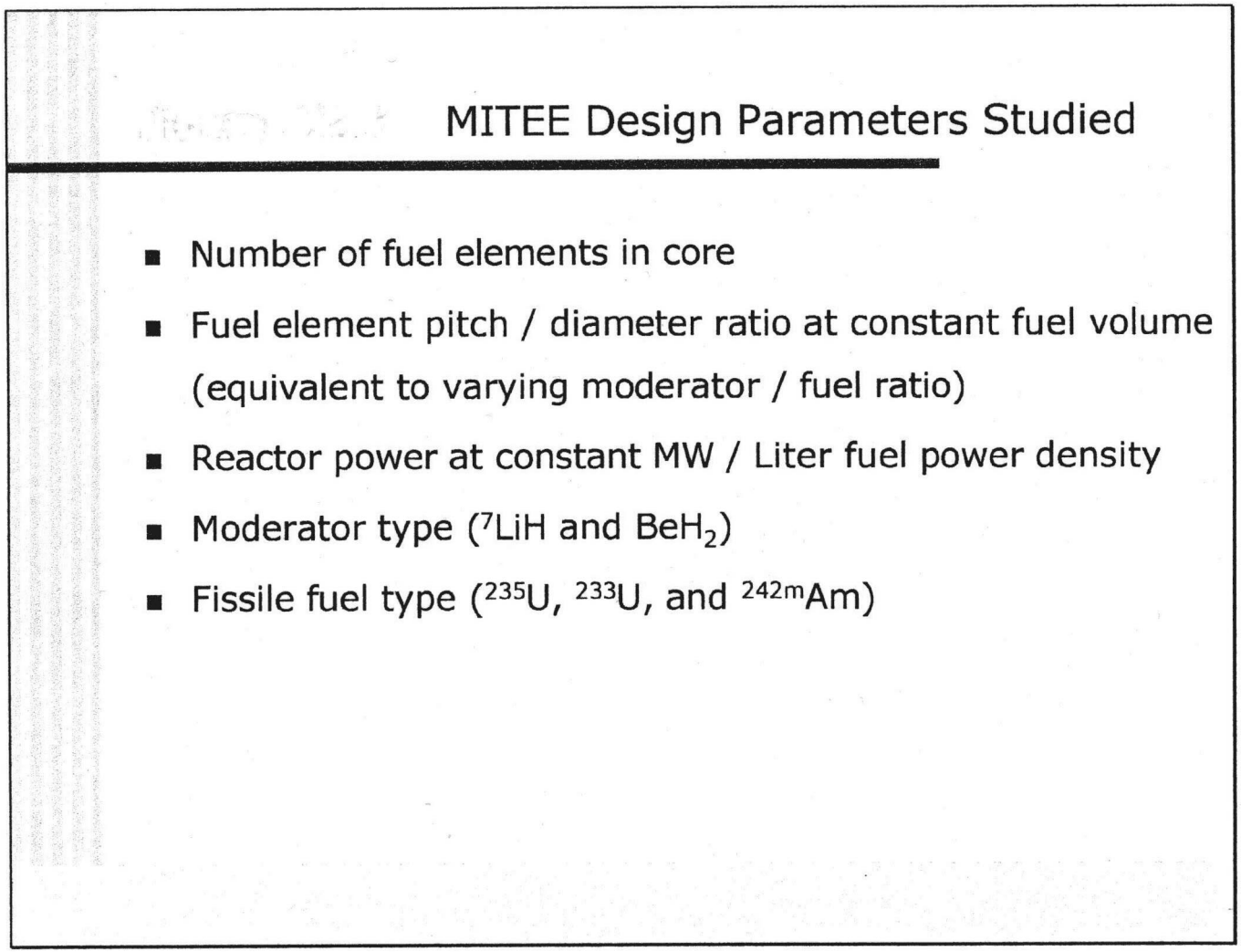

Figure 4.4.2.1 Design parameters studied for MITEE nuclear rocket

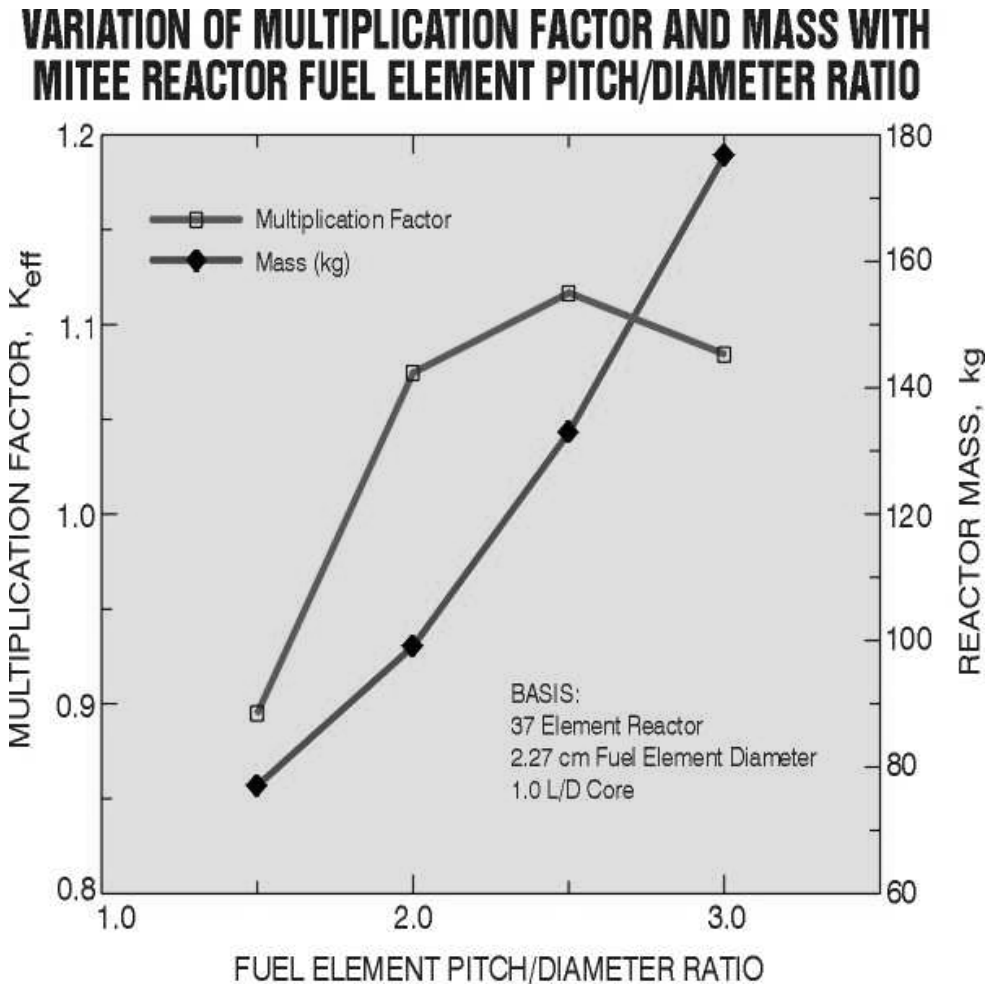

Figure 4.4.2.2 Variation of multiplication factor and mass with MITEE reactor fuel element pitch/diameter ratio

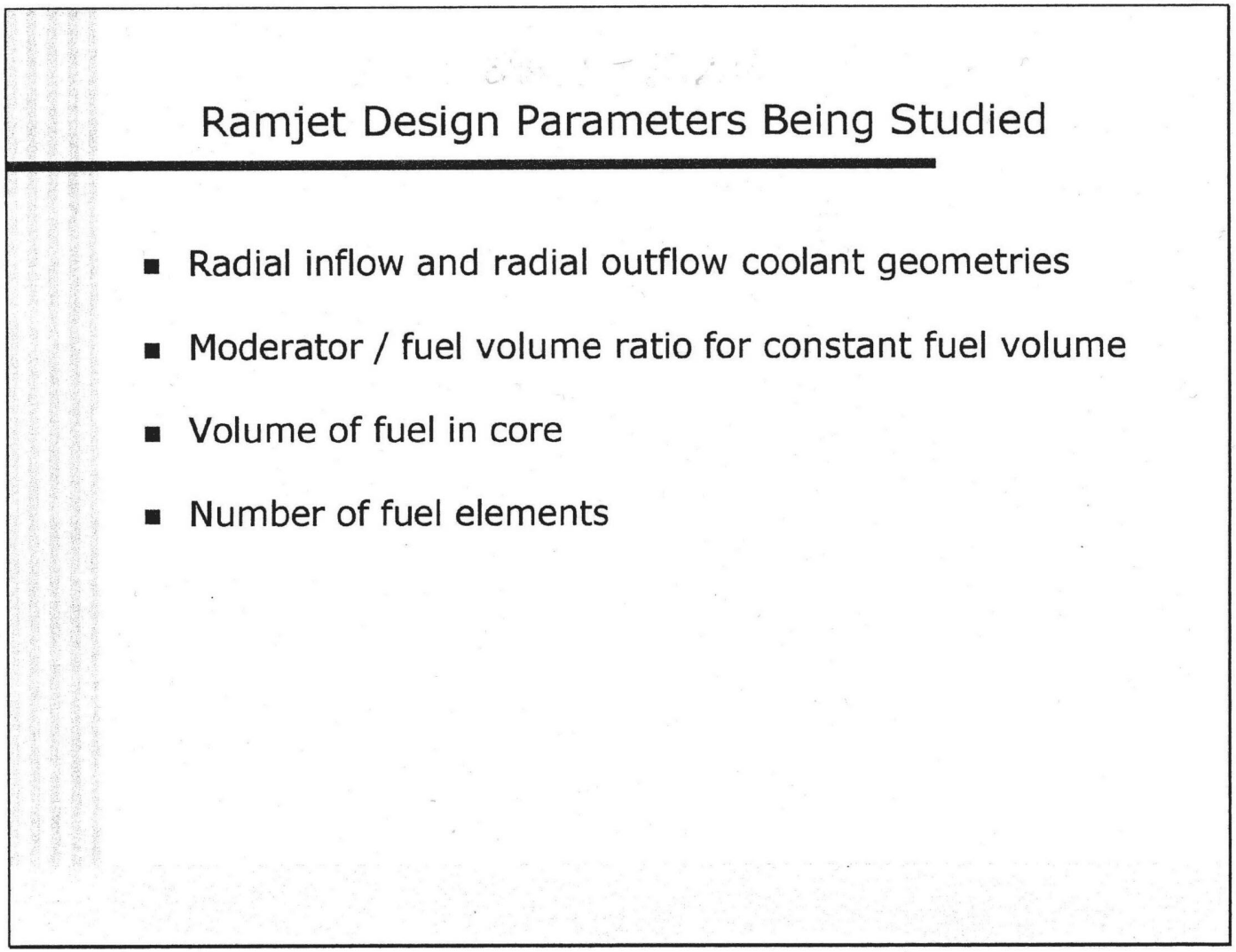

Figure 4.4.2.3 Jupiter ramjet design parameters studied

GEOMETRICAL CONFIGURATION OF CORE

- ASSUME ELEMENTS ARE ARRANGED IN A HEXAGONAL LATTICE
- ASSUME THAT INLET DUCT DIAMETER, RATIO OF INLET DUCT AREA/OUTLET DUCT AREA, AND MODERATOR VOLUME/FUEL VOLUME ARE GIVEN
- THE FOLLOWING RELATIONSHIPS FOLLOW:

$$V_f = \pi.(r_3^2 - r_2^2).y.P.N_e$$

$$(3)^{0.5}.P^2/2 - \pi.r_3^2 = \beta.\pi.r_1^2$$

$$\alpha.(r_3^2 - r_2^2) = (r_2^2 - r_1^2)$$

Where:

V_f = Fuel volume
r_3 = Outer fuel radius
r_2 = Inner fuel radius
r_1 = Inlet duct radius
y = Number of fuel element rings
N_e = Number of elements
P = Pitch
α = V_m/V_f
β = Oulet duct area/Inlet duct area

$$((3)^{0.5}.\alpha/2.\pi)^{0.5}.(\alpha.V_f/\pi.y.N_e) = (r_2^2 - r_1^2).\{(1 + \alpha).r_2^2 + (\alpha.\beta - 1).r_1^2\}^{0.5}$$

Figure 4.4.2.4 Geometrical configuration of the reactor core for Jupiter Ramjet (radial outflow through fuel region)

Figure 4.5.1 Overall Features of MITEE Nuclear Ramjet Engine

- Tungsten/UO_2 Cermet Nuclear Fuel (50 vol % UO_2)
- 1500 K H_2/He Outlet Propellant Temperature
- 7LiH Moderator and Reflector
- 37 Elements with W/UO2 Fuel and ^{7}LiH Moderator in Reactor Core
- H_2/He Inlet Propellant Flows Axially through Central Cylindrical Duct into Each Element
- H_2/He Propellant Flows from the Central Duct Radially Outward through Annular Moderator Region Enclosing the Duct, and the through Outer W/UO_2 Annular Fuel Region
- Hot H_2/He Propellant the Flows Axially through Spaces between the Elements to the Nozzle Chamber
- Fuel Element Ducts are Tapered to Reduce Pressure Drops. Inlet Duct Diameter is Maximum at Inlet End and Minimum at the Outlet End.

Figure 4.5.2 Design Parameters of MITEE Ramjet Engine

- 10 Liters Fuel (W/UO_2) Volume
- 100 MW(th) Reactor Power Output at 10 MW/LITER Power Density
- 160 kilograms total reactor mass
- 8.2 cm Element Outer Diameter at Inlet End of Reactor; 7.8 cm Element Outer Dia. at Outlet End
- 2 mm Radial Thickness of W/UO2 Fuel Region in Element (Avg.)
- 2.8 cm ID at Inlet Flow Duct, i.e., at Inlet End of Reactor; 0.4 cm ID at Outlet End of Reactor
- Ratio of Average Outlet Hot Flow Area / Inlet Cold Flow Area = 4/1
- Ratio of Moderator Volume / Fuel Volume = 6.5
- 8.5 cm Element Pitch
- Reactor Core Diameter = Core Height = 60 cm
- Criticality Constant (k_{eff}) = 1.07

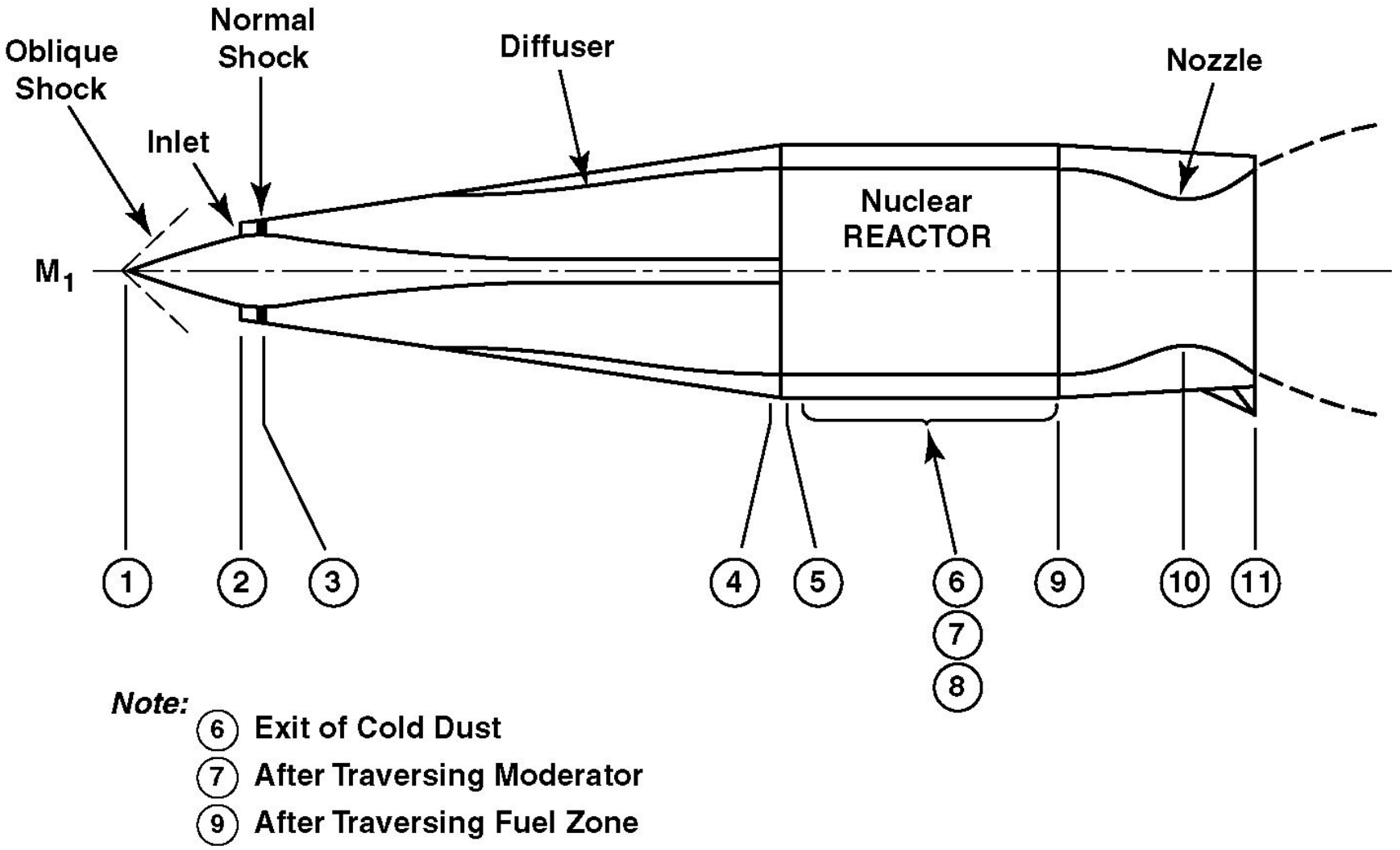

Figure 5.1 Schematic for Nuclear Ramjet Engine

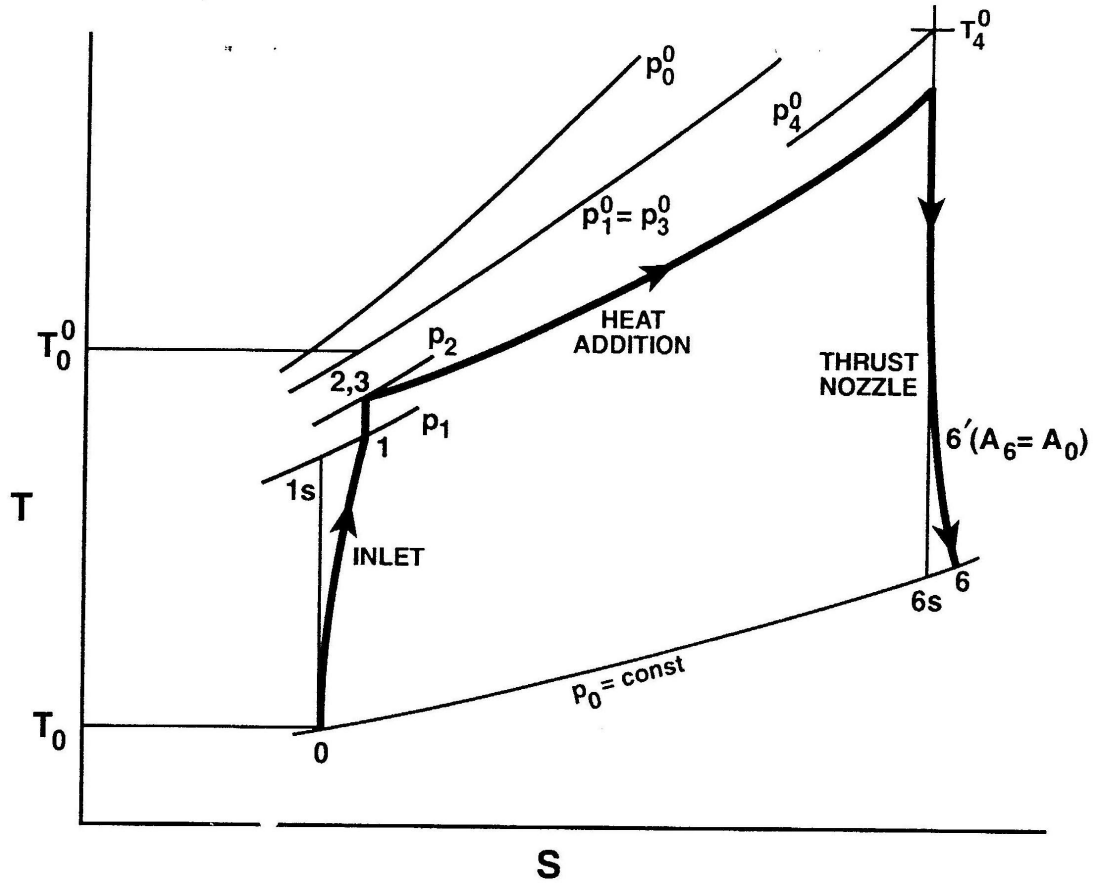

Figure 5.1.1 Temperature-Entropy diagram of ramjet engine cycle

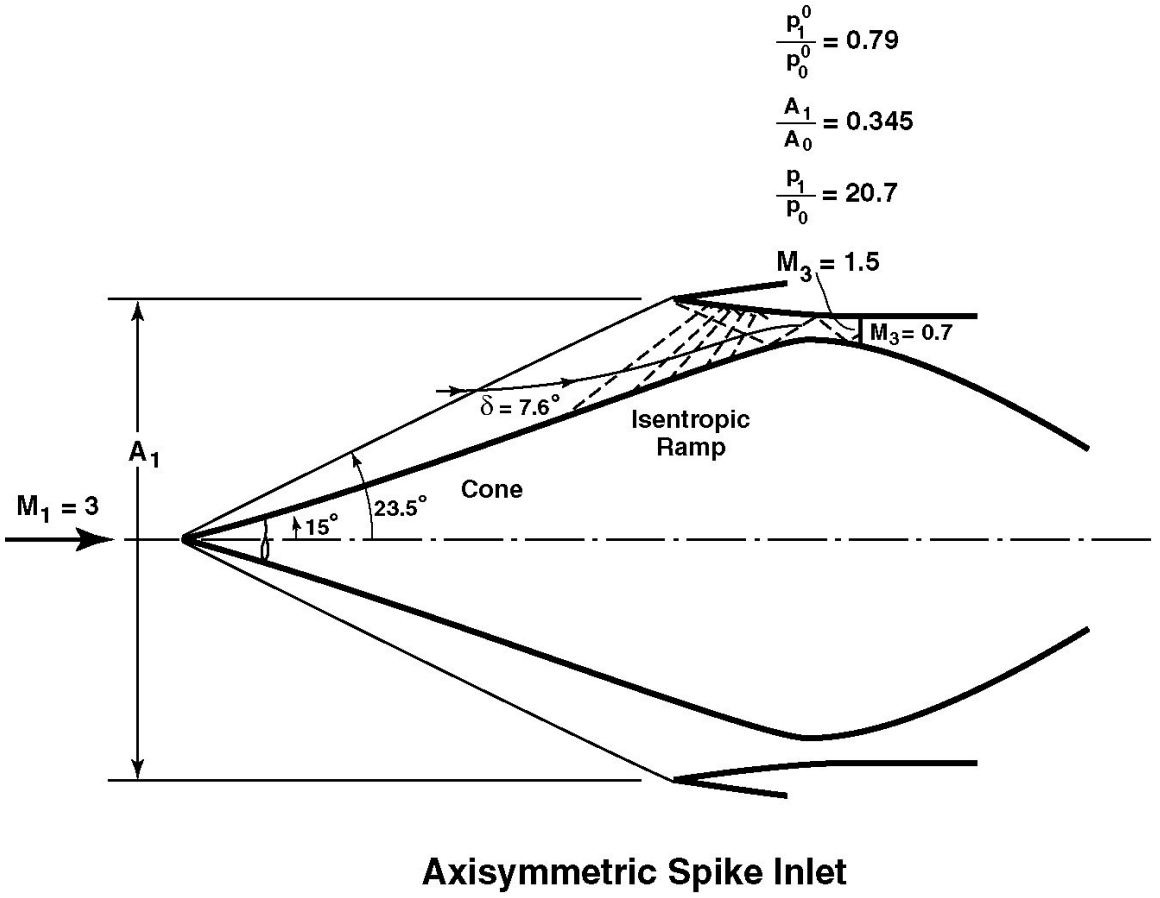

Figure 5.1.2 Axisymmetric Spike Inlet

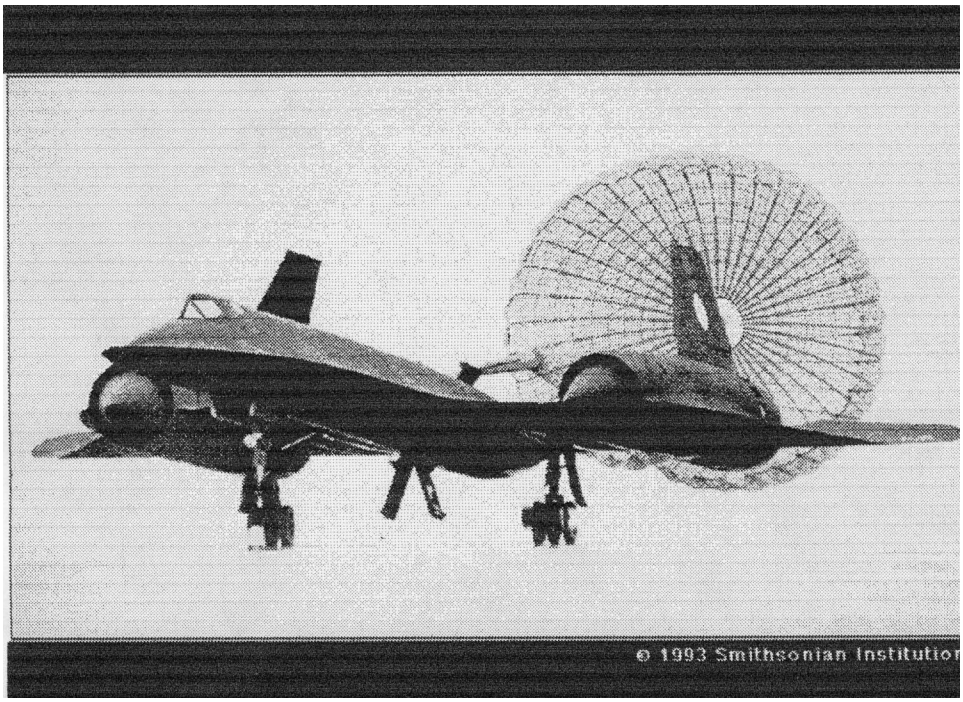

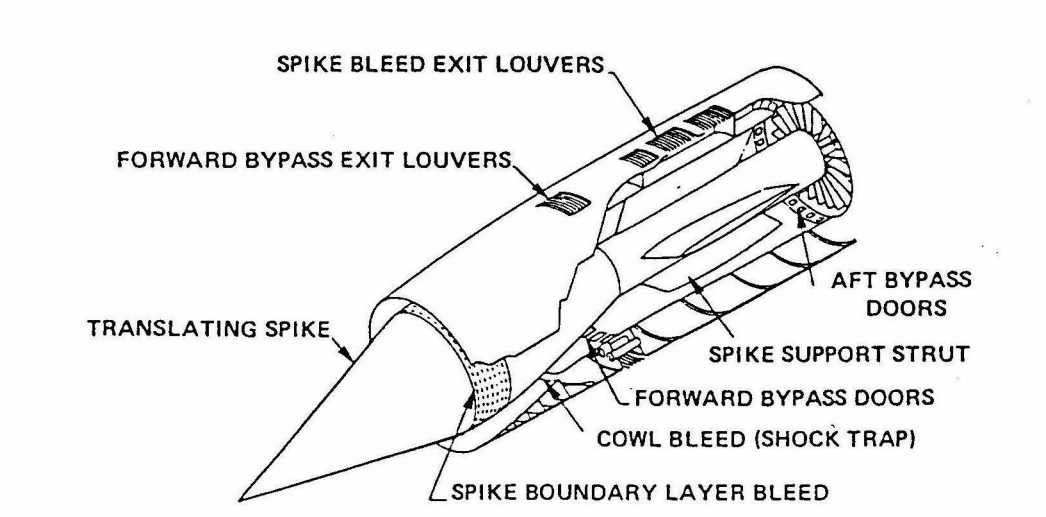

Figure 5.2.1.2 Blackbird Mach 3 Aircraft with Axisymmetric Inlets

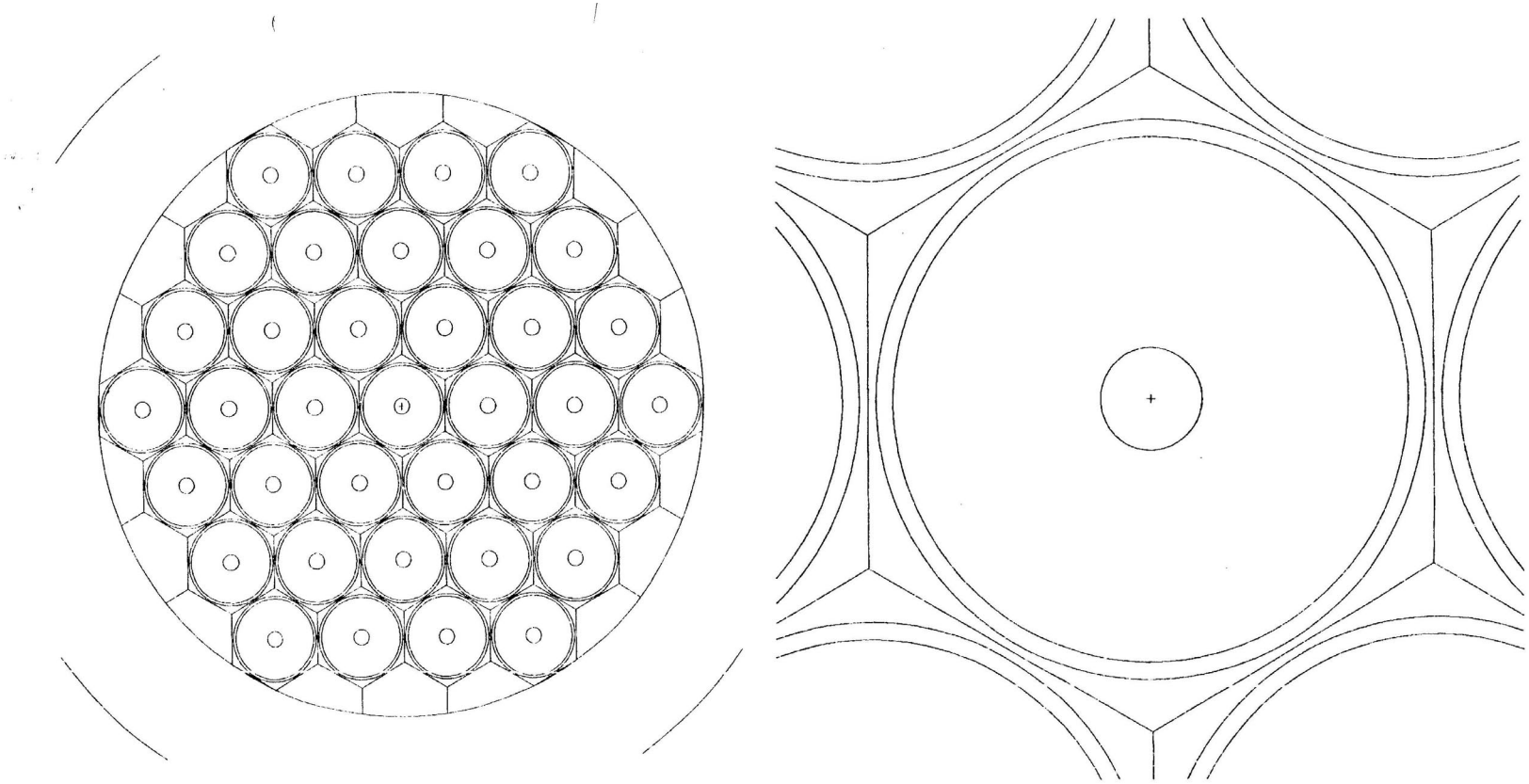

Cross section through MITEE-1 reactor

Cross section of MITEE-1 pressure tube/fuel element

Figure 5.2.2.1 Configuration of Nuclear Reactor for Ramjet Engine

Figure 5.3.2.1 Thrust Coefficient vs. Cycle Temperature, M_1=3

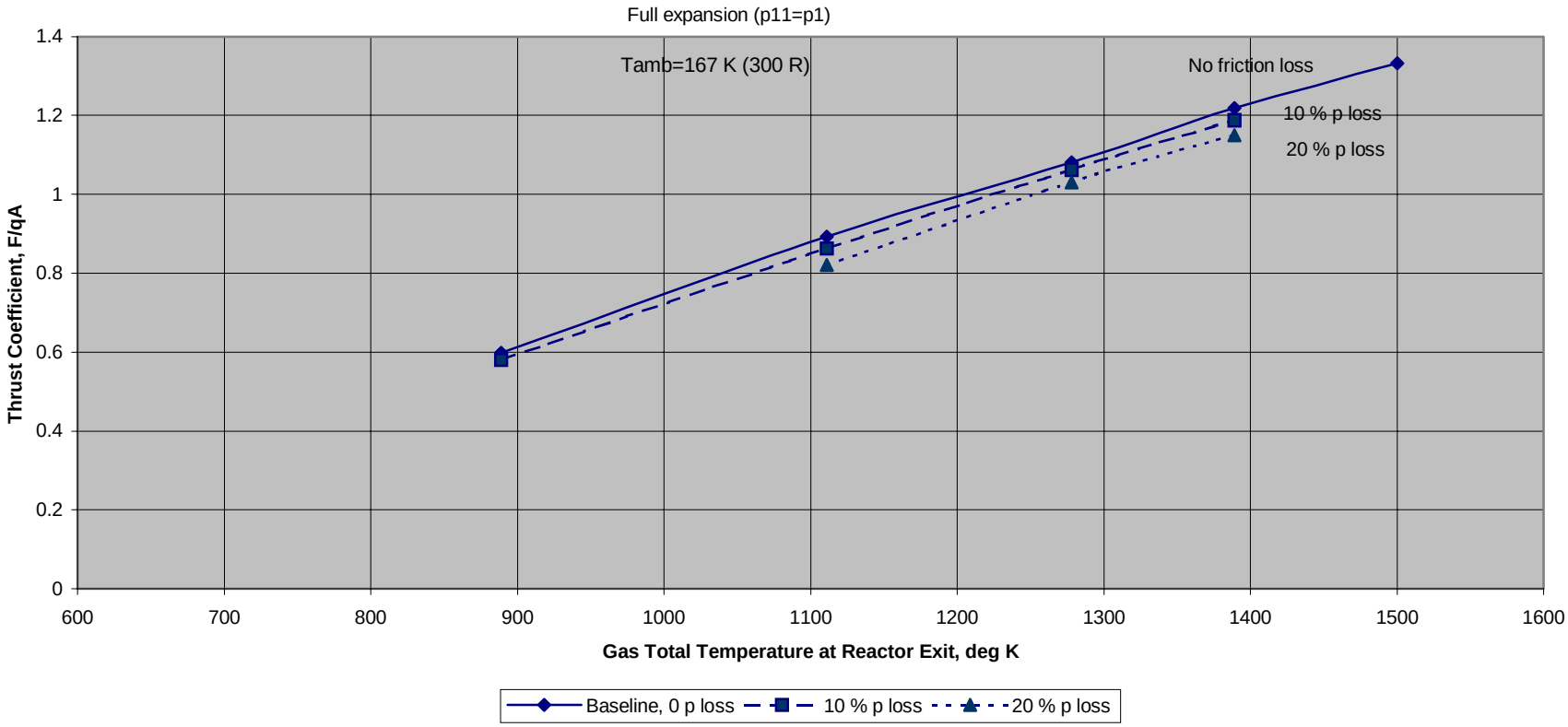

Figure 5.3.2.1 Thrust coefficient vs Cycle Temperature, M_1=3

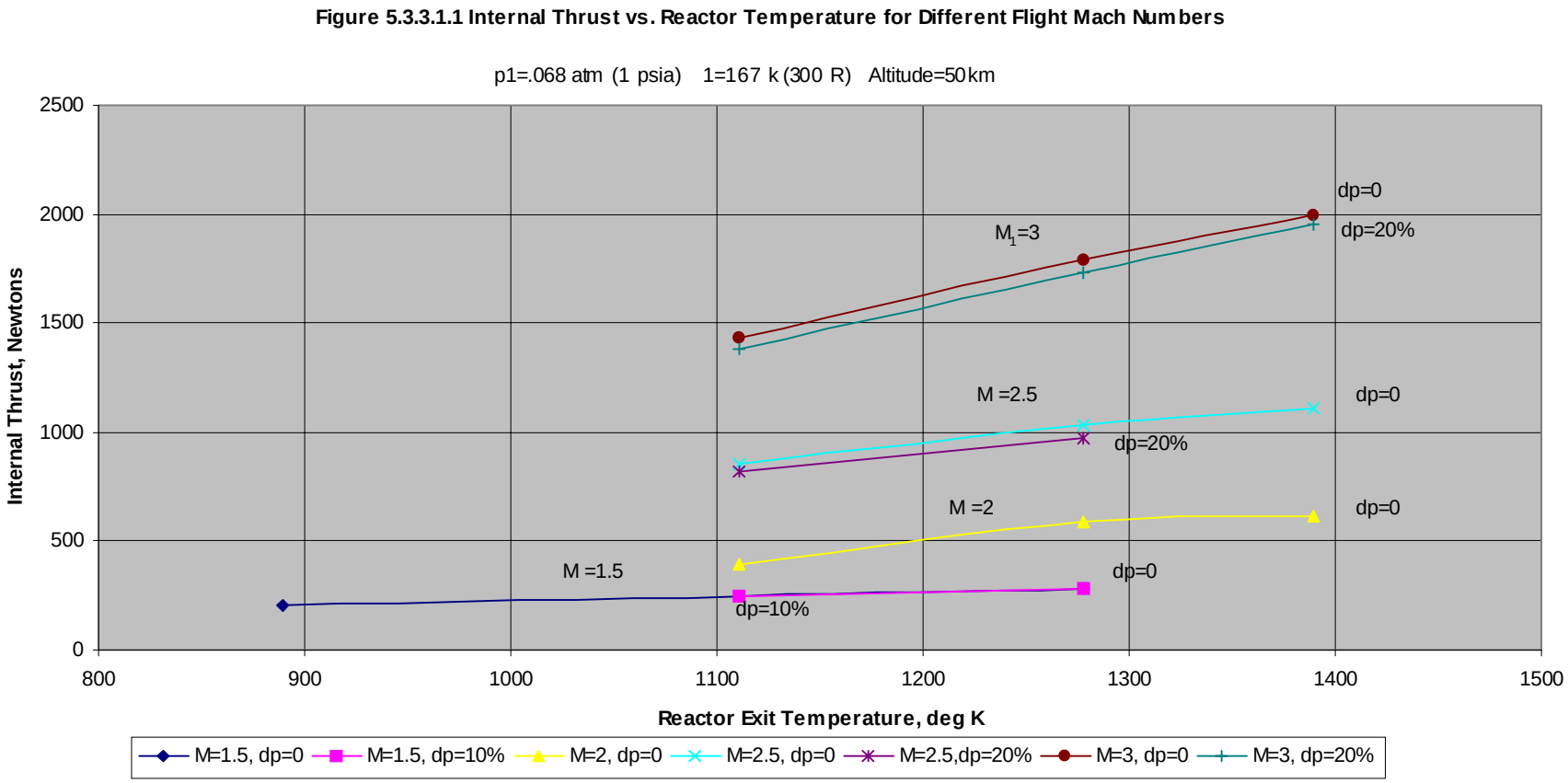

Figure 5.3.3.1.1 Internal Thrust vs Temperature for various M_1 and cycle Temperatures

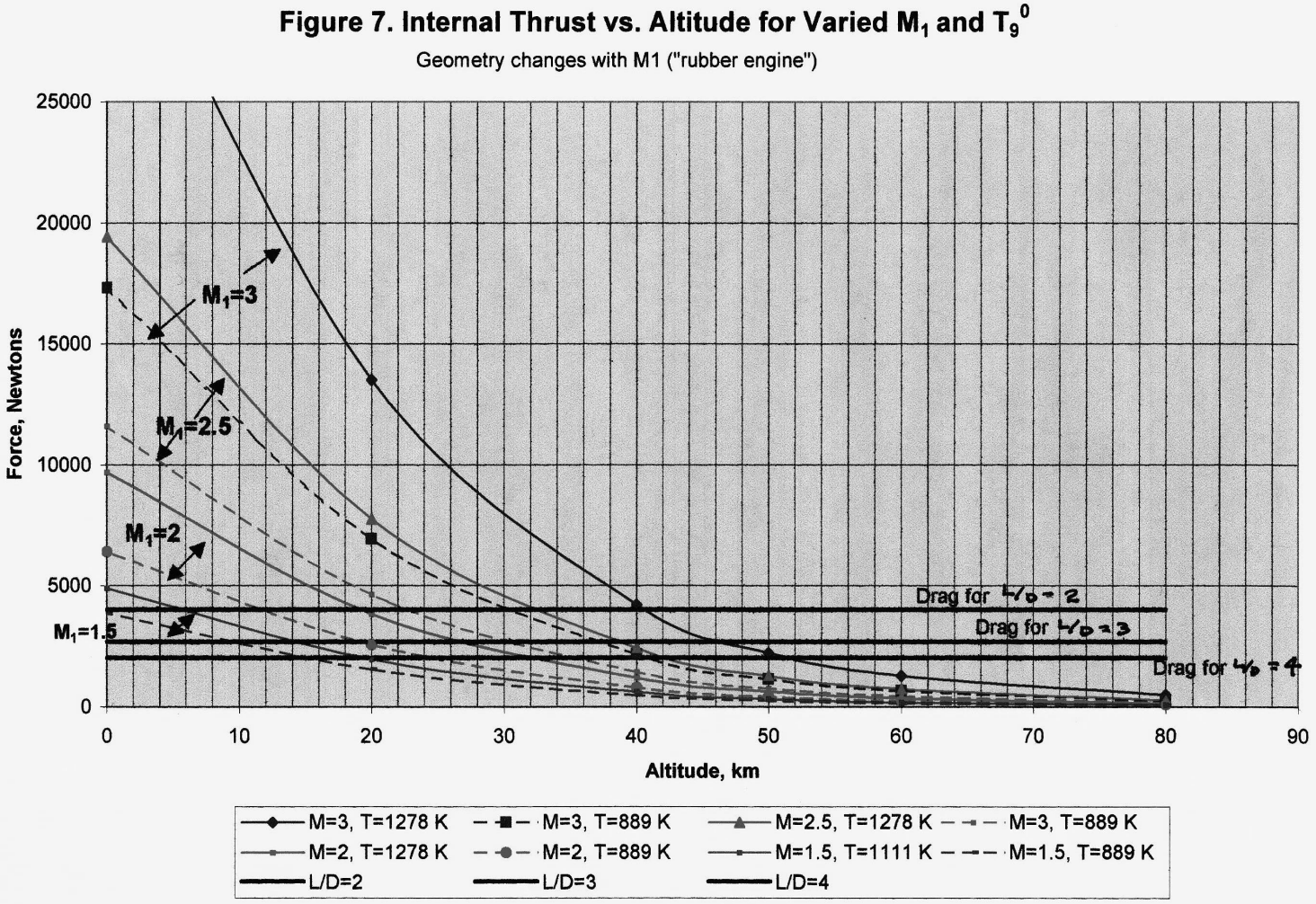

Figure 5.3.2.2.1 Internal Thrust vs Altitude for Various M_1

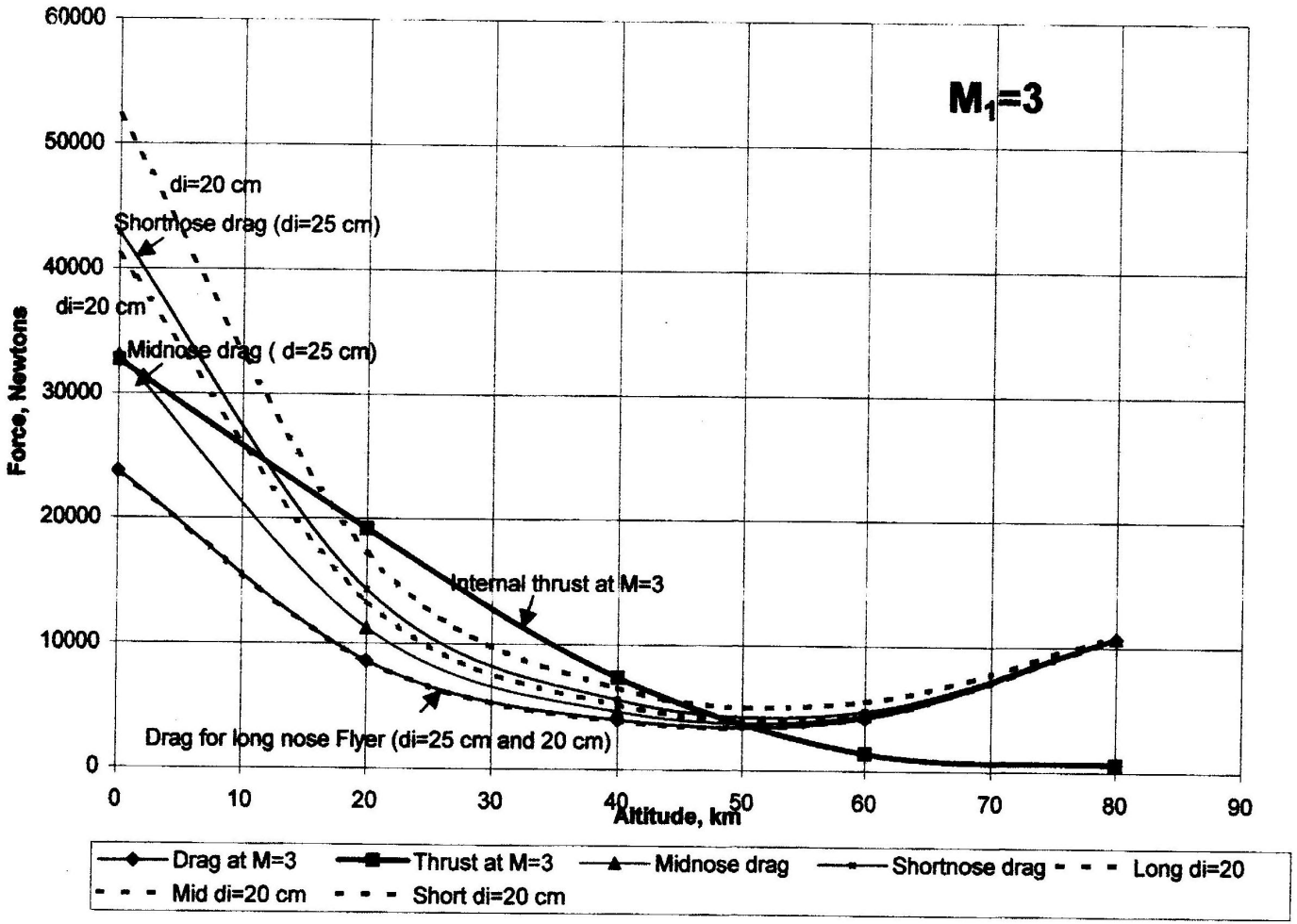

Figure 5.3.3.2.2 Internal Thrust and Vehicle Drag vs Altitude for M_1=3

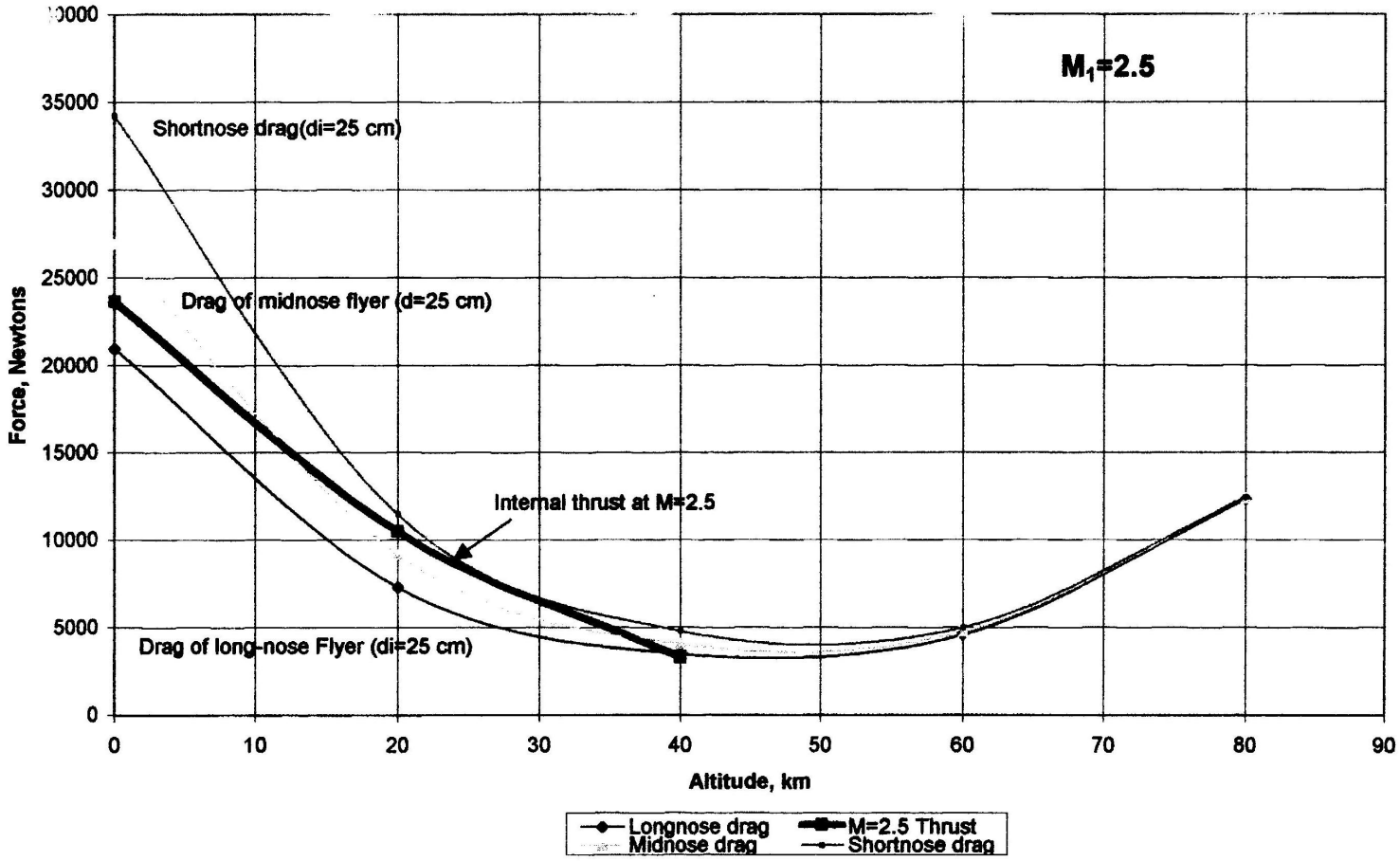

Figure 5.3.3.2.3 Internal Thrust and Vehicle Drag vs Altitude for M_1=2.5

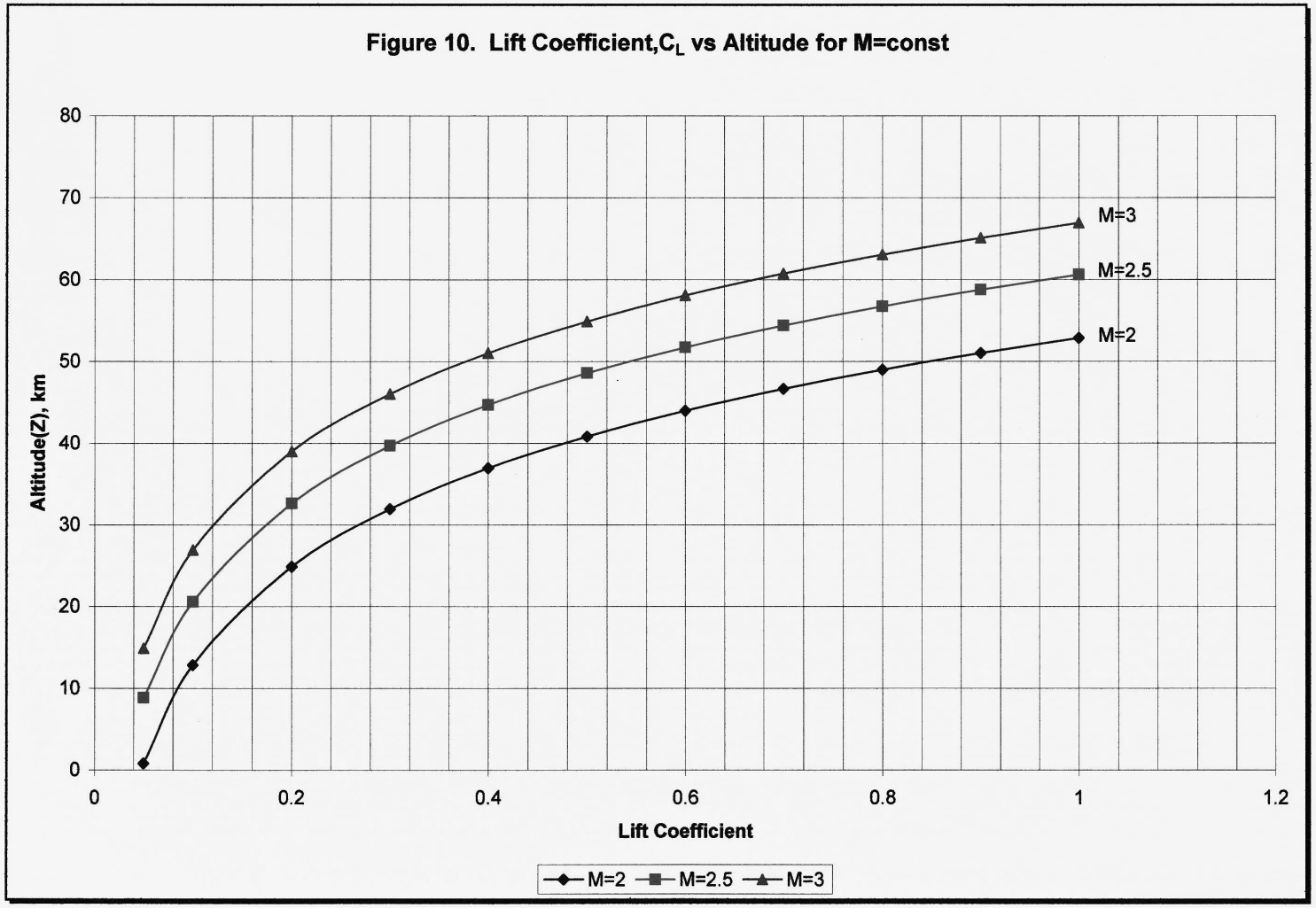

Figure 5.3.3.2.4 Lift Coefficient vs Altitude for Various Flight Mach Numbers

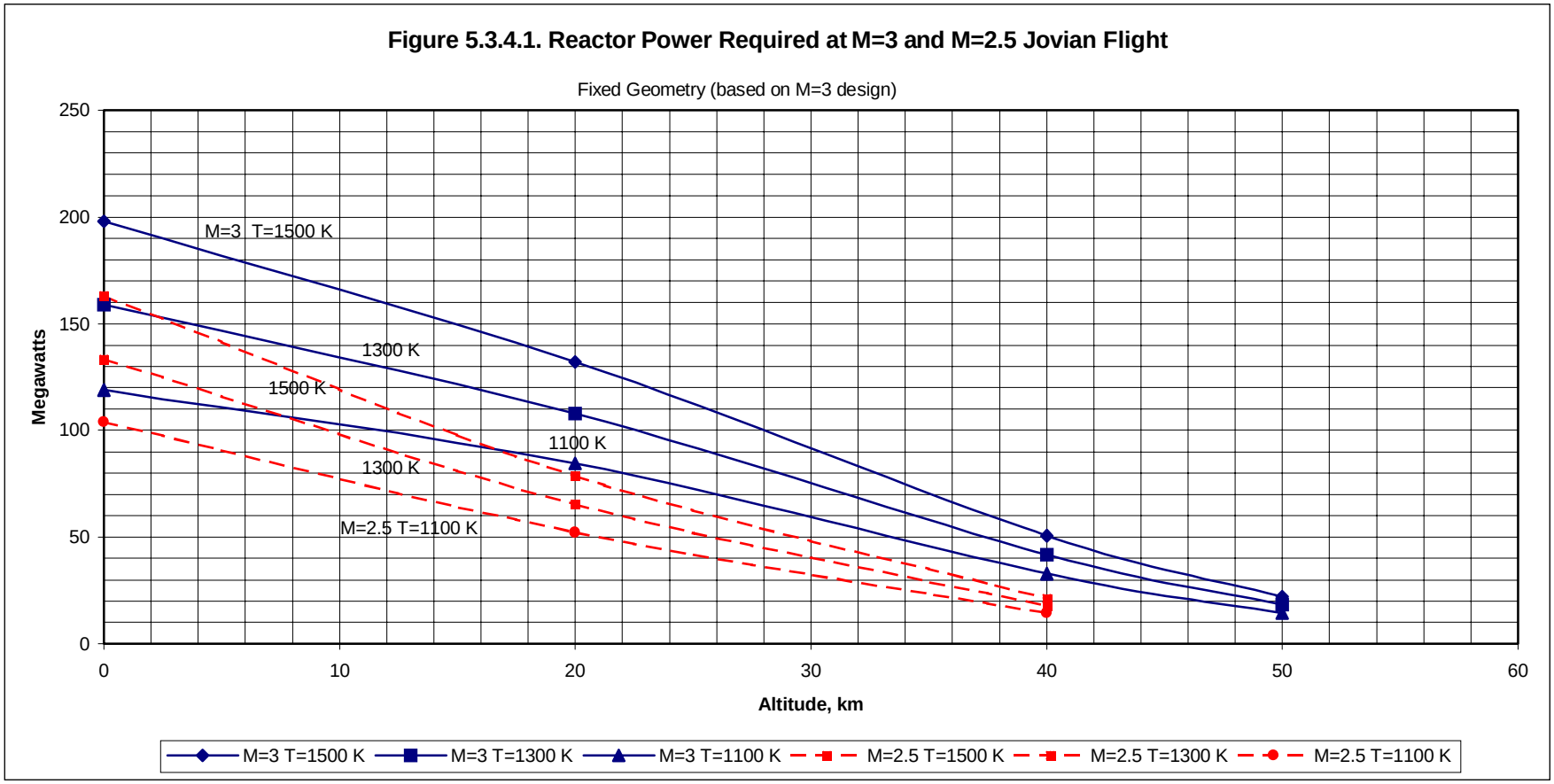

Figure 5.3.4.1 Power Input in MW vs Altitude for M_1=3 and 2.5

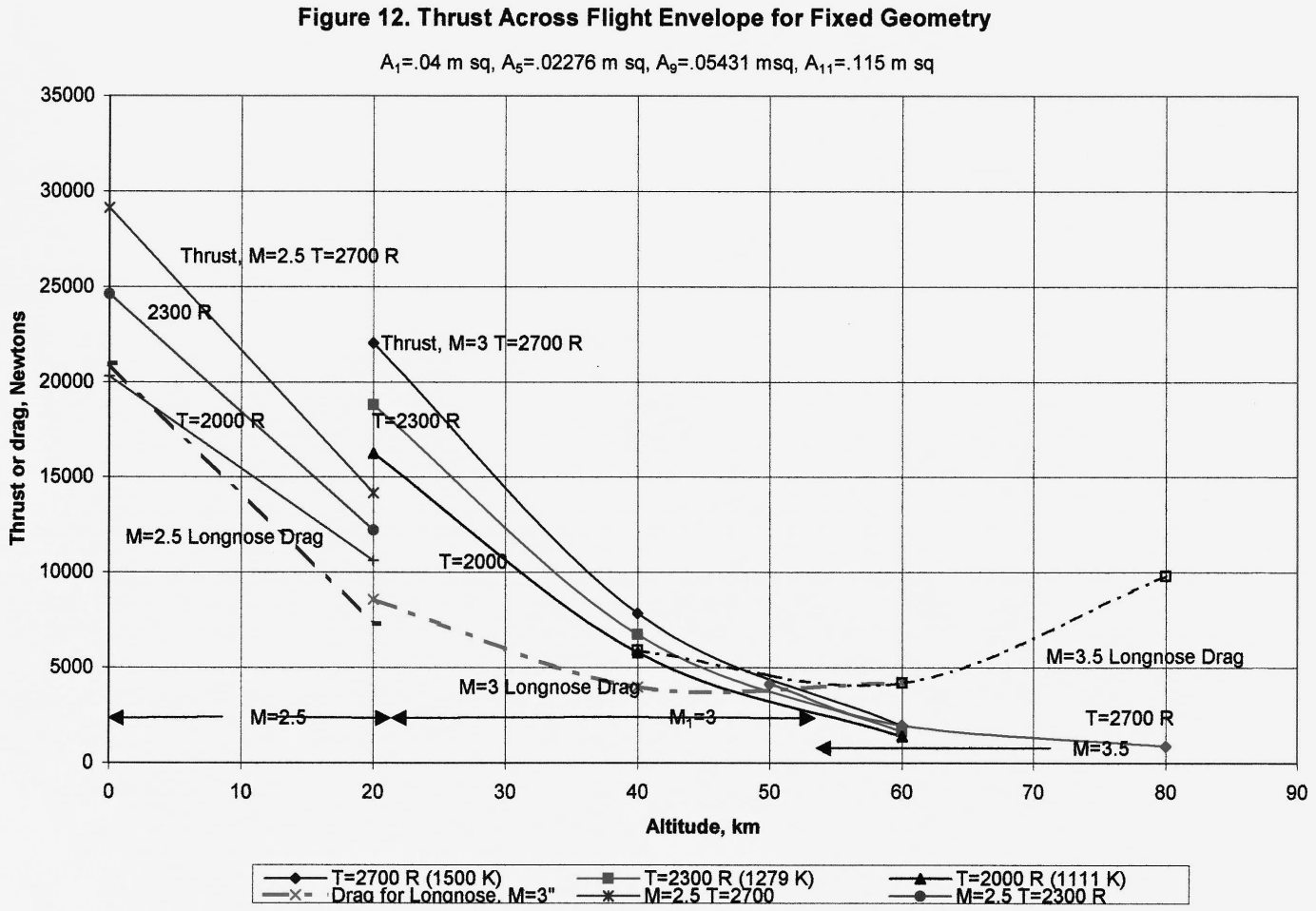

Figure 5.3.4.2 Internal Thrust and Vehicle Drag Across Flight Envelope for Finalized Fixed Geometry

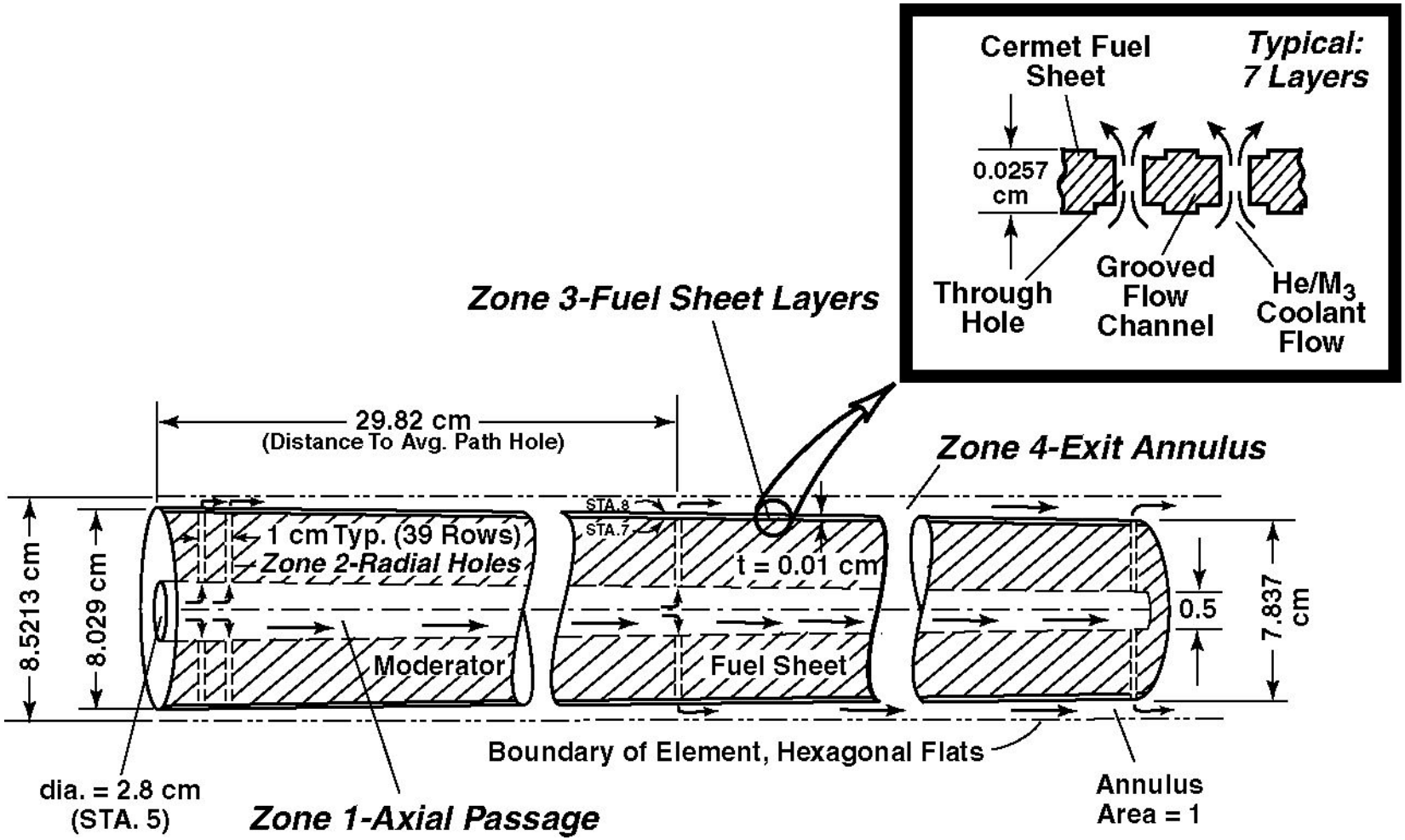

Figure 5.4.1 Diagram of Reactor Flow Passages and Heat Transfer

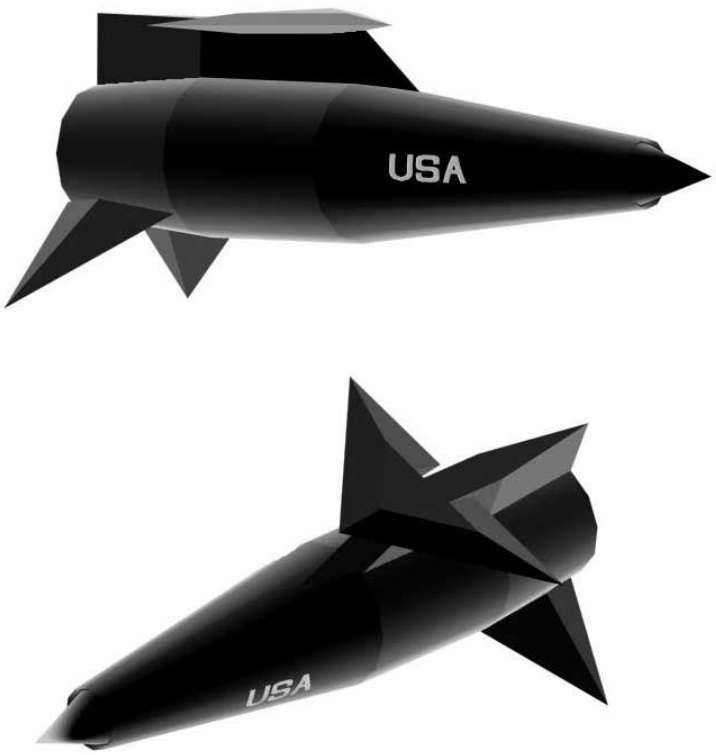

Figure 6.1.3.1 Two views of Ramjet Flyer JF-6

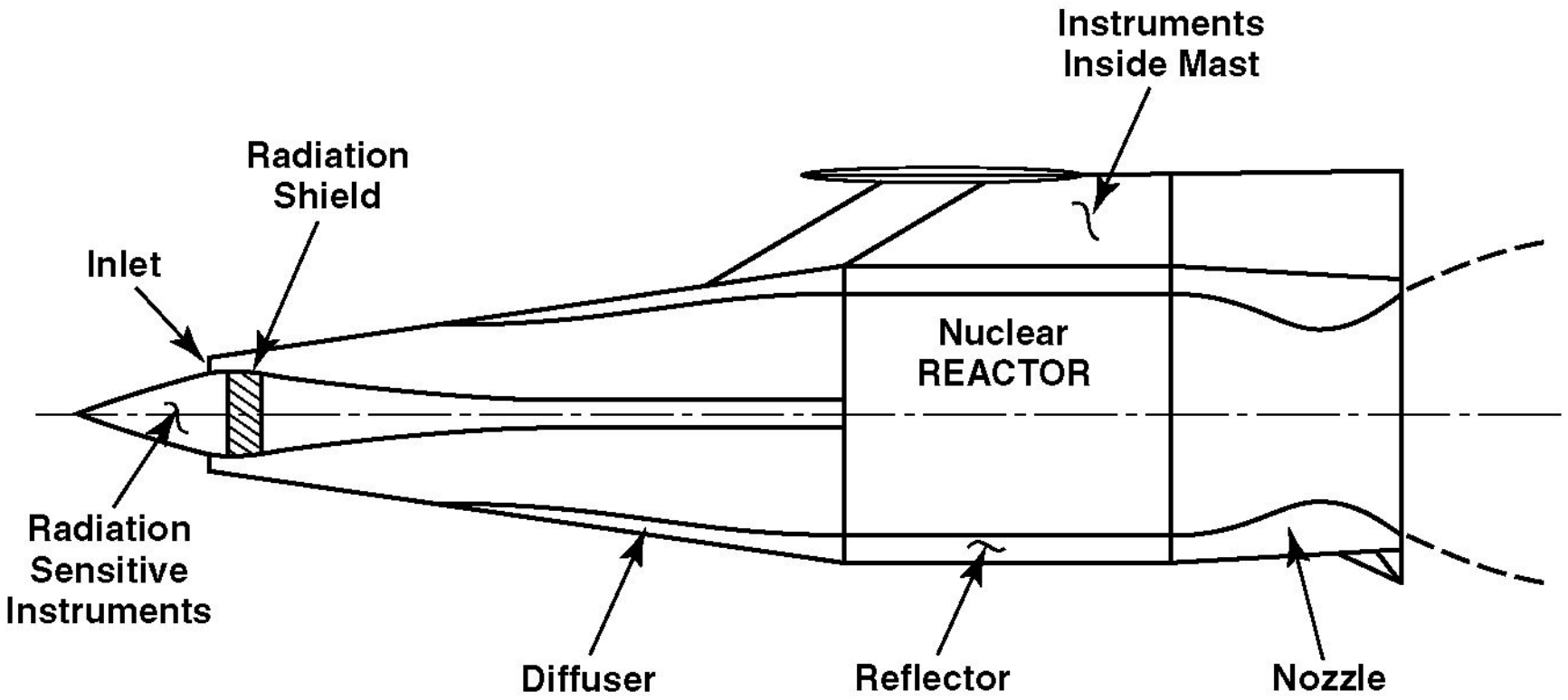

Figure 6.1.3.2 Cross sectional view of Ramjet Flyer showing the location of instruments and the radiation shield

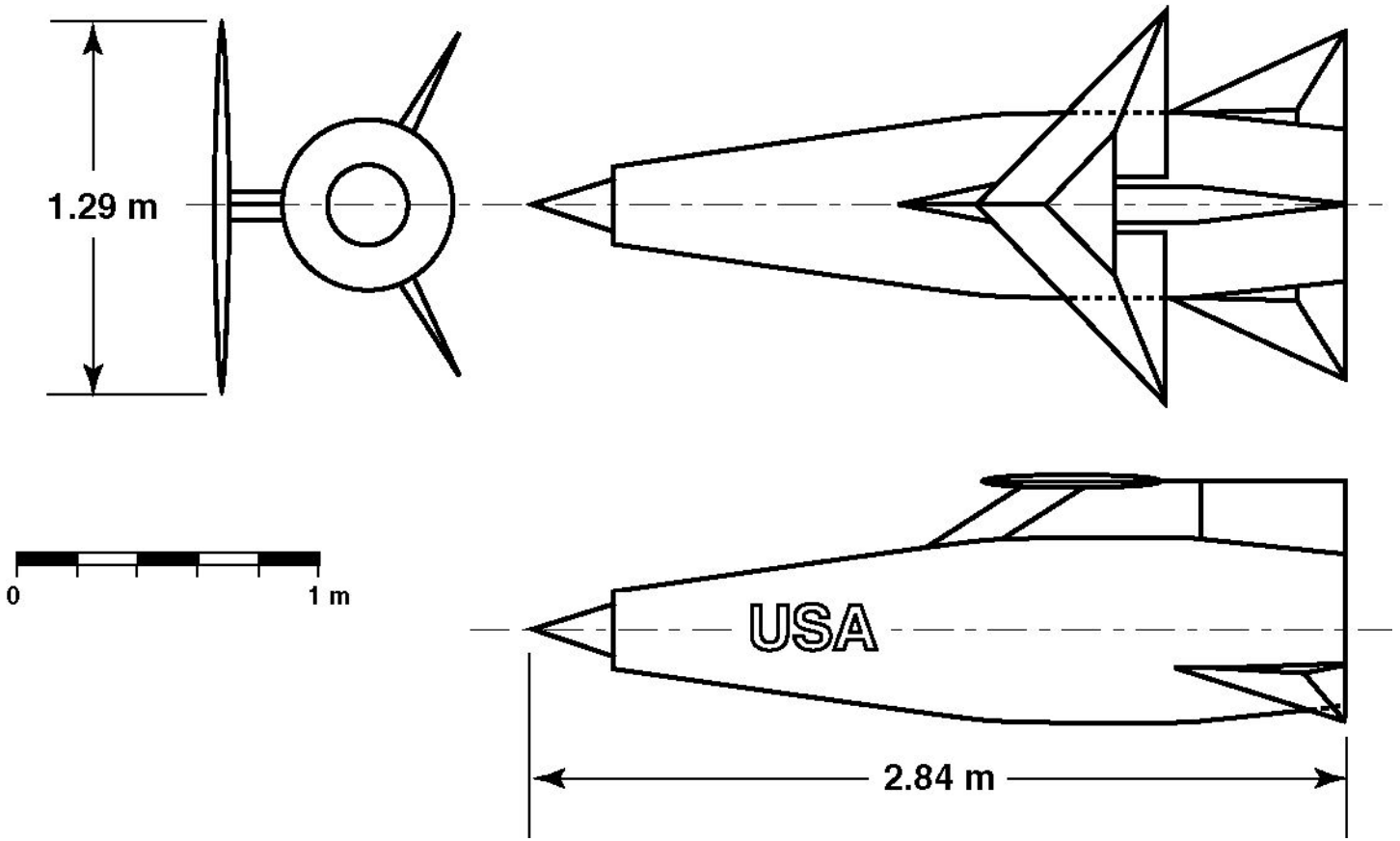

Figure 6.1.3.3 Layout drawing of the Ramjet Flyer JF-6

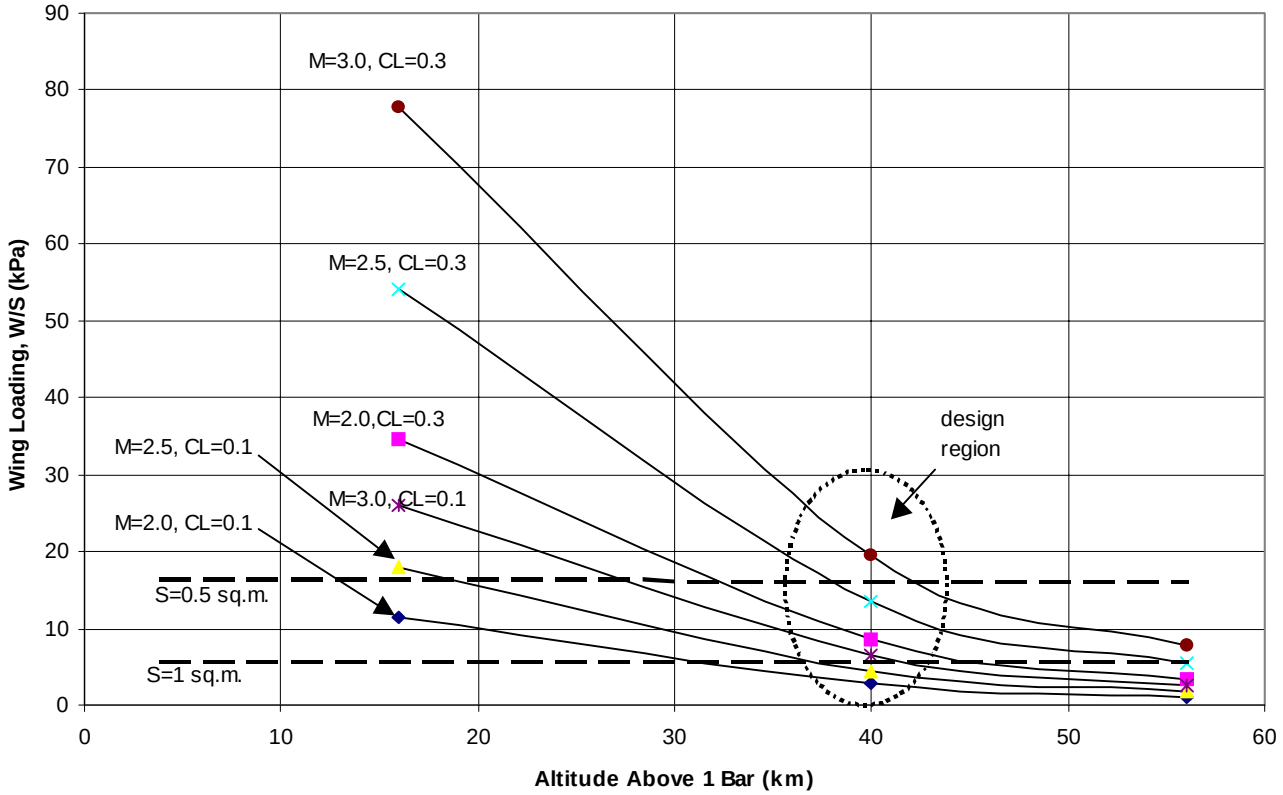

Figure 6.1.5.1 Wing loading is shown as a function of altitude for various pairs of M and C_L. Also shown are lines of constant W/S for a 326 kg vehicle and the corresponding wing area. The design region illustrates the altitude range of primary interest.

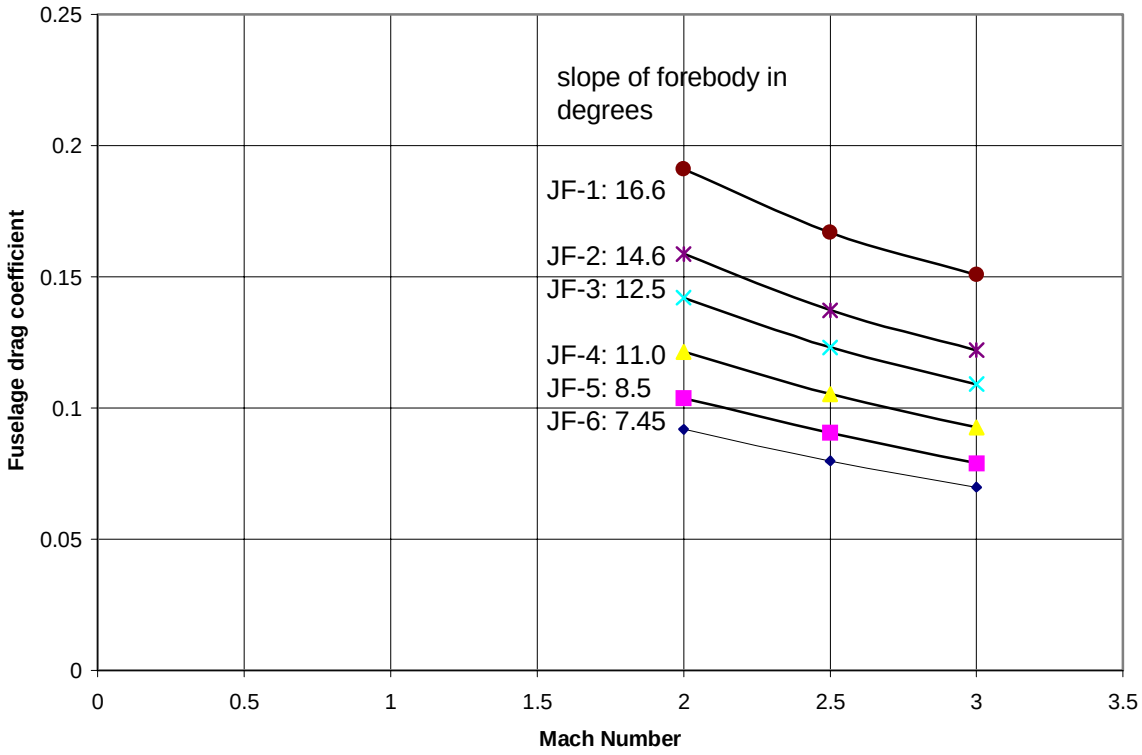

Fig. 6.1.8.1 Drag coefficients of 6 fuselage shapes as a function of Mach number at 40km altitude.

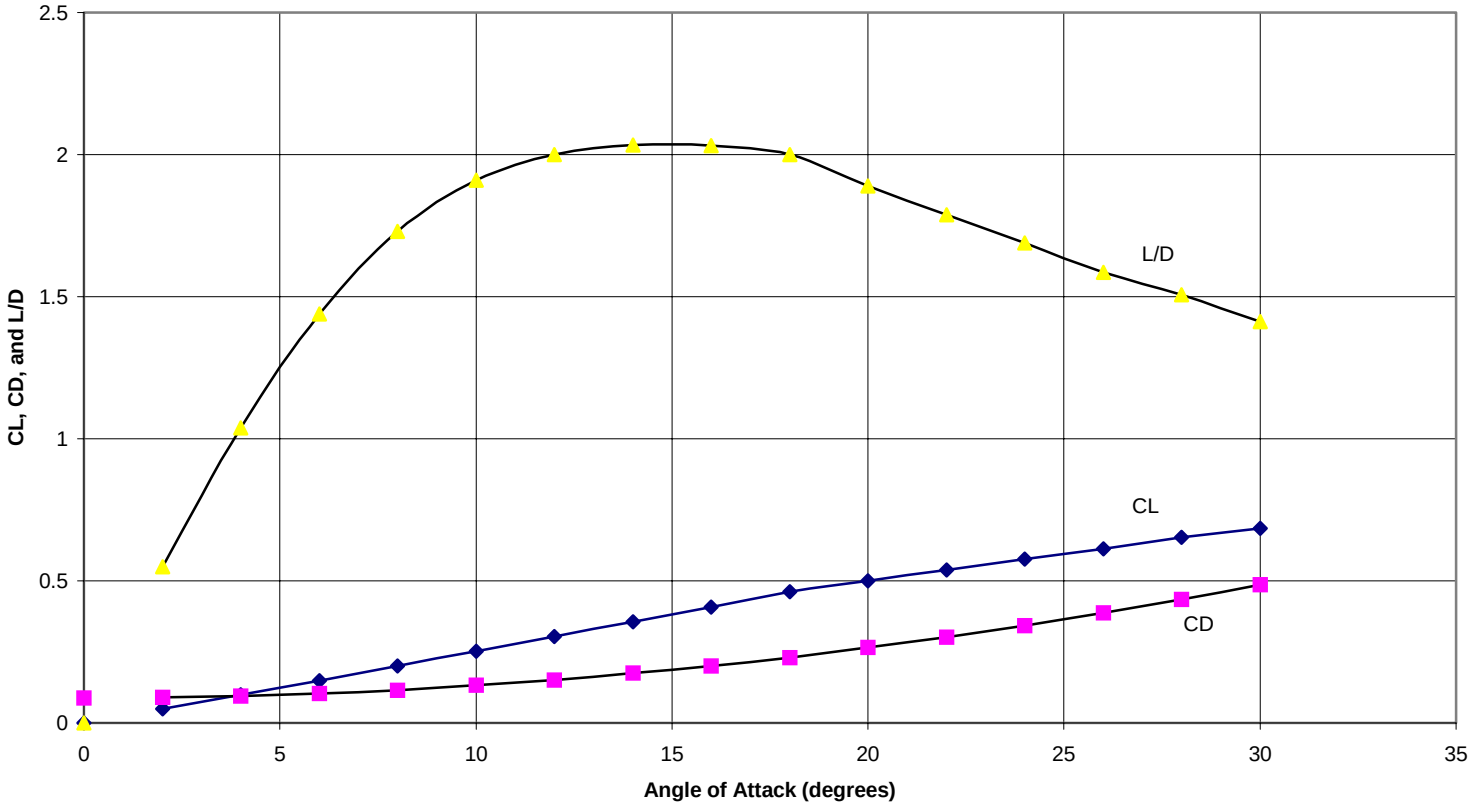

Figure 6.1.10.1 Lift and drag coefficients and lift to drag ratio for the JF-6 as a function of angle of attack

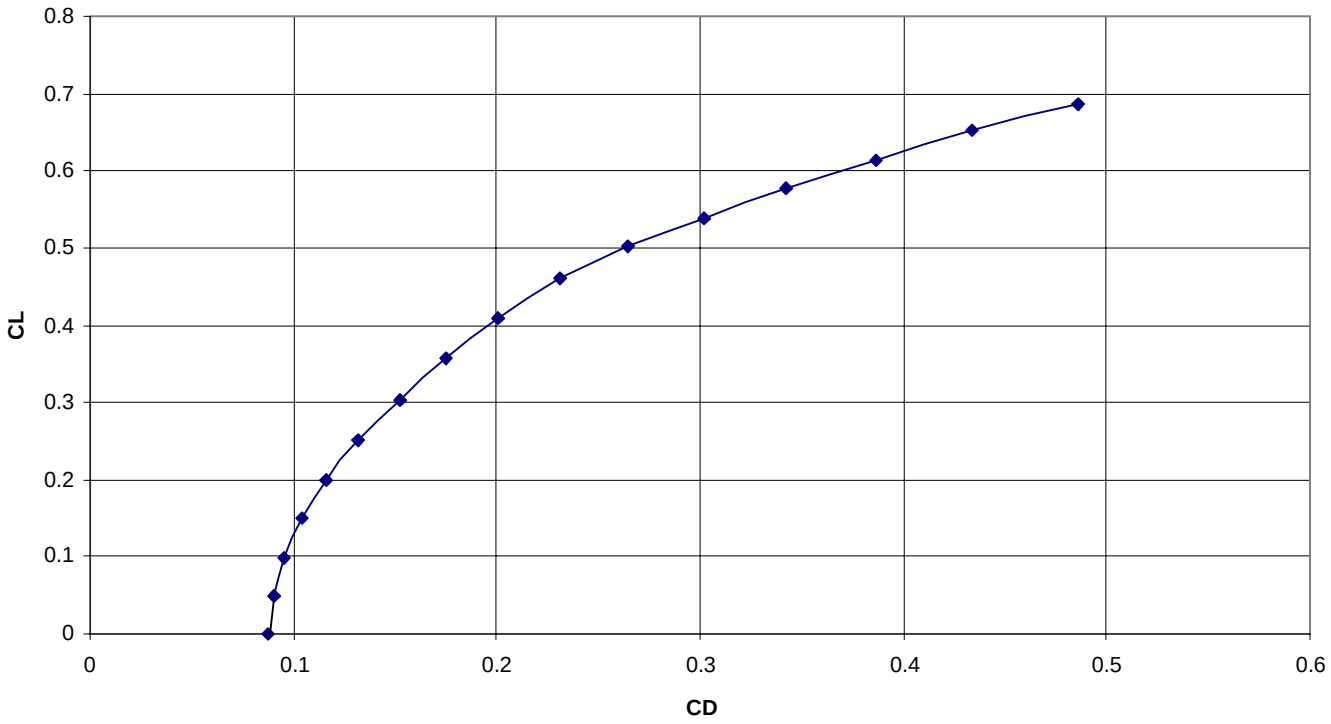

Fig. 6.1.10.2 Drag polar for the JF-6 at Mach 3 and 40 km altitude

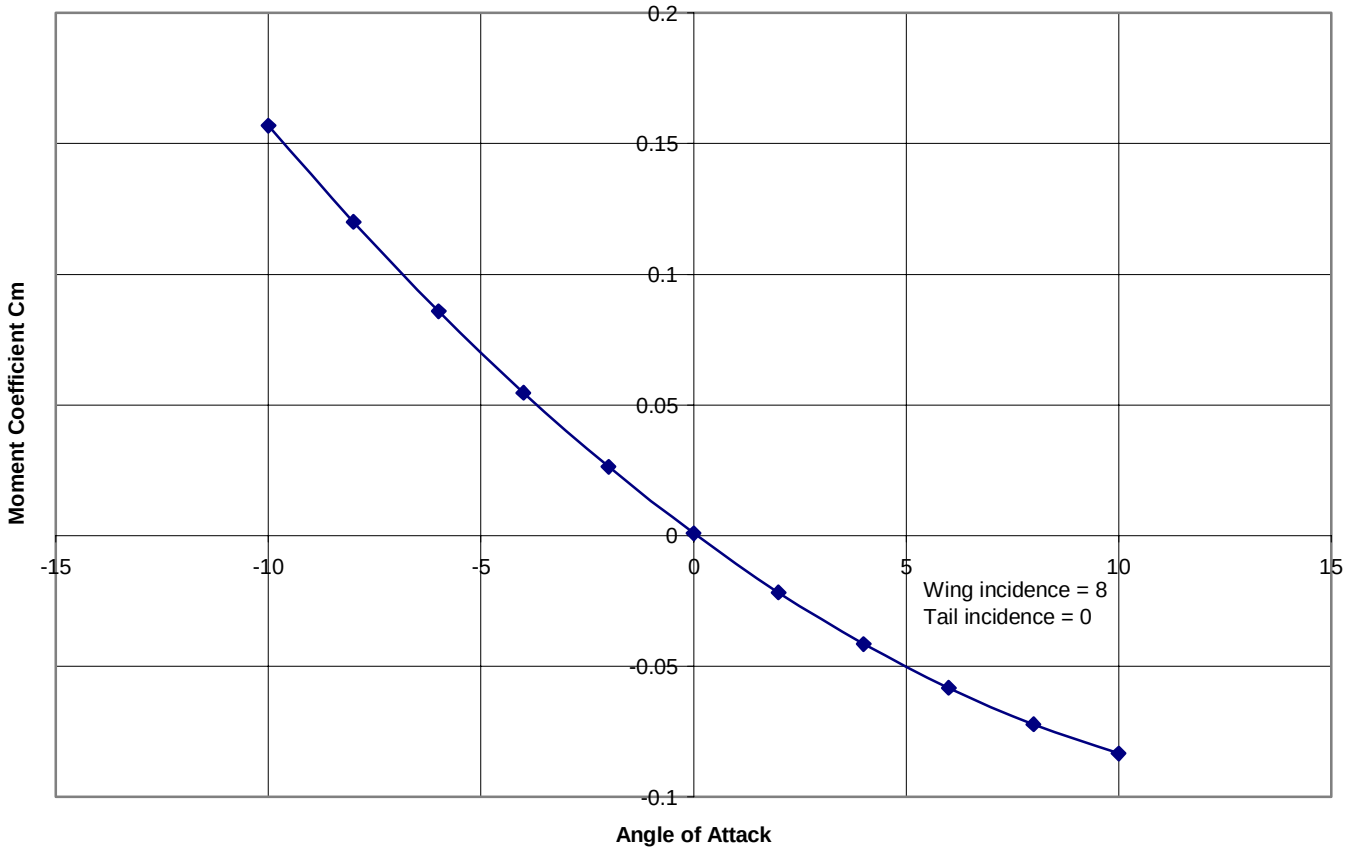

Fig. 6.3.1.1 Pitching moment coefficient of the JF-6 as a function of angle of attack of the fuselage centerline. Setting wing incidence to 8 degrees and tail incidence to zero yields a trim point at zero angle of attack.

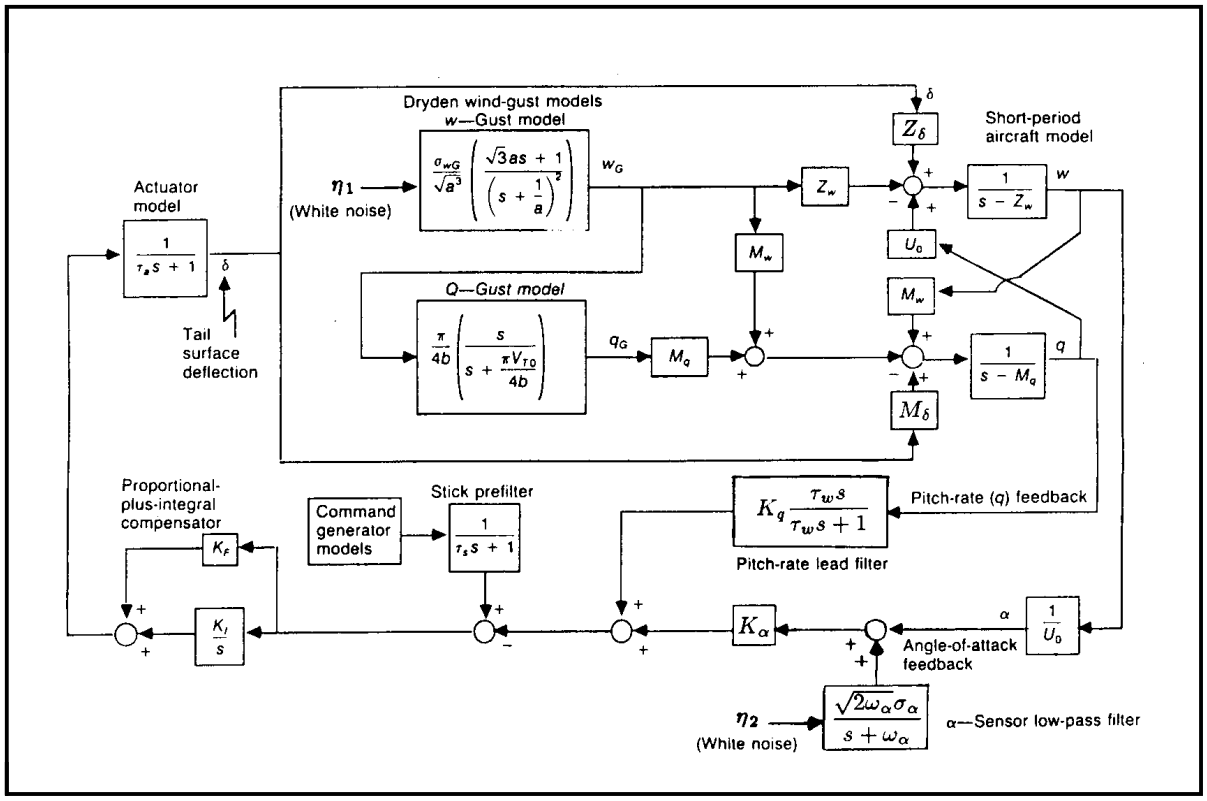

Figure 6.3.15.1 Typical Control System Design for the Pitch Channel

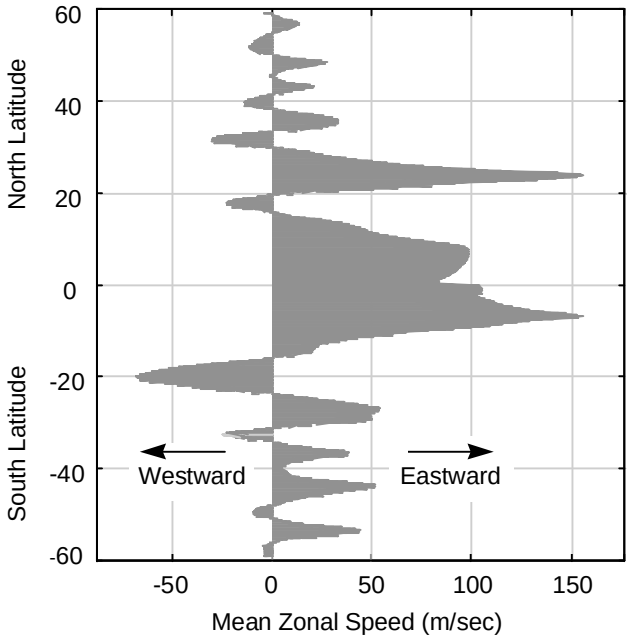

Figure 6.3.15.2 Jovian Mean Zonal Wind Speeds at Cloud Level

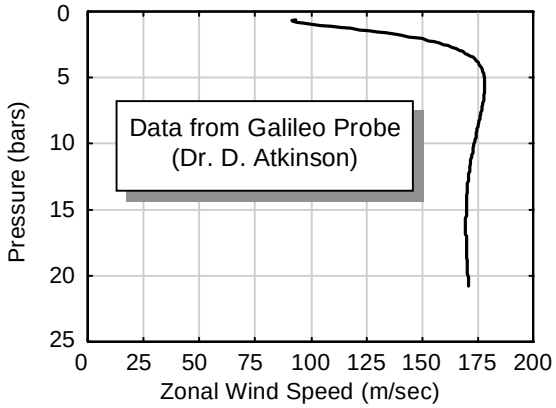

Figure 6.3.15.3 Jovian Wind Speed vs. Pressure (Altitude) from Galileo Probe

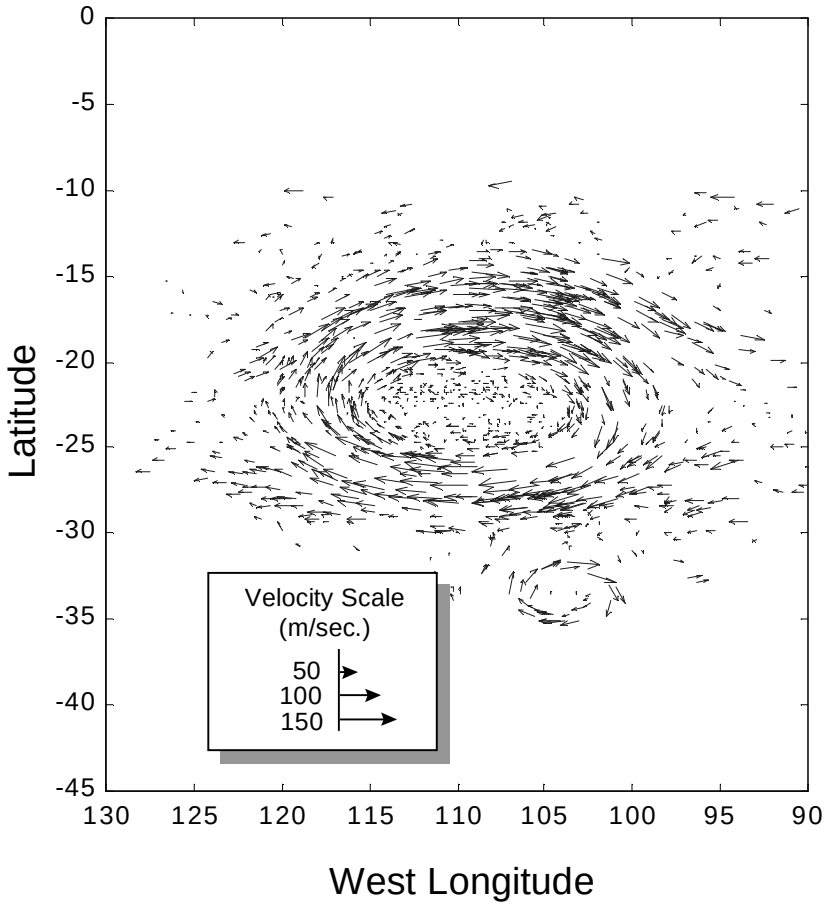

Figure 6.3.15.4 Velocity field for the Great Red Spot

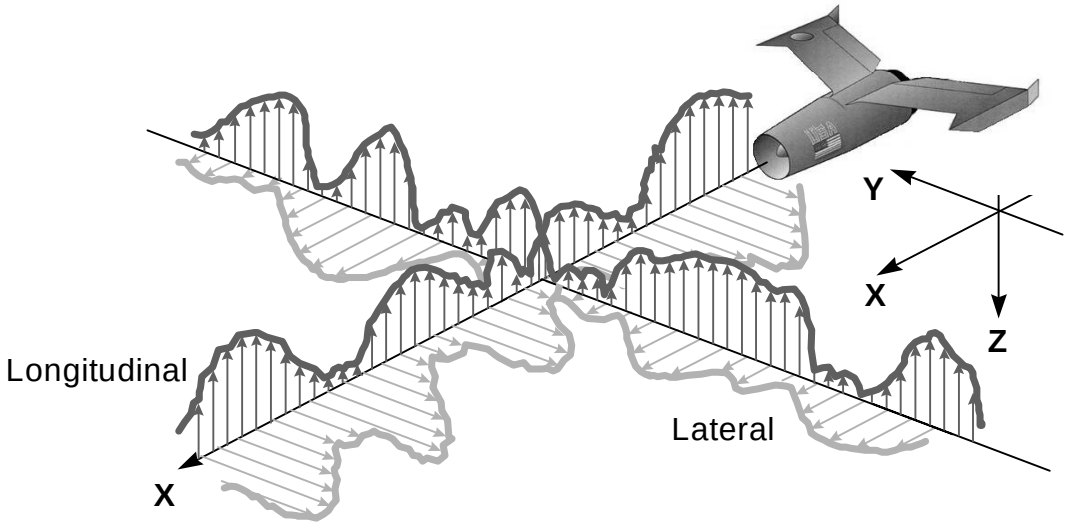

Figure 6.3.15.5 Jovian Turbulence Model: Wind Gust Components

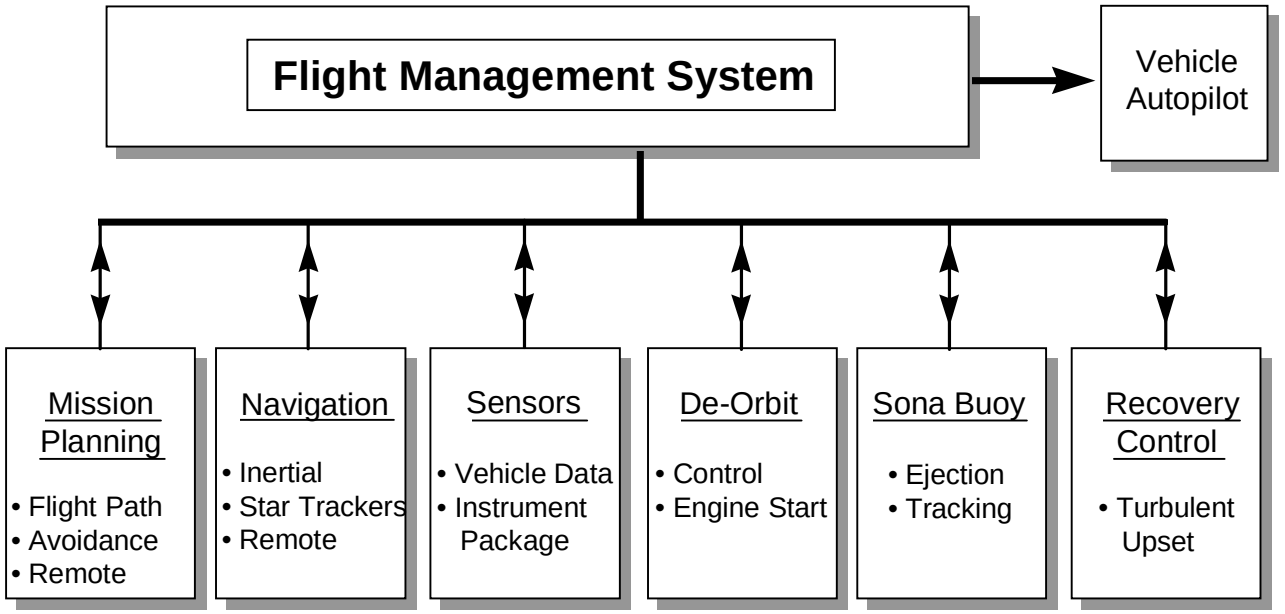

Figure 6.3.15.6 Ramjet Flyer Flight Management System (Autonomous Control)

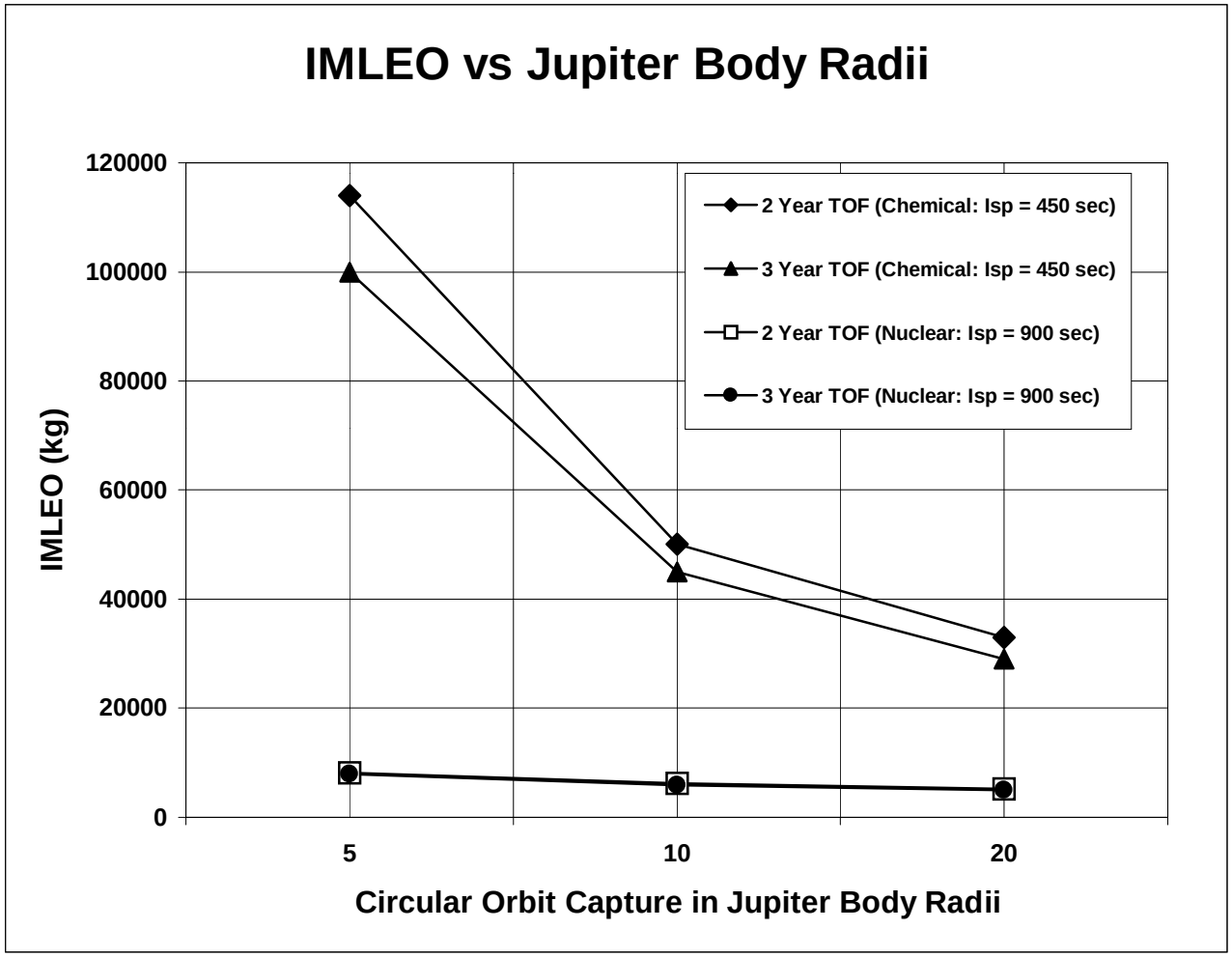

Figure 7.1 IMLEO vs Jupiter body radii

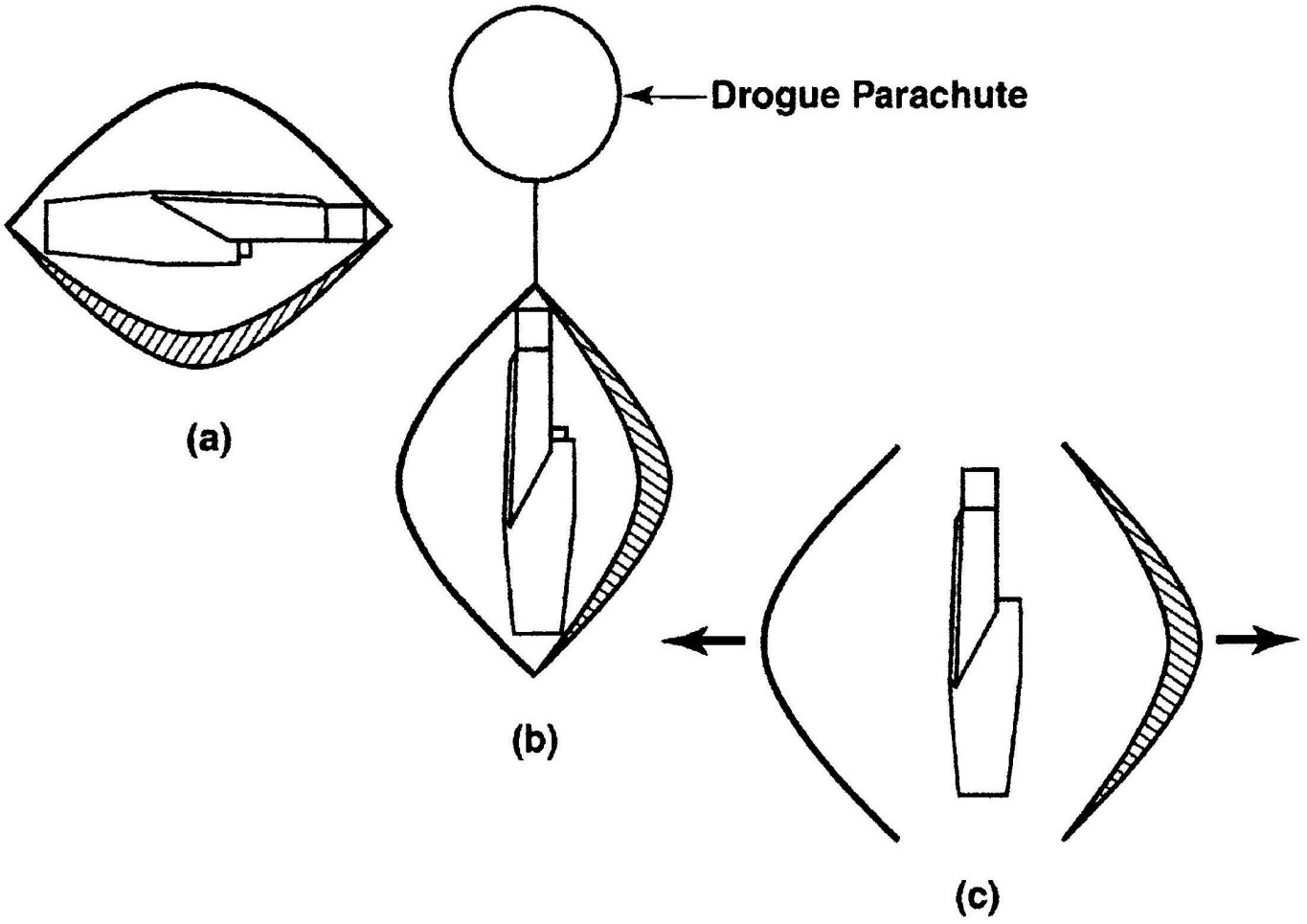

Figure 7.2 Separation of flyer from entry capsule

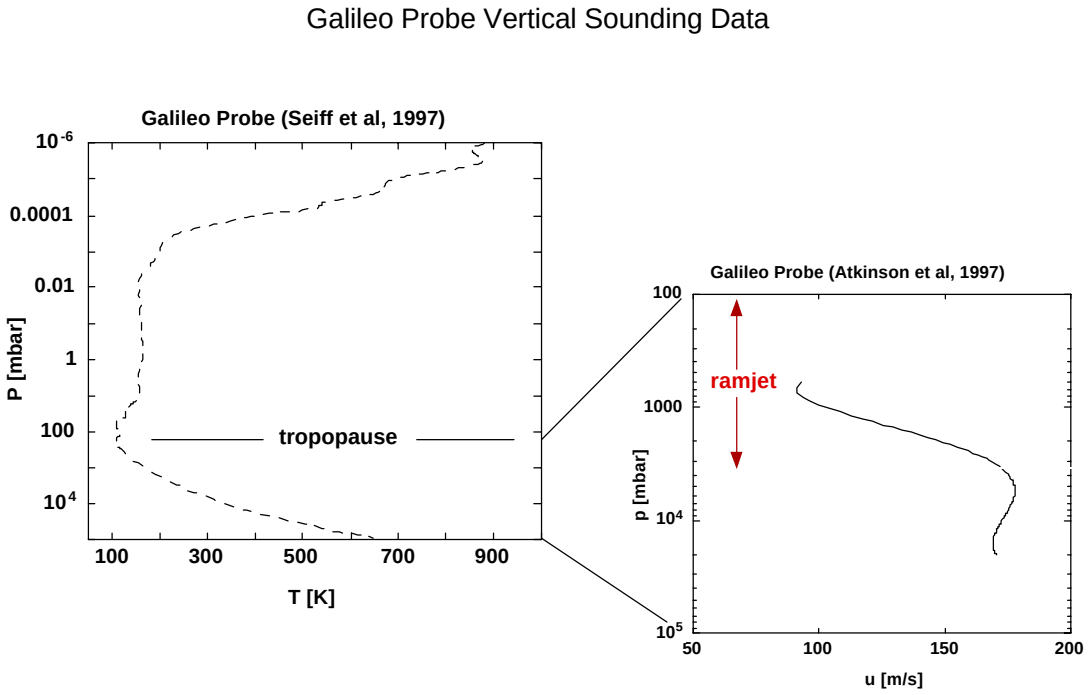

Figure 8.1 Temperature, T, and horizontal wind speed, u, versus pressure, p, on Jupiter as determined by the Galileo Probe. The tropopause marks the temperature minimum that separates the troposphere and stratosphere. The nominal operating range for the ramjet is the upper troposphere. Significantly, this is where the Doppler Probe tracking experiment (Atkinson et al, 1997) indicates there is a significant vertical shear, at least at the southern rim of 5-μm hot spots.

Figure 8.2 Configuration of dropsondes mounted in the NASA ER-2 belly pod during the Summer 2001 CAMEX-4 experiment.

Figure 9.1 Development Tasks, Schedule, and Cost for MITEE Nuclear Ramjet Engine

Phase 1 [$100 M; 3 years]	Phase 2 [$300 M; 3 years]	Phase 3 [$200 M; 2 years]
Task 1: H_2 testing of cerment fuel (non-nuclear)	Task 1: Nuclear testing of full size element with flowing H_2 coolant (Themal/hydraulic code validation)	Task 1: Full-scale testing of nuclear ramjet engine at full power over full range of anticipated operating conditions (Inlet T and P, outlet T, power level, etc.)
Task 2: Nuclear burnup tests of cermet fuel	Task 2: Neutronic tests of low power critical assemblies (power distribution, criticality constant, temp. constant, etc.)	Task 2: Design engineering for integration of ramjet engine into Jupiter Flyer mission.
Task3: Thermal/hydraulic tests of single element (electrically heated, non-nuclear)	Task 3: Construction of H2/He flow loop for full-scale testing of nuclear ramjet engine	
Task 4: 3-D Monte Carlo neutronic aanlysis of ramjet reactor	Task 4: Construction and low power testing of full-scale nuclear ramjet engine	
Task 5: Other - control systems, transient startup, coolant flow/power density matching		